for updating associations between sensory information and desirable outcomes.

A candidate brain region that could be critical for facilitating flexible response selection is the perirhinal cortex (PER), an area within the medial temporal lobe that receives direct input from all sensory modalities (Burwell & Amaral, 1998a; Suzuki & Amaral, 1994). The PER is involved in both memory (Buffalo et al., 1999; Suzuki, Zola-Morgan, Squire, & Amaral, 1993) and higher-order sensory perception (Barense, Gaffan, & Graham, 2007; Barense, Ngo, Hung, & Peterson, 2012; Bartko, Winters, Cowell, Saksida, & Bussey, 2007a, 2007b). Moreover, the PER shares reciprocal connections with the mPFC (Agster & Burwell, 2009; Burwell & Amaral, 1998a; Delatour & Witter, 2002; McIntyre, Kelly, & Staines, 1996; Sesack et al., 1989) and the hippocampus (Naber, Witter, & Lopez da Silva, 1999; Witter, Wouterlood, Naber, & Van Haeften, 2000; Witter et al., 2000). Furthermore, communication within the mPFC-PER-hippocampal circuit is necessary for an animal's ability to detect when the relationship between an object and its spatial location has changed (Barker, Bird, Alexander, & Warburton, 2007; Barker & Warburton, 2008, 2015). Thus, the PER is positioned to contribute stimulus-specific information as well as link activity patterns in the hippocampus to the mPFC in support of flexible behavior. Consistent with this idea, mPFC activity enhances interactions between the PER and entorhinal cortex (Paz, Bauer, & Pare, 2007). As PER-entorhinal cortical interactions are believed to gate the flow of information into the hippocampus (de Curtis & Pare, 2004), mPFC modulation of rhinal cortical activity is likely critical for higher cognitive function.

Although the mPFC is necessary for an animal's ability to inhibit an incorrect response (Lee & Byeon, 2014; Lee & Solivan, 2008), and mPFC-PER communication is involved in an animal's ability to detect novel object-place associations (Barker & Warburton, 2008, 2015; Barker et al., 2007; Jo & Lee, 2010a, 2010b), it is not known if communication between these brain areas is critical for flexible behavior. The objective of the current experiments was to examine whether mPFC-PER communication is necessary for performance on the object-place paired association (OPPA) task (Jo & Lee, 2010b), which tests an animal's ability to flexibly update which of two objects is rewarded based on an incrementally learned object-in-place rule that requires knowledge of both object identity and current spatial location. After rats acquired the biconditional association, the necessity of mPFC-PER communication was investigated by infusing the $GABA_A$ receptor agonist muscimol (MUS) into one hemisphere of the mPFC and the contralateral PER to reversibly disconnect these areas. This approach capitalizes on the fact that the mPFC and PER are densely connected within the same hemisphere, but not across hemispheres (Bedwell, Billett, Crofts, MacDonald, & Tinsley, 2015). Thus, unilateral mPFC and contralateral PER inactivation blocks communication between these areas. Importantly, because only one hemisphere of each region is inactivated, the PER and mPFC remain functional as independent entities.

2. Materials and methods

2.1. Subjects and handling

Twelve male Fischer 344 rats (NIA colony at Taconic; 6-13 mo. old) were single housed and kept on a reverse 12-h light/dark cycle, with all testing occurring during the dark phase. After histological verification of cannula placement (see below), 9 rats were included in the current analyses. Upon arrival to the facility, rats acclimated to the colony room for 7 days. After acclimation, the rats were handled by the experimenters for several days before being placed on food restriction. Rats were restricted to 85% of their initial free-feeding body weight, with *ad libitum* access to water for the duration of the experiment. For all surgical and behavioral procedures, adequate measures were taken to minimize pain or discomfort to all animals. All protocols were in accordance with the *Guide for the Care and Use of Laboratory Animals* and the University of Florida Institutional Animal Care and Use Committee.

2.2. Habituation and training

Rats were habituated to the OPPA arena (Fig. 1A) for 10 min a day for 2 days prior to training. For all experiments, a two-arm maze constructed from wood and sealed with waterproof black paint was used (Fig. 1A; Hernandez et al., 2015). The two arms of the maze were separated by black poster board with distinctive markings on each side to prevent the rat from seeing the opposite arm while providing environmental cues to differentiate the two arms. The arms radiated from a starting platform that was 48.3 cm in diameter. Each arm was 84.0 cm long and had a rectangular choice platform (31.8 cm × 24.1 cm) attached at the end. Each choice platform contained two food wells (2.5 cm in diameter) that were recessed into the maze floor by 1.0 cm and were separated by 12.8 cm. The arms and choice platforms had 5.5 cm high walls. During habituation, food rewards (Froot Loops; Kellogg's, Battle Creek, Michigan) were scattered throughout the maze to encourage exploration. Once comfortable with foraging, rats were shaped to alternate arms by placing a single reward on the choice platform of the unoccupied arm. After the rat retrieved the reward, the opposite arm was baited. Once a rat consistently alternated 30 times in less than 20 min, they began training on the OPPA task.

2.3. Object-place paired-association task and pre-training

Rats were trained to use an object-in-place rule, in which the rewarded object of a pair was contingent on the spatial location (see, Hernandez et al., 2015; Lee & Solivan, 2008) prior to surgery for cannula placement. Rats began the trial in either the left or right arm of the maze, randomly chosen. During pre-training, rats were required to traverse between the left and right arms for a total of 32 trials, regardless of how many correct choices were made. Arms were not blocked so rats had to correctly remember to alternate. A failure to alternate was recorded as a working memory error. The incidence of this type of error was low ($\leqslant$1/testing session), and did not significantly vary across infusion conditions ($p > 0.05$ for all comparisons). Because rats freely alternated between the 2 arms to initiate a new trial, the inter-trial interval was based on the amount of time it took a rat to ambulate from one arm to the next and variable across trials.

The same two objects were presented in both arms of the maze, with a food reward hidden in the well beneath the correct object. For example, in the left arm, the "chicks" object was always the correct choice, regardless of whether it was presented on the left or right well (Fig. 1B). In the right arm, the "chicks" object was the incorrect choice, and instead the "frog" object was always rewarded. The locations of objects within the arms pseudorandomly varied across trials in order to ensure that the left and right wells were equally rewarded. The rat was required to push the object off of the well it was covering to retrieve the food reward beneath the correct object. If the incorrect object was pushed or touched by the rat's nose, the objects and the food reward were removed from the arm and the rat was not allowed to make another choice in that arm.

During testing, as well as during all training and control sessions, the experimenter stood behind the choice platforms so that the next trial could be set up before the rat exited the current arm it was in. The barrier located between the arms ensured that the rat could not observe which well was baited. All rats completed 32 tri-

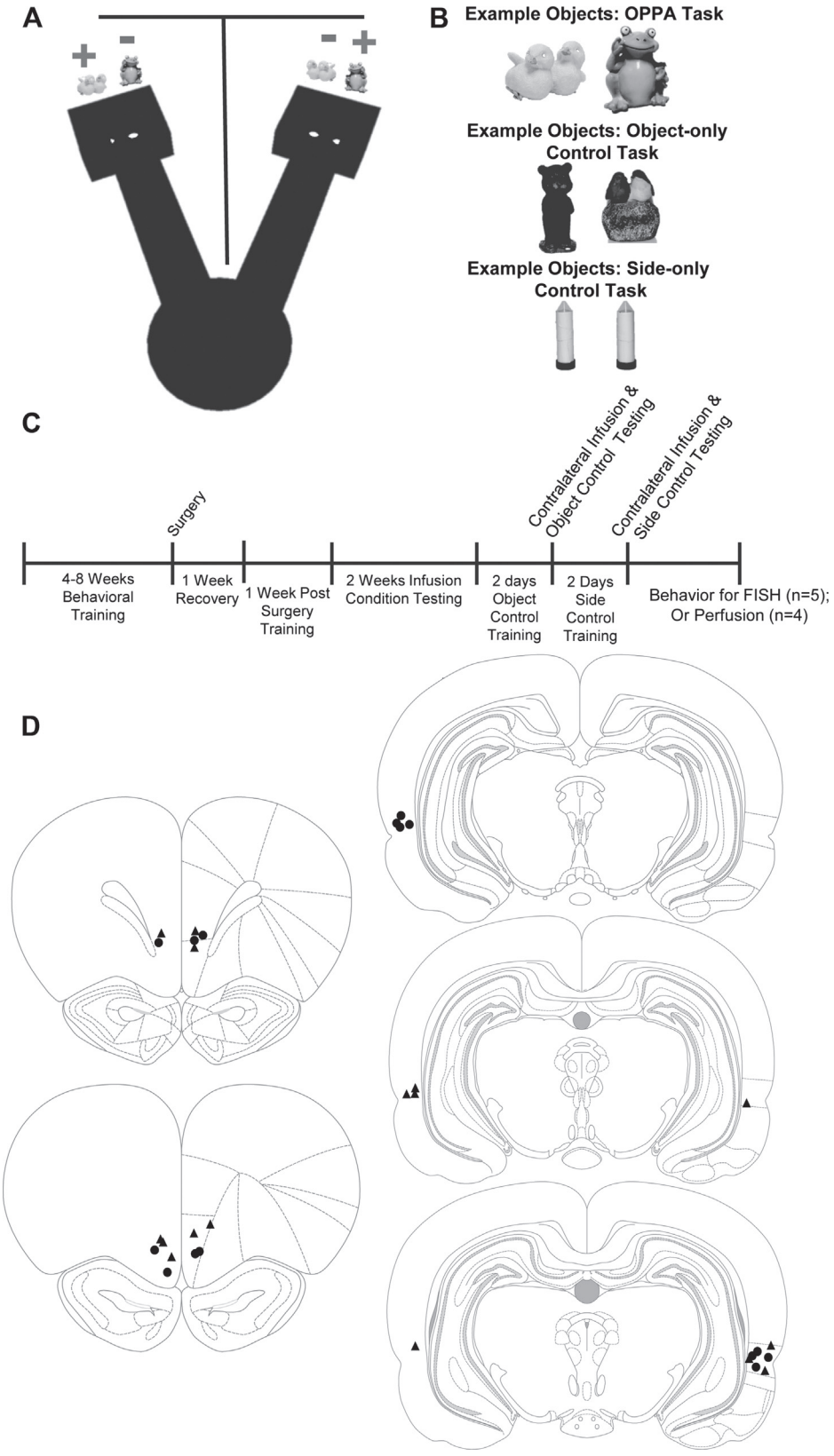

Fig. 1. Experimental design and cannulae placement. (A) The Object-Place Paired Association (OPPA) Task apparatus. Two objects were placed at the end of each arm, covering a food well with a hidden food reward underneath the correct object. The rat had to choose the correct choice in each arm while alternating back and forth. Arms were separated by black poster board with different markings on each side to prevent the rat from viewing the opposite arm and to differentiate between the two arm locations. Each object was correct in only one arm of the maze and the same objects were used within a test condition. The same apparatus was used for object-only and side-only control tasks with one arm blocked off during each task. (B) Representative objects used during the OPPA task (top), object only control task (middle), and the left versus right side discrimination control task (bottom). (C) Timeline of experimental procedures. (D) Bilateral cannulae placement in the mPFC and PER shown for each rat included in analyses. Triangles indicate the placement from animals in which tracts were verified with histology and circles represent placements from animals in which *Arc in situ* hybridization was used to verify selectivity of inactivation.

als/day for 6 days a week until they achieved criterion performance of 26/32 correct trials 2 days in a row. In cases in which there was a delay between OPPA training and cannulation surgery, rats were tested 3 days per week to maintain OPPA performance.

2.4. Surgery

Each rat was stereotaxically implanted with cannulae bilaterally targeting the mPFC (infralimbic cortex) and PER under isoflurane anesthesia (1–3%). An incision was made to expose Bregma. Small holes were drilled for the placement of 22-gauge guide cannulae (Plastics One, Roanoke, VA; C313G-L20/SPC) at +3.2 mm AP and ±0.9 mm ML from Bregma and 3.8 mm ventral to the skull surface for mPFC, and −5.5 mm AP, ±6.6 mm ML from Bregma and 6.5 mm ventral to the skull surface for PER. The mPFC coordinates were determined based on a previous study showing a role for the infralimbic cortex in the conceptual set-shifting task of behavioral flexibility (Beas, McQuail, Bañuelos, Setlow, & Bizon, 2016). Anchoring screws (1/8″ length; 00-120) were placed in the skull and all hardware was secured with dental cement. Dust caps with dummy stylets were screwed into each cannula to prevent tubing from becoming obstructed. During surgery and post-operatively, the non-steroidal anti-inflammatory Meloxicam (Boehringer Ingelheim Vetmedica, Inc., St. Joseph, MO; 1.0 mg/kg S.C.) was administered as an analgesic. All animals were given 7 days to recover before resuming behavioral testing.

2.5. Infusions

The $GABA_A$ receptor agonist muscimol (MUS) (0.5 μg/0.5 μl; Sigma-Aldrich, St. Louis, MO) was injected intracerebrally with a microinfusion pump (Harvard Apparatus; Holliston, MA) for the temporary inactivation of the PER and/or mPFC. Polyethylene tubing (Plastics One) was attached to a 10 μl syringe (Hamilton, Franklin, MA), backfilled with sterile water, and then loaded with 2 μl muscimol. An air bubble of 1–2 μl volume was maintained between the backfill and drug to prevent mixing, as well as ensure that the pump was infusing the correct volume of drug. Dust caps were removed and 28-gauge needles (Plastics One, 8IC313ISPCXC) were placed into the proper guide cannulae. Each injector needle protruded 1 mm below the guide cannula into the brain, such that the depth of injection was 7.5 mm from the surface of the skull for the PER and 4.8 mm from the surface of the skull for the mPFC infusions. MUS was infused at a rate of 0.1 μl/min over 5 min. Upon infusion completion, needles were left in place for a minimum of 2 min to allow diffusion of the drug. Dust caps were reinserted and the animal was returned to their home cage for a 30-min period before testing began.

2.6. Behavioral task post surgery

Fig. 1C shows the order and timeline for all experimental procedures. Once rats recovered from surgery, they were retrained on the OPPA task until performance was at or above criterion (26/32 trials, ⩾81.25% correct) for at least 2 consecutive days. A pseudorandomized infusion schedule was used for each rat, with a baseline testing session (no infusion) between each infusion day for a total of 15 test days. The infusion conditions were: (1) bilateral mPFC MUS, (2) bilateral PER MUS, (3) left ipsilateral mPFC-PER MUS, (4) right ipsilateral mPFC-PER MUS, (5) contralateral left mPFC-right PER MUS, (6) contralateral right mPFC-left PER MUS, (7) contralateral left mPFC-right PER vehicle control, (8) contralateral right mPFC-left PER vehicle control.

Upon completion of these 8 infusion conditions, rats were trained on 2 additional control tasks. First, rats were trained on an object-only control task (Fig. 1B middle panel), during which only one choice platform of the maze was used. In this task, rats traversed back and forth between a single choice platform and the other arm, choosing a single target rewarded object regardless of its position over the left or right well. Thus, in this task only object information was required to make a correct choice. Once the rat reached criterion performance of 26/32 trials on the object-only control task, a contralateral MUS infusion was administered 30 min prior to testing. After completion of this object discrimination control task, rats were then trained on a side-only task (Fig. 1B bottom panel) in the opposite choice platform. In this control task, the correct choice of two identical objects was determined by their placement over a single well on a specific side (left versus right). For example, a rat had to learn to always select the object over the right well, and the left well never contained the reward. The rewarded well was counterbalanced across rats. Rats performed this task until a criterion of 26/32 trials was reached and a final contralateral MUS mPFC-PER infusion was administered 30 min prior to testing.

2.7. Histology and fluorescence in situ hybridization

At the conclusion of behavioral testing, rats were sacrificed and tissue collected to evaluate accurate placement of the guide cannula in the PFC and PER with either standard histological techniques (n = 7), or by labeling the expression of the activity-dependent immediate-early gene *Arc* (n = 5). For the 7 rats that underwent standard histology, a lethal dose of sodium pentobarbital (Vortech Pharmaceuticals, Dearborn, MI) was administered prior to transcardial perfusion with 4% paraformaldehyde. Brains were stored in 4% paraformaldehyde with 30% sucrose at 4 °C for 72 h and then sectioned at 40 μm on a cryostat (Microm HM550; Thermo Scientific, Waltham, MA), thaw-mounted on Superfrost Plus slides (Fisher Scientific, Waltham, MA) and nuclei were stained prior to cannulae placement confirmation with microscopy. Fig. 1D shows the cannulae placement for all rats included in the current experiments. Based on the histology 3 rats were excluded from the analyses because the guide cannula could not be localized to the mPFC and PER.

In a second subset of rats (n = 5), fluorescence *in situ* hybridization for the activity-dependent immediate-early gene *Arc* was used to provide a functional assay of MUS infusion specificity to the target regions. In these animals, MUS was infused unilaterally into the PFC and PER 30 min prior to sacrifice (left PFC-PER n = 2, right PFC-PER n = 2, control n = 1). Just prior to sacrifice, the 4 MUS infused rats performed the OPPA task for 10 min, completing an average of 46 trials (SD = 1.22). At the conclusion of the behavioral session, rats were deeply anesthetized with isoflurane (Abbott Laboratories, Chicago, IL) and euthanized by rapid decapitation. Tissue was extracted and flash frozen in chilled 2-methyl butane (Acros Organics, NJ). One additional rat was sacrificed directly from the home cage as a caged control. Tissue was stored at −80 °C until it processing for fluorescence *in situ* hybridization.

Fluorescence *in situ* hybridization (FISH) for the immediate-early gene *Arc* was performed as previously described (e.g. Burke, Hartzell, Lister, Hoang, & Barnes, 2012; Guzowski, McNaughton, Barnes, & Worley, 1999). Tissue was sliced at 20 μm thickness on a cryostat (Microm HM550) and thaw-mounted on Superfrost Plus slides (Fisher Scientific). *In situ* hybridization for *Arc* mRNA was performed and z-stacks were collected by fluorescence microscopy (Keyence; Osaka, Osaka Prefecture, Japan) to confirm that target regions were inactivated and adjacent structures did not have a significant blockage of activity-dependent *Arc* induction. Briefly, a commercial transcription kit and RNA labeling mix (Ambion REF #: 11277073910, Lot #: 10030660; Austin, TX) was used to generate a digoxigenin-labeled riboprobe using a plasmid template containing a 3.0 kb *Arc* cDNA. Tissue was incubated with the probe

overnight and *Arc* positive cells were detected with anti-digoxigenin-HRP conjugate (Roche Applied Science Ref #: 11207733910, Lot #: 10520200; Penzberg, Germany). Cyanine-3 (Cy3 Direct FISH; PerkinElmer Life Sciences, Waltham, MA) was used to visualize labeled cells and nuclei were counterstained with DAPI (Thermo Scientific). Two images were taken per region from each hemisphere of all infused rats and the caged control for the PER, mPFC, lateral entorhinal cortex (LEC), area TE and anterior cingulate cortex (AC). This process was repeated on a second section of tissue from each rat. Two rats did not have tissue analyzed for the mPFC and AC, as the *Arc* signal was degraded. For these rats, cannula placement was confirmed with fluorescence microscopy.

Following FISH, z-stacks were taken at increments of 1 μm and the percentage of *Arc* positive cells was determined by experimenters blind to infusion condition using ImageJ software. In order to exclude nuclei that were cut off by the edges of the tissue, only those cells that were visible within the median 20% of the optical planes were included for counting. All nuclei were counted with the *Arc* channel off, so as to not bias the counter. When the total number of cells in the z-stack were identified, the *Arc* channel was turned on to classify cells as positive or negative for *Arc*. A cell was counted as *Arc* positive if the fluorescent label could be detected above threshold anywhere within or around the nucleus on at least 3 adjacent planes.

2.8. Statistical analysis

To examine the effect of bilateral inactivation of the PER and mPFC on the percent of correct responses, bilateral infusions of MUS were compared to the vehicle control condition with a repeated measures analysis of variance (ANOVA) with 3 different drug conditions of: (1) vehicle control (n = 9), (2) bilateral MUS in PER (n = 9), and (3) bilateral MUS in mPFC (n = 7). Because the primary comparisons of interest were the rats' performances following inactivation of the PER or mPFC relative to vehicle controls, a planned simple contrast was used to compare each bilateral MUS condition to the control.

In order to examine the effects of contralateral mPFC and PER inactivation on OPPA task performance, a second repeated measures ANOVA was used to test the effects of 3 different infusion conditions on behavior: (1) vehicle control (n = 9), (2) contralateral mPFC-PER inactivation (n = 9), and (3) ipsilateral mPFC-PER inactivation (n = 9). For the conditions in which there were two infusions in different brain hemispheres, the mean was determined for each rat such that sample size (n) was the number of rats for each infusion type rather than the total number of infusions. This was done as to not arbitrarily inflate statistical power. In order to quantify the effect of blocking mPFC-PER communication on behavior, the comparisons of interest were contralateral mPFC-PER inactivation relative to the vehicle control and to the ipsilateral mPFC-PER inactivation. Therefore, a planned simple contrast was used to test whether there was a statistical difference between the contralateral mPFC-PER MUS infusion relative to the vehicle control, and relative to the ipsilateral mPFC-PER MUS infusion. Table 1 summarizes the statistical tests used for the primary comparisons of infusion condition described above.

The same statistical model described above was also used to test the effect of inactivation condition on the side and object bias indices. Rats often display response biases during the acquisition of the OPPA task prior to learning the object-in-place rule (Hernandez et al., 2015; Jo & Lee, 2010a, 2010b; Lee & Byeon, 2014). Thus, indices of a side bias (left vs. right well) and object bias (e.g. "chicks" vs "frog") were calculated during initial training and for each infusion condition. Side bias was calculated as the absolute value of (total number left choices-total number right choices)/total number of trials. The object bias was calculated as the absolute value of (total number of object 1 choices-total number of object 2 choices)/total number of choices.

Finally, for two-way comparisons of the effects of hemisphere on performance, and *Arc* expression in infused versus non-infused hemispheres, significance was tested with paired-samples *T* tests. All analyses were performed with the Statistical Package for the Social Sciences v23 (IBM, Armonk, NY), and statistical significance was considered at p values less than 0.05.

3. Results

3.1. Muscimol selectively blocked activity-dependent arc expression in perirhinal and medial prefrontal cortices

To confirm the MUS infusion in the current study, the expression of the neural activity-dependent gene *Arc* was used to determine if MUS infusion blocked neuronal activity selectively in the PER and mPFC. Specifically, if MUS blocked PER/mPFC activity then the expression of *Arc* should be reduced in these brain areas compared to adjacent areas not targeted for inactivation: LEC, area TE and AC. To test this idea, 4 rats received ipsilateral infusions of MUS 30 min prior to performing the OPPA task, while the other hemisphere served as the non-infused control. These rats were tested on OPPA for 10 min and were then immediately sacrificed. In 2 of these rats, tissue was processed for the PER, LEC, area TE, mPFC, and AC. In the other 2 animals, *Arc* labeled tissue was not available for the mPFC and AC. Fig. 2 shows representative images from the hemisphere that received MUS infusion and the control hemisphere for the mPFC (Fig. 2A) and the PER (Fig. 2B). Note the reduced *Arc* signal (red[1]) in the MUS infused regions. Fig. 2C shows the mean proportion of *Arc* positive cells in the PER, mPFC, area TE, LEC, and AC for the hemisphere infused with MUS, the control hemisphere, and the caged controls. Repeated-measures ANOVA with the within subjects factor of infusion hemisphere (muscimol versus control) and the between subjects factor of brain region (targeted for muscimol versus adjacent, non-targeted area) revealed a significant main effect of brain region ($F_{[1,14]} = 8.13$, $p < 0.02$), such that the targeted regions (PER and mPFC) had fewer *Arc* positive neurons compared to the non-targeted regions. Moreover, there was a trend towards a significant interaction effect of infusion hemisphere and target region ($F_{[1,14]} = 3.20$, $p = 0.09$). Post hoc analysis indicated that the percent of *Arc* positive cells in the mPFC and PER was significantly reduced in the hemisphere that received MUS infusions relative to the non-infused hemisphere ($p < 0.04$; Tukey), which was not the case for adjacent regions not targeted for infusions ($p > 0.73$; Tukey).

The percent of *Arc* positive cells in the caged control rat was low (4.0%; SD = 3.53). For the mPFC and PER the levels of *Arc* expression after MUS infusion were not significantly different than those observed in the caged controls ($T_{[5]} = 0.51$, $p = 0.63$; one sample). In contrast, in the hemisphere that was not infused, *Arc* expression was significantly greater relative to the caged control ($T_{[5]} = 3.37$, $p < 0.02$; one sample). Moreover, in the adjacent brain regions that were not targeted for inactivation, *Arc* expression in the MUS infused hemisphere was significantly greater than the caged control ($T_{[9]} = 4.55$, $p < 0.01$; one sample). The observation that MUS blocked *Arc* expression is consistent with previous data (Kubik, Miyashita, Kubik-Zahorodna, & Guzowski, 2012). Moreover, the reduction in activity-dependent *Arc* expression observed in the mPFC and PER, but not LEC, area TE or AC, of MUS infused hemispheres indicates that neural activity in the target regions of the current experiments was selectively blocked. Although this was

[1] For interpretation of color in Fig. 2, the reader is referred to the web version of this article.

Table 1
Summary of infusion condition statistical model. The effect of infusion condition was tested with repeated measures ANOVAs and planned contrasts.

Main effect	Statistical test	Comparison	n	Statistic	p value
Bilateral infusion (3 levels: PER, mPFC, control)	Repeated measures ANOVA	Vehicle control vs bilateral MUS in PER	9	Simple contrast	$p < 0.01$
	$F[2,12] = 10.25$, $p < 0.01$	Vehicle control vs bilateral MUS in mPFC	7	Simple contrast	$p < 0.01$
Disconnection infusion (3 levels: contralateral mPFC-PER, ipsilateral mPFC-PER, control)	Repeated measures ANOVA	Contralateral mPFC-PER MUS vs Vehicle control	9	Simple contrast	$p < 0.01$
	$F[2,12] = 23.62$, $p < 0.001$	Contralateral mPFC-PER MUS vs Ipsilateral mPFC-PER MUS	9	Simple contrast	$p < 0.01$

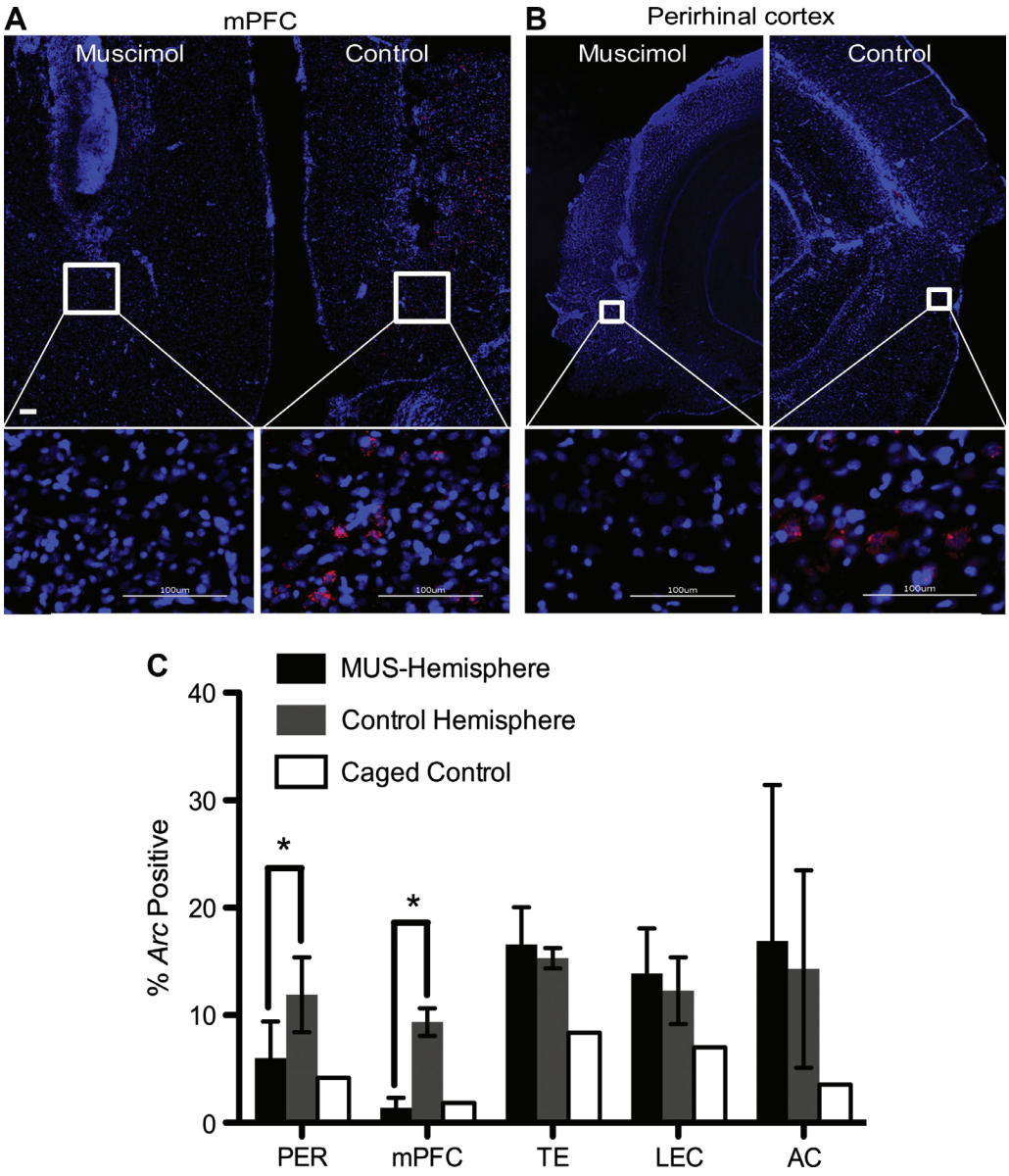

Fig. 2. *Arc* expression following muscimol (MUS) infusion. (A) A representative image of *Arc* expression in the mPFC in which the left hemisphere was inactivated with MUS and the right was intact (*top*). 40× images of the regions of interest outlined in top panel from MUS infused (left panel) and non-infused tissue (right panel) (*bottom*). (B) A representative image of *Arc* expression the PER in which the right hemisphere was infused with MUS and the left as intact (*top*). 40× images of the regions of interest outlined in top panel from non-infused (left panel) and MUS infused tissue (right panel) (*bottom*). (C) Percent of *Arc* positive cells in the perirhinal cortex (PER), medial prefrontal cortex (mPFC), area TE, lateral entorhinal cortex (LEC), and anterior cingulate cortex (AC) in the MUS infused (black) and non-infused control (grey) hemispheres relative to caged controls (white). For the PER and mPFC, there was a significantly greater percent of *Arc* positive cells in the hemisphere that was not infused with MUS ($p < 0.05$), indicating that the MUS inhibited activity-dependent gene expression in the mPFC and PER. This was not the case for the adjacent brain regions (TE, LEC and AC) that were not targeted for infusions ($p > 0.05$ for all comparisons). Error bars are ±1 Standard error of the mean (SEM).

qualitatively the case for both the PER and mPFC, it was not possible to compare *Arc* expression across hemispheres for the individual regions due to lack of statistical power from the small sample sizes.

3.2. Pre-training and initial response bias

During the initial training sessions on the OPPA task, rats exhibit a "side bias" for selecting the object over a well on a particular side,

regardless of the object or the arm of the maze (Hernandez et al., 2015; Jo & Lee, 2010a; Lee & Byeon, 2014; Lee & Kim, 2010). This bias has to be suppressed, presumably through mPFC activity projecting back to sensorimotor areas (Lee & Byeon, 2014) before OPPA task performance shows an improvement. The mean side bias and percent correct responses as a function of days before reaching criterion performance are shown in Fig. 3A and B, respectively. The rats in the current study began with a side bias and over the course of 20 days of testing, this bias decreased as indicated by a significant main effect of test day ($F_{[19,76]} = 12.80$, $p < 0.001$; repeated measures). Planned orthogonal contrasts comparing the side bias on each day to the mean of the preceding days indicated that the side bias did not significantly change across testing days until one day prior to reaching criterion performance ($p > 0.1$ for all comparisons; difference contrast). The day before criterion performance was achieved, however, the mean side bias significantly decreased from the preceding day ($p < 0.005$; difference contrast; Fig. 3A). Importantly, the significant shift away from a side bias corresponded with rats' improved performances on the OPPA task. In fact, although rats showed a significant main effect of testing day on performance ($F_{[19,76]} = 14.22$, $p < 0.001$), planned orthogonal contrasts comparing performance on each test day to the mean of the preceding test days did not detect a significant performance improvement across testing days ($p > 0.1$ for all comparisons; difference contrast) until one day prior to reaching criterion performance ($p < 0.001$; difference contrast; Fig. 3A). Together these data suggest that the rats perseverated, using a maladaptive response strategy that prevented them from making incremental progress on the task over weeks of training, and that reductions in this side bias were associated with rats reaching criterion performance. Consistent with this idea, when the response bias was plotted against percent correct for all testing days, there was a significant negative correlation over all days of testing between the response bias and percent correct on the OPPA task ($R^2_{[181]} = 0.71$, $p < 0.001$; Fig. 3C). When a correlation value was calculated separately for each rat so that an animal only contributed 1 data point, the mean correlation was also significant ($R^2_{[8]} = 0.87$, $p < 0.01$). Together, these data indicate that rats must move away from using a non-adaptive side bias in order to acquire the biconditional response of flexibly choosing the correct object associated a given maze arm.

3.3. Bilateral inactivation of the mPFC or PER impaired behavioral flexibility

Before examining the effect of disconnecting the mPFC and PER, whether these regions are independently critical for normal performance on the OPPA task was tested. Rats were bilaterally infused with MUS into the mPFC or PER during separate testing sessions. Infusions involving the left mPFC cannula were excluded for 2 of the 9 rats due to this cannula being misplaced, but the PER infusion conditions were included for these animals. Mean performance was 90.23% correct (SD = 9.10) for vehicle control infusions. Bilateral MUS infusion into the mPFC decreased the percent of correct trials to 69.64% (SD = 16.43) and bilateral PER MUS infusions resulted in 63.67% correct (SD = 15.76; Fig. 4). The overall main effect of bilateral infusion condition was statistically significant ($F_{[2,12]} = 10.25$, $p < 0.01$). Planned comparisons of performance across the different drug conditions indicated that the percent correct trials was significantly greater during the vehicle control relative to the bilateral mPFC inactivation ($p < 0.01$; simple contrast) and to the bilateral PER inactivation ($p < 0.01$; simple contrast). Importantly, the amount of time it took rats to complete the 32 trials within a test session did not significantly vary between the MUS and vehicle control conditions for either the mPFC ($T_{[8]} = 1.53$, $p = 0.16$) or PER ($T_{[8]} = 1.36$, $p = 0.21$) inactivation. This observation indicates that the MUS infusions did not cause any overt sensorimotor or motivational impairments that influenced performance.

When the effect of drug condition on the side bias and object bias indices was quantified, there was a significant main effect of infusion condition on an animal's tendency to choose one side over another (i.e., the side bias; $F_{[2,12]} = 9.99$, $p < 0.01$). Planned comparisons indicated that, relative to the vehicle control, the side bias was greater for both the bilateral mPFC MUS ($p < 0.02$; simple contrast) and PER MUS ($p < 0.01$; simple contrast) conditions (Fig. 4B). In contrast, there was no main effect of infusion condition on the object bias ($F_{[2,12]} = 2.94$, $p = 0.09$; Fig. 4C). This suggests when either the mPFC or PER is inactivated, rats regress to their initial strategy during training in which they select one side, regardless of the object or arm of the maze. Together, these results are consistent with previous studies (Jo & Lee, 2010b; Lee & Solivan, 2008) and suggest that the PER and mPFC may need to interact in order to suppress non-adaptive object selection and use the object-in-place rule for optimal performance.

3.4. mPFC-PER disconnection impaired behavioral flexibility relative to ipsilateral inactivation

To investigate whether communication between the mPFC and PER is necessary for OPPA task performance, percent correct following contralateral MUS infusions was compared to ipsilateral MUS infusions and vehicle controls. Since inter-region projections are typically more extensive within same hemisphere compared to across hemispheres (Bedwell et al., 2015), this approach blocks communication between inactivated regions while leaving one hemisphere of each brain region intact to support behavior. For the contralateral infusions, MUS or saline was infused simultaneously into the mPFC of one hemisphere and the PER of the contralateral hemisphere. Ipsilateral mPFC and PER infusions of MUS

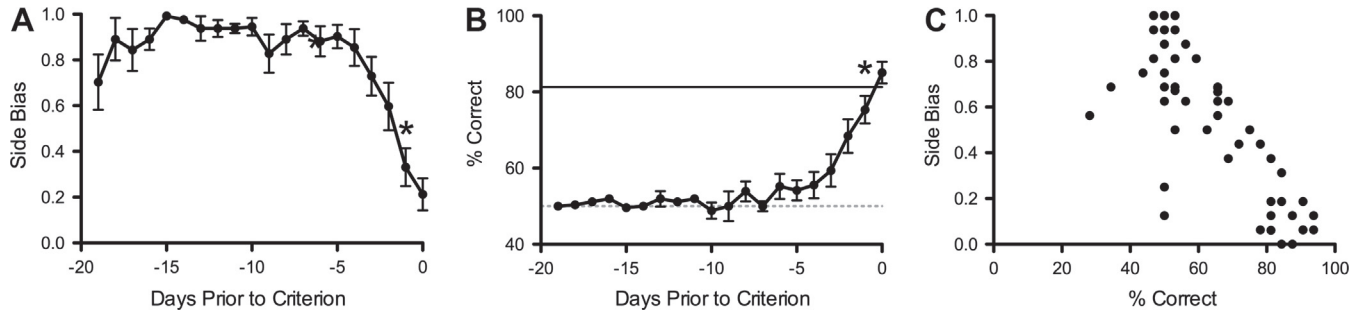

Fig. 3. Side bias during pre-training. (A) The mean side bias (Y axis) as a function of days before reaching criterion performance (X axis). During initial training, there was a response bias for a particular side. This bias did not significantly change across testing days until 1 day prior to hitting criterion performance ($^*p < 0.005$). (B) The percent correct responses (Y axis) as a function of days before reaching criterion performance (X axis). The mean percent correct did not significantly improve across testing days until one day prior to hitting criterion performance ($^*p < 0.001$). (C) There was a significant negative correlation over all days of testing between the side bias and percent correct on the OPPA task ($R^2_{[181]} = 0.71$, $p < 0.001$). Error bars are ±1 SEM.

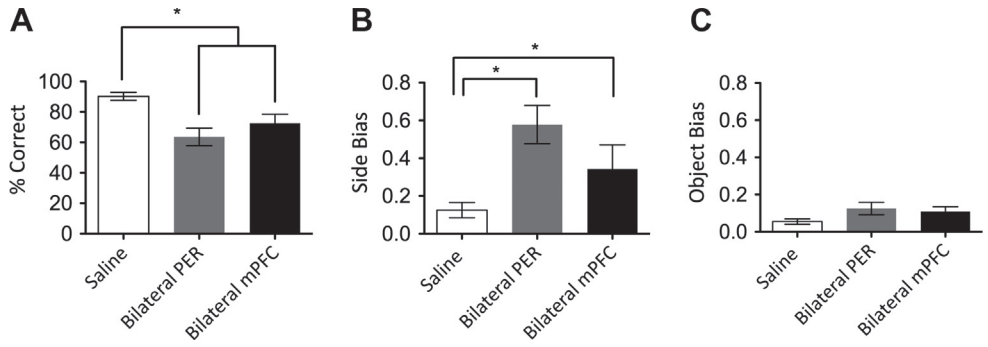

Fig. 4. Effects of bilateral mPFC or PER inactivation on OPPA task performance. (A) The Y axis shows percent correct for the bilateral MUS versus the vehicle control (saline) infusions (X axis). Bilateral mPFC and bilateral PER inactivation impaired performance relative to the vehicle control ($^{*}p < 0.01$ for both comparisons). (B) Side bias of rats' tendencies to choose one side over the other during the different infusion conditions. The side bias was significantly higher during both bilateral inactivation conditions relative to the vehicle control infusion ($^{*}p < 0.01$ for both comparisons). (C) Object bias during bilateral PER and mPFC MUS infusions and vehicle control infusions was not significantly different ($p = 0.09$). Error bars are ±1 SEM.

were used to measure the effect of unilateral inactivation when mPFC-PER communication was left intact. Fig. 5A shows the percent correct trials following the different infusion conditions. During ipsilateral MUS infusions, rats maintained 77.29% correct (SD = 16.19), which was not significantly different from criterion ($T_{[8]} = 0.24$, $p = 0.81$). In contrast, contralateral MUS infusions resulted in a reduction of correct responses (59.79%; SD = 15.76). In fact, overall there was a significant main effect of infusion condition ($F_{[2,16]} = 23.62$, $p < 0.001$). Planned comparisons with a corrected α level of $p < 0.017$ (for 3 comparisons) were used to determine if there was a significant difference between different infusion conditions. The percent correct during contralateral mPFC-PER MUS infusions was significantly different when compared to the vehicle control ($p < 0.01$; simple contrast) as well as when compared with ipsilateral mPFC-PER MUS infusions ($p < 0.01$; simple contrast). There was a trend towards an effect of ipsilateral MUS inactivation relative to vehicle infusion that did not reach statistical significance ($p = 0.04$; simple contrast). This is consistent with several studies that have shown behavioral deficits following unilateral inactivation of higher-level association cortical areas (Poe et al., 2000; Tanninen, Morrissey, & Takehara-Nishiuchi, 2013; Wilson, Langston et al., 2013; Wilson, Watanabe, Milner, & Ainge, 2013). Importantly, the amount of time it took rats to complete 32 trials within a testing session did not significantly vary between any of the infusion conditions (contralateral, ipsilateral, or vehicle control; $p > 0.13$ for all comparisons), indicating that MUS infusions did not cause sensorimotor or motivational impairments. Together these data show that blocking mPFC-PER communication impaired the ability of rats to update the selection of the correct object in the different spatial locations, compared to control conditions.

Fig. 5B and C shows the side and object biases, respectively, for the different infusion conditions. There was a main effect of MUS infusion compared to vehicle controls on side bias ($F_{[2,16]} = 19.56$, $p < 0.01$). Planned comparisons indicated that the side bias was greater for the ipsilateral ($p < 0.03$) and contralateral ($p < 0.01$) conditions relative to saline. There was no main effect of MUS infusions relative to saline controls on object bias during the task for either the ipsilateral or contralateral conditions ($F_{[2,16]} = 0.464$, $p = 0.64$). Importantly, these data indicate that, similar to the bilateral mPFC and PER infusions, disconnecting these regions also resulted in an inability to flexibly update response selection, with rats regressing back to the side bias that is observed early in training.

3.5. Side of infusion and repeated infusions did not alter behavioral performance

In order to examine whether or not different hemispheres were similarly affected by inactivation, the lateralization of infusions was compared. This analysis showed there was no significant effect of left versus right hemisphere ($T_{[6]} = 0.04$, $p = 0.97$; Fig. 6A). The two possible disconnection positions, left mPFC and contralateral PER and right mPFC and contralateral PER, were also found to not differ significantly ($T_{[6]} = 0.14$, $p = 0.89$; Fig. 6B).

The potential effect of repeating the infusions over days was also assessed. Multiple infusions did not adversely affect behavior over the course of testing. Specifically, performance on the OPPA task between infusion days remained above criterion with an average percent correct of 91.95% (SD = 0.10). Moreover, performance on the first non-infusion day was not significantly different than performance on the last non-infusion day ($T_{[7]} = 0.06$, $p = 0.96$),

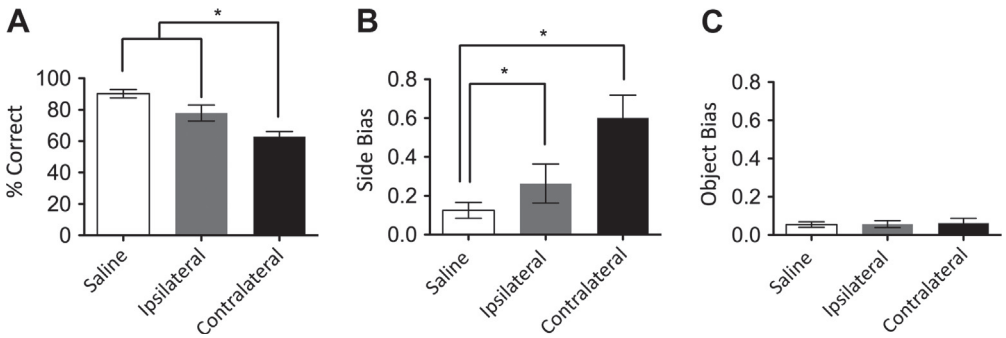

Fig. 5. Effects of contralateral mPFC-PER MUS infusions on OPPA task performance. (A) Percent correct (Y axis) for the disconnection versus ipsilateral and vehicle control infusion conditions. Contralateral infusions that disconnected the mPFC and PER impaired performance when compared to vehicle control or to ipsilateral inactivation ($p < 0.01$ for both comparisons). (B) The side bias during ipsilateral and contralateral MUS infusions was significantly greater compared to contralateral vehicle control infusions ($p < 0.05$ for both comparisons). (C) The object bias (Y axis) was not significantly different across infusion conditions (X axis; $p = 0.64$). Error bars are ±1 SEM.

demonstrating that rats were not experiencing adverse effects of multiple infusion conditions. Additionally, there was not a significant difference between vehicle infusion and non-infusion days ($T_{[7]} = 0.64$, $p = 0.54$).

3.6. Contralateral inactivation did not impair performance on control conditions

Object-only and side-only control tasks were used to determine if communication between the mPFC and PER is needed for the individual elements of the OPPA task, namely the ability to discriminate between rewarded sides or objects, which does not require the animal to update their responses across trials and minimizes the working memory component across trials. There was no significant effect of contralateral MUS infusion on performance during the object-only ($T_{[6]} = 1.54$, $p = 0.18$) or side-only ($T_{[5]} = 0.35$, $p = 0.74$) control tasks when compared to the previous day of testing with no infusion (Fig. 7). Importantly, these data suggest that the behavioral deficit resulting from the mPFC-PER disconnection was selective to a behavior that required the integration of object and place information in order to facilitate rule shifting between different target objects.

4. Discussion

The current study examined the extent to which an animal's ability to update the selection of a rewarded object when the correct choice is contingent on spatial location requires communication between medial prefrontal (mPFC) and perirhinal cortices (PER). Blocking neural activity with muscimol (MUS) infusions into either region bilaterally, resulted in significant impairments. This finding confirms previous reports that both regions are necessary for object-place paired association (OPPA) task performance (Jo & Lee, 2010a, 2010b; Lee & Solivan, 2008). The novel insight from the current data is that inactivation of one mPFC hemisphere and the contralateral PER resulted in a decline in OPPA task performance when compared to ipsilateral mPFC-PER inactivations and a regression back to the side bias that is observed early in training. This observation supports the conclusion that mPFC-PER communication is required for rule switching and retrieval of the appropriate biconditional response based on the current spatial location. As rats are able to use both intra- and extra-maze cues to aid response selection, these data are also consistent with previous work showing that communication across the mPRC and PER is necessary for an animal's ability to use spatial or contextual information to guide behavior (Barker et al., 2007), even when the hippocampus remains intact. Conversely, animals' performance on object-only and place-only discrimination tasks, which do not require the association of an object with a location or behavioral flexibility across trials, remained normal after mPFC-PER disconnection. This indicates that mPFC-PER communication is not necessary when the correct response only depends on either stimulus or spatial information and does not vary across trials.

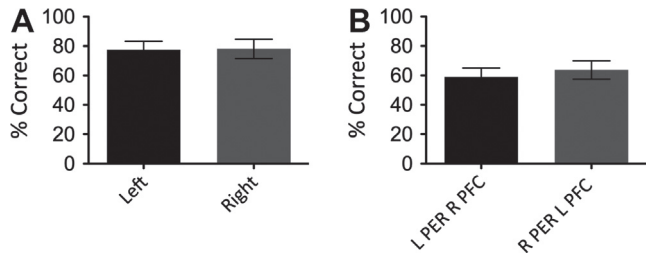

Fig. 6. Contralateral and ipsilateral infusion conditions did not show lateralization effects. (A) The Y axis shows percent correct on the OPPA task across the different hemispheres inactivated ipsilaterally (X axis). Left versus right hemisphere ipsilateral inactivation were not significantly different from each other ($p = 0.97$). (B) Percent correct (Y axis) on the OPPA task during left hemisphere mPFC/right hemisphere PER inactivation versus right hemisphere mPFC/left hemisphere PER inactivation (X axis). There was not a significant lateralization effect of infusion side between the disconnection conditions ($p = 0.87$). Error bars are ±1 SEM.

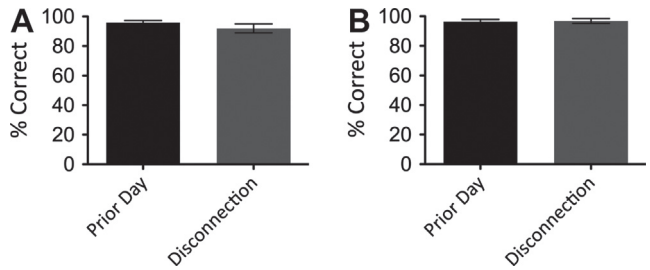

Fig. 7. Contralateral MUS infusions did not affect performance on side only or object only control tasks. Percent correct during an object-only control task (A) and a side-only control task (B) was not significantly different between the contralateral MUS inactivation compared to the previous non-infused day ($p > 0.18$ for both comparisons). Error bars are ±1 SEM.

Medial PFC and PER inactivation was verified by visualizing expression of the activity-dependent immediate-early gene *Arc* in rats that were ipsilaterally infused with MUS 30 min prior to testing on the OPPA task. Similar to previous reports (Kubik et al., 2012), blockade of *Arc* expression only occurred in the MUS infused hemisphere, as shown by the presence of *Arc* predominantly in the non-infused hemisphere. Moreover, *Arc* expression was not significantly blocked in brain regions adjacent to the MUS infusion site. Interestingly, in the current experiment, the proportion of *Arc* positive cells observed following OPPA behavior in the non-infused PER hemisphere was only 11%. A previous study reported that over 20% of cells were activated following object exploration (Burke, Hartzell et al., 2012). There are several possibilities for this apparent discrepancy. In the previous experiment, rats were presented with 5 objects, as opposed to 2 used in the current study. These data suggest that encountering a greater number of stimuli leads to greater PER activity. An alternative, but not mutually exclusive, possibility is that ipsilateral inactivation led to lower neuronal activity levels overall, which is consistent with the modest deficit in performance following ipsilateral inactivation. These possibilities will need to be explored with future experiments.

The mPFC supports OPPA task performance through several possible and potentially related mechanisms. First, the role of the mPFC may be to govern interactions among medial temporal lobe structures. The PER communicates heavily with the entorhinal cortex, both of which send projections to the hippocampus (Burwell & Amaral, 1998b). During distinct stages of learning, this interaction is facilitated by the mPFC (Paz et al., 2007). It could be that during the OPPA task, the mPFC updates representations in the rhinal cortices, based on reward prediction, to gate the flow of information between the hippocampus and neocortex. Consistent with this hypothesis is the observation that disconnection lesions of the PFC and inferotemporal cortex in monkeys impair delayed nonmatching-to-sample performance (Browning, Baxter, & Gaffan, 2013) and object-in-place scene memory (Wilson, Gaffan, Mitchell, & Baxter, 2007). Additional evidence for a unified mPFC-PER network that supports performance on the OPPA task is that the theta rhythm in the mPFC and hippocampus becomes more synchronized after acquisition of the OPPA task rule (Kim, Delcasso, & Lee, 2011). Because there are limited direct projections from mPFC to dorsal hippocampus, this synchrony may require that information flows through the rhinal cortices, thus making the PER an integral part of this circuit. The PER, however, is not the only structure reciprocally connected with both the hippocam-

pus and prefrontal cortex. In fact, the nucleus reuniens of the ventral midline thalamus in also anatomically poised to functionally link the prefrontal cortex to the hippocampus (McKenna & Vertes, 2004; Vertes, 2002, 2006, 2015; Vertes, Hoover, Do Valle, Sherman, & Rodriguez, 2006; Vertes, Linley, & Hoover, 2015). Moreover, inactivation of the nucleus reuniens leads to deficits in strategy switching (Cholvin et al., 2013), suggesting that this brain area may be critical for flexibility by modulating prefrontal-hippocampal interactions. (Cassel et al., 2013). The fact that either PER or nucleus reuniens lesions produce behavioral flexibility deficits indicates that, while both regions are necessary for prefrontal-hippocampal interactions, neither structure alone is sufficient.

The mPFC has also been shown to be involved in the flexible control of behavioral responses (Beas et al., 2013; Chadick, Zanto, & Gazzaley, 2014; Ridderinkhof, Ullsperger, Crone, & Nieuwenhuis, 2004), as well as working memory (Sloan, Good, & Dunnett, 2006), both of which may be involved in OPPA task performance. Previous studies using MUS to inactivate the mPFC have reported deficits in rats' abilities to inhibit incorrect responses (Izaki, Maruki, Hori, & Nomura, 2001). Additionally, blocking glutamatergic transmission in the mPFC enhances impulsivity and leads to compulsive perseveration in rats (Carli, Baviera, Invernizzi, & Balducci, 2006). Rats show a significant side bias during the acquisition of the OPPA task and inhibiting this perseveration is essential to being able to learn the object-in-place rule (Hernandez et al., 2015; Lee & Byeon, 2014). Although rats may not stop displaying a side bias, in the days after acquisition of the rule, they may show inhibitory behavior towards the object on the preferred side. In line with this idea, mPFC neurons show selective firing for trials requiring this inhibition before object selection (Lee & Byeon, 2014). Thus, the importance of communication between the mPFC and PER may be to ensure that actions with unwanted outcomes are inhibited, enabling subjects to make the choice with a more desirable outcome. Additionally, the OPPA task requires some active maintenance of previously visited locations in order to correctly alternate. In fact, because the order of left versus right arm trials was not randomized in the current study, rats could have successfully performed the task by alternating between object selection regardless of arm location. Future experiments will randomize left versus right arm trials and increase the inter-trial interval to determine the relative contribution of working memory versus flexibility in OPPA performance.

A final possibility is that the mPFC is necessary for the expression of memory at remote time points (Takehara-Nishiuchi, Nakao, Kawahara, Matsuki, & Kirino, 2006). It is theorized that the mPFC initially relies on the hippocampus to form memories, but later may independently use previous experience to guide adaptive responses (Takehara-Nishiuchi & McNaughton, 2008). In line with this idea, hippocampal-dependent memory consolidation causes changes in the synaptic density in the mPFC that support the retrieval of remote memories (Insel & Takehara-Nishiuchi, 2013; Restivo, Vetere, Bontempi, & Ammassari-Teule, 2009). Thus, disconnecting the mPFC and PER could prevent the PER from having access to consolidated object-place associations. If the mPFC selectively supports remote memories that are dependent on the hippocampus shortly after acquisition, it is possible that infusing MUS into the mPFC during an earlier time point in training, or before acquisition, would not result in a deficit. This idea would predict that rats over-trained for a month on the OPPA task would be able to complete the task without the hippocampus. While previous bilateral inactivation of the hippocampus during the OPPA task has shown a performance deficit (Jo & Lee, 2010a; Lee & Solivan, 2008), the time frame of hippocampal involvement has not been explicitly examined.

One critical component of OPPA task performance is the ability to identify the different objects. The dense connectivity of the PER with different sensory cortical areas enables it to link individual features of an object in order to identify it as a single entity (Murray & Bussey, 1999; Suzuki & Amaral, 1990, 1994). In fact, lesions to the PER cause impairments in object recognition, but not in spatial memory (Bussey, Muir, & Aggleton, 1999), and lesion data indicate the PER contributes to both object perception and memory (Buckley & Gaffan, 1998b; Murray & Bussey, 1999). Furthermore, a portion of PER neurons are selectively activated by different objects (Burke, Maurer et al., 2012; Deshmukh, Johnson, & Knierim, in press), even when the environment in which they are presented is changed (Burke, Hartzell et al., 2012). Although it is clear that the PER encodes object information, it is unlikely its contribution to the OPPA task is limited to object representations. Synaptic weight changes within the PER support associations between object pairs (Fujimichi et al., 2010; Higuchi & Miyashita, 1996; Murray & Richmond, 2001), and it is conceivable that this could extend across modalities. In fact, the PER is critical for linking visual to tactile information (Buckley & Gaffan, 1998a; Goulet & Murray, 2001; Jacklin, Cloke, Potvin, Garrett, & Winters, 2016; Parker & Gaffan, 1998; Reid, Jacklin, & Winters, 2014). A similar situation may occur when an object is associated with a place. While PER cells do not show spatial selectivity (Burke, Maurer et al., 2012; Burwell, Shapiro, O'Malley, & Eichenbaum, 1998), plasticity within PER may bias the retrieval of one object representation over another when the animal is in a specific location and this interaction could be modulated by projections from the mPFC (Paz et al., 2007). A critical issue not addressed by the current study is the necessity of mPFC-PER connectivity to acquire new object-place associations. Although not explicitly tested here, available data indicating that communication between these brain regions is necessary for an animal's ability to detect novel object-place associations (Barker & Warburton, 2008; Barker et al., 2007) suggest that this component of task performance would also be impaired by a mPFC-PER disconnection.

The mPFC-PER disconnection would disrupt any one of the aforementioned aspects of mPFC influence on the medial temporal lobe circuitry. Alternatively, it is possible that the deficit resulting from blocking communication across these regions is due to the inability to deal with proactive interference based on the rule used in the previous trial. This scenario, however, would predict that rats would default back to the correct choice on the previous trial and show an object bias. This behavioral outcome was not observed following the mPFC-PER disconnection, rather rats regressed to the side bias seen during pre-training.

It is likely that the role of the mPFC on the network is diverse and may encompass several aspects of learning and memory in regards to both behavioral flexibility and object-place associations. The observation that a contralateral deficit impaired performance on the OPPA task, which requires flexibility in selecting the correct object based on spatial location, but not the control tasks, is interesting in the context of aging and disease. The PER (Burke, Ryan, & Barnes, 2012; Khan et al., 2014; Reagh et al., 2016; Ryan et al., 2012) and mPFC (Griffith et al., 2014; Morrison & Baxter, 2012) are among the most vulnerable brain regions to age-related dysfunction. Even when these areas are compromised, however, aged animals are still able to perform object discriminations and differentiate the left from right side (Beas et al., 2013; Burke et al., 2011; Hernandez et al., 2015). Therefore, behaviors that require large-scale integration across different neural networks may be particularly sensitive to aging. Because individual brain regions may not age in the same manner, it is vital that potential treatments for cognitive aging and dementia not only alleviate dysfunction in an individual area, but also maintain the balance in global network interactions.

Funding

This work was supported by the Eveyln F. McKnight Brain Research Foundation, The National Institute on Aging at the National Institutes of Health (Claude D. Pepper Older Americans Independence Center Scholar Award Grant No. P30 AG028740 subaward to SNB, and Grant Nos. R01 AG049711 to SNB, and R01 AG029421 to JLB, R03 1R03AG049411 to APM and SNB), University of Florida Howard Hughes Medical Institute Science for Life, and the University of Florida Research Opportunity Seed Fund.

Acknowledgements

We would like to thank Michael G. Burke for maze construction, and Sofia Beas, Ph.D., Shannon Wall, Caitlin Orsini Ph.D., and Barry Setlow Ph.D. for help completing the experiments.

References

Agster, K. L., & Burwell, R. D. (2009). Cortical efferents of the perirhinal, postrhinal, and entorhinal cortices of the rat. *Hippocampus, 19*, 1159–1186.

Barense, M. D., Fox, M. T., & Baxter, M. G. (2002). Aged rats are impaired on an attentional set-shifting task sensitive to medial frontal cortex damage in young rats. *Learning & Memory, 9*, 191–201.

Barense, M. D., Gaffan, D., & Graham, K. S. (2007). The human medial temporal lobe processes online representations of complex objects. *Neuropsychologia, 45*, 2963–2974.

Barense, M. D., Ngo, J. K., Hung, L. H., & Peterson, M. A. (2012). Interactions of memory and perception in amnesia: The figure-ground perspective. *Cerebral Cortex, 22*, 2680–2691.

Barker, G. R., Bird, F., Alexander, V., & Warburton, E. C. (2007). Recognition memory for objects, place, and temporal order: A disconnection analysis of the role of the medial prefrontal cortex and perirhinal cortex. *Journal of Neuroscience, 27*, 2948–2957.

Barker, G. R., & Warburton, E. C. (2008). NMDA receptor plasticity in the perirhinal and prefrontal cortices is crucial for the acquisition of long-term object-in-place associative memory. *Journal of Neuroscience, 28*, 2837–2844.

Barker, G. R., & Warburton, E. C. (2015). Object-in-place associative recognition memory depends on glutamate receptor neurotransmission within two defined hippocampal-cortical circuits: A critical role for AMPA and NMDA receptors in the hippocampus, perirhinal, and prefrontal cortices. *Cerebral Cortex, 25*, 472–481.

Bartko, S. J., Winters, B. D., Cowell, R. A., Saksida, L. M., & Bussey, T. J. (2007a). Perceptual functions of perirhinal cortex in rats: Zero-delay object recognition and simultaneous oddity discriminations. *Journal of Neuroscience, 27*, 2548–2559.

Bartko, S. J., Winters, B. D., Cowell, R. A., Saksida, L. M., & Bussey, T. J. (2007b). Perirhinal cortex resolves feature ambiguity in configural object recognition and perceptual oddity tasks. *Learning & Memory, 14*, 821–832.

Beas, B. S., McQuail, J. A., Bañuelos, C., Setlow, B., & Bizon, J. L. (2016). Prefrontal cortical GABAergic signaling and impaired behavioral flexibility in aged F344 rats. *Neuroscience* (in press).

Beas, B. S., Setlow, B., & Bizon, J. L. (2013). Distinct manifestations of executive dysfunction in aged rats. *Neurobiology of Aging, 34*, 2164–2174.

Beckstead, R. M. (1979). An autoradiographic examination of corticocortical and subcortical projections of the mediodorsal-projection (prefrontal) cortex in the rat. *Journal of Comparative Neurology, 184*, 43–62.

Bedwell, S. A., Billett, E. E., Crofts, J. J., MacDonald, D. M., & Tinsley, C. J. (2015). The topology of connections between rat prefrontal and temporal cortices. *Frontiers in Systems Neuroscience, 9*, 80.

Birrell, J. M., & Brown, V. J. (2000). Medial frontal cortex mediates perceptual attentional set shifting in the rat. *Journal of Neuroscience, 20*, 4320–4324.

Bissonette, G. B., & Powell, E. M. (2012). Reversal learning and attentional set-shifting in mice. *Neuropharmacology, 62*, 1168–1174.

Browning, P. G., Baxter, M. G., & Gaffan, D. (2013). Prefrontal-temporal disconnection impairs recognition memory but not familiarity discrimination. *The Journal of Neuroscience, 33*, 9667–9674.

Buckley, M. J., & Gaffan, D. (1998a). Learning and transfer of object-reward associations and the role of the perirhinal cortex. *Behavioral Neuroscience, 112*, 15–23.

Buckley, M. J., & Gaffan, D. (1998b). Perirhinal cortex ablation impairs visual object identification. *Journal of Neuroscience, 18*, 2268–2275.

Buckner, R. L. (2004). Memory and executive function in aging and AD: Multiple factors that cause decline and reserve factors that compensate. *Neuron, 44*, 195–208.

Buffalo, E. A., Ramus, S. J., Clark, R. E., Teng, E., Squire, L. R., & Zola, S. M. (1999). Dissociation between the effects of damage to perirhinal cortex and area TE. *Learning & Memory, 6*, 572–599.

Burgos-Robles, A., Vidal-Gonzalez, I., Santini, E., & Quirk, G. J. (2007). Consolidation of fear extinction requires NMDA receptor-dependent bursting in the ventromedial prefrontal cortex. *Neuron, 53*, 871–880.

Burke, S. N., Hartzell, A. L., Lister, J. P., Hoang, L. T., & Barnes, C. A. (2012). Layer V perirhinal cortical ensemble activity during object exploration: A comparison between young and aged rats. *Hippocampus, 22*, 2080–2093.

Burke, S. N., Maurer, A. P., Hartzell, A. L., Nematollahi, S., Uprety, A., Wallace, J. L., & Barnes, C. A. (2012). Representation of three-dimensional objects by the rat perirhinal cortex. *Hippocampus, 22*, 2032–2044.

Burke, S. N., Ryan, L., & Barnes, C. A. (2012). Characterizing cognitive aging of recognition memory and related processes in animal models and in humans. *Frontiers in Aging Neuroscience, 22*(10), 2080–2093.

Burke, S. N., Wallace, J. L., Hartzell, A. L., Nematollahi, S., Plange, K., & Barnes, C. A. (2011). Age-associated deficits in pattern separation functions of the perirhinal cortex: A cross-species consensus. *Behavioral Neuroscience, 125*, 836–847.

Burwell, R. D., & Amaral, D. G. (1998a). Cortical afferents of the perirhinal, postrhinal, and entorhinal cortices of the rat. *The Journal of Comparative Neurology, 398*, 179–205.

Burwell, R. D., & Amaral, D. G. (1998b). Perirhinal and postrhinal cortices of the rat: Interconnectivity and connections with the entorhinal cortex. *The Journal of Comparative Neurology, 391*, 293–321.

Burwell, R. D., Shapiro, M. L., O'Malley, M. T., & Eichenbaum, H. (1998). Positional firing properties of perirhinal cortex neurons. *NeuroReport, 9*, 3013–3018.

Bussey, T. J., Muir, J. L., & Aggleton, J. P. (1999). Functionally dissociating aspects of event memory: The effects of combined perirhinal and postrhinal cortex lesions on object and place memory in the rat. *Journal of Neuroscience, 19*, 495–502.

Carli, M., Baviera, M., Invernizzi, R. W., & Balducci, C. (2006). Dissociable contribution of 5-HT1A and 5-HT2A receptors in the medial prefrontal cortex to different aspects of executive control such as impulsivity and compulsive perseveration in rats. *Neuropsychopharmacology, 31*, 757–767.

Cassel, J. C., Pereira de Vasconcelos, A., Loureiro, M., Cholvin, T., Dalrymple-Alford, J. C., & Vertes, R. P. (2013). The reuniens and rhomboid nuclei: Neuroanatomy, electrophysiological characteristics and behavioral implications. *Progress in Neurobiology, 111*, 34–52.

Chadick, J. Z., Zanto, T. P., & Gazzaley, A. (2014). Structural and functional differences in medial prefrontal cortex underlie distractibility and suppression deficits in ageing. *Nature Communications, 5*, 4223.

Cholvin, T., Loureiro, M., Cassel, R., Cosquer, B., Geiger, K., De Sa Nogueira, D., ... Cassel, J. C. (2013). The ventral midline thalamus contributes to strategy shifting in a memory task requiring both prefrontal cortical and hippocampal functions. *Journal of Neuroscience, 33*, 8772–8783.

Clapp, W. C., Rubens, M. T., Sabharwal, J., & Gazzaley, A. (2011). Deficit in switching between functional brain networks underlies the impact of multitasking on working memory in older adults. *Proceedings of the National Academy of Sciences, 108*, 7212–7217.

Cunha, P. J., Gonçalves, P. D., Ometto, M., Dos Santos, B., Nicastri, S., Busatto, G. F., & de Andrade, A. G. (2013). Executive cognitive dysfunction and ADHD in cocaine dependence: Searching for a common cognitive endophenotype for addictive disorders. *Frontiers in Psychiatry, 4*, 126.

de Curtis, M., & Pare, D. (2004). The rhinal cortices: A wall of inhibition between the neocortex and the hippocampus. *Progress in Neurobiology, 74*, 101–110.

Delatour, B., & Witter, M. P. (2002). Projections from the parahippocampal region to the prefrontal cortex in the rat: Evidence of multiple pathways. *European Journal of Neuroscience, 15*, 1400–1407.

Demakis, G. J. (2003). A meta-analytic review of the sensitivity of the Wisconsin Card Sorting Test to frontal and lateralized frontal brain damage. *Neuropsychology, 17*, 255–264.

Deshmukh, S. S., Johnson, J. L., & Knierim, J. J. (2012). Perirhinal Cortex Represents Nonspatial, But Not Spatial, Information in Rats Foraging in the presence of objects: Comparison with lateral entorhinal cortex. *Hippocampus* (in press).

Dias, R., Robbins, T. W., & Roberts, A. C. (1996a). Dissociation in prefrontal cortex of affective and attentional shifts. *Nature, 380*, 69–72.

Dias, R., Robbins, T. W., & Roberts, A. C. (1996b). Primate analogue of the Wisconsin Card Sorting Test: Effects of excitotoxic lesions of the prefrontal cortex in the marmoset. *Behavioral Neuroscience, 110*, 872–886.

Enomoto, T., Tse, M. T., & Floresco, S. B. (2011). Reducing prefrontal gamma-aminobutyric acid activity induces cognitive, behavioral, and dopaminergic abnormalities that resemble schizophrenia. *Biological Psychiatry, 69*, 432–441.

Floresco, S. B., Block, A. E., & Tse, M. T. (2008). Inactivation of the medial prefrontal cortex of the rat impairs strategy set-shifting, but not reversal learning, using a novel, automated procedure. *Behavioural Brain Research, 190*, 85–96.

Fujimichi, R., Naya, Y., Koyano, K. W., Takeda, M., Takeuchi, D., & Miyashita, Y. (2010). Unitized representation of paired objects in area 35 of the macaque perirhinal cortex. *European Journal of Neuroscience, 32*, 659–667.

Goulet, S., & Murray, E. A. (2001). Neural substrates of crossmodal association memory in monkeys: The amygdala versus the anterior rhinal cortex. *Behavioral Neuroscience, 115*, 271–284.

Griffith, W. H., Dubois, D. W., Fincher, A., Peebles, K. A., Bizon, J. L., & Murchison, D. (2014). Characterization of age-related changes in synaptic transmission onto F344 rat basal forebrain cholinergic neurons using a reduced synaptic preparation. *Journal of Neurophysiology, 111*, 273–286.

Guzowski, J. F., McNaughton, B. L., Barnes, C. A., & Worley, P. F. (1999). Environment-specific expression of the immediate-early gene Arc in hippocampal neuronal ensembles. *Nature Neuroscience, 2*(12), 1120–1124.

Hernandez, A. R., Maurer, A. P., Reasor, J. E., Turner, S. M., Barthle, S. E., Johnson, S. A., & Burke, S. N. (2015). Age-related impairments in object-place associations are not due to hippocampal dysfunction. *Behavioral Neuroscience, 129*, 599–610.
Higuchi, S., & Miyashita, Y. (1996). Formation of mnemonic neuronal responses to visual paired associates in inferotemporal cortex is impaired by perirhinal and entorhinal lesions. *Proceedings of the National Academy of Sciences, 93*, 739–743.
Insel, N., & Takehara-Nishiuchi, K. (2013). The cortical structure of consolidated memory: A hypothesis on the role of the cingulate-entorhinal cortical connection. *Neurobiology of Learning and Memory, 106*, 343–350.
Izaki, Y., Maruki, K., Hori, K., & Nomura, M. (2001). Effects of rat medial prefrontal cortex temporal inactivation on a delayed alternation task. *Neuroscience Letters, 315*, 129–132.
Jacklin, D. L., Cloke, J. M., Potvin, A., Garrett, I., & Winters, B. D. (2016). The dynamic multisensory engram: Neural circuitry underlying crossmodal object recognition in rats changes with the nature of object experience. *Journal of Neuroscience, 36*, 1273–1289.
Jo, Y. S., & Lee, I. (2010a). Disconnection of the hippocampal-perirhinal cortical circuits severely disrupts object-place paired associative memory. *Journal of Neuroscience, 30*, 9850–9858.
Jo, Y. S., & Lee, I. (2010b). Perirhinal cortex is necessary for acquiring, but not for retrieving object-place paired association. *Learning & Memory, 17*, 97–103.
Kaczorowski, C. C., Davis, S. J., & Moyer, J. R. (2012). Aging redistributes medial prefrontal neuronal excitability and impedes extinction of trace fear conditioning. *Neurobiology of Aging, 33*, 1744–1757.
Khan, U. A., Liu, L., Provenzano, F. A., Berman, D. E., Profaci, C. P., Sloan, R., ... Small, S. A. (2014). Molecular drivers and cortical spread of lateral entorhinal cortex dysfunction in preclinical Alzheimer's disease. *Nature Neuroscience, 17*, 304–311.
Kim, J., Delcasso, S., & Lee, I. (2011). Neural correlates of object-in-place learning in hippocampus and prefrontal cortex. *Journal of Neuroscience, 31*, 16991–17006.
Kubik, S., Miyashita, T., Kubik-Zahorodna, A., & Guzowski, J. F. (2012). Loss of activity-dependent Arc gene expression in the retrosplenial cortex after hippocampal inactivation: Interaction in a higher-order memory circuit. *Neurobiology of Learning and Memory, 97*, 124–131.
Lavoie, K., & Everett, J. (2001). Schizophrenia and performance on the Wisconsin Card Sorting Test (WCST): Deficits and rehabilitation. *Encephale, 27*, 444–449.
Lee, I., & Byeon, J. S. (2014). Learning-dependent changes in the neuronal correlates of response inhibition in the prefrontal cortex and hippocampus. *Experimental Neurobiology, 23*, 178–189.
Lee, I., & Kim, J. (2010). The shift from a response strategy to object-in-place strategy during learning is accompanied by a matching shift in neural firing correlates in the hippocampus. *Learning & Memory, 17*, 381–393.
Lee, I., & Solivan, F. (2008). The roles of the medial prefrontal cortex and hippocampus in a spatial paired-association task. *Learning & Memory, 15*, 357–367.
Logue, S. F., & Gould, T. J. (2014). The neural and genetic basis of executive function: Attention, cognitive flexibility, and response inhibition. *Pharmacology, Biochemistry and Behavior, 123*, 45–54.
Malá, H., Andersen, L. G., Christensen, R. F., Felbinger, A., Hagstrøm, J., Meder, D., ... Mogensen, J. (2015). Prefrontal cortex and hippocampus in behavioural flexibility and posttraumatic functional recovery: Reversal learning and set-shifting in rats. *Brain Research Bulletin, 116*, 34–44.
McIntyre, D. C., Kelly, M. E., & Staines, W. A. (1996). Efferent projections of the anterior perirhinal cortex in the rat. *Journal of Comparative Neurology, 369*, 302–318.
McKenna, J. T., & Vertes, R. P. (2004). Afferent projections to nucleus reuniens of the thalamus. *Journal of Comparative Neurology, 480*, 115–142.
Milad, M. R., & Quirk, G. J. (2002). Neurons in medial prefrontal cortex signal memory for fear extinction. *Nature, 420*, 70–74.
Moore, T. L., Killiany, R. J., Herndon, J. G., Rosene, D. L., & Moss, M. B. (2003). Impairment in abstraction and set shifting in aged rhesus monkeys. *Neurobiology of Aging, 24*, 125–134.
Moore, T. L., Schettler, S. P., Killiany, R. J., Rosene, D. L., & Moss, M. B. (2009). Effects on executive function following damage to the prefrontal cortex in the rhesus monkey (*Macaca mulatta*). *Behavioral Neuroscience, 123*, 231–241.
Morrison, J. H., & Baxter, M. G. (2012). The ageing cortical synapse: Hallmarks and implications for cognitive decline. *Nature Reviews Neuroscience, 13*, 240–250.
Murray, E. A., & Bussey, T. J. (1999). Perceptual-mnemonic functions of the perirhinal cortex. *Trends in Cognitive Sciences, 3*, 142–151.
Murray, E. A., & Richmond, B. J. (2001). Role of perirhinal cortex in object perception, memory, and associations. *Current Opinion in Neurobiology, 11*, 188–193.
Naber, P. A., Witter, M. P., & Lopez da Silva, F. H. (1999). Perirhinal cortex input to the hippocampus in the rat: evidence for parallel pathways, both direct and indirect. A combined physiological and anatomical study. *European Journal of Neuroscience, 11*, 4119–4133.
Owen, A. M., Roberts, A. C., Polkey, C. E., Sahakian, B. J., & Robbins, T. W. (1991). Extra-dimensional versus intra-dimensional set shifting performance following frontal lobe excisions, temporal lobe excisions or amygdalo-hippocampectomy in man. *Neuropsychologia, 29*, 993–1006.
Parker, A., & Gaffan, D. (1998). Interaction of frontal and perirhinal cortices in visual object recognition memory in monkeys. *European Journal of Neuroscience, 10*, 3044–3057.
Paz, R., Bauer, E. P., & Pare, D. (2007). Learning-related facilitation of rhinal interactions by medial prefrontal inputs. *Journal of Neuroscience, 27*, 6542–6551.
Poe, G. R., Teed, R. G., Insel, N., White, R., McNaughton, B. L., & Barnes, C. A. (2000). Partial hippocampal inactivation: Effects on spatial memory performance in aged and young rats. *Behavioral Neuroscience, 114*, 940–949.
Quirk, G. J., & Mueller, D. (2008). Neural mechanisms of extinction learning and retrieval. *Neuropsychopharmacology, 33*, 56–72.
Reagh, Z. M., Ho, H. D., Leal, S. L., Noche, J. A., Chun, A., Murray, E. A., & Yassa, M. A. (2016). Greater loss of object than spatial mnemonic discrimination in aged adults. *Hippocampus, 26*(4), 417–422.
Reid, J. M., Jacklin, D. L., & Winters, B. D. (2014). Delineating prefrontal cortex region contributions to crossmodal object recognition in Rats. *Cerebral Cortex, 24*, 2108–2119.
Restivo, L., Vetere, G., Bontempi, B., & Ammassari-Teule, M. (2009). The formation of recent and remote memory is associated with time-dependent formation of dendritic spines in the hippocampus and anterior cingulate cortex. *Journal of Neuroscience, 29*, 8206–8214.
Ridderinkhof, K. R., Ullsperger, M., Crone, E. A., & Nieuwenhuis, S. (2004). The role of the medial frontal cortex in cognitive control. *Science, 306*, 443–447.
Ryan, L., Cardoza, J. A., Barense, M. D., Kawa, K. H., Wallentin-Flores, J., Arnold, W. T., & Alexander, G. E. (2012). Age-related impairment in a complex object discrimination task that engages perirhinal cortex. *Hippocampus, 22*, 1978–1989.
Sesack, S. R., Deutch, A. Y., Roth, R. H., & Bunney, B. S. (1989). Topographical organization of the efferent projections of the medial prefrontal cortex in the rat: An anterograde tract-tracing study with Phaseolus vulgaris leucoagglutinin. *Journal of Comparative Neurology, 290*, 213–242.
Sloan, H. L., Good, M., & Dunnett, S. B. (2006). Double dissociation between hippocampal and prefrontal lesions on an operant delayed matching task and a water maze reference memory task. *Behavioural Brain Research, 171*, 116–126.
Suzuki, W. A., & Amaral, D. G. (1990). Cortical inputs to the CA1 field of the monkey hippocampus originate from the perirhinal and parahippocampal cortex but not from area TE. *Neuroscience Letters, 115*, 43–48.
Suzuki, W. A., & Amaral, D. G. (1994). Perirhinal and parahippocampal cortices of the macaque monkey: cortical afferents. *Journal of Comparative Neurology, 350*, 497–533.
Suzuki, W. A., Zola-Morgan, S., Squire, L. R., & Amaral, D. G. (1993). Lesions of the perirhinal and parahippocampal cortices in the monkey produce long-lasting memory impairment in the visual and tactual modalities. *Journal of Neuroscience, 13*, 2430–2451.
Takehara-Nishiuchi, K., & McNaughton, B. L. (2008). Spontaneous changes of neocortical code for associative memory during consolidation. *Science, 322*, 960–963.
Takehara-Nishiuchi, K., Nakao, K., Kawahara, S., Matsuki, N., & Kirino, Y. (2006). Systems consolidation requires postlearning activation of NMDA receptors in the medial prefrontal cortex in trace eyeblink conditioning. *Journal of Neuroscience, 26*, 5049–5058.
Tanninen, S. E., Morrissey, M. D., & Takehara-Nishiuchi, K. (2013). Unilateral lateral entorhinal inactivation impairs memory expression in trace eyeblink conditioning. *PLoS ONE, 8*, e84543.
Uylings, H. B., Groenewegen, H. J., & Kolb, B. (2003). Do rats have a prefrontal cortex? *Behavioural Brain Research, 146*, 3–17.
Vertes, R. P. (2002). Analysis of projections from the medial prefrontal cortex to the thalamus in the rat, with emphasis on nucleus reuniens. *Journal of Comparative Neurology, 442*, 163–187.
Vertes, R. P. (2006). Interactions among the medial prefrontal cortex, hippocampus and midline thalamus in emotional and cognitive processing in the rat. *Neuroscience, 142*, 1–20.
Vertes, R. P. (2015). Major diencephalic inputs to the hippocampus: Supramammillary nucleus and nucleus reuniens. Circuitry and function. *Progress in Brain Research, 219*, 121–144.
Vertes, R. P., Hoover, W. B., Do Valle, A. C., Sherman, A., & Rodriguez, J. J. (2006). Efferent projections of reuniens and rhomboid nuclei of the thalamus in the rat. *Journal of Comparative Neurology, 499*, 768–796.
Vertes, R. P., Linley, S. B., & Hoover, W. B. (2015). Limbic circuitry of the midline thalamus. *Neuroscience and Biobehavioral Reviews, 54*, 89–107.
Wais, P. E., & Gazzaley, A. (2014). Distractibility during retrieval of long-term memory: Domain-general interference, neural networks and increased susceptibility in normal aging. *Frontiers in Psychology, 5*, 280.
Wilson, C. R., Gaffan, D., Mitchell, A. S., & Baxter, M. G. (2007). Neurotoxic lesions of ventrolateral prefrontal cortex impair object-in-place scene memory. *European Journal of Neuroscience, 25*, 2514–2522.
Wilson, D. I., Langston, R. F., Schlesiger, M. I., Wagner, M., Watanabe, S., & Ainge, J. A. (2013). Lateral entorhinal cortex is critical for novel object-context recognition. *Hippocampus, 23*, 352–366.
Wilson, D. I., Watanabe, S., Milner, H., & Ainge, J. A. (2013). Lateral entorhinal cortex is necessary for associative but not nonassociative recognition memory. *Hippocampus, 23*, 1280–1290.
Witter, M. P., Naber, P. A., van Haeften, T., Machielsen, W. C., Rombouts, S. A., Barkhof, F., ... Lopes da Silva, F. H. (2000). Cortico-hippocampal communication by way of parallel parahippocampal-subicular pathways. *Hippocampus, 10*, 398–410.
Witter, M. P., Wouterlood, F. G., Naber, P. A., & Van Haeften, T. (2000). Anatomical organization of the parahippocampal-hippocampal network. *Annals of the New York Academy of Sciences, 911*, 1–24.

Neurobiology of Aging 49 (2017) 79–85

Contents lists available at ScienceDirect

Neurobiology of Aging

journal homepage: www.elsevier.com/locate/neuaging

Epigenetic regulation of estrogen receptor α contributes to age-related differences in transcription across the hippocampal regions CA1 and CA3

Lara Ianov [a,b], Ashok Kumar [a,*], Thomas C. Foster [a,b,*]

[a] Department of Neuroscience, McKnight Brain Institute, University of Florida, Gainesville, FL, USA
[b] Genetics and Genomics Program, Genetics Institute, University of Florida, Gainesville, FL, USA

ARTICLE INFO

Article history:
Received 11 August 2016
Received in revised form 20 September 2016
Accepted 20 September 2016
Available online 28 September 2016

Keywords:
Aging
Estrogen receptor alpha
Hippocampus
Transcription
DNA methylation

ABSTRACT

The expression of estrogen receptor alpha (ERα) varies across brain regions and changes with age and according to the previous history of estradiol exposure. ERα is regulated by a number of mechanisms including the level of mRNA (*Esr1*) expression. For this study, we took advantage of regional differences in hippocampal ERα expression to investigate DNA ERα promoter methylation at CpG dinucleotide sites as a potential epigenetic mechanism for regulating gene expression. Young and aged female Fischer 344 rats were ovariectomized, and *Esr1* expression and ERα promoter methylation were examined in hippocampal regions CA1 and CA3, either 3 or 14 weeks following surgery. The results indicate that reduced *Esr1* expression in region CA1 relative to CA3 was associated with an increase in DNA methylation in region CA1, particularly for the first CpG site. Additionally, differential methylation of distal CpG sites, 11–17, was associated with altered *Esr1* expression during aging or following long-term hormone deprivation. The results support the idea that methylation of site 1 may be the primary regulatory region for cross-regional patterns in ERα expression, while distal sites are modifiable across the life span and may act as a feedback mechanism for ERα activity.

© 2016 Elsevier Inc. All rights reserved.

1. Introduction

Estradiol (E2) influences several biological processes that likely contribute to neuroprotection (Bean et al., 2014). The relative levels and subcellular distributions of estrogen receptor alpha (ERα) vary across brain regions and according to the previous history of E2 exposure (Mehra et al., 2005; Milner et al., 2001; Mitra et al., 2003; Mitterling et al., 2010). Differences in ERα expression/activity likely contribute to regional differences in vulnerability to ischemia and oxidative stress (Merchenthaler et al., 2003; Zhang et al., 2009). While the expression profile for ERα in the hippocampus is well characterized by age and hippocampal subregions, the molecular mechanisms that regulate estrogen receptor expression in the hippocampus are not well understood (Bean et al., 2014).

One mechanism for the regulation of gene expression is through methylation of cytosines in guanine-cytosine–rich areas of the gene promoter region, termed CpG islands. In several tissues, ERα promoter methylation increases with age and is associated with decreased ERα expression and increased incidence of disease (Li et al., 2004; Post et al., 1999). Similarly, in the brain, ERα promoter methylation is associated with a decrease in ERα expression and underlies physiological and behavioral differences across the lifespan (Gore et al., 2011; Schwarz et al., 2010). We examined the DNA methylation status of the 17 CpG sites within the ERα promoter exon 1b region in ovariectomized female rats to test the hypothesis that CpG DNA methylation is an active epigenetic regulator of regional and age-related differences in the expression of ERα mRNA, *Esr1*. For this study, we took advantage of regional differences in hippocampal ERα expression, with increased expression in region CA3 relative to region CA1 (Mehra et al., 2005; Rune et al., 2002), and possible autoregulation of ERα promoter activity by E2 (Castles et al., 1997; Donaghue et al., 1999; Pinzone et al., 2004), which may underlie effects of hormone deprivation on ERα expression (Bean et al., 2014). The results suggest that differential methylation of sites within the ERα promoter may regulate transcription of *Esr1* across hippocampal regions and that DNA methylation of distal CpG sites may have a function in age-related expression changes relative to upstream sites in the promoter.

* Corresponding author at: Department of Neuroscience, McKnight Brain Institute, University of Florida, PO Box 100244, Gainesville, FL 32610-0244, USA. Tel.: (352) 394-0033; fax: (352) 392-8347.
E-mail addresses: Kash@ufl.edu (A. Kumar), foster1@ufl.edu (T.C. Foster).

0197-4580/$ – see front matter © 2016 Elsevier Inc. All rights reserved.
http://dx.doi.org/10.1016/j.neurobiolaging.2016.09.013

2. Materials and methods

2.1. Animals

Procedures involving animal subjects have been reviewed and approved by the Institutional Animal Care and Use Committee and were in accordance with guidelines established by the U.S. Public Health Service Policy on Humane Care and Use of Laboratory Animals. Female Fischer 344 rats of two ages, young (3 months, n = 21) and aged (18 months, n = 22), were obtained from National Institute on Aging colony at Charles River Laboratories, through the University of Florida Animal Care and Service facility. Animals were maintained on a 12:12 hours light schedule and provided ad lib access to food and water.

2.2. Surgery and tissue collection

Ovariectomy (OVX) was performed as previously described (Bean et al., 2015; Sharrow et al., 2002). Briefly, rats were handled for 5 minutes a day for at least 1 week prior to surgery. Female rats were ovariectomized under isoflurane (Piramal Healthcare) in oxygen using a VetEquip anesthesia system. Bilateral incisions were made to expose the ovaries, which were cleared from the fat tissue and dissected out. Subsequent to the closure of the incisions, buprenorphine (0.03 mg/kg) and saline (5–10 mL) were given by subcutaneous injection. Following OVX, the food of the animals was exchanged to a casein-based chow, which contains lower levels of phytoestrogens. Three weeks (wk) following OVX (young, n = 10 and aged, n = 11), rats were overdosed with CO_2, decapitated, and the hippocampi were dissected. The same procedure was repeated for the remaining animals after a 14-week period (young, n = 11 and aged, n = 11) (Fig. 1). Hippocampal regions (CA1 and CA3) were separated, placed in tubes, immediately frozen in liquid nitrogen, and stored in −80 °C until processed.

2.3. RNA isolation and reverse transcription quantitative polymerase chain reaction

RNA was isolated from each hippocampal region (n = 5–6 per region of each age and OVX duration group) using the RNeasy Lipid Tissue Mini kit (Qiagen, catalog number: 74804), and DNase digestion was performed with the RNase-Free DNase Set (Qiagen, catalog number: 79254). Following isolation, the concentration was measured using the NanoDrop 2000 spectrophotometer (Thermo Scientific). Reverse transcription was performed using the QuantiTect Reverse Transcription kit (Qiagen, catalog number: 205311), and quantitative polymerase chain reaction was completed using the TaqMan Gene Expression Assays (*Esr1*: Rn01640372_m1, *Gapdh*: Rn01775763_g1) in a 7300 real-time polymerase chain reaction (PCR) system with SDS software version 1.3.1 (Applied Biosystems). The ΔΔCT method (Livak and Schmittgen, 2001) was used to determine the relative cDNA levels, and the CA1 region from young short-term rats was used as the calibrator samples.

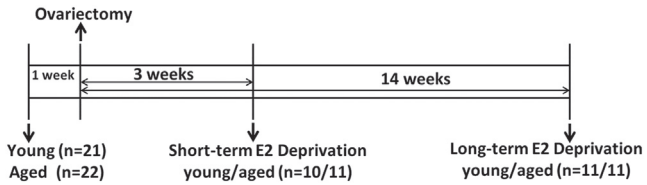

Fig. 1. Experimental research design. Young (3 months) and aged (18 months) F344 female rats were handled for 5 minutes a day for 1 week prior to OVX surgery and killed following a short-term E2 deprivation time (3 weeks) or a long-term E2 deprivation time (14 weeks). Abbreviation: OVX, ovariectomy.

2.4. Sodium bisulfite sequencing

Genomic DNA was isolated from the CA1 and CA3 areas (n = 5 per age group and OVX time) using the DNeasy Blood and Tissue kit (Qiagen, catalog number: 69504). The DNA concentration was quantified using the NanoDrop 2000 spectrophotometer, and sodium bisulfite conversion was performed with the EZ DNA Methylation-Gold kit (Zymo Research, catalog number: D5005) according to the manufacturer's directions. The exon 1b promoter region of ERα (GenBank accession number: X98236) was amplified with the following modifications from previous reports (Champagne et al., 2006; Kurian et al., 2010). The thermocycler parameters included an initial denaturation cycle of 5 minutes at 94 °C, 40 cycles of 1 minute at 94 °C (denaturing), 3 minutes at 56 °C (annealing) and 1 minute at 72 °C (extension), followed by a final extension cycle of 15 minutes at 72 °C. The following bisulfite sequencing PCR (BSP) primers were used: outer forward 5′TAGTATATTTTGATTGTTA TTTTAT3′; outer reverse 5′CTAAACAAAAAAATAAATTACTTTC3′. The PCR product was used for nested PCR with the same thermocycler parameters with the following BSP nested primers: forward 5′TTTATTTGTGGTTTATAGATATTT3′ and reverse 5′ACAAAAAAAAAA AAATCAAAACAC3′. In addition, a preliminary check of bisulfite conversion efficiency of each sample was assessed by performing a separate nested PCR reaction. The same thermocycler conditions were used with wild-type sequence-specific primers, which map to the unconverted DNA sequence of the exon 1b promoter region of ERα (outer forward 5′CAGCACACTTTGACTGCCATTCTAC3′; outer reverse 5′CTAGGCAGAAAGGTAAGTTGCTTTC3′; nested forward 5′TTTATCTGTGGTTTACAGACATCT3′; nested reverse 5′ACAGAAAGA GGGAAATCAAAACAC3′). Amplification of the target sequence with wild-type primers would indicate incomplete bisulfite conversion. All samples demonstrated complete bisulfite conversion. Unconverted DNA was used as the positive control for the wild-type primers.

The nested product (459 bp) of each PCR reaction using BSP primers was cloned with the TOPO TA cloning kit for Sequencing (Life Technologies, catalog number: K4575-J10) with the following modifications to the transformation reaction: TOP10 cells were heat shocked for 45 seconds at 42 °C and immediately transferred to ice for 7 minutes before the addition of S.O.C. medium. Positive clones were confirmed by colony PCR using nested BSP primers, and miniprep was performed on each positive clone (PureLinkquick plasmid DNA miniprep, Life Technologies, catalog number: K2100-10). The samples were sent for Sanger sequencing at the Interdisciplinary Center for Biotechnology Research, University of Florida. The DNA methylation status of all 17 CpG sites from each region was analyzed using BiQ analyzer (Bock et al., 2005) retaining the default parameters. All positive clones contained conversion rates from 97%–100%, and FASTA files which contained a gap in more than one CpG site were removed. After quality filtering, the average number of clones per animal/region was 10 (±standard error of the mean 2) and the average number of clones per age and OVX groups was 51 (±standard error of the mean 4). In addition, the total number of clones for each hippocampal region was 204 for CA1 and 203 for CA3. Hierarchical clustering and heatmap figures were generated in Partek Genomics Suite 6.6 (Partek Inc) using clones which contained at least one site methylated to illustrate the DNA methylation pattern in site 1 to sites 2–17.

2.5. Statistical analysis

All statistical analyses were performed using StatView 5.0 (SAS Institute Inc, NC, USA). Analyses of variance (ANOVAs) were used to determine significant main effects for RNA expression. For CpG methylation, repeated measures ANOVAs were employed to determine main effects of age and hippocampal region across CpG sites. Fisher's protected least significant difference post hoc comparisons with $p < 0.05$ were employed to localize differences related to differential expression across CpG sites. For interactions of CpG sites with age, OVX duration, or hippocampal region, post hoc ANOVAs were employed to localize differences within each site. A chi-square analysis was employed to examine the independence of methylation across CpG sites.

3. Results

3.1. Region and aging effects on ERα mRNA expression

Fig. 2 illustrates the expression of *Esr1* associated with age (young: 3 months, aged: 18 months), OVX duration (short term: 3 weeks, long term: 14 weeks), and region (CA1 or CA3). An increase in *Esr1* expression was observed in older animals (Fig. 2A). Similarly, expression was increased for the long-term OVX relative to short-term OVX (Fig. 2B). Finally, the largest difference was observed as a threefold increase in *Esr1* expression in CA3 relative to CA1 (Fig. 2C). A three-factor ANOVA for expression of *Esr1* confirmed significant main effects of age [$F(1,38) = 33.14$, $p < 0.001$], OVX duration [$F(1,38) = 56.0$, $p < 0.0001$], and region [$F(1,38) = 155.42$, $p < 0.0001$]. Additionally, there was an interaction of OVX duration and age [$F(1,38) = 13.31$, $p < 0.001$], region and age [$F(1,38) = 9.25$, $p < 0.01$], and a tendency ($p = 0.063$) for a region by OVX duration interaction.

The interaction of age and OVX duration was due to increased *Esr1* expression limited to the short duration OVX (Fig. 2D). To examine the interaction of age and OVX duration, post hoc ANOVAs were conducted within respective OVX durations and revealed an age difference for short-term OVX [$F(1,18) = 40.27$, $p < 0.001$], with an age by region interaction [$F(1,18) = 9.52$, $p < 0.01$]. Examination of each region indicated that, for short-term OVX, an age-related increase in *Esr1* expression was observed in region CA1 [$F(1,9) = 27.6$, $p < 0.001$] and in region CA3 [$F(1,9) = 24.6$, $p < 0.0001$] (Fig. 2D).

Long-term OVX was associated with an increase in *Esr1* expression in CA1 and CA3 for younger animals. For older animals, long-term OVX increased expression only in region CA1 (Fig. 2D). To localize effects of E2 deprivation, effects of OVX duration within each region and each age group were examined. The results indicated that relative to young short-term OVX, *Esr1* expression increased in CA1 [$F(1,9) = 26.68$, $p < 0.001$] and CA3 [$F(1,9) = 60.6$, $p < 0.0001$] of young long-term OVX animals (Fig. 2D). For aged animals, long-term OVX increased *Esr1* expression [$F(1,10) = 10.45$, $p < 0.01$] in CA1 relative to aged short-term OVX rats (Fig. 2D). Thus, it appears that *Esr1* expression is increased due to age and

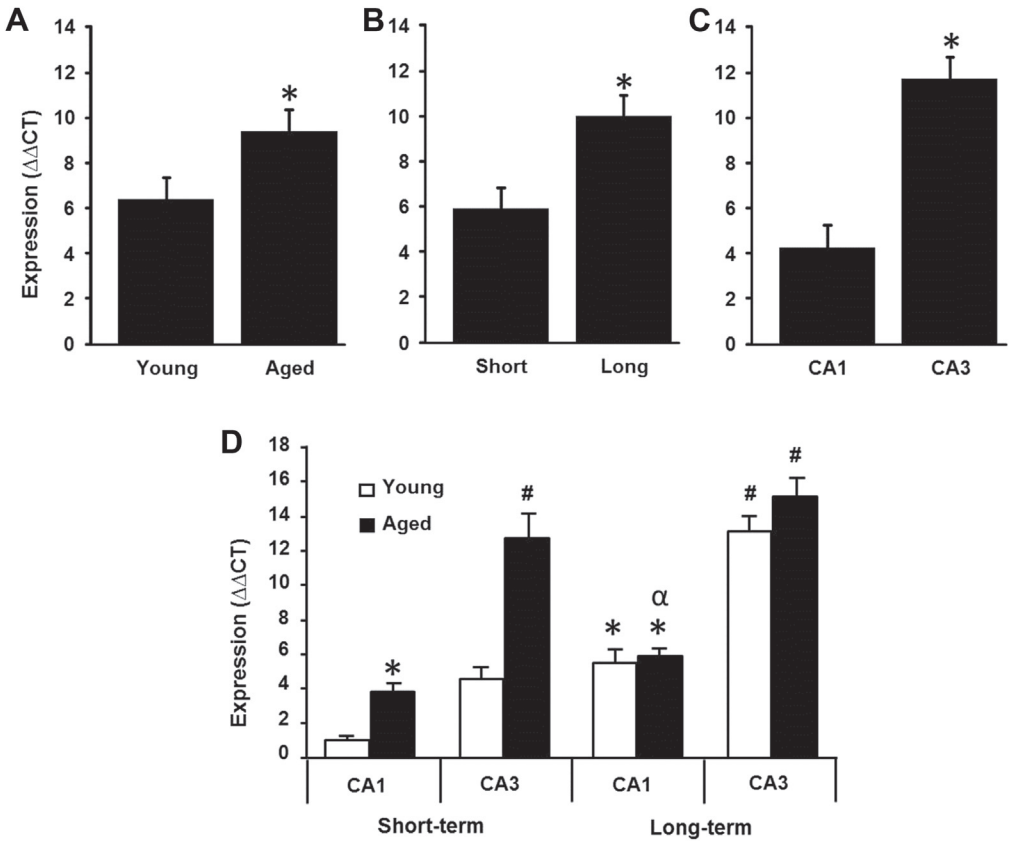

Fig. 2. Illustration of differences in *Esr1* expression. The CA1 region from young short-term rats was used as the calibrator sample in calculating the ΔΔCT. For (A–C), each bar represents the mean (+SEM) of *Esr1* expression for the relevant variable, collapsed across all other variables. *Esr1* expression is increased with (A) age, (B) long-term OVX, and (C) in region CA3 relative to region CA1. Asterisks in (A–C) indicated a significant ($p < 0.001$) main effect. (D) Examination of interactions, where each bar represents the mean (+SEM) of *Esr1* expression for young (n = 5–6; open bars) and aged (n = 6; filled bars), across regions CA1 and CA3 according to OVX duration (short term: 3 week, long term: 14 weeks). Asterisk indicates a significant ($p < 0.05$) increase in region CA1 relative to young short-term OVX CA1. Pound sign indicates a significant ($p < 0.05$) increase in region CA3 relative to young short-term OVX CA3. For aged animals, long-term OVX was associated with increased expression relative to aged short-term OVX for region CA1 only (α, $p < 0.05$). Abbreviations: OVX, ovariectomy; SEM, standard error of the mean.

long-term E2 deprivation. We confirmed this by comparing young short-term OVX relative to aged long term in CA1 [$F(1,9) = 100.83$, $p < 0.0001$] and in CA3 [$F(1,9) = 75.80$, $p < 0.0001$] (Fig. 2D).

3.2. Methylation of the ERα promoter

Considerable variability in methylation was observed across the 17 CpG sites of the ERα promoter region. In general, the pattern of methylation was similar across the two regions with the greatest methylation observed at site 1 and minimal methylation for sites 2–10. Modest methylation was observed for distal sites 11–17 (Fig. 3A). A repeated measures ANOVA was conducted across the 17 DNA CpG methylation sites examining main effects of region, age, and OVX duration. As expected, a significant difference in methylation was observed across CpG sites [$F(16,512) = 26.91$, $p < 0.0001$] indicative of the considerable variability in CpG methylation. Post hoc tests across all sites, collapsed across age, region, and OVX duration, indicated the first CpG site exhibited methylation that was significantly greater than all other sites. In addition, considerable methylation was observed for sites 11, 15, and 17, which were greater than sites 2–7, 9, and 14 (Table 1). No significance difference was observed for any of the main effects; however, there was an interaction of CpG site and region [$F(16,512) = 2.49$, $p < 0.005$] and a CpG site by age by region interaction [$F(16,512) = 2.13$, $p < 0.01$].

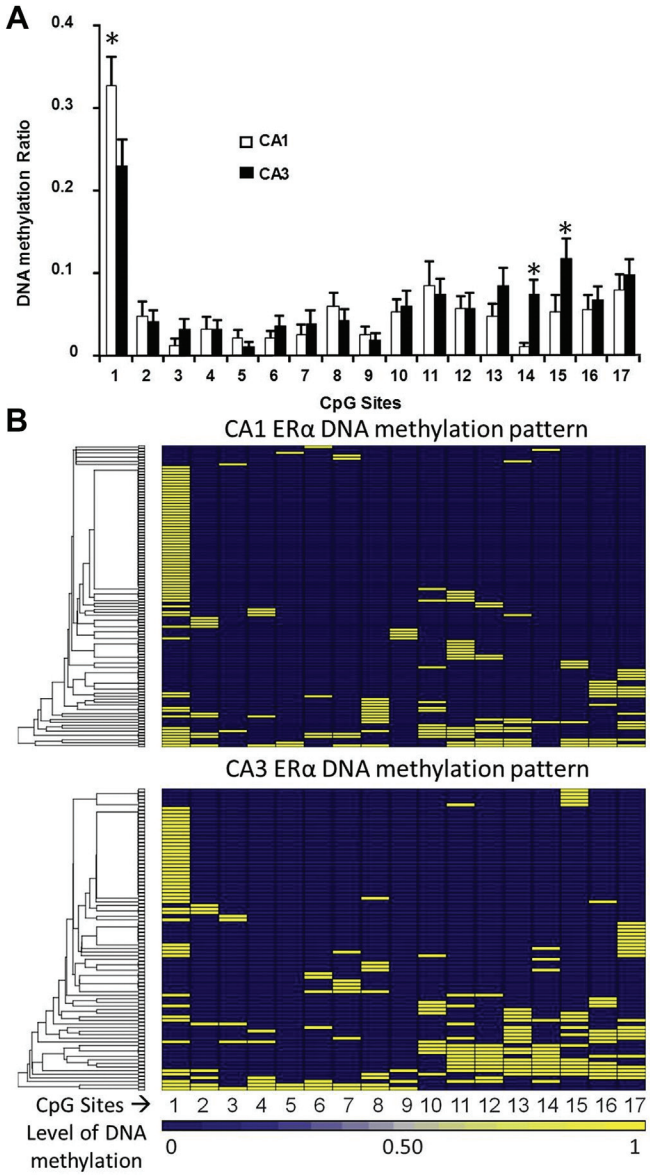

Fig. 3. Site-specific DNA methylation of CpG sites across CA1 and CA3 regions. (A) Each bar represents the mean (+SEM) DNA methylation ratio for sites 1–17 in CA1 (open bars) and CA3 (filled bars). Regional differences in CpG site methylation included increased methylation of site 1 in CA1 and sites 14 and 15 in CA3 (n = 20 per region). Asterisk indicates a significant ($p < 0.05$) increase in methylation. (B) Hierarchical clustering and heatmap of the clones which contained ≥1 methylated site [CA1: 104 clones (51%) and CA3: 84 clones (41%)]. Abbreviation: SEM, standard error of the mean.

ANOVAs were conducted within each site to examine the site by region interaction. Increased methylation was observed in region CA1 for site 1 [$F(1,38) = 4.30$, $p < 0.05$], and methylation was increased in region CA3 for site 14 [$F(1,38) = 10.34$, $p < 0.005$] and site 15 [$F(1,38) = 4.12$, $p < 0.05$] (Fig. 3A). Due to the higher DNA methylation ratio on site 1 relative to downstream sites, a closer examination of the clones that contained at least one site methylated in the promoter was performed by chi-square analysis between DNA methylation in site 1 to sites 2–17.

For region CA1, chi-square analysis showed no significant associations between site 1 methylation and distal CpG methylation on sites 2–17, suggesting that methylation of these sites is independent of methylation of the first site in the exon 1b promoter (Fig. 3B). For region CA3, site 1 methylation was independent from the other sites with the exception of a significant association to DNA methylation in site 15. The analysis showed that when site 1 is not methylated, there is a higher probability of methylation on site 15 ($X^2 = 4.662$, $p < 0.05$).

To examine the site by age by region interaction, ANOVAs were conducted within each site and region to examine age effects (Fig. 4A and B). A significant age-related increase in methylation was observed for sites 11 [$F(1,18) = 6.49$, $p < 0.05$] and 12 [$F(1,18) = 6.09$, $p < 0.05$] in CA3. In contrast, young animals exhibited a significant increase in methylation at site 15 [$F(1,18) = 4.76$, $p < 0.05$] in CA1 and site 17 [$F(1,18) = 5.57$, $p < 0.05$] in CA3.

Because *Esr1* expression was increased in area CA1 and CA3 of young animals by long-duration OVX, age differences in DNA methylation may have been masked by effects of long-term OXV in young. Therefore, we separated young animals according to OVX duration and for sites 11–17, we compared young short-term OVX, young long-term OVX, and all aged animals. For region CA1, a significant group difference was observed for site 11 [$F(2,17) = 3.96$, $p < 0.05$] and site 14 [$F(2,17) = 4.24$, $p < 0.05$]. Post hoc tests indicated that in each case, methylation was increased in young short term, relative to young long term and aged animals (Fig. 4C and D). For region CA3, a significant group difference was observed for site 13 [$F(2,17) = 3.80$, $p < 0.05$] and post hoc tests indicated that methylation was decreased in young short-term OVX, relative to young long-term OVX (Fig. 4E).

Table 1
Fisher's PLSD for CpG sites in *Esr1* promoter

DNA methylation on CpG site	*p*-value
1 > 16 sites (2–17)	<0.05
8 > 1 sites (5)	<0.05
10 > 2 sites (5, 9)	<0.05
11 > 8 sites (2–7, 9, 14)	<0.05
12 > 3 sites (3, 5, 9)	<0.05
13 > 3 sites (3–7, 9)	<0.05
15 > 9 sites (2–9, 14)	<0.05
16 > 4 sites (3, 5, 6, 9)	<0.05
17 > 8 sites (2–7, 9, 14)	<0.05

Key: PLSD, protected least significant difference.

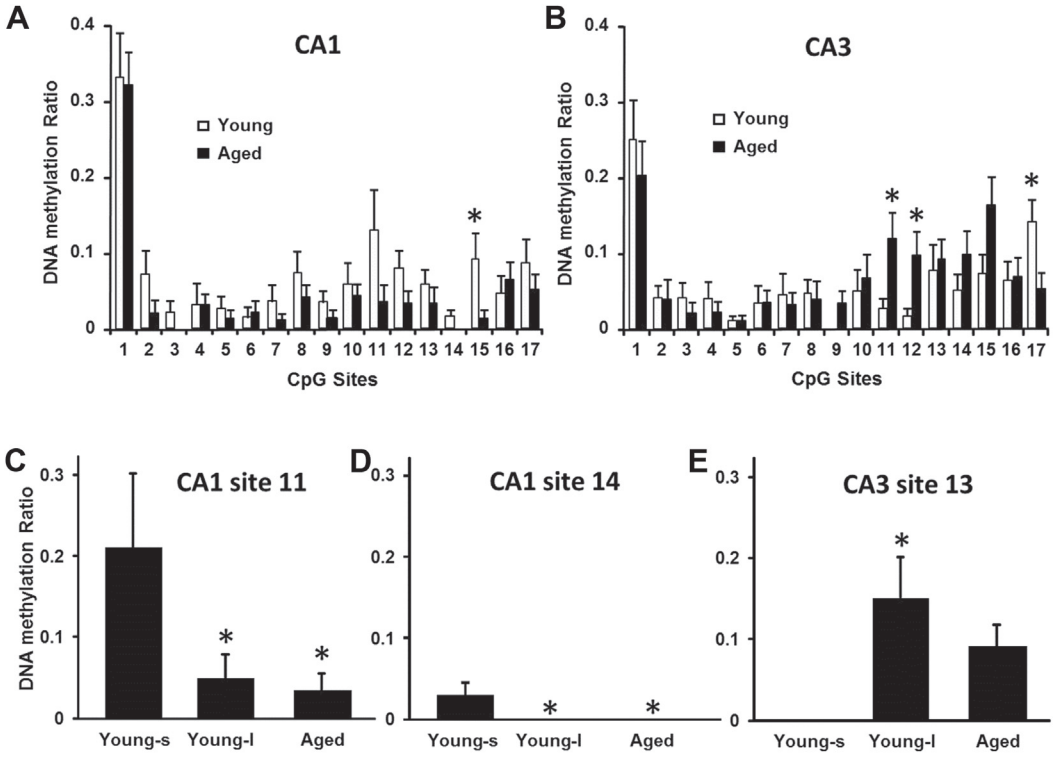

Fig. 4. ERα promoter DNA methylation is altered in regions CA1 and CA3 during aging. Age-related differences in CpG site methylation for (A) area CA1 were observed as an increase in DNA methylation for site 15 for young animals (open bars, n=10) relative to aged animals (filled bars, n = 10). (B) For area CA3, site 17 contained higher methylation in young rats, and sites 11 and 12 showed higher methylation in aged rats. Due to the influence of OVX duration on transcription, young animals were separated into short-term OVX (young-s) and long-term OVX (young-l) and compared to all aged animals for sites 11–17. Specific differences were observed in CA1 for (C) site 11 and (D) site 14. (E) For region CA3, a difference was observed for site 13. Bars represent the mean (+SEM) of the methylation ratio. Asterisks indicate a significant ($p < 0.05$) increase in (A) and (B) and a significant ($p < 0.05$) difference from young short-term in (C–E). Abbreviations: ERα, estrogen receptor alpha; OVX, ovariectomy; SEM, standard error of the mean.

4. Discussion

Previous research using rat models indicates region and age-related changes in ERα protein expression within the hippocampus, with elevated expression in region CA3 relative to CA1 and altered expression in both regions with age or E2 deprivation (Bohacek and Daniel, 2009; Mehra et al., 2005; Zhang et al., 2011). While the effect of age on *Esr1* expression is unclear (Ishunina and Swaab, 2007; Tohgi et al., 1995), *Esr1* messenger levels increase following E2 deprivation (Sarvari et al., 2014) and are higher in area CA3 relative to CA1 (Rune et al., 2002). In the current study, we confirmed that *Esr1* expression is elevated in region CA3 relative to region CA1, suggesting that transcriptional regulation contributes to differential expression of the receptor across the two regions. The age difference in *Esr1* expression was limited to the short-term OVX animals, with increased expression in all aged animals. Furthermore, expression in young animals was elevated in region CA1 following long-term hormone deprivation, such that expression was similar to that of aged animals. These results are consistent with work indicating that hormone state can regulate *Esr1* expression and indicate that long-term E2 deprivation may up regulate *Esr1*, possibly as a compensatory mechanism for a loss of ERα activity (Han et al., 2013). Nevertheless, it should be noted that the level of CA1 *Esr1* expression was consistently reduced relative to area CA3, regardless of age or OVX duration.

In other brain regions and tissues, DNA methylation of the ERα promoter is thought to contribute to differential *Esr1* expression. The promoter exon 1b region was chosen for examination as this has been shown to be the active promoter in the rat brain and contains a number of CpG sites previously associated with the regulation of the *Esr1* gene (Champagne et al., 2006; Freyschuss and Grandien, 1996; Kurian et al., 2010). Considerable variability in methylation was observed across the 17 CpG sites located in this promoter region. In general, the greatest methylation was observed at site 1 and minimal methylation was observed for sites 2–10. Modest methylation was observed for sites 11–17 with sites 11, 15, and 17 exhibiting higher methylation relative to upstream sites 2–7.

DNA methylation is involved in heritable gene silencing or gene inactivation (Bird and Wolffe, 1999; Newell-Price et al., 2000). While promoter regions that are highly methylated tend to be less transcriptionally active, the relationship between DNA methylation and gene expression is far from clear. In the current study, the largest difference in *Esr1* expression was observed across hippocampal subregions and the site of the greatest DNA methylation, site 1, also exhibited differential methylation across subregions, with increased methylation in region CA1 associated with reduced *Esr1* expression. Similarly, the increase in mRNA expression in CA1 with age was associated with decreased methylation of site 15 in CA1, and the increase in *Esr1* for young long-term OVX and aged animals was associated with decreased methylation in CA1 of sites 11 and 14, compared to young short-term OVX animals. The results indicate that for sites with the greatest methylation (i.e., site 1), variability in methylation is associated with changes in *Esr1* expression. Furthermore, for more distal sites (i.e., 11, 14, 15), methylation is more modest and can be modified across the lifespan. Each of these points are addressed below.

The idea that increased methylation of site 1 is related to decreased mRNA expression is consistent with previous work in other brain regions (Kurian et al., 2010). However, we also observed increased methylation for sites 14 and 15 in region CA3 associated

with increased *Esr1* expression. Similarly, Gore et al. (2011) have reported that exposure to an estrogenic endocrine disruptor increased DNA methylation at one site, identified as site 14 of the *Esr1* promoter in the current study, which was associated with increased mRNA levels in the preoptic area (Gore et al., 2011). Thus, it should be emphasized that the variability in methylation, increasing or decreasing, only provides a correlate of mRNA expression. A mechanism through which differential DNA methylation might regulate *Esr1* expression remains to be elucidated.

The idea that methylation of these distal sites can be modified across the lifespan to regulate *Esr1* expression is supported by previous work, which demonstrates that maternal care and hormonal manipulations altered *Esr1* expression in the medial preoptic area and amygdala, and the changes in *Esr1* expression were associated with differential methylation of sites 11–16 (Champagne et al., 2006; Edelmann and Auger, 2011; Gore et al., 2011). Across hippocampal subregions, there is heterogeneity in DNA methylation, gene expression, and in the transcriptional response to aging (Xu, 2015; Zeier et al., 2011). Previous studies have highlighted distinct patterns in DNA methylation and transcription across cell types including different neuronal cell types (Angermueller et al., 2016; Brunner et al., 2009; Kozlenkov et al., 2014, 2016), suggesting that variability in DNA methylation observed in the current study could be due to cell-type heterogeneity. However, it should also be noted that mRNA for ERα has been observed in both pyramidal cells and interneurons in the hippocampus and expression is higher in region CA3 relative to CA1 (Rune et al., 2002). Regardless, it will be important for future studies to determine if the relationship of DNA methylation and *Esr1* expression is specific to certain cell types.

Several transcriptional and post-translational feedback mechanisms control estrogen receptor expression (Bean et al., 2014). However, most of this work has been performed in breast cancer cell cultures, and the molecular mechanisms that regulate estrogen receptor expression in the hippocampus are not well understood. In mice, functional knockout of ERα or ERβ induces a compensatory increase in hippocampal *Esr1* and *Esr2* transcription, respectively, suggesting a feedback mechanism (Han et al., 2013). The current study suggests that a shift in DNA methylation, particularly for distal sites, could be involved in feedback regulation of ERα expression. Previous studies have reported a link between ERα expression, DNA methyltransferase activity, and ERα promoter methylation during development, aging, and in disease states (Wang et al., 2012; Westberry et al., 2010; Yang et al., 2001). Methylation of the promoter may influence mRNA expression by regulating the binding of transcription factors. A number of putative transcriptional factors binding sites have been reported for the exon 1b region (Gore et al., 2011); however, only the binding of one transcriptional factor (Stat5b) has been found to be associated with ERα methylation (Champagne et al., 2006). In addition, DNA methyltransferase interacts with transcription repressor proteins (e.g., histone deacetylase) to alter chromatin structure and the pattern of DNA methylation (Robertson, 2002). Transcription repressors, Hdac2 and Sap18, influence *Esr1* transcription (Bicaku et al., 2008; Ellison-Zelski et al., 2009) and E2 treatment decreases the expression of *Hdac2* and *Sap18* in the hippocampus (Aenlle et al., 2009). Thus, altered expression of transcription repressor proteins may interact with DNA methylation as part of a feedback mechanism.

Finally, the ratio of hippocampal ERα and ERβ expression interacts with the level of E2 to influence transcription and synaptogenesis and a shift in the ERα/ERβ ratio may determine the ability of E2 to influence cognition (Bean et al., 2014, 2015; Hall and McDonnell, 1999; Han et al., 2013; Pettersson et al., 2000). The increase in *Esr1* and *Esr2* transcription in estrogen receptor knockout mice is diminished for *Esr1*, but not *Esr2*, during aging (Han et al., 2013). It is also interesting to note that E2 treatment of aged animals increases hippocampal synaptic expression of ERβ, but not ERα (Waters et al., 2011), suggesting differential regulation of estrogen receptors during aging. Due to the interaction of ERα and ERβ in determining functional outcome, it will be important to map out differences in the regulation of these two estrogen receptors during aging.

In summary, transcriptional levels of *Esr1* were altered across hippocampal CA1 and CA3 subregions, with increased expression in region CA3 relative to CA1. In addition, an age-related increase in expression was found in region CA1 relative to young short-term OVX rats. Furthermore, the results support the idea that DNA methylation is an active epigenetic mechanism for the regulation of *Esr1* in the hippocampus, where methylation of site 1 may be the primary regulatory region for cross-regional patterns in ERα expression. Additionally, differential methylation of distal CpG sites, 11–17, was associated with aging or E2 deprivation, suggesting that these sites are modifiable across the life span and may act as a feedback mechanism for ERα activity.

Disclosure statement

The authors have no conflicts of interest to disclose.

Acknowledgements

Financial support by National Institute on Aging grants R01AG037984, R37AG036800, R01AG49711, and RO1AG052258, and the Evelyn F. McKnight Brain Research Foundation is highly appreciated.

References

Aenlle, K.K., Kumar, A., Cui, L., Jackson, T.C., Foster, T.C., 2009. Estrogen effects on cognition and hippocampal transcription in middle-aged mice. Neurobiol. Aging 30, 932–945.

Angermueller, C., Clark, S.J., Lee, H.J., Macaulay, I.C., Teng, M.J., Hu, T.X., Krueger, F., Smallwood, S.A., Ponting, C.P., Voet, T., Kelsey, G., Stegle, O., Reik, W., 2016. Parallel single-cell sequencing links transcriptional and epigenetic heterogeneity. Nat. Methods 13, 229–232.

Bean, L.A., Ianov, L., Foster, T.C., 2014. Estrogen receptors, the hippocampus, and memory. Neuroscientist 20, 534–545.

Bean, L.A., Kumar, A., Rani, A., Guidi, M., Rosario, A.M., Cruz, P.E., Golde, T.E., Foster, T.C., 2015. Re-opening the critical window for estrogen therapy. J. Neurosci. 35, 16077–16093.

Bicaku, E., Marchion, D.C., Schmitt, M.L., Munster, P.N., 2008. Selective inhibition of histone deacetylase 2 silences progesterone receptor-mediated signaling. Cancer Res. 68, 1513–1519.

Bird, A.P., Wolffe, A.P., 1999. Methylation-induced repression–belts, braces, and chromatin. Cell 99, 451–454.

Bock, C., Reither, S., Mikeska, T., Paulsen, M., Walter, J., Lengauer, T., 2005. BiQ Analyzer: visualization and quality control for DNA methylation data from bisulfite sequencing. Bioinformatics 21, 4067–4068.

Bohacek, J., Daniel, J.M., 2009. The ability of oestradiol administration to regulate protein levels of oestrogen receptor alpha in the hippocampus and prefrontal cortex of middle-aged rats is altered following long-term ovarian hormone deprivation. J. Neuroendocrinol. 21, 640–647.

Brunner, A.L., Johnson, D.S., Kim, S.W., Valouev, A., Reddy, T.E., Neff, N.F., Anton, E., Medina, C., Nguyen, L., Chiao, E., Oyolu, C.B., Schroth, G.P., Absher, D.M., Baker, J.C., Myers, R.M., 2009. Distinct DNA methylation patterns characterize differentiated human embryonic stem cells and developing human fetal liver. Genome Res. 19, 1044–1056.

Castles, C.G., Oesterreich, S., Hansen, R., Fuqua, S.A., 1997. Auto-regulation of the estrogen receptor promoter. J. Steroid Biochem. Mol. Biol. 62, 155–163.

Champagne, F.A., Weaver, I.C., Diorio, J., Dymov, S., Szyf, M., Meaney, M.J., 2006. Maternal care associated with methylation of the estrogen receptor-alpha1b promoter and estrogen receptor-alpha expression in the medial preoptic area of female offspring. Endocrinology 147, 2909–2915.

Donaghue, C., Westley, B.R., May, F.E., 1999. Selective promoter usage of the human estrogen receptor-alpha gene and its regulation by estrogen. Mol. Endocrinol. 13, 1934–1950.

Edelmann, M.N., Auger, A.P., 2011. Epigenetic impact of simulated maternal grooming on estrogen receptor alpha within the developing amygdala. Brain Behav. Immun. 25, 1299–1304.
Ellison-Zelski, S.J., Solodin, N.M., Alarid, E.T., 2009. Repression of ESR1 through actions of estrogen receptor alpha and Sin3A at the proximal promoter. Mol. Cell. Biol. 29, 4949–4958.
Freyschuss, B., Grandien, K., 1996. The 5' flank of the rat estrogen receptor gene: structural characterization and evidence for tissue- and species-specific promoter utilization. J. Mol. Endocrinol. 17, 197–206.
Gore, A.C., Walker, D.M., Zama, A.M., Armenti, A.E., Uzumcu, M., 2011. Early life exposure to endocrine-disrupting chemicals causes lifelong molecular reprogramming of the hypothalamus and premature reproductive aging. Mol. Endocrinol. 25, 2157–2168.
Hall, J.M., McDonnell, D.P., 1999. The estrogen receptor beta-isoform (ERbeta) of the human estrogen receptor modulates ERalpha transcriptional activity and is a key regulator of the cellular response to estrogens and antiestrogens. Endocrinology 140, 5566–5578.
Han, X., Aenlle, K.K., Bean, L.A., Rani, A., Semple-Rowland, S.L., Kumar, A., Foster, T.C., 2013. Role of estrogen receptor alpha and beta in preserving hippocampal function during aging. J. Neurosci. 33, 2671–2683.
Ishunina, T.A., Swaab, D.F., 2007. Alterations in the human brain in menopause. Maturitas 57, 20–22.
Kozlenkov, A., Roussos, P., Timashpolsky, A., Barbu, M., Rudchenko, S., Bibikova, M., Klotzle, B., Byne, W., Lyddon, R., Di Narzo, A.F., Hurd, Y.L., Koonin, E.V., Dracheva, S., 2014. Differences in DNA methylation between human neuronal and glial cells are concentrated in enhancers and non-CpG sites. Nucleic Acids Res. 42, 109–127.
Kozlenkov, A., Wang, M., Roussos, P., Rudchenko, S., Barbu, M., Bibikova, M., Klotzle, B., Dwork, A.J., Zhang, B., Hurd, Y.L., Koonin, E.V., Wegner, M., Dracheva, S., 2016. Substantial DNA methylation differences between two major neuronal subtypes in human brain. Nucleic Acids Res. 44, 2593–2612.
Kurian, J.R., Olesen, K.M., Auger, A.P., 2010. Sex differences in epigenetic regulation of the estrogen receptor-alpha promoter within the developing preoptic area. Endocrinology 151, 2297–2305.
Li, L.C., Shiina, H., Deguchi, M., Zhao, H., Okino, S.T., Kane, C.J., Carroll, P.R., Igawa, M., Dahiya, R., 2004. Age-dependent methylation of ESR1 gene in prostate cancer. Biochem. Biophys. Res. Commun. 321, 455–461.
Livak, K.J., Schmittgen, T.D., 2001. Analysis of relative gene expression data using real-time quantitative PCR and the 2−ΔΔCT method. Methods 25, 402–408.
Mehra, R.D., Sharma, K., Nyakas, C., Vij, U., 2005. Estrogen receptor alpha and beta immunoreactive neurons in normal adult and aged female rat hippocampus: a qualitative and quantitative study. Brain Res. 1056, 22–35.
Merchenthaler, I., Dellovade, T.L., Shughrue, P.J., 2003. Neuroprotection by estrogen in animal models of global and focal ischemia. Ann. N. Y. Acad. Sci. 1007, 89–100.
Milner, T.A., McEwen, B.S., Hayashi, S., Li, C.J., Reagan, L.P., Alves, S.E., 2001. Ultrastructural evidence that hippocampal alpha estrogen receptors are located at extranuclear sites. J. Comp. Neurol. 429, 355–371.
Mitra, S.W., Hoskin, E., Yudkovitz, J., Pear, L., Wilkinson, H.A., Hayashi, S., Pfaff, D.W., Ogawa, S., Rohrer, S.P., Schaeffer, J.M., McEwen, B.S., Alves, S.E., 2003. Immunolocalization of estrogen receptor beta in the mouse brain: comparison with estrogen receptor alpha. Endocrinology 144, 2055–2067.
Mitterling, K.L., Spencer, J.L., Dziedzic, N., Shenoy, S., McCarthy, K., Waters, E.M., McEwen, B.S., Milner, T.A., 2010. Cellular and subcellular localization of estrogen and progestin receptor immunoreactivities in the mouse hippocampus. J. Comp. Neurol. 518, 2729–2743.
Newell-Price, J., Clark, A.J., King, P., 2000. DNA methylation and silencing of gene expression. Trends Endocrinol. Metab. 11, 142–148.
Pettersson, K., Delaunay, F., Gustafsson, J.A., 2000. Estrogen receptor beta acts as a dominant regulator of estrogen signaling. Oncogene 19, 4970–4978.
Pinzone, J.J., Stevenson, H., Strobl, J.S., Berg, P.E., 2004. Molecular and cellular determinants of estrogen receptor alpha expression. Mol. Cell. Biol. 24, 4605–4612.
Post, W.S., Goldschmidt-Clermont, P.J., Wilhide, C.C., Heldman, A.W., Sussman, M.S., Ouyang, P., Milliken, E.E., Issa, J.P., 1999. Methylation of the estrogen receptor gene is associated with aging and atherosclerosis in the cardiovascular system. Cardiovasc. Res. 43, 985–991.
Robertson, K.D., 2002. DNA methylation and chromatin - unraveling the tangled web. Oncogene 21, 5361–5379.
Rune, G.M., Wehrenberg, U., Prange-Kiel, J., Zhou, L., Adelmann, G., Frotscher, M., 2002. Estrogen up-regulates estrogen receptor alpha and synaptophysin in slice cultures of rat hippocampus. Neuroscience 113, 167–175.
Sarvari, M., Kallo, I., Hrabovszky, E., Solymosi, N., Liposits, Z., 2014. Ovariectomy and subsequent treatment with estrogen receptor agonists tune the innate immune system of the hippocampus in middle-aged female rats. PLoS One 9, e88540.
Schwarz, J.M., Nugent, B.M., McCarthy, M.M., 2010. Developmental and hormone-induced epigenetic changes to estrogen and progesterone receptor genes in brain are dynamic across the life span. Endocrinology 151, 4871–4881.
Sharrow, K.M., Kumar, A., Foster, T.C., 2002. Calcineurin as a potential contributor in estradiol regulation of hippocampal synaptic function. Neuroscience 113, 89–97.
Tohgi, H., Utsugisawa, K., Yamagata, M., Yoshimura, M., 1995. Effects of age on messenger RNA expression of glucocorticoid, thyroid hormone, androgen, and estrogen receptors in postmortem human hippocampus. Brain Res. 700, 245–253.
Wang, Y.S., Chou, W.W., Chen, K.C., Cheng, H.Y., Lin, R.T., Juo, S.H., 2012. MicroRNA-152 mediates DNMT1-regulated DNA methylation in the estrogen receptor alpha gene. PLoS One 7, e30635.
Waters, E.M., Yildirim, M., Janssen, W.G., Lou, W.Y., McEwen, B.S., Morrison, J.H., Milner, T.A., 2011. Estrogen and aging affect the synaptic distribution of estrogen receptor beta-immunoreactivity in the CA1 region of female rat hippocampus. Brain Res. 1379, 86–97.
Westberry, J.M., Trout, A.L., Wilson, M.E., 2010. Epigenetic regulation of estrogen receptor alpha gene expression in the mouse cortex during early postnatal development. Endocrinology 151, 731–740.
Xu, X., 2015. DNA methylation and cognitive aging. Oncotarget 6, 13922–13932.
Yang, X., Phillips, D.L., Ferguson, A.T., Nelson, W.G., Herman, J.G., Davidson, N.E., 2001. Synergistic activation of functional estrogen receptor (ER)-alpha by DNA methyltransferase and histone deacetylase inhibition in human ER-alpha-negative breast cancer cells. Cancer Res. 61, 7025–7029.
Zeier, Z., Madorsky, I., Xu, Y., Ogle, W.O., Notterpek, L., Foster, T.C., 2011. Gene expression in the hippocampus: regionally specific effects of aging and caloric restriction. Mech. Ageing Dev. 132, 8–19.
Zhang, Q.G., Han, D., Wang, R.M., Dong, Y., Yang, F., Vadlamudi, R.K., Brann, D.W., 2011. C terminus of Hsc70-interacting protein (CHIP)-mediated degradation of hippocampal estrogen receptor-alpha and the critical period hypothesis of estrogen neuroprotection. Proc. Natl. Acad. Sci. U. S. A. 108, E617–E624.
Zhang, Q.G., Raz, L., Wang, R., Han, D., De Sevilla, L., Yang, F., Vadlamudi, R.K., Brann, D.W., 2009. Estrogen attenuates ischemic oxidative damage via an estrogen receptor alpha-mediated inhibition of NADPH oxidase activation. J. Neurosci. 29, 13823–13836.

Systems/Circuits

Movement Enhances the Nonlinearity of Hippocampal Theta

Alex Sheremet,[1] Sara N. Burke,[3,4] and Andrew P. Maurer[2,3]

[1]Engineering School of Sustainable Infrastructure and Environment (ESSIE) and [2]Department of Biomedical Engineering, University of Florida, Gainesville, Florida 32611, [3]Department of Neuroscience, McKnight Brain Institute, College of Medicine, University of Florida, Gainesville, Florida 32610, and [4]Institute of Aging, University of Florida, Gainesville, Florida 32603

The nonlinear, metastable dynamics of the brain are essential for large-scale integration of smaller components and for the rapid organization of neurons in support of behavior. Therefore, understanding the nonlinearity of the brain is paramount for understanding the relationship between brain dynamics and behavior. Explicit quantitative descriptions of the properties and consequences of nonlinear neural networks, however, are rare. Because the local field potential (LFP) reflects the total activity across a population of neurons, nonlinearites of the nervous system should be quantifiable by examining oscillatory structure. We used high-order spectral analysis of LFP recorded from the dorsal and intermediate regions of the rat hippocampus to show that the nonlinear character of the hippocampal theta rhythm is directly related to movement speed of the animal. In the time domain, nonlinearity is expressed as the development of skewness and asymmetry in the theta shape. In the spectral domain, nonlinear dynamics manifest as the development of a chain of harmonics statistically phase coupled to the theta oscillation. This evolution was modulated across hippocampal regions, being stronger in the dorsal CA1 relative to more intermediate areas. The intensity and timing of the spiking activity of pyramidal cells and interneurons was strongly correlated to theta nonlinearity. Because theta is known to propagate from dorsal to ventral regions of the hippocampus, these data suggest that the nonlinear character of theta decreases as it travels and supports a hypothesis that activity dissipates along the longitudinal axis of the hippocampus.

Key words: CA1; dorsoventral; oscillation; place cell; rat

Significance Statement

We describe the first explicit quantification regarding how behavior enhances the nonlinearity of the nervous system. Our findings demonstrate uniquely how theta changes with increasing speed due to the altered underlying neuronal dynamics and open new directions of research on the relationship between single-neuron activity and propagation of theta through the hippocampus. This work is significant because it will encourage others to consider the nonlinear nature of the nervous system and higher-order spectral analyses when examining oscillatory interactions.

Introduction

The nonlinear character of the brain (Buzsáki, 2006) has been recognized for >50 years (Ashby, 1947; Wiener, 1966) as the foundation of large-scale integration across local neuron structures (Steriade, 2001; Buzsáki and Draguhn, 2004) and for the metastable dynamics critical for rapid neuron organization in support of behavior (Engström et al., 1996; Friston, 1997; Tognoli and Kelso, 2014). Understanding brain nonlinearity is therefore fundamental for determining how brain dynamics translate to behavior (Hasselmo, 2015; Marder, 2015), yet quantitative descriptions of brain nonlinearity are scarce (Buzsáki, 2006). Using a thermodynamics analogy, "understanding the brain" can be achieved by describing either its microscopic states (complete description of the state of each neuron) or its macroscopic states (sets of "statistically equivalent" microscopic states). Although the former does not seem achievable (Marder, 2015), even with new high-density measures of real-time neural activity (Ziv et al., 2013), a macroscopic model of brain dynamics could be built on existing measurement techniques, such as the local-field potential (LFP). The LFP reflects the activity of a larger number of neurons (Buzsáki, 2002; Buzsáki et al., 2012; Schomburg et al., 2012), providing a macroscopic signature of microscopic activity.

Although the characteristics of the hippocampal LFP in relation to behavior are well documented (Buzsáki, 2005), its nonlin-

Received Sept. 24, 2015; revised Feb. 29, 2016; accepted March 2, 2016.

Author contributions: A.P.M. designed research; S.N.B. and A.P.M. performed research; A.S., S.N.B., and A.P.M. contributed unpublished reagents/analytic tools; A.S., S.N.B., and A.P.M. analyzed data; A.S., S.N.B., and A.P.M. wrote the paper.

This work was supported by the McKnight Brain Research Foundation, the University of Florida Research Seed Opportunity Fund, the Claude D. Pepper Older Americans Independence Center, and The National Institutes of Health (Grant R03AG049411). We thank the reviewers for their thoughtful comments in revision.

The authors declare no competing financial interests.

Correspondence should be addressed to Andrew P. Maurer, Department of Neuroscience, University of Florida College of Medicine, P.O. Box 100244, 1149 Newell Drive, McKnight Brain Institute, L1-100 Gainesville, FL 32610. E-mail: drewmaurer@ufl.edu.

DOI:10.1523/JNEUROSCI.3564-15.2016

Copyright © 2016 the authors 0270-6474/16/364218-13$15.00/0

earity has not been examined explicitly. The goal of the current investigation was to quantify the nonlinearity of the hippocampal theta rhythm in relation to movement. Theta is a dominant feature of hippocampal LFP commonly reported as a 4–12 Hz oscillation associated with active exploration and REM sleep (Jung and Kornmüller, 1938; Green and Arduini, 1954; Vanderwolf, 1969) that may serve to organize hippocampal neuron firing. During movement, principal cells of the hippocampus express spatial receptive fields (O'Keefe and Dostrovsky, 1971). As an animal passes through a neuron's place field, the spike timing systematically shifts to earlier phases of theta between adjacent cycles (O'Keefe and Recce, 1993). The rate at which this precession occurs varies along the longitudinal axis of the hippocampus (Maurer et al., 2005). Interestingly, differences between dorsal and more ventral regions of the hippocampus are also observed in theta amplitude and the firing rate of neurons, such that firing rates and theta power in intermediate CA1 show less velocity modulation than in dorsal CA1 (Maurer et al., 2005). This suggests that dynamic interactions between hippocampal neurons and LFP may reflect the behavioral state of an animal, but this varies according to longitudinal position.

In addition to amplitude, the shape of the theta wave is sensitive to movement, with a transition from a sinusoid to sawtooth shape at faster running speeds (Buzsáki et al., 1983; Terrazas et al., 2005). Moreover, a 16 Hz oscillation has been observed to develop as a function of velocity (Czurko et al., 1999; Terrazas et al., 2005), described as the second harmonic of theta (Harper, 1971; Coenen, 1975; Leung et al., 1982; Leung, 1982). The standard technique used to investigate theta, however, has typically been based on Fourier power-spectrum analysis. Because it ignores phases, this approach is fundamentally linear. Therefore, the nonlinear mechanisms underlying the relationship between the 16 Hz oscillation and the sawtooth shape of theta in relation to running speed (Skaggs, 1995) and dorsoventral position is not well understood.

The theta rhythm is also known to propagate along the hippocampal longitudinal axis (Lubenov and Siapas, 2009; Patel et al., 2012), losing amplitude as it moves into more ventral regions (Maurer et al., 2005; Royer et al., 2010). It is not known, however, how this relates to longitudinal differences in the modulation of neuron activity by velocity. To understand the nature of the sawtooth shape of theta and the 16 Hz frequency component in the hippocampus, we investigated the nonlinear character of the theta rhythm in the dorsal and intermediate regions of the hippocampal CA1 subregion. The nonlinearity was quantified in terms of phase coupling between different Fourier frequency bands that were estimated using third-order Fourier statistics.

Materials and Methods

Subjects and behavior. Neurophysiology data were obtained from three Brown Norway/Fisher-344 hybrid male rats between 8 and 12 months of age. The rats were housed individually and maintained on a 12 h light/dark cycle. Recordings took place during the dark phase of the cycle. Surgery was conducted according to the National Institutes of Health's guidelines for rodents and approved Institutional Animal Care and Use Committee protocols.

Before surgery, the animals were food deprived to 85% of their *ad libitum* weight. During this time period, the rats were trained to run on circular tracks for food reinforcement. Food was given on either side of the barrier and at the 180° opposite point. Rats ran for ~20 min, resulting in a variable number of laps per session depending on motivation and other factors. Each track running session was flanked by a rest period in which the rat rested in a towel lined pot located near the track. For the present analyses, only data obtained during running conditions are presented.

Surgical procedures. Neuronal recordings were made in the dorsal and intermediate CA1 subregion of the hippocampus. Before surgery, rats were administered ampicillin (Bicillin; Wyeth Laboratories; 30,000 U, i.m., in each hindlimb). The rats were implanted, under isofluorane anesthesia, with an array of 14 separately movable microdrives ("hyperdrive"). This device, implantation methods, and the parallel recording technique have been described in detail previously (Gothard et al., 1996). Briefly, each microdrive consisted of a drive screw coupled by a nut to a guide cannula. Twelve guide cannulae contained tetrodes (McNaughton et al., 1983; Recce and O'Keefe, 1989), four-channel electrodes constructed by twisting together four strands of insulated 13 μm nichrome wire (H.P. Reid). Two additional tetrodes with their individual wires shorted together served as an indifferent reference and an EEG recording probe. A full turn of the screw advanced the tetrode 318 μm.

For 1 rat, the tetrodes were divided into 2 groups of 7 ("split bundle drive"), permitting recording simultaneously from the septal (3.0 mm posterior, 1.8 mm lateral to bregma) and middle (6 mm posterior, 5.0 mm lateral to bregma) regions of the hippocampus. For the other 2 rats, recordings were made sequentially, first from the intermediate (5.7 mm posterior, 5.0 mm lateral to bregma). After intermediate recordings were completed, the implant was removed. Rats were then implanted with a new array in dorsal/septal (3.0 mm posterior, 1.4 mm lateral to bregma) regions. In all cases, the implant was cemented in place with dental acrylic anchored by dental screws. A ground lead was connected to one of the jeweler's screws placed in the skull. After surgery, rats were orally administered 26 mg of acetaminophen (Children's Tylenol *Elixir; McNeil). They also received 2.7 mg/ml acetaminophen in the drinking water for 1–3 d after surgery and oral ampicillin (Bicillin; Wyeth Laboratories) on a 10 d on/10 d off regimen for the duration of the experiment. Data from these animals have been used in other unrelated analyses that have been published previously (Maurer et al., 2005; Maurer et al., 2006a, 2006b; Maurer et al., 2012), drawing from a database of ~900 well isolated pyramidal neurons.

Electrophysiological recording. Twelve tetrodes were lowered after surgery into the hippocampus, allowed to stabilize for several days just above the CA1 hippocampal subregion, and then gradually advanced into the CA1 stratum pyramidale. Another probe was used as a neutral reference electrode and was located in or near the corpus callosum. The final probe was used to record theta field activity from the vicinity of the hippocampal fissure. Each tetrode was attached to four separate channels of a 50-channel unity-gain head stage (Neuralynx). A multiwire cable connected the head stage to digitally programmable amplifiers (Neuralynx). The spike signals were amplified by a factor of 1000–5000, band-pass filtered between 600 and 6 kHz, and transmitted to the Cheetah Data Acquisition system (Neuralynx). Signals were digitized at 32 kHz and events that reached a predetermined threshold were recorded for a duration of 1 ms. Spikes were sorted offline on the basis of the amplitude and principal components from the four tetrode channels by means of a semiautomatic clustering algorithm (BBClust; P. Lipa, University of Arizona, Tucson, AZ, and KlustaKwik; K.D. Harris, Rutgers University, Newark, NJ). The resulting classification was corrected and refined manually with custom-written software (MClust; A.D. Redish, University of Minnesota, Minneapolis, MN), resulting in a spike-train time series for each of the well isolated cells. No attempt was made to match cells from one daily session to the next, so the numbers of recorded cells reported does not take into account possible recordings from the same cells on consecutive days. However, because the electrode positions were adjusted from one day to the next, recordings from the same cell over days were probably relatively infrequent. Putative pyramidal neurons were identified by means of the standard parameters of firing rate, burstiness, spike waveform shape characteristics (Ranck, 1973), and the first moment of the autocorrelation (Csicsvari et al., 1998).

Theta activity in the CA1 layer was taken from the tetrode that collected the most pyramidal neurons while the fissure LFP was recorded from a separate probe that was positioned 0.5 mm below the CA1 pyramidal layer. LFP signals were band-pass filtered between 1 and 300 Hz and sampled at 2.4 kHz, amplified on the head stage with unity gain, and

then amplified again with variable gain amplifiers (up to 5000). Several light-emitting diodes were mounted on the head stage to allow position tracking. The position of the diode array was detected by a television camera placed directly above the experimental apparatus and recorded with a sampling frequency of 60 Hz. The sampling resolution was such that a pixel was 0.3 cm.

Time-series analysis. Throughout the current study, the phrase "time series" will be used in its traditional sense of a sequence of unprocessed measurements (numbers) indexed in time, synonymous to raw, unfiltered voltage traces of the EEG. This study assumes that EEG time series express essential properties of the underlying physical processes of the brain; that is, the physiological interactions contributing to the extracellular transmembrane currents. In principle, these processes could be represented using a mathematical formalism that uses a set of differential equations to describe their time evolution. The term "system" will therefore be used as it is in "dynamical systems" theory, to denote the differential equations that describe the brain processes and the time evolution of their solutions. Therefore, "system" can be thought of as a mathematical abstraction completely describing the brain processes.

In the mathematical description introduced above, EEGs are functions of, and carry information about, the state of the underlying system. The central focus of this study is the nonlinear character of the system and the central observation that the nonlinearity of the brain is reflected in the EEG time series. If the system is linear, then known solutions can be added to construct new solutions; that is, the solution space is a linear space. Under quite general uniformity conditions, sinusoids form a basis of the solution space, the Fourier basis. The general solution is a superposition of sinusoids with different amplitudes (which include the initial phase) and thus completely defined by the distribution of amplitudes. The stochastic general solution is a superposition of sinusoids with random amplitudes. The joint probability density of the amplitude set defined completely the statistics of the solution. Therefore, the geometry of the solution space of a linear system is trivial: any point in the space spanned by the Fourier basis is a solution to the system and the general solution is completely characterized by the projections on the elements of the basis (amplitudes).

In contrast, in the case of nonlinear systems, two solutions cannot be added to construct a new solution, which makes them rather intractable unless some simplifying assumptions can be made. Our central assumption is that the brain is a weakly nonlinear system and, for weakly nonlinear systems, the general solution can still be represented, in the leading order, as a superposition of sinusoids. However, the amplitudes cannot be constant (otherwise, the system would be linear) and therefore have to evolve. Indeed, decomposition on a linear basis (e.g., the Fourier one) yields a system of equations that describes the evolution of amplitudes through mutual interactions.

The geometry of the nonlinear solution space becomes nontrivial: a general solution is a trajectory in the space spanned by the Fourier basis. The stochastic solution will therefore be characterized by statistically correlated amplitudes and phases. Phase correlations are expressed in the peculiar appearance of the shape of the solution, for example, in the development of time series asymmetries. It follows that such a solution is not completely defined by its power spectrum and knowledge about the phase correlations is essential.

The analysis of the theta spectral band EEG time series used in the current study was based on standard techniques used for stationary signals (Priestley, 1981; Papoulis and Pillai, 2002). We assume that the EEG time series $g(t)$ is a stochastic process, stationary in the relevant statistics, and decompose it using the discrete Fourier transform (DFT) as follows:

$$g_j = \frac{1}{N}\sum_{n=1}^{N} G_n \, exp(2\pi f_n t_j);\; G_n = \sum_{j=1}^{N} g_j \, exp(-2\pi f_n t_j); \qquad (1)$$

Where $g_j = g(t_j)$ is a sequence of N points collected at times $t_j = j\Delta t$, with $j = 1, 2, \ldots, N$, Δt is the sampling interval, and $G_n = G(f_n)$ is the sequence of complex Fourier coefficients corresponding to the following frequencies:

$$f_n = \frac{n}{N\Delta t}, \text{ with } n = 1, 2, \ldots, N. \qquad (2)$$

The family of sequences $s_n(t_j) = exp(-2\pi f_n t_j)$ form the Fourier basis, also called modes. The second-order (linear) statistics of the Fourier spectrum of time series g are characterized by the spectral density as follows:

$$S_n = S(f_n) = \mathbf{E}[G_n G_n^*] \qquad (3)$$

Where G_n is the series of complex Fourier coefficients of process g, f_n is a frequency band in the Fourier representation (Eq. 2), and $\mathbf{E}[\ldots]$ is the expected-value operator. Spectral densities describe the frequency distribution of variance. If the process g is linear, it is completely characterized by its variance and consequently its variance density S_n. A realization of the process can be derived by assigning a set of random phases (uniformly distributed in $[-\pi, \pi]$) to modal amplitudes defined e.g., as $\sqrt{(S_n)}/2$. Note that the spectral density contains no information about phases, their correlation, and, therefore, about the nonlinearity of the process.

The nonlinear character of the system, expressed in phase correlations across spectral components, is described in the lowest order by the bispectrum, first proposed for ocean waves by Hasselmann et al. (1963) and further developed by Rosenblatt and Van Ness (1965) and others (Kim and Powers, 1979; Masuda and Kuo, 1981; Elgar, 1987), as follows:

$$B_{n,m} = B(f_n, f_m) = \mathbf{E}[G_n G_m G_{m+n}^*], \qquad (4)$$

Where f_n and f_m are two frequencies in the Fourier sequence in Equation 2. In other words, in this notation, f_n and f_m are waves of different frequencies. When the bispectrum is derived from a single time series, the result is described as the auto-bicoherence (simply referred to as bicoherence in the present study). The bispectrum is statistically zero if the Fourier coefficients are mutually independent; that is, for a linear system. For nonlinear systems, the bispectrum will exhibit peaks at triads (f_n, f_m, f_{n+m}) that are phase correlated, measuring the degree of three-wave coupling. The real and imaginary part of the bispectrum B provide measures of third-order statistics (Masuda and Kuo, 1981; Elgar, 1987), as follows:

$$\sigma^{-3}\sum_{n,m} B_{n,m} = \zeta + iA \qquad (5)$$

Where ζ is the skewness and A is the asymmetry of the process (Haubrich and MacKenzie, 1965; Masuda and Kuo, 1981) and σ is its SD, with the sign of ζ and A ($\pm$) indicating the direction of the skew or asymmetry. Both ζ and A are "global" measures of the nonlinearity of the process (Fourier modes obviously have zero skewness and asymmetry). Meaningful skewness/asymmetry estimates can be defined for a frequency band only if it is wide enough (see below) to contain all of the relevant phase-coupled modes.

To eliminate the distortion induced by the variance distribution, the bispectrum can be normalized (Haubrich and MacKenzie, 1965) as follows:

$$b_{n,m} = \frac{B_{n,m}}{\left(\mathbf{E}\left[\left|G_n G_m\right|^2\right]\mathbf{E}\left[\left|G_{n+m}\right|^2\right]\right)^{1/2}}. \qquad (6)$$

The squared modulus and the phase of the normalized bispectrum are called bicoherence and biphase. Although definition 5 does not insure that $|b_{n,m}| < 1$ (see, e.g., Kim and Powers, 1979; Elgar and Guza, 1985), it was adopted here for its simplicity and ease of implementation. Equation 4 implies that the real and imaginary part of the normalized bispectrum can be interpreted as the "frequency distribution" of skewness and asymmetry. In the sequel, we will refer to the real and imaginary parts of the normalized bispectrum as skewness and asymmetry distributions as follows:

$$\zeta_{n,m} = \mathbf{R}\{b_{n,m}\};\; A_{n,m} = \mathbf{I}\{b_{n,m}\}, \qquad (7)$$

Where $\mathbf{R}\{z\}$ and $\mathbf{I}\{z\}$ are the real and imaginary parts of the complex number z, respectively.

The bispectrum (and thus the normalized bispectrum) has well known symmetries with respect to its arguments (Rosenblatt and Van Ness,

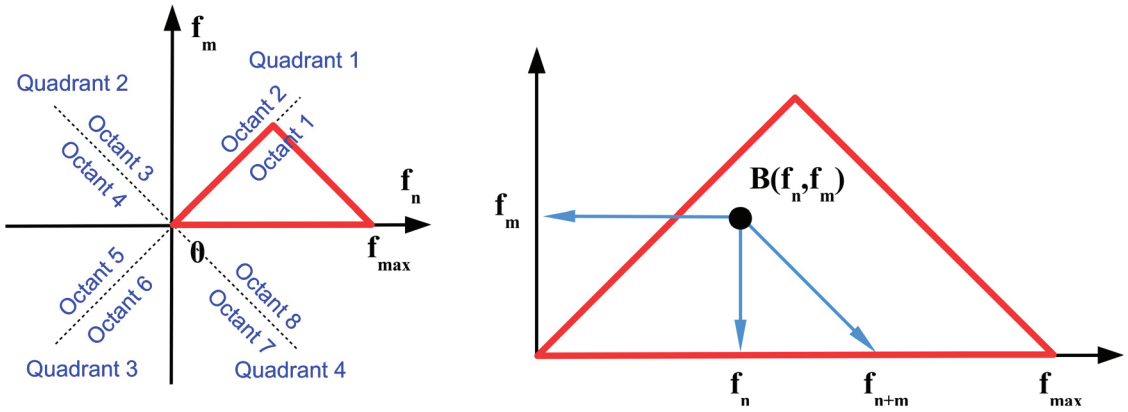

Figure 1. Bispectral symmetries (see Eq. 7–9). Left, Quadrant and octants of the frequency plane. Red triangle represents the area containing nonredundant information for the DFT. Right, Peak in the bispectral estimate (represented by the black dot) represents a phase-coupled triplet (f_n, f_m, f_{n+m}), where f_n, f_m are two frequencies in the Fourier representation sequence defined in Equation 1. If a bispectral peak (black dot) is on the first diagonal, then $m = n$, meaning that frequency f_n is phase correlated to its second harmonic $f_{2n} = 2f_n$.

1965; Fig. 1), which is equivalent to saying that different regions in the plane spanned by (f_n, f_m) contain equivalent (redundant) bispectral information, as follows:

$$B(-f_n, -f_m) = B^*(f_n, f_m) \quad \text{Quadrants } 1-3 \text{ and } 2-4 \text{ are equivalent.} \tag{8}$$

$$B(f_m, f_n) = B(f_n, f_m) \quad \text{Octants } 1-2 \text{ are equivalent.} \tag{9}$$

$$B(f_n, f_m) = B^*(f_n, -f_m, f_m) \quad \text{Octants } 1-8 \text{ and } 2-7 \text{ are equivalent.} \tag{10}$$

From rules 8–10, it follows that the first octant of the plane (f_n, f_m) contains all nonredundant bispectral information. For the DFT, the nonredundant domain reduces to a segment of the first octant bounded by a line parallel to the second diagonal passing through the maximum (Nyquist) frequency. The nonredundant domain in the (f_n, f_m) plane is illustrated in Figure 1. The figure contains a basic, minimal receipt for understanding bispectral distributions. At any point in the (f_n, f_m) plane, the value of the bispectrum $B(f_n, f_m)$ represents the phase correlation between the Fourier modes with frequencies f_n, f_m, and $f_{n+m} = f_n + f_m$,. In other words, the triad contains the two coordinates of the point and the frequency defined by the intersection of the second diagonal with the horizontal axis.

Implementation of bispectral analysis. To estimate second-order Fourier statistics, the time series were de-meaned, linearly de-trended, and divided into 50% overlapping segments of ~4 s windows (2^{13}-point windows for the sampling rate $f_s = 1988$ Hz for rats 7951 and 8042; 214 for $f_s = 936$ Hz for rat 7805), with a frequency resolution of $\sim\Delta f = 0.25$ Hz. The total time intervals for analysis were chosen so as to yield a number of degrees of freedom (DOF) >170 for all data analyzed and DOF = 300 for the data presented. The statistics of the bispectrum of stationary processes are well understood (Haubrich and MacKenzie, 1965; Elgar and Guza, 1985; Elgar and Sebert, 1989; and many others). Briefly, for the normalization used here (Eq. 6), the probability density function (PDF) is approximated by the noncentral χ^2 distribution, where $|b|^2$ is the mean value of the bicoherence, and the parameters n and α are given by the following (equations 6–8 in Elgar and Sebert, 1989).

$$f\left(\frac{|b|^2}{\alpha}\right) \approx \chi^2(|b|^2, n) \quad \text{with } n = \frac{DOF\,|b|^2}{2(1-|b|^2)^3}, \text{ and } \alpha = \frac{|b|^2}{n} \tag{11}$$

Knowledge of the theoretical PDF allows for estimating confidence limits for any mean value of the bicoherence. Because zero mean that bicoherence is meaningful for distinguishing between linear and nonlinear stochastic processes, an important consequence of the above discussion is that the zero-mean bicoherence is χ^2 distributed with $n = 2$. From this, a confidence level can be derived. With DOF = 300, the zero-mean bicoherence $|b| < 0.05$ at 90% confidence level and bicoherence $|b| < 0.1$ at 95%. This is consistent with Elgar and Guza's (1985) estimate of $|b| < \sqrt{\frac{6}{DOF}} \approx 0.15$ at 99% (Haubrich and MacKenzie, 1965 gives this relation for a different bispectral normalization and for the confidence level of 95%).

The time–frequency representation (windowed Fourier transform; Mallat, 1999) was used to represent the time evolution of the EEG frequency content (2^{12}-point window at 90% overlap). Bispectral analysis was used to examine the nonlinearity of the EEG time series and was implemented using a lower-frequency resolution and increased DOF by using 210-point windows (0.5 s) segments.

To compare the nonlinear character of theta across hippocampal regions and velocity conditions, we defined a global nonlinearity measure as the square root of the bicoherence integrated over the frequency domain (Sheremet et al., 2002), as follows:

$$\phi = \left[\sum_{n,m=1}^{n} 8\left|\bar{b}_{n,m}\right|^2 \Delta f^2 \left(1 - \frac{1}{2}\delta_{n,m}\right)\right]^{\frac{1}{2}} \tag{12}$$

where

$$\bar{b}_{n,m} = \begin{cases} b_{n,m} & \text{if } b_{n,m} > 0.1 \\ 0 & \text{otherwise} \end{cases} \tag{13}$$

The value 0.1 is the 95% confidence level of $|\bar{b}_{n,m}| = 0$, where $|b_{n,m}|$ is the normalized bispectrum matrix (Eq. 6); $\Delta f = \frac{1}{N\Delta t}$ is the frequency increment, δ is the Kronecker symbol, as in the following:

$$\delta_{n,m} = \begin{cases} 1 & \text{if } n = m \\ 0 & \text{otherwise} \end{cases}, \tag{14}$$

and the rest of the symbols have the same meaning as in Equation 6. The measure φ is proportional to the Euclidean norm of the matrix $|b_{n,m}|$, where the coefficient $\left(1 - \frac{1}{2}\delta_{n,m}\right)$ accounts for the symmetries of $b_{n,m}$, that is, for the diagonal appearing only four times in the full matrix.

All calculations were coded in MATLAB using its implementation of the DFT. The bispectral estimates were computed using code based on modified functions of the HOSA toolbox (Swami et al., 2000).

Spike spectrogram. To determine the frequency in which neuronal spiking occurred, we implemented spectral analyses on spike trains (Leung and Buzsáki, 1983). First, action potentials were sorted based upon the velocity of the rat. Spikes between either 10–20 cm/s or 60–70

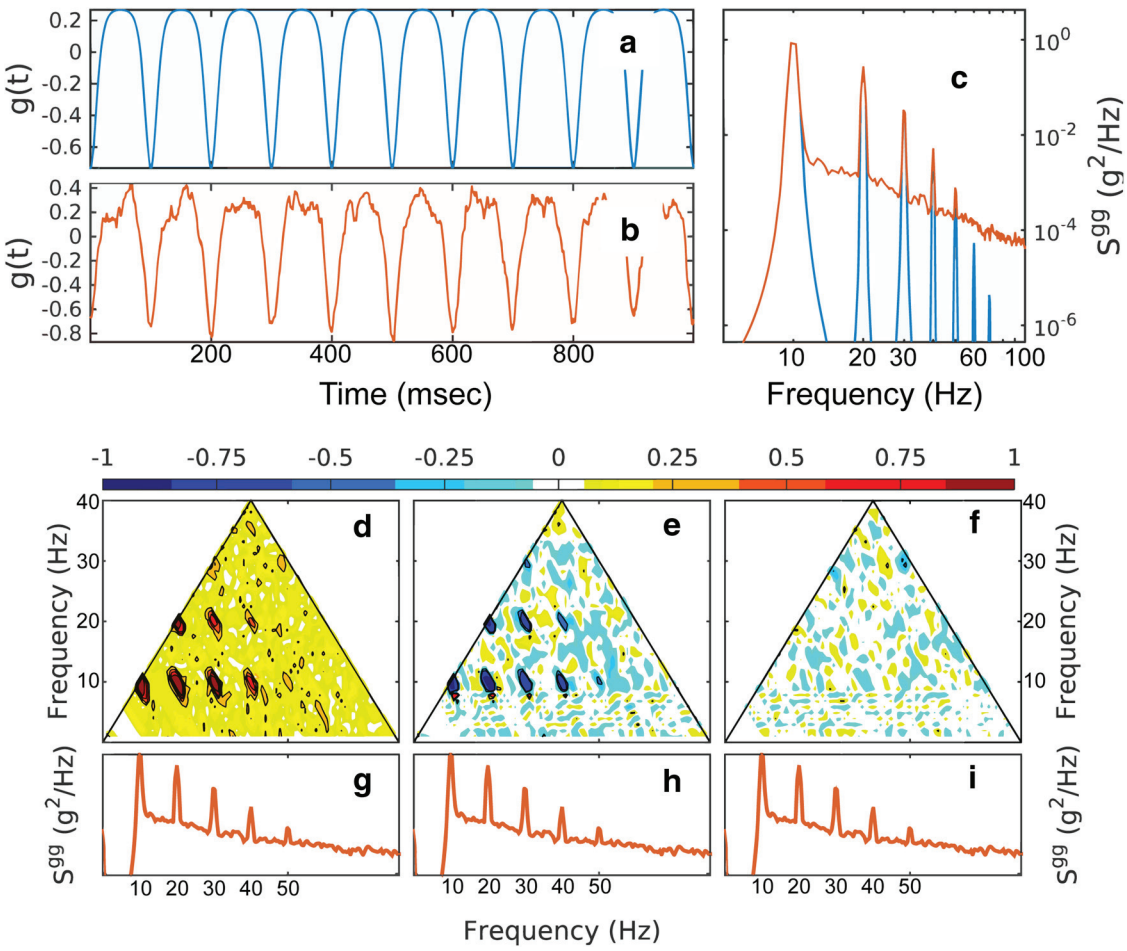

Figure 2. Bispectral analysis of a noisy time series with negative skewness. ***a***, Signal based on a cnoidal function. ***b***, Signal with added f^{-2} Gaussian noise with at 20% signal variance. ***c***, Spectra of the two time series. ***d–f***, Normalized bispectrum of the noisy time series depicting the modulus (***d***), the real part (***e***; skewness distribution), and the imaginary part (***f***; asymmetry distribution). The power spectra of the signal with added f^{-2} Gaussian noise are repeated in ***g–i*** for reference.

cm/s were analyzed separately, placing the spikes for each velocity segment into 1 ms bins for the duration of the recording. This often resulted in a sparse, but periodic vector of spike counts. The power spectra of the spike trains were then calculated via the Thomson multitaper method.

Results

Simplified nonlinear EEG model

Here, we constructed a simplified model that illustrates the bispectral signature of stochastic processes with measurable global skewness and asymmetry. The model consists of two nonlinear time series (Figs. 2, 3) constructed using periodic analytical functions (period 1 s) based on elliptic Jacobi functions (Whitham, 2011) deformed to have controllable asymmetry (Figs. 2*a*, 3*a*). The process analyzed in Figure 2 has negative skewness and zero asymmetry; the process analyzed in Figure 3 has zero skewness and positive asymmetry (Figs. 2*a*, 3*a*). For a realistic aspect, a Gaussian noise process with a spectral law of f^{-2} (Figs. 2*b*,*c*, 3*b*,*c*) is added to the analytic functions. The spectra of the time series (both analytic and "noisified") exhibit peaks at the harmonics of the fundamental frequency of 10 Hz. Note that the DOF values for the model are arbitrary, so the statistics of the processes represented in Figures 2, 3, and 4 are arbitrarily close to the theoretical ones.

Different components of the bispectrum of the noisified time series are shown in Figures 2*d–f*, 3*d–f*, and 4*d–f*. The modulus of the normalized bispectrum (Eq. 6, Fig. 2*d*, 3*d*) exhibits seven, but potentially more, distinct peaks. Based on the diagram in Figure 1, these indicate the frequency triplets that are strongly phase coupled. One can distinguish coupling up to the sixth harmonic of the peak: (f_p, f_p, $2f_p$), (f_p, $2f_p$, $3f_p$), (f_p, $3f_p$, $4f_p$), (f_p, $4f_p$, $5f_p$), ($2f_p$, $2f_p$, $4f_p$), ($2f_p$, $3f_p$, $5f_p$), ($2f_p$, $4f_p$, $6f_p$), as well as ($3f_p$, $3f_p$, $6f_p$). For the first nonlinear time series (Fig. 2), the skewness distribution γ (real part of the normalized bispectrum, Eq. 6, Figs 2*e*, 3*e*) shows the same peaks, but negative, in accordance with the global skewness of the time series. Because the time series has no asymmetry, the asymmetry distribution α is statistically zero (Fig. 2*f*). Alternatively, for the nonskewed but asymmetric time series (Fig. 3), the skewness distribution is statistically zero (Fig. 3*e*), but the asymmetry distribution is positive (Fig. 3*f*).

The contrast spectral and bispectral analysis and the effectiveness of the bispectral components in detecting nonlinearity is illustrated in Figure 4. Here, a linear time series is constructed by assigning Fourier modes random phases uniformly distributed in $[-\pi,\pi]$ to amplitudes derived from the spectral density of the negatively skewed, symmetric time series (Fig. 2*b*), as described above. Importantly, a simple spectral density analysis does not distinguish between the linear and the nonlinear time series because these two oscillations have the same spectral density characteristics (Fig. 4*c*). This illustrates the point that spectral density estimators contain no information about phase correlation across the spectrum, and thus no information about the nonlin-

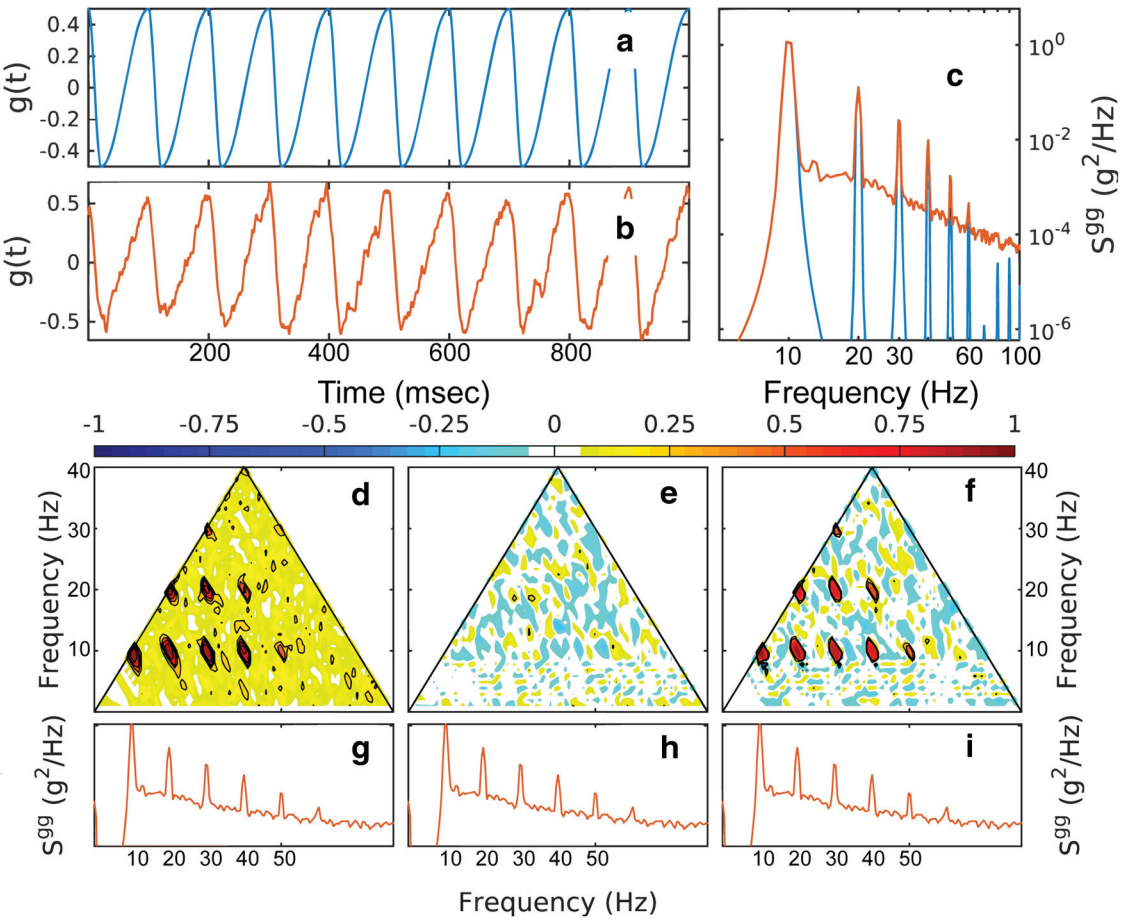

Figure 3. Bispectral analysis of a noisy time series with positive asymmetry. ***a***, Signal based on a sinusoidal function. ***b***, Signal with added f^{-2} Gaussian noise with at 20% signal variance. ***c***, Spectra of the two time series. ***d–f***, Normalized bispectrum of the noisy time series depicting the modulus (***d***), the real part (***e***; skewness distribution, and the imaginary part (***f***; asymmetry distribution). The power spectra of the signal with added f^{-2} Gaussian noise are repeated in ***g–i*** for reference.

ear character of the process. Bispectral analysis (cf. Figs. 2*d–f*, 4*d–f*), however, reveals clearly the linear character of the linear time series in Figure 4*b*. The normalized bispectrum and all of its components are statistically zero.

This simple example makes several points: (1) the bispectrum can identify phase coupling, (2) the different components of the bispectrum are useful to identify the effect of the phase coupling on the skewness and asymmetry of the process, and (3) the presence of phase coupling can be detected even in the presence of Gaussian noise and below the noise level. Finally, this analysis suggests a more general meaning for the concept of harmonics. Harmonics can be defined in several ways. A mode G_{kn} with frequency $f_{kn} = kf_n$, with k integer, is called the kth harmonic of mode Gn. This definition is trivial and not useful: because spectral estimates are never exactly zero at any frequency, such harmonics always exist but have no statistical relationship with the mode G_n. It is tempting to describe spectral distributions such as that in Figure 3 as fundamental frequency and its harmonics.

The inability of the spectral density estimators to distinguish between linear and nonlinear systems makes another important point: the presence of peaks in spectral densities at multiples of a given frequency (harmonics) might have different meanings. For linear systems, harmonics are statistically independent and their presence does not modify the statistics of the process. For nonlinear systems, the presence of harmonics might be accompanied by phase correlations that have significant and fundamental effects on the shape and statistics of the process.

Based on this discussion, hereafter, we reserve the term "harmonic" only for cases in which there is a phase correlation between the harmonics and the fundamental frequency (mode). The determination of whether certain modes are or not harmonics of a spectral peak has to involve an examination of the bispectral characteristics.

Relation between theta and velocity in EEG measured in the dorsal and intermediate CA1

An examination of LFP time series showed obvious changes in the shape of the hippocampal theta (Fig. 5), in agreement with previous studies (Harper, 1971; Coenen, 1975; Leung et al., 1982; Leung, 1982; Terrazas et al., 2005). The unfiltered LFP trace was well approximated by a near-sinusoidal 6–8 Hz band-pass signal for running speeds <20 cm/s (Fig. 5*a*,*c*). At running speeds >20 cm/s (Fig. 5*b*), the dorsal LFP trace became asymmetric and skewed, departing significantly from the 6–8 Hz signal. Note that the departure of the raw LFP from the 6–8 Hz filter was attenuated in the intermediate hippocampus, even at fast running speeds (Fig. 5*d*). These data suggest the development of cycle skew and asymmetry may be associated with the 16 Hz frequency noted in prior investigations.

Velocity and the CA1 spectrogram

To examine the effect of running speed on the LFP, the average shape of the power spectrogram as a function of running speed was calculated (Fig. 6). At low speeds, the 4–60 Hz frequency

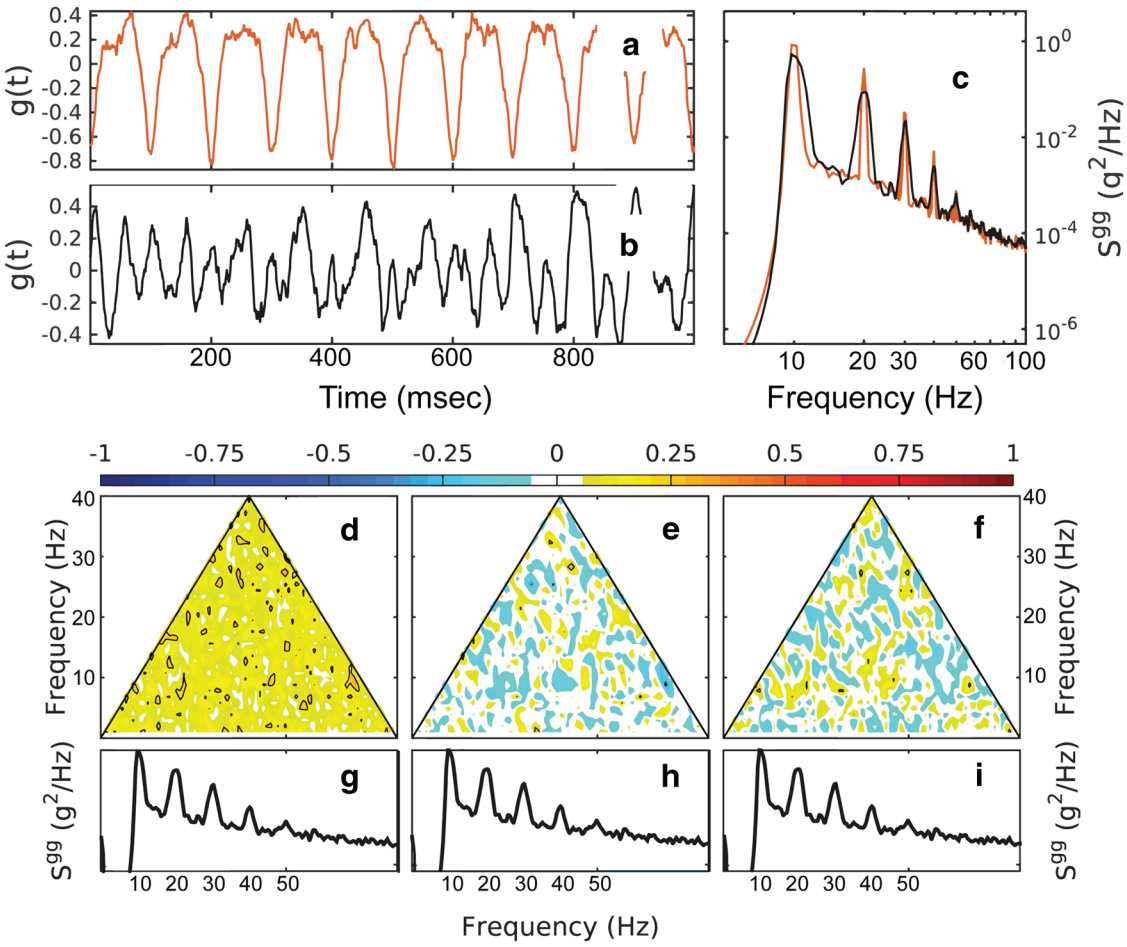

Figure 4. Bispectral analysis of a linear and nonlinear time series. ***a***, ***b***, Nonlinear signal (***a***; red) and linear signal (***b***; black) constructed from the spectrum of the nonlinear signal using random phases uniformly distributed in [0, 2π]. ***c***, Spectra of the nonlinear and linear time series (red and black, respectively). ***d***–***f***, Normalized bispectrum of the linear time series (cf. Figs. 2, 3) for the modulus (***d***), the real part (***e***; skewness distribution), and imaginary part (***f***; asymmetry distribution). The power spectra of the linear decomposition are repeated in ***g***–***i*** for reference.

band was dominated by a single spectral peak located approximately between 6 and 7 Hz (Fig. 6*a*–*d*). As the speed increased, the peak quickly narrowed, became more prominent, and shifted toward 8 Hz while additional peaks developed at frequencies $n f_\theta$ ($n > 1$ integer) where $f_\theta = 8$ Hz. For simplicity, we will call the $n f_\theta$ peaks putative theta "harmonics" (see simulation above). The dominance of the putative harmonics increased with movement speed at the expense of the bands separating them. This effect was more pronounced in the dorsal region of the hippocampus, where harmonics could be identified up to $n = 6$ (Fig. 6*a*,*b*), whereas the intermediate region developed no more than $n = 2$ (Fig. 6*c*,*d*).

Phase dependence of spectral peaks

The development of spectral peaks in the 16 Hz range and higher have considerable overlap with beta (10–30 Hz) (Penttonen and Buzsáki, 2003) and low-gamma (25–50 Hz) (Colgin et al., 2009; Belluscio et al., 2012). Therefore, the development of higher frequencies at faster velocities may be due to the appearance of rhythms other than the evolution of theta harmonics. Beta and low-gamma, however, are meaningful as distinct rhythms only if they are statistically independent of the theta rhythm. Therefore, the identity of harmonics can be tested simply by checking their statistical relation to theta. In the lowest order, this can be achieved by using bispectral analysis. Compared with other methods for examining frequency coupling between two different frequencies (Lachaux et al., 1999), this approach has the advantage that it provides direct measures of phase coupling between Fourier frequency bands with no *a priori* (arbitrary) band identification (filtering). Bispectrum components provide complementary information about the stochastic process analyzed. The absolute value of the normalized bispectrum (bicoherence; Fig. 2) is a measure of the nonlinearity of the signal and is statistically zero for independent frequency bands (stochastic process with uncorrelated phases). The real and imaginary parts provide measures of the contribution of different bands to the skewness (Fig. 3) and asymmetry (Fig. 4) of the total signal. For low-velocity conditions (Fig. 7*a*), dorsal CA1 bicoherence estimates (Fig. 7*a*,*d*) were statistically zero over the entire Fourier space (no phase correlation). This implies that the asymmetry and skewness measures were also statistically zero (Fig. 7*b*,*c*). That is, the LFP process was nearly sinusoidal. This agreed with the general aspect of the trace (Fig. 5*a*,*c*). In contrast, bispectral measures estimated for high-velocity conditions exhibited a distinct pattern of peaks, coinciding with the location and development of the harmonics (see Fig. 1 for instructions on how to read the plots). The bicoherence showed significant phase coupling between theta and the harmonics, with correlations distinguishable for up to the sixth harmonic in dorsal CA1. The bicoherence peaks were reproduced in the skewness and asymmetry distributions shown in Fig. 7, *e* and *f*, where the negative sign indicates the type of skewness and asymmetry produced by the peaks. Remark-

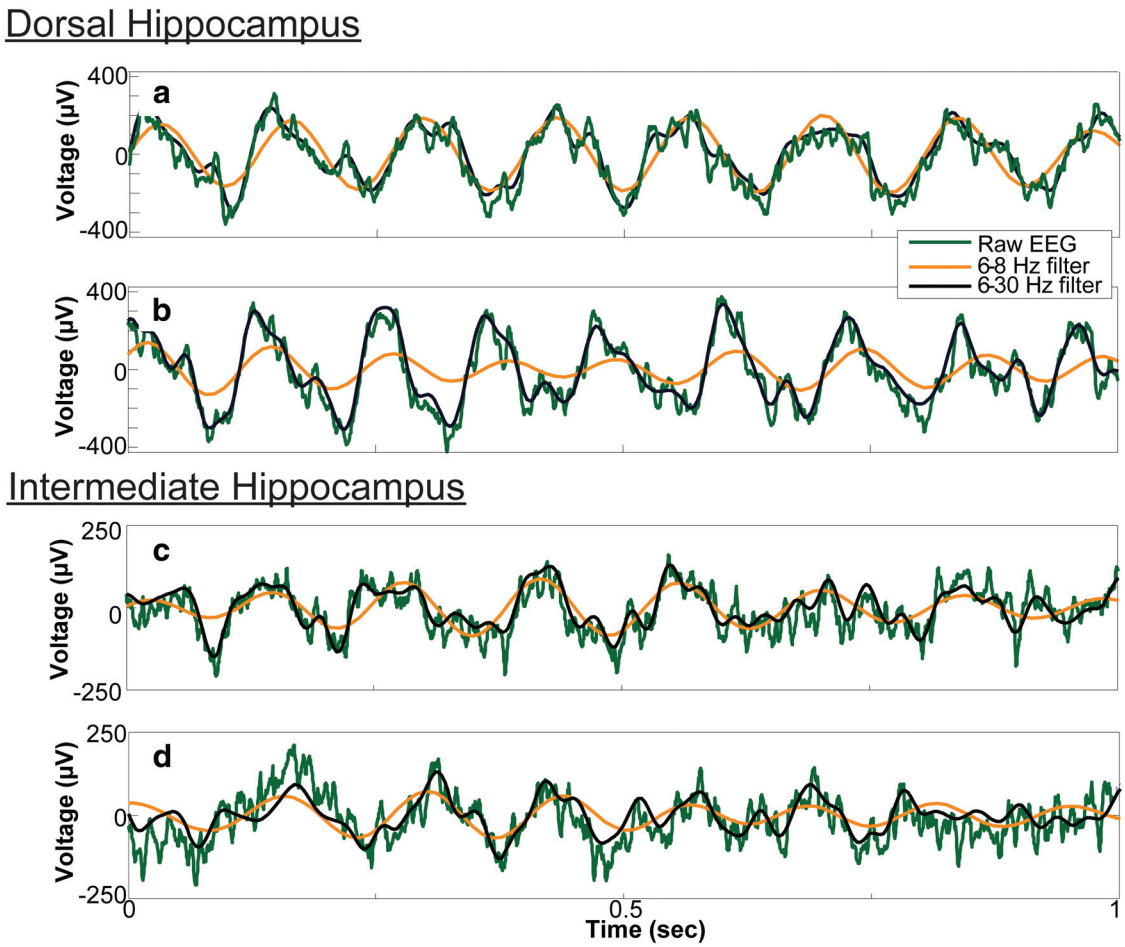

Figure 5. Change of LFP shape as a function of rat running speed. Representative examples of LFP during low running speeds (<20 cm/s; ***a***, ***c***) and high running speeds (>20 cm/s; ***b***, ***d***) showing the raw data (green), narrow filter (orange), and wide-band filter (black) that captures the asymmetry that developed as a function of running velocity in the dorsal hippocampus.

ably, the nonlinearity of theta was modulated across the hippocampal regions. The same analysis performed for intermediate CA1 (Fig. 7*j–r*) exhibited weaker nonlinearity, with coupling only between theta and the second harmonic clearly distinguishable.

To compare the magnitude of the EEG nonlinearity across hippocampal regions and velocity conditions directly, the mean global nonlinearity measure (Eq. 12–14) for each rat in the dorsal and intermediate hippocampus for the low and high velocities was calculated. Figure 8 illustrates the effects of speed on theta nonlinearity for the three rats tested. The nonlinearity measure φ is consistently higher for higher speeds, with the nonlinearity of the dorsal CA1 region dominating the nonlinearity of the intermediate CA1 region. This comparison revealed that there was a significant main effect of hippocampal region ($F_{(1,4)} = 30.6$, $p < 0.01$; repeated measures) on the magnitude of the nonlinearity such that the EEG in the dorsal hippocampus was more nonlinear than the intermediate. Although there was no overall main effect of velocity (low vs high) on nonlinearity ($F_{(1,4)} = 5.9$, $p = 0.08$; repeated measures), the interaction between hippocampal region and velocity was significant ($F_{(1,4)} = 9.1$, $p < 0.05$; repeated measures). *Post hoc* analysis indicated that this interaction effect was due to a significant difference in EEG nonlinearity across velocity conditions in the dorsal hippocampus ($p < 0.05$), but not in the intermediate hippocampus ($p = 0.2$). Together, these data indicate that EEG in the dorsal hippocampus is more nonlinear and more sensitive to changes in speed of movement relative to the intermediate hippocampus.

Neuronal activity and theta nonlinearity

Because theta has been hypothesized to organize spike timing of neurons (O'Keefe and Recce, 1993; Lisman and Idiart, 1995; Skaggs et al., 1996; Harris et al., 2003), we examined action potential frequency as a function of velocity for single cells in dorsal and intermediate CA1 using spectral density estimates (Fig. 9). The spectral power of spiking in the theta band demonstrated that dorsal neurons were sensitive to changes in velocity. There was a significant increase in both frequency ($t_{(5)} = 7.75$, $p < 0.001$) and amplitude ($t_{(5)} = 3.58$, $p < 0.02$) between slow and fast velocities, which is consistent with a previous report (Geisler et al., 2010). This was not the case in the intermediate hippocampus, in which neither the frequency ($t_{(5)} = 0.48$, $p = 0.66$) nor the amplitude ($t_{(5)} = 1.12$, $p < 0.33$) was significantly affected by velocity. Second harmonic peaks were seen to develop for the pyramidal cell action potential spectrograms in the dorsal and intermediate region of the hippocampus, but not for the interneurons. The arrows in Figure 9 indicate a second harmonic peak that is significantly different from 0 ($p < 0.05$ for both comparisons) for the pyramidal cell spike spectrogram in high-velocity conditions only. Given the appearance of harmonics exclusively in principal neurons, it suggests that harmonic activity may be related to rebound activity after inhibition (Cobb et al., 1995; Diba et al., 2014). Specifically, velocity-dependent increases of interneuron activity may invoke rebound excitation, leading to pyramidal cells firing two distinct bursts within a single theta cycle (see Discussion).

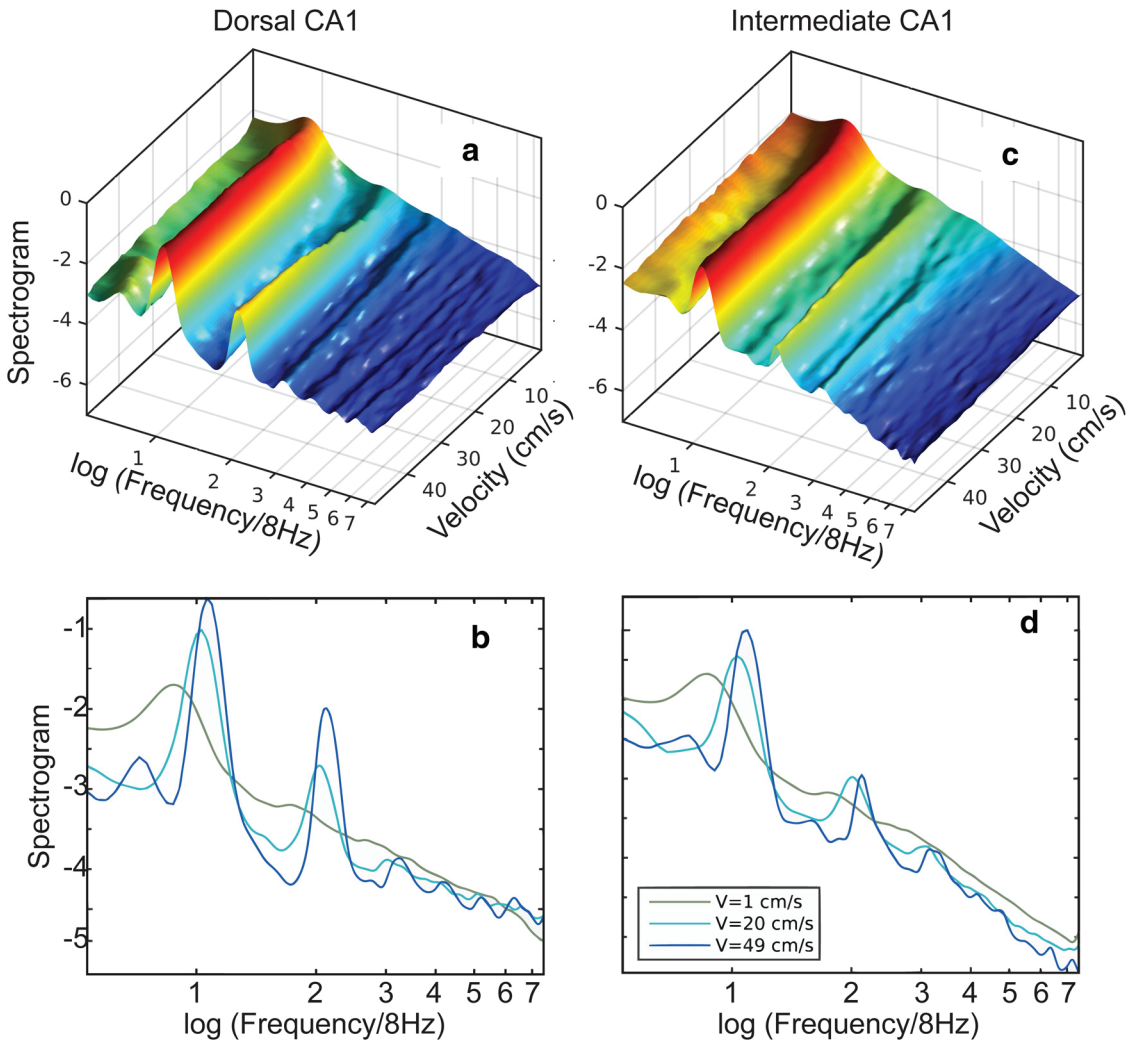

Figure 6. Power spectral density as a function of movement velocity. Normalized spectral density (logarithmic scale) as a function of velocity averaged over four rats (see Materials and Methods) for dorsal CA1 (***a***) and intermediate CA1 (***c***). The frequency axis was normalized by 8 Hz. Spectral densities (logarithmic scale) are shown for three velocities for dorsal CA1 (***b***) and intermediate CA1 (***d***).

Discussion

Using bispectral analysis, the current study documents the novel findings that (1) the CA1 subregion of the hippocampus has harmonics that are statistically dependent on theta; (2) higher-order harmonics emerge as a function of running speed in dorsal CA1 and, to a lesser extent, in intermediate CA1; and (3) harmonics were the source of the overall deformation of the LFP shape (negative skewness and asymmetry). Therefore, theta harmonics are in fact the spectral signature of the shape change of the LFP and express the increased nonlinearity of the theta rhythm in response to faster running speeds and increased neural activity. The harmonics cannot be regarded as a distinct (statistically independent) set of oscillations and are therefore not related to the beta and low-gamma rhythms.

These results show that the theta rhythm changed in response to running behavior, becoming more nonlinear as the animal's movement velocity increased. In the time domain, this is expressed as the development of skewness and asymmetry in the theta shape; in the spectral domain, it is expressed as the development of a chain of harmonics statistically phase coupled to the theta oscillation. This evolution is reflected in the spiking activity of principal cells (Maurer et al., 2005) and modulated across regions of the hippocampus: it is stronger in the dorsal CA1 than in the intermediate CA1. The current findings add to our understanding of how dynamic activity patterns vary as a function of anatomical position along the longitudinal axis of the hippocampus. Because theta is known to propagate from dorsal to ventral regions (Petsche and Stumpf, 1960; Lubenov and Siapas, 2009; Patel et al., 2012), these data suggest that the nonlinear character of theta decreases as it travels and suggests a hypothesis that activity during movement dissipates along the longitudinal axis of the hippocampus. Future studies will need to test this idea directly.

Although the potential mechanisms that attenuate theta nonlinearity as it travels are not known, the dorsal and ventral regions of the hippocampus are dissociated in terms of patterns of gene expression and the behavioral impact of lesions (Nadel, 1968; Stevens and Cowey, 1973; Sinnamon et al., 1978; Moser et al., 1993; Moser et al., 1995; Long and Kesner, 1996; Moser and Moser, 1998; Kjelstrup et al., 2002; Burton et al., 2009; Wang et al., 2015). In fact, it has been proposed that the hippocampal longitudinal axis is functionally organized along a gradient (Strange et al., 2014; Long et al., 2015) and others have even proposed that the dorsal and ventral hippocampus should be

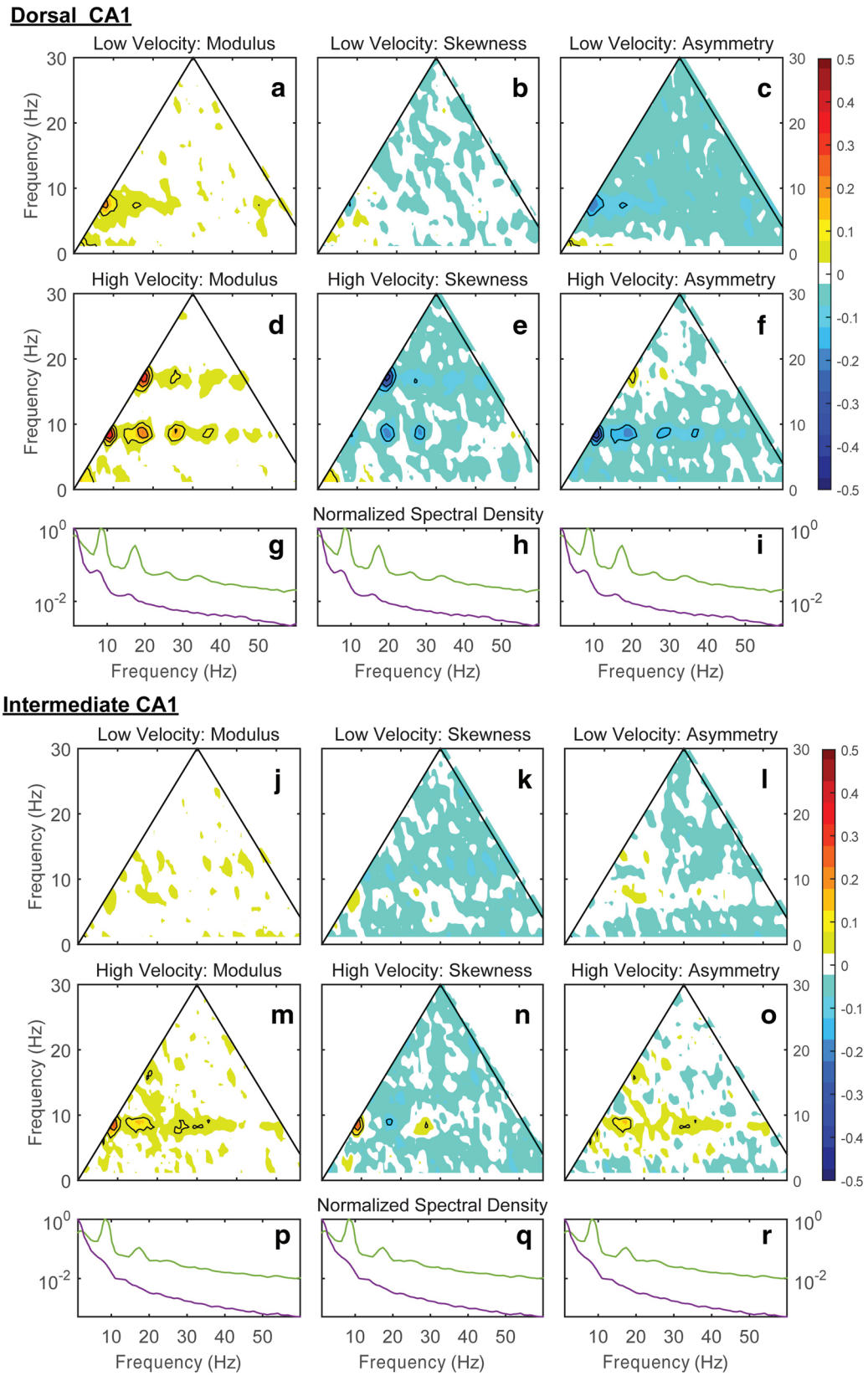

Figure 7. Representative bispectral properties of hippocampal LFP in the dorsal and intermediate CA1 region from rat 7805. The variability of the normalized bispectral distribution as a function of running speed (***a***–***c***: speed <10 cm/s; ***d***–***f***: speed >30 cm/s) for the modulus (***a***, ***d***), the real part (***b***, ***e***; skewness distribution), and the imaginary part (***c***, ***f***; asymmetry distribution). ***g***, ***h***, Normalized power spectral densities (maximum value = 1) are provided for reference (red, low speed; blue, high speed). Note that, in ***d***, the contour lines outline 6 distinct regions of triad phase correlations (using the format f_n, f_m, f_{n+m} depicted in Fig. 1: [8 Hz, 8 Hz, 16 Hz], [16 Hz, 8 Hz, 24 Hz], [24 Hz, 8 Hz, 32 Hz], and [32 Hz, 8 Hz, 40 Hz], [16 Hz, 16 Hz, 32 Hz], [24 Hz 16 Hz 48 Hz]). ***j***–***r*** are equivalent to ***a***–***i*** except that data were obtained from intermediate CA1. Bispectral maps are colored for absolute values >90% (>0.05) and contoured for absolute values >95% (>0.1). Contour lines are drawn with an increment of 0.05.

considered distinct structures (Fanselow and Dong, 2010). The observation that the theta rhythm is more nonlinear in the dorsal relative to intermediate hippocampus supports the idea that information may be processed differently along the dorsoventral axis. It also leaves open the question of whether different behavioral parameters could more strongly modulate theta nonlinearity in the intermediate and ventral areas. Specifically, whereas spatial cognitive behaviors are attributed to the dorsal hippocampus, the ventral hippocampus is often associated with emotional processing, stress and affect (for review, see Fanselow and Dong, 2010). This presents the possibility that LFP nonlinearity in more ventral regions of the hippocampus might be influenced by the emotional valence of an experience rather than by the animal's movement.

The development of the theta harmonic with faster running speeds was reflected in the spectrogram of principal cell firing. Although the correlation between theta nonlinearity and neuron spiking is obvious, establishing causality is more difficult. One can make the argument that spiking activity contributes to the background field (Geisler et al., 2010) and, therefore, that altered spiking dynamics with velocity would change the LFP shape. This argument, however, may be circular in that the evolution of theta with velocity alters the spike timing by mechanisms such as ephatic coupling (Buzsáki et al., 1991; Anastassiou et al., 2011). Perhaps more importantly, theta is not carried by the spiking of neurons, but rather is the summed activity of excitatory and inhibitory postsynaptic potentials (for review, see Buzsáki, 2005). Because hippocampal pyramidal neurons project to local interneurons (Csicsvari et al., 1998), which in turn provide dense feedback inhibition to several hundred principal neurons (Sik et al., 1995), local recurrent dynamics have been proposed to support the local generation of theta (Leung, 1998). In the model of Leung (1998), two inputs are responsible for the theta dipole across the CA1 layer: one onto the soma and proximal dendrites of pyramidal neurons carried by rhythmic basket cells and the other from input onto distal apical dendrites. Moreover, the interneurons across these regions exhibit differences in their phase preference (Klausberger et al., 2003; Somogyi and Klausberger, 2005), providing structured IPSPs along different pyramidal neuron domains (Allen and Monyer, 2015). Therefore, the consequence of two inhibitory rhythmic inputs at ~8 Hz

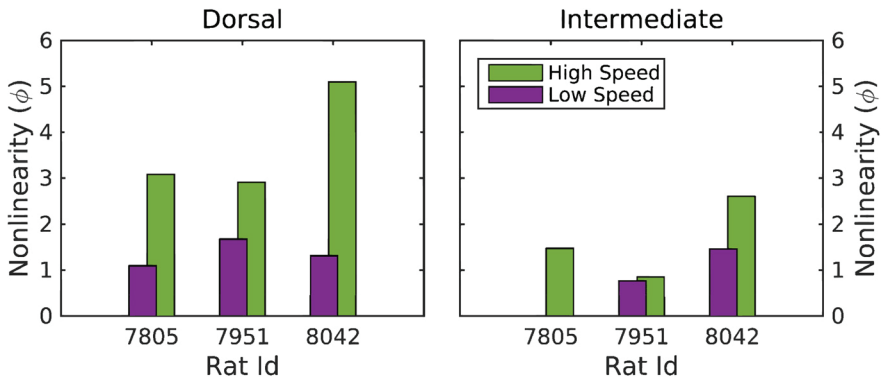

Figure 8. Theta nonlinearity of the three rats tested in the dorsal (left) and intermediate (right) CA1 regions and low (green) and high (purple) running velocities. The nonlinearity measure φ (Eq. 12) is defined only for bispectral values exceeding the 95% confidence level of the zero modulus of the normalized bispectrum (Eq. 13): the missing low-speed bar for rat 7805 for intermediate CA1 indicates that, at low speed, the normalized bispectrum is statistically zero. There was a significant main effect of hippocampal region ($F_{(1,\ 4)} = 30.6$, $p < 0.01$; repeated measures) on the magnitude of the nonlinearity such that the EEG in the dorsal hippocampus was more nonlinear than the intermediate. There was not a significant main effect of velocity (low vs high) on nonlinearity ($F_{(1,\ 4)} = 5.9$, $p = 0.08$; repeated measures), but the interaction between hippocampal region and velocity was significant ($F_{(1,\ 4)} = 9.1$, $p < 0.05$; repeated measures). *Post hoc* analysis indicated that this interaction effect was due to a significant difference in EEG nonlinearity across velocity conditions in the dorsal hippocampus ($p < 0.05$), but not in the intermediate hippocampus ($p = 0.2$).

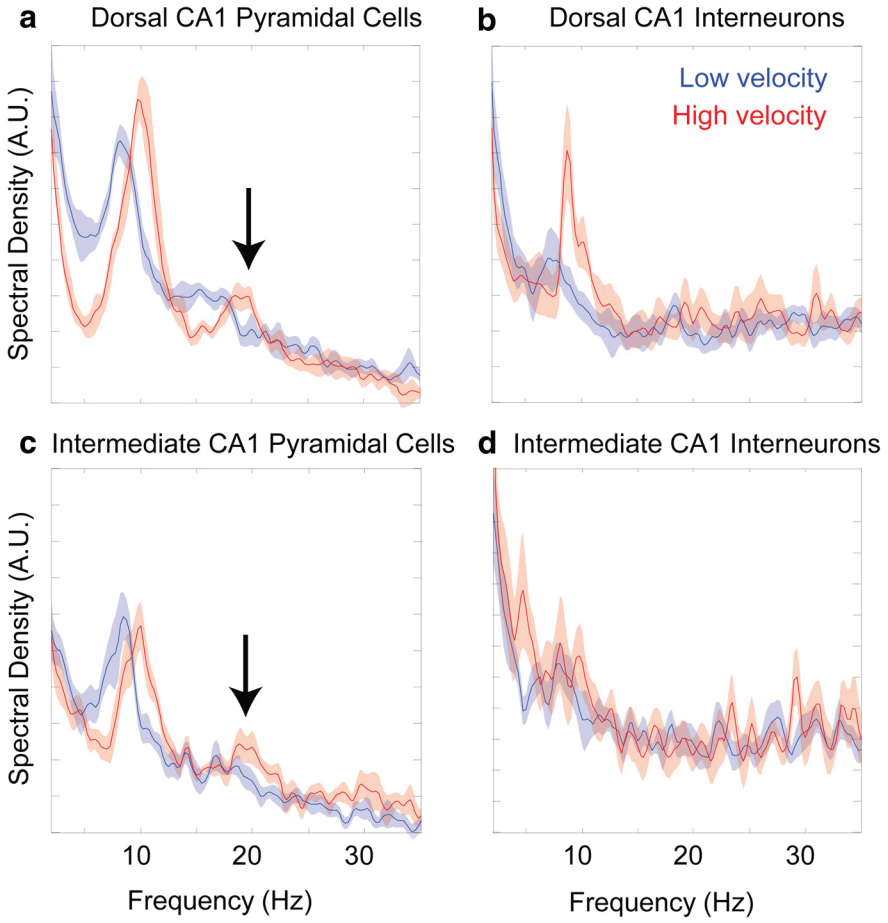

Figure 9. Spike spectrogram versus velocity. ***a***, ***b***, Dorsal CA1: pyramidal cells (***a***) and interneurons (***b***). ***c***, ***d***, Intermediate CA1: pyramidal cells (***c***) and interneurons (***d***). Because the analysis was conducted on binary spike trains, power units are arbitrary, although the axes are constant across respective cell classes. Low-velocity epochs are 10–20 cm/s and high-velocity epochs are 60–70 cm/s. Values are mean and SEM. Note the presence of a significant fundamental harmonic frequency, ~16 Hz, evident in the spectrogram of the spikes for the pyramidal cells at high velocities (arrows).

across distinct subcompartments of CA1 pyramidal neurons will interact, providing the basis for the 16 Hz modulation seen in Figure 9. Because there are fewer neurons active in the intermediate region of the hippocampus at any given moment in time (Maurer et al., 2006a) and these cells are less sensitive to changes in velocity (Maurer et al., 2005), fewer excitatory and inhibitory events contribute to the theta rhythm and the harmonic. Nonetheless, the intermediate pyramidal cells are still influenced by the structured inhibition, yielding a harmonic in the firing patterns.

This brings to the forefront the question of the role of the theta oscillation in the architecture of the brain. Although axons tend to propagate in a hierarchical manner (Felleman and Van Essen, 1991), the brain's architecture is more akin to a recurrent network in which neurons generate, as well as add, their own information to the activity propagating through the networks (Buzsáki, 2006). Because the theta rhythm is theorized to play a role in the coordination of brain activity, the nonlinear nature of wave propagation may govern the organization of spike timing. This idea is supported by the brain's capacity for large-scale integration of small components (Steriade, 2001; Buzsáki and Draguhn, 2004) and self-organized dynamics (Ashby, 1947; Kelso, 1997), as well as the simple observations that neurons fire during sleep and quiescent periods, when integration is largely disabled. The self-organized emergence of these oscillatory patterns, which reflects the excitatory (or inhibitory) state of the local groups of neurons (Haken, 1984), allows the firing patterns among assemblies of neurons to be "constrained" or timed via fluxes in the extracellular ionic concentration that modifies ionic driving force (Anastassiou et al., 2011). Although there have been significant theoretical advancements in describing self-organized, nonlinear dynamics in the nervous system (Amari, 1982; Haken, 1984; Freeman, 1992; McKenna et al., 1994; Kelso, 1997), the majority of our knowledge has been gained via linear methods, which ignore important elements of the complexity of the brain (Buzsáki, 2006). Future research attempting to untangle the dynamics of the nervous system should integrate nonlinear methods to understand the interaction between anatomy and activity.

References

Allen K, Monyer H (2015) Interneuron control of hippocampal oscillations. Curr Opin Neurobiol 31:81–87. CrossRef Medline

Amari S (1982) Chapter XIV: A mathematical theory of self-organizing nerve systems. In: Biomathematics in 1980: Papers presented at a workshop on biomathematics: current status and future perspective, Salerno, April 1980, p 159. Amsterdam: Elsevier.

Anastassiou CA, Perin R, Markram H, Koch C (2011) Ephaptic coupling of cortical neurons. Nat Neurosci 14:217–223. CrossRef Medline

Ashby WR (1947) Principles of the self-organizing dynamic system. J Gen Psychol 37:125–128. CrossRef Medline

Belluscio MA, Mizuseki K, Schmidt R, Kempter R, Buzsáki G (2012) Cross-frequency phase-phase coupling between theta and gamma oscillations in the hippocampus. J Neurosci 32:423–435. CrossRef Medline

Burton BG, Hok V, Save E, Poucet B (2009) Lesion of the ventral and intermediate hippocampus abolishes anticipatory activity in the medial prefrontal cortex of the rat. Behav Brain Res 199:222–234. CrossRef Medline

Buzsáki G (2002) Theta oscillations in the hippocampus. Neuron 33: 325–340. CrossRef Medline

Buzsáki G (2005) Theta rhythm of navigation: link between path integration and landmark navigation, episodic and semantic memory. Hippocampus 15:827–840. CrossRef Medline

Buzsáki, G (2006) Rhythms of the brain. New York: OUP.

Buzsáki G, Draguhn A (2004) Neuronal oscillations in cortical networks. Science 304:1926–1929. CrossRef Medline

Buzsáki G, Leung LW, Vanderwolf CH (1983) Cellular bases of hippocampal EEG in the behaving rat. Brain Res 287:139–171. Medline

Buzsáki G, Hsu M, Slamka C, Gage FH, Horváth Z (1991) Emergence and propagation of interictal spikes in the subcortically denervated hippocampus. Hippocampus 1:163–180. CrossRef Medline

Buzsáki G, Anastassiou CA, Koch C (2012) The origin of extracellular fields and currents–EEG, ECoG, LFP and spikes. Nat Rev Neurosci 13:407–420. CrossRef Medline

Cobb SR, Buhl EH, Halasy K, Paulsen O, Somogyi P (1995) Synchronization of neuronal activity in hippocampus by individual GABAergic interneurons. Nature 378:75–78. CrossRef Medline

Coenen AM (1975) Frequency analysis of rat hippocampal electrical activity. Physiol Behav 14:391–394. CrossRef Medline

Colgin LL, Denninger T, Fyhn M, Hafting T, Bonnevie T, Jensen O, Moser MB, Moser EI (2009) Frequency of gamma oscillations routes flow of information in the hippocampus. Nature 462:353–357. CrossRef Medline

Csicsvari J, Hirase H, Czurko A, Buzsáki G (1998) Reliability and state dependence of pyramidal cell-interneuron synapses in the hippocampus: an ensemble approach in the behaving rat. Neuron 21:179–189. CrossRef Medline

Czurko A, Hirase H, Csicsvari J, Buzsáki G (1999) Sustained activation of hippocampal pyramidal cells by 'space clamping' in a running wheel. Eur J Neurosci 11:344–352. CrossRef Medline

Diba K, Amarasingham A, Mizuseki K, Buzsáki G (2014) Millisecond timescale synchrony among hippocampal neurons. J Neurosci 34:14984–14994. CrossRef Medline

Elgar S (1987) Relationships involving third moments and bispectra of a harmonic process. IEEE Transactions on Acoustics, Speech and Signal Processing 35:1725–1726. CrossRef

Elgar S, Guza R (1985) Observations of bispectra of shoaling surface gravity waves. Journal of Fluid Mechanics 161:425–448. CrossRef

Elgar S, Sebert G (1989) Statistics of bicoherence and biphase. J Geophys Res Oceans 94:10993–10998. CrossRef

Engström DA, Kelso JS, Holroyd T (1996) Reaction-anticipation transitions in human perception-action patterns. Human Movement Science 15: 809–832. CrossRef

Fanselow MS, Dong HW (2010) Are the dorsal and ventral hippocampus functionally distinct structures? Neuron 65:7–19. CrossRef Medline

Felleman DJ, Van Essen DC (1991) Distributed hierarchical processing in the primate cerebral cortex. Cereb Cortex 1:1–47. Medline

Freeman WJ (1992) Tutorial on neurobiology: from single neurons to brain chaos. International Journal of Bifurcation and Chaos 2:451–482. CrossRef

Friston KJ (1997) Transients, metastability, and neuronal dynamics. Neuroimage 5:164–171. CrossRef Medline

Geisler C, Diba K, Pastalkova E, Mizuseki K, Royer S, Buzsáki G (2010) Temporal delays among place cells determine the frequency of population theta oscillations in the hippocampus. Proc Natl Acad Sci U S A 107: 7957–7962. CrossRef Medline

Gothard KM, Skaggs WE, Moore KM, McNaughton BL (1996) Binding of hippocampal CA1 neural activity to multiple reference frames in a landmark-based navigation task. J Neurosci 16:823–835. Medline

Green JD, Arduini AA (1954) Hippocampal electrical activity in arousal. J Neurophysiol 17:533–557. Medline

Haken H (1984) The science of structure: synergetics. New York: Van Nostrand Reinhold.

Harper RM (1971) Frequency changes in hippocampal electrical activity during movement and tonic immobility. Physiol Behav 7:55–58. CrossRef Medline

Harris KD, Csicsvari J, Hirase H, Dragoi G, Buzsáki G (2003) Organization of cell assemblies in the hippocampus. Nature 424:552–556. CrossRef Medline

Hasselmann K, Munk W, MacDonald G (1963) Bispectra of ocean waves. In: Time series analysis (Rosenblatt M, ed), pp 125–139. New York: John Wiley & Sons.

Hasselmo ME (2015) If I had a million neurons: potential tests of cortico-hippocampal theories. Prog Brain Res 219:1–19. CrossRef Medline

Haubrich RA, MacKenzie GS (1965) Earth noise, 5 to 500 millicycles per second: 2. Reaction of the Earth to oceans and atmosphere. Journal of Geophysical Research 70:1429–1440. CrossRef

Jung R, Kornmüller A (1938) Eine methodik der ableitung iokalisierter potentialschwankungen aus subcorticalen hirngebieten. European Archives of Psychiatry and Clinical Neuroscience 109:1–30.

Kelso, JS (1997) Dynamic patterns: The self-organization of brain and behavior. Cambridge, MA: MIT.

Kim YC, Powers EJ (1979) Digital bispectral analysis and its applications to nonlinear wave interactions. IEEE Transactions on Plasma Science 7:120–131. CrossRef

Kjelstrup KG, Tuvnes FA, Steffenach HA, Murison R, Moser EI, Moser MB (2002) Reduced fear expression after lesions of the ventral hippocampus. Proc Natl Acad Sci U S A 99:10825–10830. CrossRef Medline

Klausberger T, Magill PJ, Márton LF, Roberts JD, Cobden PM, Buzsáki G, Somogyi P (2003) Brain-state- and cell-type-specific firing of hippocampal interneurons in vivo. Nature 421:844–848. CrossRef Medline

Lachaux JP, Rodriguez E, Martinerie J, Varela FJ (1999) Measuring phase synchrony in brain signals. Hum Brain Mapp 8:194–208. CrossRef Medline

Leung LS (1982) Nonlinear feedback model of neuronal populations in hippocampal CAl region. J Neurophysiol 47:845–868. Medline

Leung LS (1998) Generation of theta and gamma rhythms in the hippocampus. Neurosci Biobehav Rev 22:275–290. CrossRef Medline

Leung LW, Buzsáki G (1983) Spectral analysis of hippocampal unit train in relation to hippocampal EEG. Electroencephalogr Clin Neurophysiol 56: 668–671. CrossRef Medline

Leung LW, Lopes da Silva FH, Wadman WJ (1982) Spectral characteristics of the hippocampal EEG in the freely moving rat. Electroencephalogr Clin Neurophysiol 54:203–219. CrossRef Medline

Lisman JE, Idiart MA (1995) Storage of 7 ± 2 short-term memories in oscillatory subcycles. Science 267:1512–1515. CrossRef Medline

Long JM, Kesner RP (1996) The effects of dorsal versus ventral hippocampal, total hippocampal, and parietal cortex lesions on memory for allocentric distance in rats. Behav Neurosci 110:922–932. CrossRef Medline

Long LL, Bunce JG, Chrobak JJ (2015) Theta variation and spatiotemporal scaling along the septotemporal axis of the hippocampus. Front Syst Neurosci 9:37. Medline

Lubenov EV, Siapas AG (2009) Hippocampal theta oscillations are travelling waves. Nature 459:534–539. CrossRef Medline

Mallat S (1999) A wavelet tour of signal processing. San Diego: Academic.

Marder E (2015) Understanding brains: details, intuition, and big data. PLoS Biol 13:e1002147. CrossRef Medline

Masuda A, Kuo YY (1981) A note on the imaginary part of bispectra. Deep Sea Research Part A Oceanographic Research Papers 28:213–222. CrossRef

Maurer AP, Vanrhoads SR, Sutherland GR, Lipa P, McNaughton BL (2005) Self-motion and the origin of differential spatial scaling along the septotemporal axis of the hippocampus. Hippocampus 15:841–852. CrossRef Medline

Maurer AP, Cowen SL, Burke SN, Barnes CA, McNaughton BL (2006a) Organization of hippocampal cell assemblies based on theta phase precession. Hippocampus 16:785–794. CrossRef Medline

Maurer AP, Cowen SL, Burke SN, Barnes CA, McNaughton BL (2006b) Phase precession in hippocampal interneurons showing strong functional coupling to individual pyramidal cells. J Neurosci 26:13485–13492. CrossRef Medline

Maurer AP, Burke SN, Lipa P, Skaggs WE, Barnes CA (2012) Greater running speeds result in altered hippocampal phase sequence dynamics. Hippocampus 22:737–747. CrossRef Medline

McKenna TM, McMullen TA, Shlesinger MF (1994) The brain as a dynamic physical system. Neuroscience 60:587–605. CrossRef Medline

McNaughton BL, O'Keefe J, Barnes CA (1983) The stereotrode: a new technique for simultaneous isolation of several single units in the central nervous system from multiple unit records. J Neurosci Methods 8: 391–397. CrossRef Medline

Moser E, Moser MB, Andersen P (1993) Spatial learning impairment parallels the magnitude of dorsal hippocampal lesions, but is hardly present following ventral lesions. J Neurosci 13:3916–3925. Medline

Moser MB, Moser EI (1998) Distributed encoding and retrieval of spatial memory in the hippocampus. J Neurosci 18:7535–7542. Medline

Moser MB, Moser EI, Forrest E, Andersen P, Morris RG (1995) Spatial learning with a minislab in the dorsal hippocampus. Proc Natl Acad Sci U S A 92:9697–9701. CrossRef Medline

Nadel L (1968) Dorsal and ventral hippocampal lesions and behavior. Physiol Behav 3:891–900. CrossRef

O'Keefe J, Dostrovsky J (1971) The hippocampus as a spatial map: preliminary evidence from unit activity in the freely-moving rat. Brain Res 34: 171–175. Medline

O'Keefe J, Recce ML (1993) Phase relationship between hippocampal place units and the EEG theta rhythm. Hippocampus 3:317–330. CrossRef Medline

Papoulis A, Pillai SU (2002) Probability, random variables, and stochastic processes. Delhi, India: Tata McGraw-Hill Education.

Patel J, Fujisawa S, Berényi A, Royer S, Buzsáki G (2012) Traveling theta waves along the entire septotemporal axis of the hippocampus. Neuron 75:410–417. CrossRef Medline

Penttonen M, Buzsáki G (2003) Natural logarithmic relationship between brain oscillators. Thalamus and Related Systems 2:145–152.

Petsche H, Stumpf C (1960) Topographic and toposcopic study of origin and spread of the regular synchronized arousal pattern in the rabbit. Electroencephalogr Clin Neurophysiol 12:589–600. CrossRef Medline

Priestley MB (1981) Spectral analysis and time series. New York: Elsevier.

Ranck JB Jr (1973) Studies on single neurons in dorsal hippocampal formation and septum in unrestrained rats. I. Behavioral correlates and firing repertoires. Exp Neurol 41:461–531. Medline

Recce ML, O'Keefe J (1989) The tetrode: an improved technique for multiunit extracellular recording. Soc Neurosci Abstr 15:1250.

Rosenblatt, M, Van Ness, JW (1965) Estimation of the bispectrum. Annals of Mathematical Statistics 36:1120–1136.

Royer S, Sirota A, Patel J, Buzsáki G (2010) Distinct representations and theta dynamics in dorsal and ventral hippocampus. J Neurosci 30:1777–1787. CrossRef Medline

Schomburg EW, Anastassiou CA, Buzsáki G, Koch C (2012) The spiking component of oscillatory extracellular potentials in the rat hippocampus. J Neurosci 32:11798–11811. CrossRef Medline

Sheremet, A, Guza RT, Elgar S, Herbers THC (2002) Observations of nearshore infragravity waves: seaward and shoreward propagating components. J Geophys Res 107:3095. CrossRef

Sik A, Penttonen M, Ylinen A, Buzsáki G (1995) Hippocampal CA1 interneurons: an in vivo intracellular labeling study. J Neurosci 15:6651–6665. Medline

Sinnamon HM, Freniere S, Kootz J (1978) Rat hippocampus and memory for places of changing significance. J Comp Physiol Psychol 92:142–155. CrossRef Medline

Skaggs WE (1995) Relations between the theta rhythm and activity patterns of hippocampal neurons. PhD thesis, University of Arizona.

Skaggs WE, McNaughton BL, Wilson MA, Barnes CA (1996) Theta phase precession in hippocampal neuronal populations and the compression of temporal sequences. Hippocampus 6:149–172. CrossRef Medline

Somogyi P, Klausberger T (2005) Defined types of cortical interneurone structure space and spike timing in the hippocampus. J Physiol 562:9–26. CrossRef Medline

Steriade M (2001) Impact of network activities on neuronal properties in corticothalamic systems. J Neurophysiol 86:1–39. Medline

Stevens R, Cowey A (1973) Effects of dorsal and ventral hippocampal lesions on spontaneous alternation, learned alternation and probability learning in rats. Brain Res 52:203–224. CrossRef Medline

Strange BA, Witter MP, Lein ES, Moser EI (2014) Functional organization of the hippocampal longitudinal axis. Nat Rev Neurosci 15:655–669. CrossRef Medline

Swami A, Mendel C, Nikias C (2000) Higher-order spectral analysis (hosa) toolbox. Version 2:3.

Terrazas A, Krause M, Lipa P, Gothard KM, Barnes CA, McNaughton BL (2005) Self-motion and the hippocampal spatial metric. J Neurosci 25: 8085–8096. CrossRef Medline

Tognoli E, Kelso JA (2014) The metastable brain. Neuron 81:35–48. CrossRef Medline

Vanderwolf CH (1969) Hippocampal electrical activity and voluntary movement in the rat. Electroencephalogr Clin Neurophysiol 26:407–418. CrossRef Medline

Wang J, Bast T, Wang YC, Zhang WN (2015) Hippocampus and two way active avoidance conditioning: contrasting effects of cytotoxic lesion and temporary inactivation. Hippocampus 25:1517–1531. CrossRef Medline

Whitham GB (2011) Linear and nonlinear waves: Wiley.

Wiener N (1966) Nonlinear problems in random theory, pp 142. Cambridge, MA: MIT.

Ziv Y, Burns LD, Cocker ED, Hamel EO, Ghosh KK, Kitch LJ, El Gamal A, Schnitzer MJ (2013) Long-term dynamics of CA1 hippocampal place codes. Nat Neurosci 16:264–266. CrossRef Medline

CAM

Selected Publications

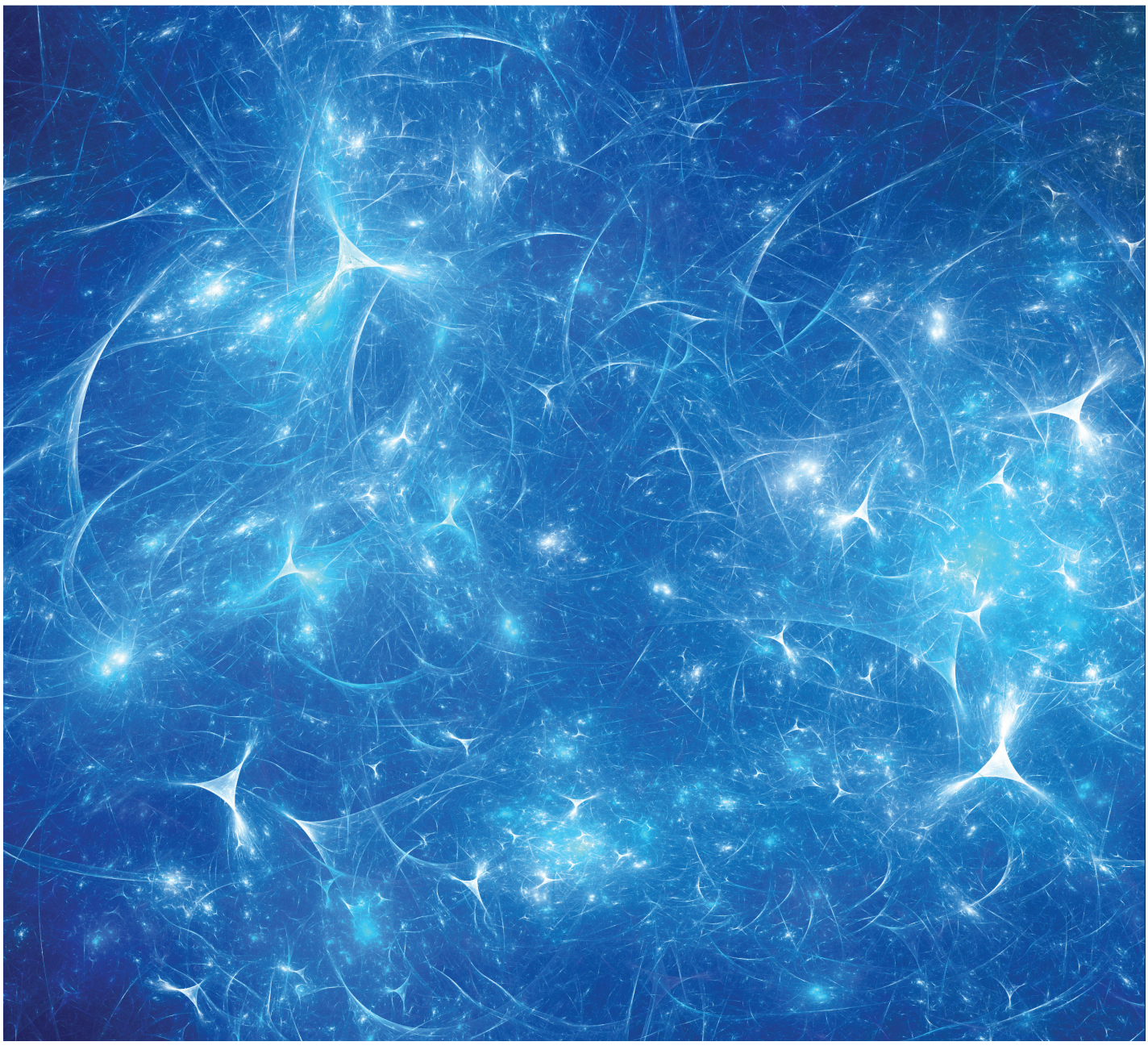

frontiers in Aging Neuroscience

METHODS
published: 19 July 2016
doi: 10.3389/fnagi.2016.00176

Statistical Approaches for the Study of Cognitive and Brain Aging

Huaihou Chen[1,2], Bingxin Zhao[1], Guanqun Cao[3], Eric C. Proges[2], Andrew O'Shea[2], Adam J. Woods[2] and Ronald A. Cohen[2]*

[1] Department of Biostatistics, University of Florida, Gainesville, FL, USA, [2] Department of Aging and Geriatric Research, Center for Cognitive Aging and Memory, Institute on Aging, McKnight Brain Institute, University of Florida, Gainesville, FL, USA, [3] Department of Mathematics and Statistics, Auburn University, Auburn, AL, USA

Neuroimaging studies of cognitive and brain aging often yield massive datasets that create many analytic and statistical challenges. In this paper, we discuss and address several limitations in the existing work. (1) Linear models are often used to model the age effects on neuroimaging markers, which may be inadequate in capturing the potential nonlinear age effects. (2) Marginal correlations are often used in brain network analysis, which are not efficient in characterizing a complex brain network. (3) Due to the challenge of high-dimensionality, only a small subset of the regional neuroimaging markers is considered in a prediction model, which could miss important regional markers. To overcome those obstacles, we introduce several advanced statistical methods for analyzing data from cognitive and brain aging studies. Specifically, we introduce semiparametric models for modeling age effects, graphical models for brain network analysis, and penalized regression methods for selecting the most important markers in predicting cognitive outcomes. We illustrate these methods using the healthy aging data from the Active Brain Study.

Keywords: semiparametric model, graphical model, penalized regression methods, structural covariance, functional connectivity

OPEN ACCESS

Edited by:
Rodrigo Orlando Kuljiš, University of Miami School of Medicine, USA

Reviewed by:
Vassiliki Nikoletopoulou, Institute of Molecular Biology and Biotechnology, Greece
Alex Zhavoronkov, The Biogerontology Research Foundation, UK

****Correspondence:***
Huaihou Chen
huaihouchen@ufl.edu

Received: *07 March 2016*
Accepted: *04 July 2016*
Published: *19 July 2016*

Citation:
Chen H, Zhao B, Cao G, Proges EC, O'Shea A, Woods AJ and Cohen RA (2016) Statistical Approaches for the Study of Cognitive and Brain Aging. Front. Aging Neurosci. 8:176. doi: 10.3389/fnagi.2016.00176

INTRODUCTION

Multimodal neuroimaging collected in cognitive aging studies provides a noninvasive way to investigate brain changes in structure, function, and metabolism as people age, and thus helps us to understand age-related cognitive changes. However, the high-dimensionality and complex structure of those multimodal neuroimaging data raise statistical challenges. Additionally, the age range is large in aging studies and very often the age effects may not be linear in the large age interval. For instance, participant's age ranges from 50 to 90 in the Active Brain Study, a successful aging cohort. To efficiently analyze those data, there is a strong need for introduction of advanced statistical methods. We will elaborate on the limitations of several existing methods and introduce three advanced statistical methods in sequence.

First, age is a complex variable and often has a nonlinear effect on the outcomes of interest. In developmental studies, flexible semiparametric models have been well used, because it is well-known that growth curves are nonlinear. However, in aging studies, linear or quadratic models are often used to characterize age-related changes. Although a majority of aging research treats aging as a linear process (constant rate of change) and linear models are often considered the gold standard method for evaluating aging effects, this approach may not be the most effective method for representing the complexity of aging data. For instance, Raz et al. (2010) used linear

mixed effects models to characterize the age-related brain structural changes in a longitudinal neuroimaging study with 76 participants whose age ranges from 49 to 85. Similarly, Resnick et al. (2003) also used linear mixed effects models to show the age-related brain structural changes in the longitudinal Baltimore study. However, as noted in Fjell et al. (2010), Gogtay et al. (2004), and Thompson et al. (2011); brain structure may show complex age-related nonlinear changes, and could be misspecified by a linear or quadratic model. We have shown that misspecified linear models can result in biased estimates and low powers in statistical tests (Chen et al., 2012). As a nonparametric method, a spline model is recommended for its flexibility and robustness. To accurately model the age trajectories of the neuroimaging markers, we will introduce a spline-based semiparametric model in the methods section and illustrate these methods using the structural neuroimaging data from the Active Brain Study in the example section. The semiparametric model excels at determining rates of global and regional brain atrophy and identifying vulnerable regions of interest (ROIs) susceptible to aging.

Second, marginal correlations are often used in brain network analyses. For example, structural covariance was studied in Mechelli et al. (2005) and Alexander-Bloch et al. (2013), which may be related to structural and functional connectivity. There is also a large literature on Pearson correlation based functional connectivity analysis, where the correlation between two functional magnetic resonance imaging (fMRI) time series [that is the blood-oxygen-level dependent (BOLD) signal] is computed. However, marginal correlation between two brain ROIs is indirect and weak in the sense that all the components in a system are correlated to some degree. Two regions can be indirectly associated with each other due to their correlation with a third region. Moreover, when the number of ROIs is large, the sample covariance/correlation matrix is unstable, as the number of parameters increases quadratically with the number of ROIs. Alternatively, graphical models are attractive for inferring brain connectivity due to their advantages over conventional marginal correlation based analysis (Lauritzen, 1996; Yuan and Lin, 2007; Koller and Friedman, 2009). Graphical models can generate either partial correlations or a binary undirected graph. Sparse penalty is used to regularize the loglikelihood function and make the solution robust. Partial correlation is a desirable measure, as it quantifies the conditional association between two ROIs given the rest of ROIs. Partial correlation can be interpreted as the adjusted correlation. Preliminary applications to neuroimaging data can be found in Salvador et al. (2005), Valdés-Sosa et al. (2005), and Smith (2012). In the methods section, we will introduce two graphical methods for brain network analysis. We will apply these methods to the cortical thickness data from the Active Brain Study for building cortical networks.

Third, the high dimensional neuroimaging markers may provide informative early signs of age-related cognitive and functional decline. For example, brain atrophy in the basal ganglia, hippocampus, and prefrontal areas often precedes the clinical diagnosis of cognitive impairment (Amieva et al., 2005; Grober et al., 2008; Jedynak et al., 2012). It is of great interest to select the informative neuroimaging markers for predicting cognitive decline. However, the high-dimensionality of the neuroimaging markers posit challenges on how to efficiently pick up the informative subset of the markers. Traditional backward or forward variable selection methods are computationally inefficient given the large number of neuroimaging markers. Also neuroimaging markers are often highly correlated with each other. The unpenalized least square based estimates often suffer from high variability or instability (that is with large variance). Moreover, when the number of neuroimaging markers is larger than the sample size, the design matrix is singular and not invertible, and thus there is no unique estimate. In contrast, penalized regression methods can lead to stable solutions and are computationally efficient by using advanced algorithms (Tibshirani, 1996; Fan and Li, 2001; Zou, 2006; Meinshausen and Bühlmann, 2010). Penalized regression methods can simultaneously select and estimate the effects of the predictors. The variable selection is achieved by the sparsity penalty. In the methods section, we will introduce penalized regression methods for selecting the optimal subset of neuroimaging biomarkers for predicting cognitive outcomes. We will illustrate those methods using structural neuroimaging and cognitive data from the Active Brain Study.

The rest of the paper is structured as follows. In the methods section, we introduce the three sets of methods including the spline-based semiparametric model, graphical models, and penalized regression methods. In the examples section, we apply those methods to the data from the Active brain study. We end our paper with general discussions.

METHODS

Semiparametric Models and Methods

We first introduce some notations. Let n be the number of subjects and let R be the number of ROIs. For the ith participant, denote t_i as the age, denote Y_{ir} as the structural/metabolic imaging markers [for instance, volume, fractional anisotropy (FA), myo-inositol (MI)] at the rth ROI, and denote $\boldsymbol{Z}_i$ as other predictors such as education and sex that we want to study. To accurately and efficiently model the age effects, we introduce the following semiparametric model (1) for neuroimaging markers in cross-sectional studies.

$$Y_{ir} = \mu_r(t_i) + \boldsymbol{Z}_i\boldsymbol{\beta}_r + \epsilon_{ir}, \quad i = 1, \cdots, n, \quad r = 1, \cdots, R, \quad (1)$$

where $\mu_r(t)$ is the unspecified aging trajectory for the older people at the rth ROI evaluated at age t, and $\boldsymbol{\beta}_r$ are the regression coefficients of the other predictors at the ROI. The measurement errors ϵ_{ir} are assumed to be independently and identically distributed and follow a normal distribution $N(0, \sigma_r^2)$ with mean zero and variance σ_r^2. Model (1) consists of both the nonparametric part $\mu_r(t)$ and the parametric part $\boldsymbol{Z}\boldsymbol{\beta}_r$, and thus it is called semiparametric model. The semiparametric model is a parsimonious way to both capture the potential nonlinear age trajectory and investigate the effects of other predictors. Notably, the traditional linear model is a special case of model (1), where the function $\mu_r(t)$ is specified as a linear function $\beta_{0r} + \beta_{1r}t$. Extension of model (1) to longitudinal data

case is straightforward, which can be accomplished by either introducing subject-specific random effects or using generalized least square methods (Wood, 2006; Wu and Zhang, 2006).

For estimation, we use spline basis functions to approximate the unspecified function $\mu_r(t)$. Particularly, we assume $\mu_r(t) = B(t)\boldsymbol{\theta}_r$, where $B(t)$ is a set of B-spline basis functions and $\boldsymbol{\theta}_r$ is the associated spline coefficients (de Boor, 1978). The B-spline basis functions are piecewise polynomial functions in the age interval. A smoothing penalty $\lambda \int [\mu_r''(t)]^2 dt$ is used to achieve smoothness of the fitted function $\hat{\mu}_r(t)$, where $\mu_r''(t)$ is the second derivative function of $\mu_r(t)$, and $\lambda \geq 0$ is a smoothing parameter controlling the degree of smoothness. The tuning parameter λ is crucial for the estimation and inference and is often chosen by data driven methods. By minimizing the penalized log-likelihood function, we can obtain the estimate for these parameters including $\boldsymbol{\theta}_r$ and $\boldsymbol{\beta}_r$. Compared to traditional linear model and methods, spline method offers flexible estimation of these functions. Based on the semiparametric model (1), we will be able to more accurately delineate the aging trajectories and their derivative functions and get unbiased estimates for the parametric part.

The spline-based semiparametric model and methods have been implemented in several R packages (R Core Team, 2012) including the *mgcv* package (Wood, 2006). The *gam* function in *mgcv* can output the estimates and inferential results for both the parametric and nonparametric parts. Specifically, for the parametric part, estimates of the regression coefficients and *p*-values are provided which is similar to a linear regression model. For the nonparametric part, the procedure provides the estimate and pointwise confidence intervals for the estimated function and a *p*-value for testing the function as a constant. The 95% point-wise confidence interval $[\mu_r^L(t), \mu_r^U(t)]$ for $\mu_r(t)$ provides the variability at the age t in the rth ROI, in addition to the magnitude. The first derivative function of $\mu_r(t)$ indicate the rate of brain atrophy, where in the linear case is the slope of the line. The first derivative functions are can be easily obtained using $B'(t)\theta$, where $B'(t)$ are the first derivative functions of the B-spline basis functions. Based on the first derivative functions of the aging trajectories, ROIs/markers show early atrophy/abnormality could be candidate biomarkers for early diagnosis of diseases. We adjust for multiple comparison by controlling the *false discovery rate* (FDR) (Benjamini and Hochberg, 1995; Benjamini and Heller, 2007).

Remark 1 Misspecified linear models could introduce bias for the estimates of $\mu_r(t)$ and $\boldsymbol{\beta}_r$, that is for both the nonparametric and parametric parts.

Remark 2 To achieve good approximations of these unspecified functions, enough number of basis functions should be used for the penalized splines. If the procedure leads to an oversmooth case, one can fit a regression cubic spline with fixed number of knots without penalty, thus the degree of freedom is fixed.

Remark 3 Computing time is not a concern for ROI-level data. Some statistical packages such as the *vows* have implemented massive parallel algorithm for voxel-level data (Reiss et al., 2014).

Graphical Model and Methods

We first define a graph $G = (V, E)$, where V is a set of vertices/nodes, and E is a set of edges connecting pairs of nodes in V. An adjacency matrix of a graph is a binary matrix indicating the connection between the nodes. We introduce graphical models for brain structural and functional network analysis. In the past decade, *Gaussian graphical model* (GGM) has been a hot topic in statistics as a tool for complex system analysis. The GGM has many advantages over the traditional marginal correlation based analysis including resulting in partial correlations, i.e., direct dependency/independence, and sparse networks. Let $\boldsymbol{Y}$ be an R-dimensional random variable following a multivariate Gaussian distribution $N(\boldsymbol{\mu}, \boldsymbol{G}^{-1})$ with mean $\boldsymbol{\mu}$ and covariance $\boldsymbol{G}^{-1}$. $\boldsymbol{G}$ is a precision matrix (inverse covariance), and the i, jth component of $\boldsymbol{G}$, $g_{rs} = 0$ indicates *conditional independence* between ROIs r and s given all the other ROIs $\{1, \cdots, R\}/\{r, s\}$. The partial correlation between ROIs r and s is defined as $\rho_{rs} = -g_{rs}/\sqrt{g_{rr}g_{ss}}$ (Lauritzen, 1996). We obtain a sparse graph by minimizing the following penalized loglikelihood function (Yuan and Lin, 2007):

$$\arg\min_{G \in \mathbb{G}} -\log|\boldsymbol{G}| + \frac{1}{n}\sum_{i=1}^{n}(\boldsymbol{Y}_i - \boldsymbol{\mu})^T \boldsymbol{G}(\boldsymbol{Y}_i - \boldsymbol{\mu}) + \lambda \sum_{r \neq s} |g_{rs}|, \quad (2)$$

where argmin stands for argument of the minimum, $\mathbb{G}$ is the set of $R \times R$ positive definite matrices, and $\lambda \geq 0$ is the tuning parameter chosen by a data-driven method. The lasso penalty (Tibshirani, 1996) is used to regularize the loglikelihood function and achieve a sparse solution. This method is often called graphical lasso (glasso) in the statistical literature. Along the same line, Meinshausen and Bühlmann (2006) proposed the node-wise regression based approach for obtaining a binary graph. Both the glasso and the node-wise regression methods have been implemented in the R package *huge* with computational efficient algorithms (Zhao et al., 2012). The *huge* function in the *huge* package can provide estimate for the precision matrix or adjacency matrix of an undirected graph. The stability selection method (Meinshausen and Bühlmann, 2010) is preferred for the selection of the tuning parameter, which controls the sparsity of the estimated precision/adjacency matrix. A large tuning parameter will penalize the loglikelihood function heavily and shrink the small elements in the precision matrix/regression coefficients to zero, while a smaller tuning parameter will barely penalize the loglikelihood function and thus leads to many tiny elements in the precision matrix/regression coefficients.

Once the graph is obtained, graph summary statistics such as centrality measures and clustering coefficient can be computed. For visualizing and summarizing graphical objects, the R package *igraph* provides a set of sophisticated tools (Csardi and Nepusz, 2006).

Penalized Regression Methods

To utilize high-dimensional markers for predicting cognitive outcomes, we introduce penalized regression methods for linear models. Penalized regression methods can reduce the dimensionality of the predictors by automatically selecting the optimal subset. The variable selection is achieved by a sparsity penalty such as lasso (Tibshirani, 1996), adaptive lasso (Zou, 2006), elastic net (Zou, 2006), SCAD (Fan and Li, 2001), or by stability method (Meinshausen and Bühlmann, 2010). For the

*i*th participant, let Y_i be the cognitive outcome, and let $\boldsymbol{X}_i$ be the stacked $p \times 1$ vector of neuroimaging markers and other covariates. We consider the following linear model and penalized method.

$$Y_i = \boldsymbol{X}_i\boldsymbol{\beta} + \epsilon_i, \quad i = 1, \cdots, n, \tag{3}$$

$$\boldsymbol{\beta} = \arg\min_{\boldsymbol{\beta}\in\mathbb{R}^p} \sum_{i=1}^{n} (Y_i - \boldsymbol{X}_i\boldsymbol{\beta})^2 + \lambda\phi(|\boldsymbol{\beta}|), \tag{4}$$

where $\boldsymbol{\beta}$ are the coefficients for neuroimaging markers and covariates, and $\phi(.)$ is a penalty function of the regression coefficients $\boldsymbol{\beta}$. By minimizing the penalized least squares (4), we can obtain the penalized estimator $\hat{\boldsymbol{\beta}}$. The sparsity penalty shrinkages those small regression coefficients to zeros, thus the procedure automatically leads to a subset of the predictors. If $\hat{\beta}_j = 0$, then the *j*th predictor X_j is not selected. The sparsity of the estimate is controlled by the tuning parameter $\lambda \geq 0$, which is usually chosen by data driven methods such as cross-validation or generalized cross-validation.

Thanks to the implementation of efficient algorithms, current software package can handle thousands of predictors simultaneously for a medium sample size such as n = 80. In general the computational time is moderate and depends on the size of the data that is the sample size n and the number of predictors p. One of the popular R package *glmnet* has implemented a few penalized methods including lasso and elastic net. The *glmnet* function in the *glmnet* package provides all the coefficient solution paths as functions of the tuning parameter λ. To get the optimal solution, the user needs to use the cross-validation method to select the optimal tuning parameter with the smallest mean squared error (MSE).

Remark 4 The penalized regression methods are applicable to generalized outcomes including binary and count data as well. For example, we can use penalized logistic regression methods to select informative neuroimaging markers in predicting risk of mild cognitive impairment (MCI).

Remark 5 Because the penalty shrinkages those regression coefficients toward to zero according to their magnitude, large differences in the original scale of those predictors can mess up the selection. Therefore, it is recommended to standardize the predictors and make all the variables in the same scale.

EXAMPLES: THE ACTIVE BRAIN STUDY

We illustrate the introduced methods using the data from the Active Brain Study. The aim of the study is to investigate the brain changes associated with age-related cognitive decline via multimodal neuroimaging. We consider n = 114 participants with structural imaging. Among them 68% are female. The mean age of the sample is 72.3 with the standard deviation (SD) 10. Those participants are well educated as can be seen from the mean education years = 16.2 (SD = 2.6). They also show high cognitive performance with mean Montreal Cognitive Assessment (MoCA) score 25.7 (SD = 2.6). The structural imaging was processed using standard procedures implemented in Freesurfer version 5.3 (Dale et al., 1999; Fischl et al., 2002). For a more detailed description of the Freesurfer processing methods used by our group see Szymkowicz et al. (2016). Brain volumetric indices including regional and global volumes of cortical and subcortical structures as well as cortical thickness were generated. Particularly, we used the anatomical cortical parcellation in Desikan et al. (2006), which generated 34 ROIs in each hemisphere. Similarly, the subcortical segmentation of a brain volume is based on the existence of an atlas containing probabilistic information on the location of structures (Fischl et al., 2002).

Aging-Related Trajectories of Brain Regional Volumes and Areas

We are interested in delineating the aging trajectories for the regional volumes and areas, while adjusting for sex, education, and the total intracranial volume (ICV). For normalization purpose, the regional volumes are divided by the ICV. To check the nonlinearity of the age trajectories of the regional volumes and areas, we first applied the loess (locally weighted scatterplot smoothing) method using the R function *loess*, which is a popular exploratory tool for checking nonlinear pattern. As a lot of ROIs show nonlinear age trajectories of brain regional volumes, we fit a semiparametric model for the normalized volume at each ROI with nonparametric age trajectory and parametric effects for sex and education using the *gam* function in the *mgcv* package. Similarly, we fit a semiparametric model for the area at each ROI with nonparametric age trajectory and parametric effects for sex, education and ICV. Penalized cubic B-splines with 10 basis functions are used to fit the age trajectories. The restricted maximum likelihood (REML, Reiss and Todd Ogden, 2009) method is used to select the tuning parameters. For comparison, we also fit linear and quadratic models for the age trajectories. The quadratic age term is centered to achieve robustness. Alternatively, orthogonal polynomial model can be used to avoid multicollinearity problem.

We choose the normalized volume of the lateral ventricle and putamen for illustration. **Figure 1** shows the estimated age trajectories (the solid lines) using different methods, and the 95% pointwise confidence intervals (the shaded area) for the B-spline fits. The lateral ventricle displays considerable expansion especially after age 70, while the putamen shows a large amount of decline especially before age 75. Both the lateral ventricle expansion and the putamen volume shrinkage indicate brain atrophy as people age. We notice that both the loess and the semiparametric fits indicate nonlinear age patterns. As displayed in **Figure 1**, linear models are not flexible enough to capture the nonlinear age trajectories. Linear models assume the rate of age-related change is constant as people age, which may not be true for all the ROIs. The deviation of the linear fits from the semiparmetric model fitted curves are large in the two ends and the middle part of the interval, that is less than 60, greater than 80, and around 70. The quadratic age trajectories show agreement with the B-spline fits around the middle of the age interval [60, 80], but not in the two ends

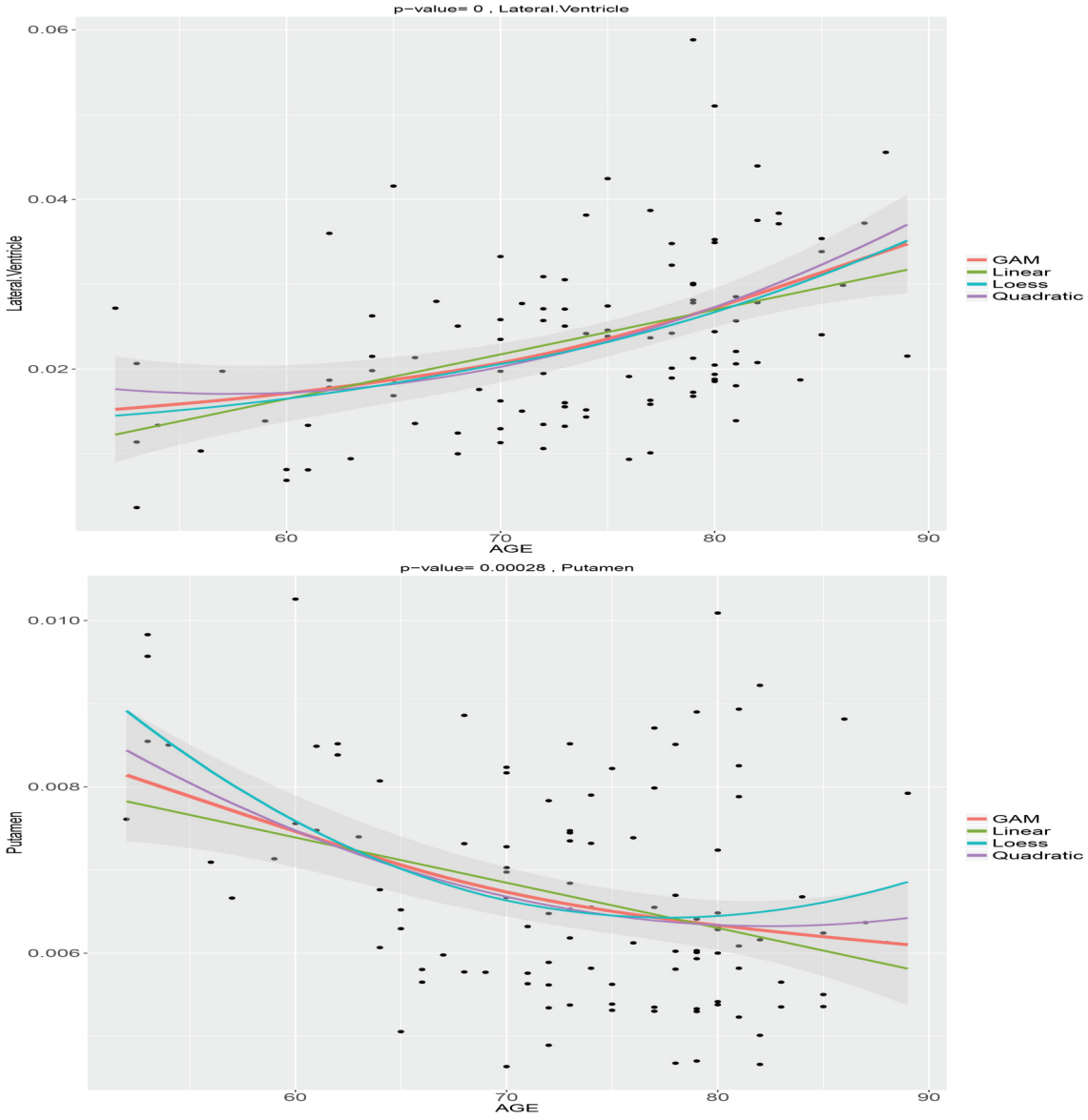

FIGURE 1 | Age trajectories of the normalized lateral ventricle and putamen volumes using the semiparametric model, loess fit, linear, and quadratic regression models.

either. The loess fits are exploratory without adjusting for sex and education. Interestingly the B-spline fits agree with the loess fit for the lateral ventricle volume but not the putamen volume.

Overall, age has significant effects on almost all of the cortical and subcortical regional volumes in both hemispheres after FDR correction. Particularly, the cortical frontal, temporal, parietal, occipital, cingulate lobes are significantly impacted by aging except the left caudal anterior cingulate, bilateral entorhinal, pericalcarine, and frontal pole. The insula shows a marginally significant age effect. The ventricle, subcortical regions, and corpus callosum are significant except for the bilateral caudate. Our findings are consistent with the literature that as people age, the brain regional volumes shrink, while the ventricle system and CSF considerably expand. We also observe that older females tend to have less brain atrophy compared to older males after FDR correction. Education does not have a significant effect on any of those regional volumes after FDR correction. Additionally, age shows similar effects on the cortical regional areas. However, after adjusting for the ICV, neither sex nor education has an effect on the cortical regional areas.

In summary, the linear/quadratic model due to its parametric nature, may not be flexible enough to capture age-related brain changes as people age. A nonparametric/semiparametric model should be used if there is a convincingly nonlinear pattern as suggested by an exploratory loess fit.

Cortical Thickness Based Cortical Network

Structural covariance has been used in the literature for studying cortical networks and patterns of neurodegeneration (Mechelli et al., 2005; Alexander-Bloch et al., 2013). Here, we are interested in applying graphical models to investigate the cortical network using the cortical thickness data from the Active Brain Study. We consider the cortical thickness at 34 ROIs in each of the hemispheres. For summary purpose, we group the 68 cortical ROIs into six lobes including the frontal, temporal, parietal, occipital, cingulate, and insula. We first compute the marginal Pearson correlation for the structural covariance/correlation. We then use the *huge* function to obtain the partial correlation (based on the precision matrix) and a binary undirected graph (or equivalently the adjacency matrix) using the glasso and node-wise regression respectively. The tuning parameters are selected by the stability method (Liu et al., 2010; Meinshausen and Bühlmann, 2010).

The results are summarized in **Figure 2**. The top two patterns in **Figure 2** display the thresholded marginal/partial correlation map for the 68 cortical ROIs (34 ROIs per hemisphere). The bottom two patterns display the undirected graph and the frontal subgraph plotted using function in the *igraph* package. The marginal correlation map is cut by 0.3. The marginal correlation and partial correlation show very different patterns. The range of the marginal correlation is much larger compared to the partial correlation. The two graphical methods share some similarity. The left and right correlation are strong even conditional on all the other ROIs. There are both inter- and intra-hemisphere correlation. Based on the bottom adjacency matrix plot, we observe that the frontal ROIs tend to be conditionally correlated (see also the bottom right panel in **Figure 2**). Other graph summary statistics can be easily calculated using functions in the *igraph* package such as degree of centrality.

In summary, the marginal correlation and partial correlation map often show different patterns. The interpretation of the two are also different. The marginal correlation between two ROIs does not account for the involvement of other ROIs, while the partial correlation between two ROIs adjusts for other ROIs. Due to the lasso penalty, the partial correlation map and the adjacency matrix are sparse that is some of the partial correlations/elements of the adjacency matrix are estimated to be zeros.

Predicting MoCA Using Brain Regional Volumes

In this section, we aim to select informative brain regional volumes in predicting the cognitive outcome MoCA. We first normalize regional volumes via dividing by the estimated intracranial volume (ICV), then standardize the variables by subtracting the sample mean and divided by sample standard deviation to make the variables comparable. The predictors we consider include the cortical and subcortical regional volumes, age, sex, and education. We used the *glmnet* function in the R package *glmnet* with both lasso and elastic net penalties. We choose the tuning parameters by 10-fold cross-validation.

Table 1 summarizes the selected variables and their coefficients using both penalties. The selected variables include regional volumes from the frontal and temporal lobes, subcortical regions, and demographic variables. Compared to the elastic net penalty, the lasso penalty tends to choose a small subset of correlated predictors. For example, the left pars opercularis (Brodmann area 44) was selected but not the right one. Consistent with the findings in the literature, we found that volumes of subcortical and cortical ROIs including the left accumbens, middle temporal, pars opercularis, temporal pole, right entorhinal, medial-orbito-frontal, pars opercularis are positively associated with MoCA.

The *glmnet* function can output the whole solution path. **Figure 3** displays the whole solution path for all the coefficients as functions of the logarithm tuning parameter λ for the lasso penalty. The vertical line corresponds to the optimal λ selected by cross-validation. When the tuning parameter λ is small (that is with less penalization), the magnitudes of the coefficients are large and the variability is large. The traditional least square estimate is similar to the small penalization case, which is not stable. As the tuning parameter increases, the variability of the coefficients declines. The regularization achieves the small variance at the cost of introducing bias. The cross-validation criterion selects the tuning parameter by balancing the variance and bias.

To check the performance of the selected subset of the regional volumes, we refit a model with the volume of the selected ROIs and compare to the model with only age, sex, and education. The selected regional volumes from the elastic net penalty explains additional 19% variance in MoCA, where R^2 increases from 16 to 35%. We conduct an ANOVA test to compare the two models, where the p-value is less than 0.001.

DISCUSSIONS

Misspecified linear models are not uncommon in the literature, which may lead to biased results and misleading conclusions. Based on our previous neuroimaging analysis (Chen et al., 2014, 2015), linear models may not always be appropriate for characterizing the age-related brain changes, although it is the default method due to its simplicity. In practice, cautions need to be raised for the potential nonlinear age-related changes. To minimize the potential bias, we introduced the spline-based semiparametric models, which are more flexible and able to capture the underlying age trends in the data. Notably a linear model is a special case of the semiparametric model. When the underlying trend is linear, semiparametric model agrees with the linear model. Semiparametric methods have been implemented in many statistical softwares such as R. One of the popular implementations is the *gam* function in the *mgcv* package. The *gam* function provides the estimated curves and inferential results for both the parametric and the nonparametric parts. Extension of the basic semiparametric model (1) has been extensively studied in the past few decades in the statistical literature. More sophisticated models such as varying coefficient models and additive models have also been developed (Wood, 2006; Wu and Zhang, 2006). All these semiparametric methods are scalable and applicable to voxel level data as well. The

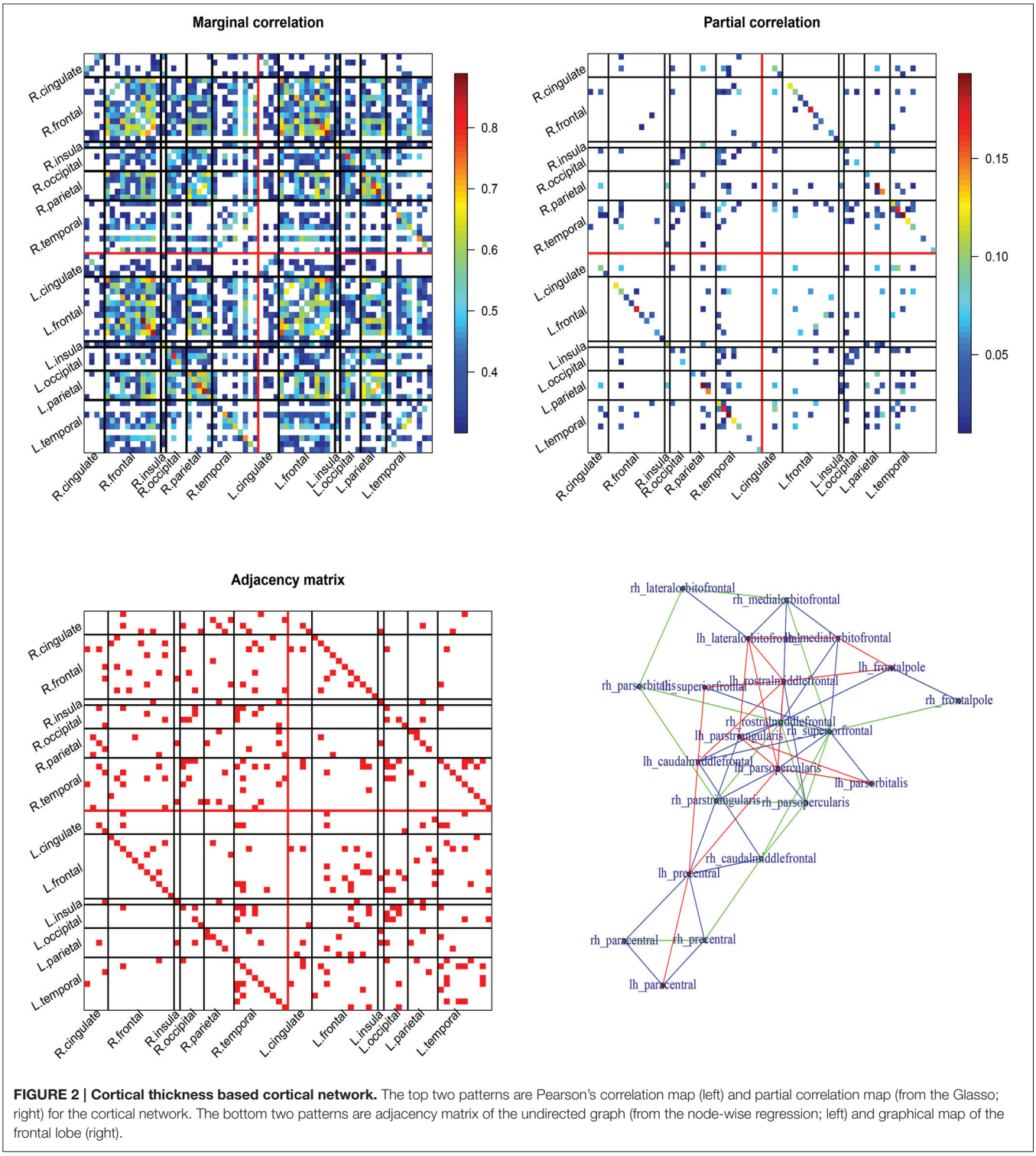

FIGURE 2 | Cortical thickness based cortical network. The top two patterns are Pearson's correlation map (left) and partial correlation map (from the Glasso; right) for the cortical network. The bottom two patterns are adjacency matrix of the undirected graph (from the node-wise regression; left) and graphical map of the frontal lobe (right).

R package *vows* has implemented semiparametric models for voxel-level data. A parallel algorithm is implemented to speed up the computational procedure.

In the neuroimaging literature, network analysis provides a systematic way to study the brain structural and functional changes. The use of network analysis is a remarkable progress from the pairwise relationship between ROIs. However, researchers often compute the marginal correlation then threshold the correlation matrix to obtain the graph/network. It is well known that sample covariance/correlation matrix is highly instable when the number of ROIs is large. The pairwise nature of the marginal correlations hurts and limits the interpretation of

TABLE 1 | Selected brain regional volumes and covariates in predicting MoCA.

	lh.middle.temporal (temporal lobe)	lh.pars.opercularis (frontal lobe)	lh.pars.orbitalis (frontal lobe)	lh.temporal.pole (temporal lobe)	rh.entorhinal (temporal lobe)	rh.medial.orbito.frontal (frontal lobe)
Elastic-net	0.047	0.345	−0.320	0.145	0.188	0.048
LASSO	0.004	0.433	−0.343	0.154	0.193	0.005
	rh.pars.opercularis (frontal lobe)	**lh.Accumbens**	**Age**	**Sex (F vs. M)**	**Education**	
Elastic-net	0.031	0.309	−0.231	0.331	0.177	
LASSO	-	0.358	−0.225	0.329	0.177	

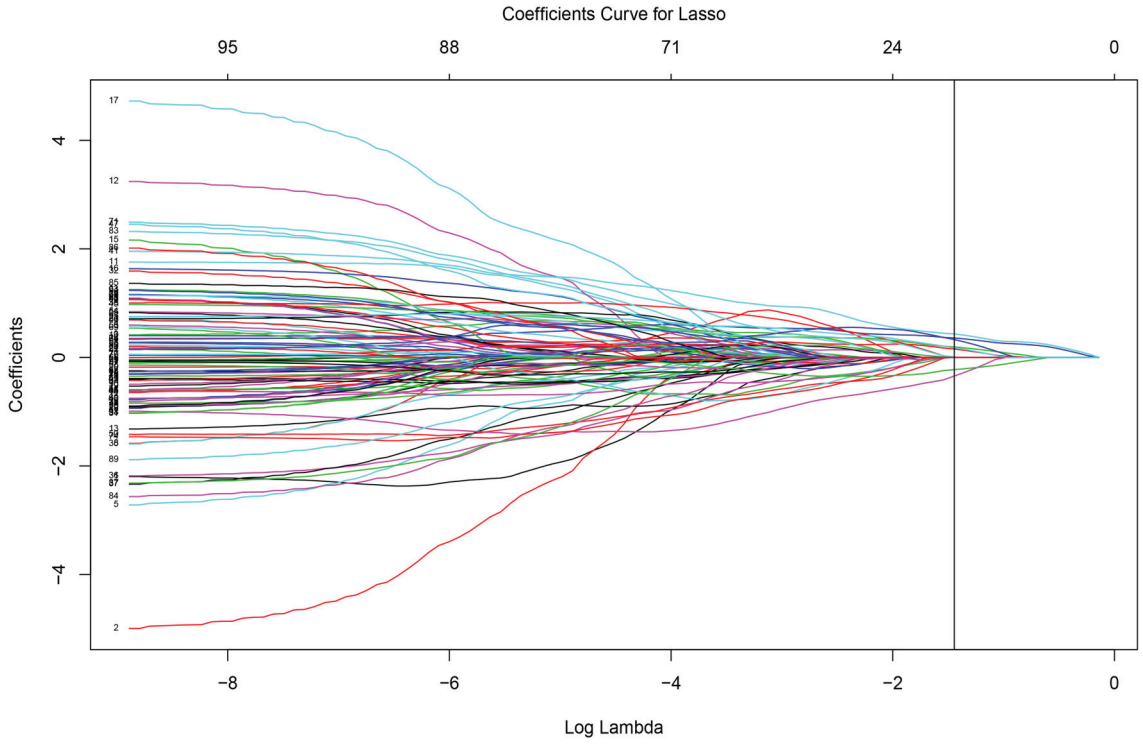

FIGURE 3 | Solution paths from the penalized regression with lasso penalty.

the subsequent network based results. To address the limitation of the marginal correlation, we introduced two Gaussian graphical models, which can generate either partial correlations or an undirected graph. Under the multivariate Gaussian assumption, a zero partial correlation for two ROIs given all the other ROIs is equivalent to conditional independence between the two ROIs. Similarly, for an undirected Gaussian graph, the edges indicate conditional dependence between ROIs. We illustrated the graphical models using the cortical thickness data, where the generated cortical networks may be related to the cortical structural connectivity. The application of graphical model to fMRI for investigating functional connectivity is straightforward, but need to be modified to account for the temporal correlation within each time series. Besides partial correlation in the time domain, there is a few works on correlation measure in the frequency domain such as the total independence (Wen et al., 2012) and partial correlation for multivariate time series (Fried and Didelez, 2005).

For testing the brain network differences between groups such as young vs. older, there are three levels of tests including the edge-level, node-level, and subgraph-level (Nichols and Holmes, 2002; Kim et al., 2014, 2015; Narayan and Allen, 2016). The edge-level testing approach first tests the group differences at the edges one by one, then applies multiple correction for the *p*-values such as FDR correction. The node-level testing method investigates the group differences in graph summary statistics at each node such as degree of centrality. The subgraph-level testing aims to detect either topologically connected cluster difference (Zalesky et al., 2010) or differences in graph overall

metrics such as clustering coefficient. The three levels of testing approaches provide complementary ways of testing the brain network differences.

Efficiently and accurately predicting cognitive decline is a central topic in cognitive and brain aging studies. In practice, very often an *a priori* subset of neuroimaging biomarkers are used to predict cognitive outcomes, which are based on the predetermined hypothesis. Hypothesis-driven methods are a recommended way to conduct research that can generate reproducible results. However, by chance, we may miss important neuroimaging markers that could indeed be predictive for cognitive decline. We introduced penalized regression methods for incorporating a large amount of neuroimaging biomarkers in predicting cognitive outcomes, where the number of predictors can be close to or even larger than the number of subjects. These data-driven methods can simultaneously estimate the regression coefficients and select a subset of the high-dimensional predictors. We illustrated those methods using the brain regional volumes in predicting MoCA outcomes. Moreover, these methods are applicable to categorical cognitive impairment outcomes such as a variable with three nominal levels: normal, mild cognitive impairment, and dementia. In addition to the penalized regression methods, some machine learning type of methods such as penalized support vector machine (SVM) can be used for building prediction/classification rule based on high dimensional neuroimaging biomarkers (Zhu et al., 2004; Zhang et al., 2006; Wu and Liu, 2007; Robinson et al., 2015). For long term followup longitudinal studies, penalized mixed effects model can be used to improve the prediction accuracy by incorporating both the individual trajectories and baseline or longitudinal neuroimaging biomarkers (Bondell et al., 2010; Ibrahim et al., 2011).

Neuroimaging data collected in studies of cognitive and brain aging raise statistical and analytic challenges due to the high dimensionality and complex structure. Fortunately, advanced statistical methods developed in the past few decades for high dimensional data and complex structured data could be applied for leveraging the multimodal neuroimaging analysis. These approaches provide a good starting point for analyzing such data. However, there is a strong need for developing new statistical methods that are specific to the multimodal neuroimaging analyses in cognitive and brain aging studies.

AUTHOR CONTRIBUTIONS

The first two authors HC and BZ conducted the analysis and initiated the paper, while the other five coauthors GC, EP, AO, AW, and RC contributed significant components for the presentations of the models and methods and the general discussions. The last two authors AW and RC are the PIs of the Active Brain Study.

ACKNOWLEDGMENTS

This work was supported by the McKnight Brain Research Foundation, the Center for Cognitive Aging and Memory at the University of Florida, and the Claude D. Pepper Center at the University of Florida (P30 AG028740). GC research was supported in part by the Simons Foundation under grant #354917.

REFERENCES

Alexander-Bloch, A., Giedd, J. N., and Bullmore, E. (2013). Imaging structural co-variance between human brain regions. *Nat. Rev. Neurosci.* 14, 322–336. doi: 10.1038/nrn3465

Amieva, H., Jacqmin-Gadda, H., Orgogozo, J.-M., Le Carret, N., Helmer, C., Letenneur, L., et al. (2005). The 9 year cognitive decline before dementia of the Alzheimer type: a prospective population-based study. *Brain* 128, 1093–1101. doi: 10.1093/brain/awh451

Benjamini, Y., and Heller, R. (2007). False discovery rates for spatial signals. *J. Am. Stat. Assoc.* 102, 1272–1281. doi: 10.1198/016214507000000941

Benjamini, Y., and Hochberg, Y. (1995). Controlling the false discovery rate: a practical and powerful approach to multiple testing. *J. R. Stat. Soc. Ser. B* 57, 289–300.

Bondell, H. D., Krishna, A., and Ghosh, S. K. (2010). Joint variable selection for fixed and random effects in linear mixed-effects models. *Biometrics* 66, 1069–1077. doi: 10.1111/j.1541-0420.2010.01391.x

Chen, H., Kelly, C., Castellanos, F. X., He, Y., Zuo, X.-N., and Reiss, P. T. (2015). Quantile rank maps: A new tool for understanding individual brain development. *NeuroImage* 111, 454–463. doi: 10.1016/j.neuroimage.2014.12.082

Chen, H., Paik, M. C., Dhamoon, M. S., Moon, Y. P., Willey, J., Sacco, R. L., et al. (2012). Semiparametric model for the dichotomized functional outcome after stroke: the northern Manhattan study. *Comput. Stat. Data Anal.* 56, 2598–2608. doi: 10.1016/j.csda.2012.02.001

Chen, H., Reiss, P. T., and Tarpey, T. (2014). Optimally weighted l2 distance for functional data. *Biometrics* 70, 516–525. doi: 10.1111/biom.12161

Csardi, G., and Nepusz, T. (2006). The igraph software package for complex network research. *InterJ. Comp. Syst.* 1695, 1–9.

Dale, A. M., Fischl, B., and Sereno, M. I. (1999). Cortical surface-based analysis: I. segmentation and surface reconstruction. *NeuroImage* 9, 179–194. doi: 10.1006/nimg.1998.0395

de Boor, C. (1978). *A Practical Guide to Splines*. New York, NY: Springer.

Desikan, R. S., Ségonne, F., Fischl, B., Quinn, B. T., Dickerson, B. C., Blacker, D., et al. (2006). An automated labeling system for subdividing the human cerebral cortex on MRI scans into gyral based regions of interest. *NeuroImage* 31, 968–980. doi: 10.1016/j.neuroimage.2006.01.021

Fan, J., and Li, R. (2001). Variable selection via nonconcave penalized likelihood and its oracle properties. *J. Am. Stat. Assoc.* 96, 1348–1360. doi: 10.1198/016214501753382273

Fischl, B., Salat, D. H., Busa, E., Albert, M., Dieterich, M., Haselgrove, C., et al. (2002). Whole brain segmentation: automated labeling of neuroanatomical structures in the human brain. *Neuron* 33, 341–355. doi: 10.1016/S0896-6273(02)00569-X

Fjell, A. M., Walhovd, K. B., Westlye, L. T., Østby, Y., Tamnes, C. K., Jernigan, T. L., et al. (2010). When does brain aging accelerate? dangers of quadratic fits in cross-sectional studies. *NeuroImage* 50, 1376–1383. doi: 10.1016/j.neuroimage.2010.01.061

Fried, R., and Didelez, V. (2005). Latent variable analysis and partial correlation graphs for multivariate time series. *Stat. Probabil. Lett.* 73, 287–296. doi: 10.1016/j.spl.2005.04.002

Gogtay, N., Giedd, J. N., Lusk, L., Hayashi, K. M., Greenstein, D., Vaituzis, A. C., et al. (2004). Dynamic mapping of human cortical development during childhood through early adulthood. *Proc. Natl. Acad. Sci. U.S.A.* 101, 8174–8179. doi: 10.1073/pnas.0402680101

Grober, E., Hall, C. B., Lipton, R. B., Zonderman, A. B., Resnick, S. M., and Kawas, C. (2008). Memory impairment, executive dysfunction, and intellectual decline

in preclinical Alzheimer's disease. *J. Int. Neuropsychol. Soc.* 14, 266–278. doi: 10.1017/S1355617708080302

Ibrahim, J. G., Zhu, H., Garcia, R. I., and Guo, R. (2011). Fixed and random effects selection in mixed effects models. *Biometrics* 67, 495–503. doi: 10.1111/j.1541-0420.2010.01463.x

Jedynak, B. M., Lang, A., Liu, B., Katz, E., Zhang, Y., Wyman, B. T., et al. (2012). A computational neurodegenerative disease progression score: method and results with the alzheimer's disease neuroimaging initiative cohort. *NeuroImage* 63, 1478–1486. doi: 10.1016/j.neuroimage.2012.07.059

Kim, J., Wozniak, J. R., Mueller, B. A., and Pan, W. (2015). Testing group differences in brain functional connectivity: using correlations or partial correlations? *Brain Connect.* 5, 214–231. doi: 10.1089/brain.2014.0319

Kim, J., Wozniak, J. R., Mueller, B. A., Shen, X., and Pan, W. (2014). Comparison of statistical tests for group differences in brain functional networks. *NeuroImage* 101, 681–694. doi: 10.1016/j.neuroimage.2014.07.031

Koller, D., and Friedman, N. (2009). *Probabilistic Graphical Models: Principles and Techniques*. Cambridge, MA: MIT press.

Lauritzen, S. L. (1996). *Graphical Models*. Oxford, UK: Oxford University Press.

Liu, H., Roeder, K., and Wasserman, L. (2010). "Stability approach to regularization selection (stars) for high dimensional graphical models," in *Advances in Neural Information Processing Systems,* Vol. 23, eds J. D. Lafferty, C. K. I. Williams, J. Shawe-Taylor, R. S. Zemel, and A. Culotta (New York, NY: Curran Associates, Inc.), 1432–1440.

Mechelli, A., Friston, K. J., Frackowiak, R. S., and Price, C. J. (2005). Structural covariance in the human cortex. *J. Neurosci.* 25, 8303–8310. doi: 10.1523/JNEUROSCI.0357-05.2005

Meinshausen, N., and Bühlmann, P. (2006). High-dimensional graphs and variable selection with the lasso. *Ann. Stat.* 34, 1436–1462. doi: 10.1214/009053606000000281

Meinshausen, N., and Bühlmann, P. (2010). Stability selection. *J. R. Stat. Soc. Ser. B* 72, 417–473. doi: 10.1111/j.1467-9868.2010.00740.x

Narayan, M. and Allen, G. I. (2016). Mixed effects models for resampled network statistics improves statistical power to find differences in multi-subject functional connectivity. *Front. neurosci.* 10:108. doi: 10.3389/fnins.2016.00108

Nichols, T. E., and Holmes, A. P. (2002). Nonparametric permutation tests for functional neuroimaging: a primer with examples. *Hum. Brain Mapp.* 15, 1–25. doi: 10.1002/hbm.1058

R Core Team (2012). *R: A Language and Environment for Statistical Computing*. Vienna: R Foundation for Statistical Computing. ISBN 3-900051-07-0.

Raz, N., Ghisletta, P., Rodrigue, K. M., Kennedy, K. M., and Lindenberger, U. (2010). Trajectories of brain aging in middle-aged and older adults: regional and individual differences. *NeuroImage* 51, 501–511. doi: 10.1016/j.neuroimage.2010.03.020

Reiss, P. T., Huang, L., Chen, Y.-H., Huo, L., Tarpey, T., and Mennes, M. (2014). Massively parallel nonparametric regression, with an application to developmental brain mapping. *J. Comput. Graph. Stat.* 23, 232–248. doi: 10.1080/10618600.2012.733549

Reiss, P. T., and Todd Ogden, R. (2009). Smoothing parameter selection for a class of semiparametric linear models. *J. R. Stat. Soc. Ser. B* 71, 505–523. doi: 10.1111/j.1467-9868.2008.00695.x

Resnick, S. M., Pham, D. L., Kraut, M. A., Zonderman, A. B., and Davatzikos, C. (2003). Longitudinal magnetic resonance imaging studies of older adults: a shrinking brain. *J. Neurosci.* 23, 3295–3301.

Robinson, M. E., O'Shea, A. M., Craggs, J. G., Price, D. D., Letzen, J. E., and Staud, R. (2015). Comparison of machine classification algorithms for fibromyalgia: neuroimages versus self-report. *J. Pain* 16, 472–477. doi: 10.1016/j.jpain.2015.02.002

Salvador, R., Suckling, J., Schwarzbauer, C., and Bullmore, E. (2005). Undirected graphs of frequency-dependent functional connectivity in whole brain networks. *Philos. Trans. R. Soc. B Biol. Sci.* 360, 937–946. doi: 10.1098/rstb.2005.1645

Smith, S. M. (2012). The future of fmri connectivity. *NeuroImage* 62, 1257–1266. doi: 10.1016/j.neuroimage.2012.01.022

Szymkowicz, S. M., McLaren, M. E., Kirton, J. W., O'Shea, A., Woods, A. J., Manini, T. M., et al. (2016). Depressive symptom severity is associated with increased cortical thickness in older adults. *Int. J. Geriatr. Psychiatry.* 31, 325–333. doi: 10.1002/gps.4324

Thompson, W. K., Hallmayer, J., and O'Hara, R. (2011). Design considerations for characterizing psychiatric trajectories across the lifespan: application to effects of APOE-e4 on cerebral cortical thickness in Alzheimer's disease. *Am. J. Psychiatry* 168, 894–903. doi: 10.1176/appi.ajp.2011.10111690

Tibshirani, R. (1996). Regression shrinkage and selection via the lasso. *J. R. Stat. Soc. Ser. B* 58, 267–288.

Valdés-Sosa, P. A., Sánchez-Bornot, J. M., Lage-Castellanos, A., Vega-Hernández, M., Bosch-Bayard, J., Melie-García, L., et al. (2005). Estimating brain functional connectivity with sparse multivariate autoregression. *Philos. Trans. R. Soc. B Biol. Sci.* 360, 969–981. doi: 10.1098/rstb.2005.1654

Wen, X., Mo, J., and Ding, M. (2012). Exploring resting-state functional connectivity with total interdependence. *NeuroImage* 60, 1587–1595. doi: 10.1016/j.neuroimage.2012.01.079

Wood, S. (2006). *Generalized Additive Models: An Introduction with R*. Boca Raton, FL: CRC Press.

Wu, H., and Zhang, J.-T. (2006). *Nonparametric Regression Methods for Longitudinal Data Analysis: Mixed-Effects Modeling Approaches*, New York, NY: John Wiley & Sons.

Wu, Y., and Liu, Y. (2007). Robust truncated hinge loss support vector machines. *J. Am. Stat. Assoc.* 102, 974–983. doi: 10.1198/016214507000000617

Yuan, M., and Lin, Y. (2007). Model selection and estimation in the gaussian graphical model. *Biometrika* 94, 19–35. doi: 10.1093/biomet/asm018

Zalesky, A., Fornito, A., and Bullmore, E. T. (2010). Network-based statistic: identifying differences in brain networks. *NeuroImage* 53, 1197–1207. doi: 10.1016/j.neuroimage.2010.06.041

Zhang, H. H., Ahn, J., Lin, X., and Park, C. (2006). Gene selection using support vector machines with non-convex penalty. *Bioinformatics* 22, 88–95. doi: 10.1093/bioinformatics/bti736

Zhao, T., Liu, H., Roeder, K., Lafferty, J., and Wasserman, L. (2012). The huge package for high-dimensional undirected graph estimation in R. *J. Mach. Learn. Res.* 13, 1059–1062.

Zhu, J., Rosset, S., Hastie, T., and Tibshirani, R. (2004). 1-norm support vector machines. *Adv. Neural Inform. Process. Syst.* 16, 49–56.

Zou, H. (2006). The adaptive lasso and its oracle properties. *J. Am. Stat. Assoc.* 101, 1418–1429. doi: 10.1198/016214506000000735

Conflict of Interest Statement: The authors declare that the research was conducted in the absence of any commercial or financial relationships that could be construed as a potential conflict of interest.

Copyright © 2016 Chen, Zhao, Cao, Proges, O'Shea, Woods and Cohen. This is an open-access article distributed under the terms of the Creative Commons Attribution License (CC BY). The use, distribution or reproduction in other forums is permitted, provided the original author(s) or licensor are credited and that the original publication in this journal is cited, in accordance with accepted academic practice. No use, distribution or reproduction is permitted which does not comply with these terms.

Archival Report

Biological Psychiatry: CNNI

Frontal Gamma-Aminobutyric Acid Concentrations Are Associated With Cognitive Performance in Older Adults

Eric C. Porges, Adam J. Woods, Richard A.E. Edden, Nicolaas A.J. Puts, Ashley D. Harris, Huaihou Chen, Amanda M. Garcia, Talia R. Seider, Damon G. Lamb, John B. Williamson, and Ronald A. Cohen

ABSTRACT

BACKGROUND: Gamma-aminobutyric acid (GABA), the brain's principal inhibitory neurotransmitter, has been associated with perceptual and attentional functioning. Recent application of magnetic resonance spectroscopy (MRS) provides in vivo evidence for decreasing GABA concentrations during adulthood. It is unclear, however, how age-related decrements in cerebral GABA concentrations contribute to cognitive decline, or whether previously reported declines in cerebral GABA concentrations persist during healthy aging. We hypothesized that participants with higher GABA concentrations in the frontal cortex would exhibit superior cognitive function and that previously reported age-related decreases in cortical GABA concentrations continue into old age.

METHODS: We measured GABA concentrations in frontal and posterior midline cerebral regions using a Mescher-Garwood point-resolved spectroscopy (MEGA-PRESS) ^{1}H-MRS approach in 94 older adults without history or clinical evidence of mild cognitive impairment or dementia (mean age, 73 years). We administered the Montreal Cognitive Assessment to assess cognitive functioning.

RESULTS: Greater frontal GABA concentrations were associated with superior cognitive performance. This relation remained significant after controlling for age, years of education, and brain atrophy. GABA concentrations in both frontal and posterior regions decreased as a function of age.

CONCLUSIONS: These novel findings from a large, healthy, older population indicate that cognitive function is sensitive to cerebral GABA concentrations in the frontal cortex, and GABA concentration in frontal and posterior regions continue to decline in later age. These effects suggest that proton MRS may provide a clinically useful method for the assessment of normal and abnormal age-related cognitive changes and the associated physiological contributors.

Keywords: Aging, Cognition, GABA, γ-Aminobutyric, MEGA-PRESS, MRS

http://dx.doi.org/10.1016/j.bpsc.2016.06.004

Gamma-aminobutyric acid (GABA) is the principal inhibitory neurotransmitter in the human nervous system and plays a fundamental role in central nervous system function (1). GABA neurotransmission is involved in nearly all neuronal coding and processing throughout the brain. It directly influences membrane potentials through ionic $GABA_A$ receptors and modulates both short- and longer-term neuronal activity via G-protein coupled $GABA_B$ receptors, modifying synaptic and network plasticity (2–6). Given this connection to synaptic plasticity, GABA has been studied in the context of the aging brain. Recent work demonstrates that GABA concentrations decline with age (7), and rodent models have shown age-related decreases in a GABA synthetic enzyme, glutamic acid decarboxylase (8). However, the relation between these long-term decreases in GABA concentrations and age-related declines in cognitive function has yet to be determined.

A large body of GABA studies relies on examination of downstream pharmacological effects of GABAergic agents (e.g., benzodiazepines) and animal models. This work links GABA to age-related cognitive decline in rodents (9), specifically noting the importance of GABA as a modulator of memory encoding (10,11). Although such studies provide a strong foundation for investigations into the relation between GABA and cognition, these methods make extensions of their results to more broad discussions of human cognition challenging. Relevant to the question at hand, then, is the development of Mescher-Garwood point-resolved spectroscopy (MEGA-PRESS) (12,13) for GABA-edited magnetic resonance spectroscopy (MRS) (12,14,15). This acquisition sequence allows for relatively rapid and reliable quantification of GABA concentrations in the brain of awake humans. Because these GABA concentrations are experimentally mutable (16,17), MEGA-PRESS more directly enables research into the regionally variable role of GABA in behavior and cognitive function.

This approach has proven to be a flexible and powerful tool for examining GABA, facilitating investigations of GABAergic contributions to specific behaviors and pathological disorders and differences in GABA concentrations between populations. Broadly, researchers have used this approach to demonstrate

© 2016 Society of Biological Psychiatry. Published by Elsevier Inc. All rights reserved.

ISSN: 2451-9022

that GABA concentrations correlate with other measures of brain activity, including functional magnetic resonance imaging indices (18,19), cerebral blood flow (19), and motor cortex gamma oscillations (20). Specifically applying this work to the intersection between GABA and cognition, several MRS studies have examined the role of GABA in sensory and motor functioning in healthy populations. Often, these studies delineate the differential importance of GABA in various brain regions for multiple sensorimotor or cognitive functions. For example, associations between sensorimotor GABA concentrations and tactile sensitivity have been demonstrated in sensorimotor cortices (21,22). GABA concentrations in the occipital cortex have been shown to relate to visual orientation discrimination (23), whereas frontal GABA concentrations correspond with working memory performance (24). Thus, some degree of specificity between cortical GABA concentration and cognitive ability seems likely. Less clear, however, is the relation between GABA and higher-order cognitive functioning and its decline in healthy aging.

Notably, although GABA concentrations tend to be stable over the short term (25), they do change over longer periods of time. A recent cross-sectional study of adults (20–76 years of age) indicated that GABA concentrations decrease with age after adolescence. This report specifically found an approximate 5% reduction in GABA concentrations with age per decade in the frontal cortex (7). Because the frontal cortex is important for numerous cognitive domains, notably those related to executive function (26–29), such a decline might correlate or even underlie alterations in related domains of cognitive function. The functional significance of these age-associated changes in GABA is not well established.

Given these considerations, the present study examined the relation between frontal and posterior GABA concentrations and cognitive function in the context of normal cognitive aging. We sought to extend previous work relating GABA and cognitive function in modality-specific cortices (e.g., occipital lobe) by investigating higher-order cognition with a general cognitive screening measure, the Montreal Cognitive Assessment (MoCA) (30). This tool, widely used in clinical settings, taps several cognitive domains, including attention/working memory, verbal memory, naming, and fluency. Because a number of these domains fall under the umbrella of executive functions, the MoCA is quite sensitive to frontal dysfunction in general (31). Convergently, older adults demonstrate changes in both frontal activation and frontally mediated cognitive functions. Thus, we placed our primary MRS voxel of interest in the frontal lobe. We predicted that GABA concentrations would continue to decrease in advanced age. We also predicted that the relation between concentrations of GABA in the frontal regions would predict general cognitive performance on the MoCA. We additionally placed a voxel in the posterior cortex to serve as a control. We predicted that, although GABA in this region would decline with age, there would be no association between GABA concentrations and global cognitive performance.

METHODS AND MATERIALS

Population

Ninety-four older volunteers (54 women, 40 men; age [mean ± SD], 73.12 ± 9.9 years; years of education, 16.25 ± 2.8 years; MoCA scores, 25.5 ± 2.5) were recruited from the local community. Subjects with a self-reported history of neurological or psychiatric disease on comprehensive medical questionnaires or magnetic resonance imaging (MRI) prescreening forms were excluded from the study. Subjects reported abstaining from alcohol on the day of MRS data collection. Of the 94 subjects, 89 had the frontal voxel collected, and 90 had the posterior voxel collected (due to time constraints in the imaging sequence, 5 participants had only a frontal voxel collected and 4 participants had only a posterior voxel collected). Ethical approval for the study was obtained via the University of Florida's Institutional Review Board, and all participants signed an informed consent form after discussion of the study with a study coordinator and review of the document.

MoCA

The MoCA is a one-page cognitive assessment that takes approximately 10 minutes to administer. A score of 0–30, reflecting general cognitive function, is derived from performance on tasks assessing the following cognitive domains: verbal memory, visuospatial abilities, executive functions, attention, working memory, naming, verbal fluency, repetition, and orientation to time and place (30). One point was added to the scores of participants who had 12 years of education or less (30). Using the MoCA total score in this analysis has a number of advantages. First, the MoCA is a widely used clinical tool with good psychometric properties (e.g., test-retest reliability and internal consistency). It has better sensitivity to mild cognitive impairment and other forms of cognitive decline, including Korsakoff's syndrome, than the Mini-Mental State Examination (32). Thus, a comparison between MoCA performance and GABA concentration allows for a discussion of these mechanisms in a translational context. Precisely because this measure is both sensitive and quick to administer, the MoCA is an efficient test to use in the clinical space. This analysis, then, allows for extension of previous GABA studies to a highly clinically relevant tool. The MoCA, however, does present a notable disadvantage. This instrument is useful when interpreted as a whole, but is not as useful at the level of subscale analysis, because the domains frequently are probed with three to five questions. This small range limits variability, and in healthy populations, many domains experience a ceiling effect. Therefore, the utility of this instrument is somewhat limited to general cognitive performance.

MRS Acquisition and Analysis, ^{1}H-MRS Spectroscopy, Spectrum Editing, and Volume-of-Interest Refraction

All scanning was performed on a 3T Philips Achieva scanner (Philips Healthcare, Best, The Netherlands) using a 32-channel head coil. A T1-weighted anatomical image (magnetization-prepared rapid gradient-echo; repetition time/echo time = 8 ms/3.7 ms, 1-mm^3 isotropic voxels) was acquired for MRS voxel placement and segmentation. GABA-edited MRS data were acquired using the MEGA-PRESS sequence (12). PRESS localization was achieved with minimum-phase amplitude-modulated excitation pulses (2-kHz bandwidth) and amplitude-modulated refocusing pulses (bandwidth, 1.3 kHz), as shown in Figure 3 of Mullins *et al.* (14). Editing was performed with 14-ms

sinc-Gaussian pulses applied at 1.9 ppm in the on experiment and 7.46 ppm in the off experiment. This editing scheme co-edits approximately 50% macromolecules at 3 ppm, which are coupled to spins at 1.7 ppm also inverted by editing pulses. Therefore, all GABA values reported refer to GABA + macromolecules. Acquisition variables were repetition time/echo time of 2 s/68 ms; 320 transients with on-off scans alternating every 2 transients; a 16-step phase cycle (with steps repeated for on and off); 2048 data points acquired at a spectral width of 2 kHz; and variable pulse power and optimized relaxation delays (VAPOR) water suppression (33). Sixteen transients of water-unsuppressed data were also acquired for quantification using the same acquisition variables. All voxels were $3 \times 3 \times 3$ cm^3. Representative voxel locations are shown in Figure 1A. Voxel locations were verified after data collection to identify placement errors. Quantitative analysis was performed using the Gannet program (version 2.0) (34). All time domain data were frequency- and phase-corrected using spectral registration (35), filtered with a 3-Hz exponential line broadening and zero-filled by a factor of 16. The 3-ppm GABA peak in the difference spectrum was fit using a five-parameter Gaussian model and quantified relative to water (fit with a Gaussian-Lorentzian model) in institutional units. To correct for tissue-related factors, controlling for cerebrospinal fluid (CSF) content in the voxel is the most common approach (36) and has been applied in populations in whom voxel tissue composition may vary (37,38). This correction involved the generation of a binary mask of the MRS voxel created with the same imaging matrix as the T1-weighted anatomical image, using Gannet's (34) integrated voxel-to-image coregistration. Segmentation of the anatomical image was performed using Segment in SPM12 (39). The voxel fraction that was CSF, gray matter, and white matter was calculated. In addition, all multiple regression models were rerun, replacing CSF with gray matter and white mater in the model. In all models, all factors significant for the CSF approach were also significant for the gray matter and white matter approach and vice versa. Thus, we only report the CSF fraction because it makes fewer assumptions as to tissue-specific

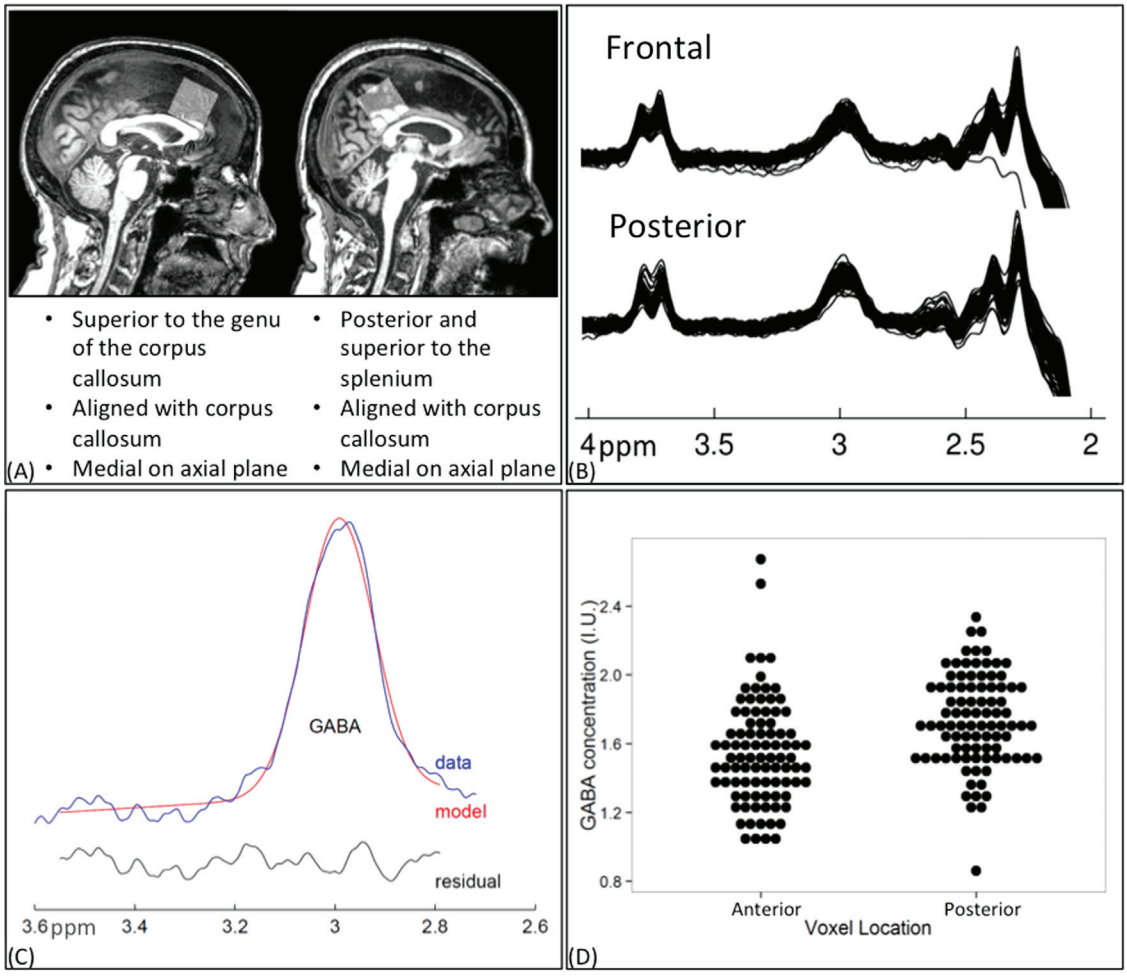

Figure 1. **(A)** Voxel locations in the frontal and posterior regions of the brain. The gray box represents the location of the $3 \times 3 \times 3$ cm voxel collected using Mescher-Garwood point-resolved spectroscopy. **(B)** Edited spectra from the frontal and posterior voxels for all subjects. Gamma-aminobutyric acid (GABA) peak is at 3.02 ppm. **(C)** Representative Gannet GABA model fit. **(D)** Stacked dot plot demonstrating greater GABA concentrations in the posterior voxel. I.U., institutional unit.

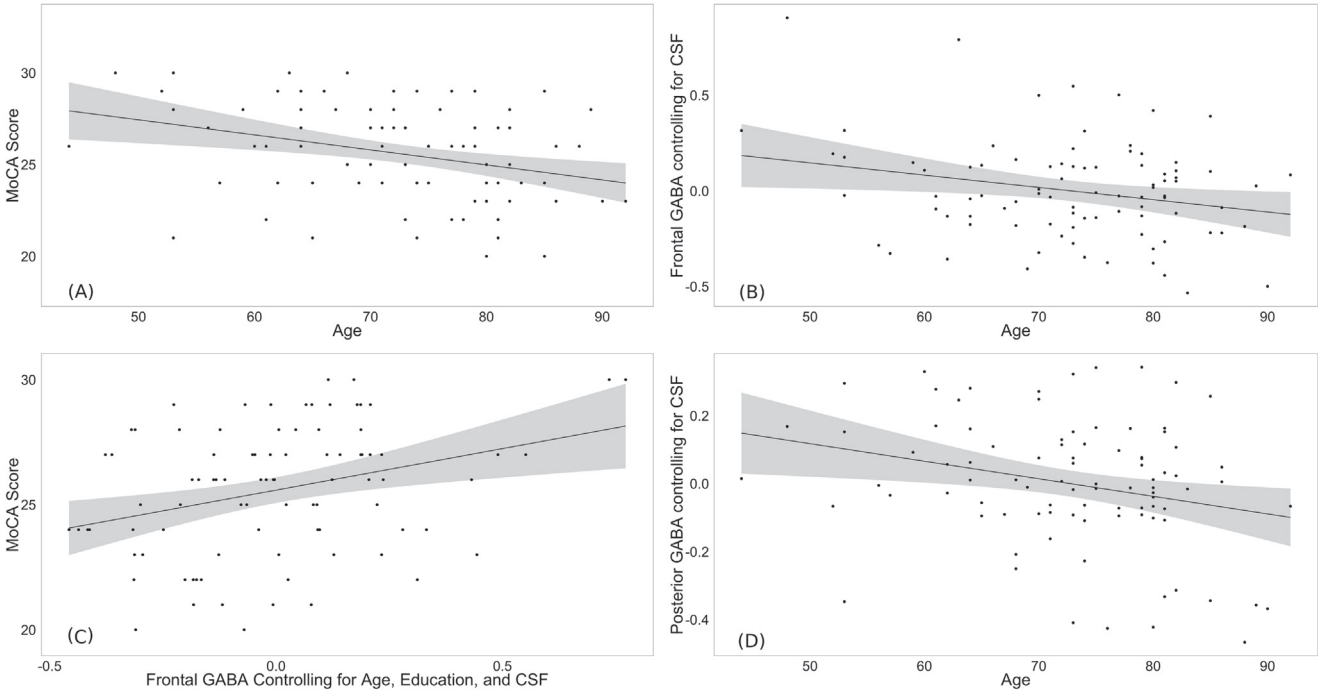

Figure 2. Confidence intervals are 95% for the regression line. **(A)** Plot demonstrating greater participant age associated with lower performance on the Montreal Cognitive Assessment (MoCA). **(B)** Plot demonstrating the age-related decrease in frontal gamma-aminobutyric acid (GABA) concentrations. **(C)** Plot demonstrating the age-related decrease in posterior GABA concentrations. **(D)** Plot demonstrating the relation between frontal GABA concentrations and MoCA scores. The relation remains significant when the two highest GABA data points are removed. CSF, cerebrospinal fluid.

GABA concentrations (36) and is more consistent with previously published approaches to age-related changes in GABA (7).

RESULTS

MoCA as a Function of Demographic Variables

MoCA scores were initially investigated with relation to the demographic variables. Multiple regression was used to analyze the predictive value of age and education for overall cognitive performance. This regression demonstrated that these demographic variables accounted for a significant proportion of variance in cognitive performance (R^2 = .1103, $F_{2,91}$ = 5.64, $p < .005$). Within this model, age significantly predicted score, such that older participants had lower scores (B = −.08, $p < .005$). Figure 2A displays the relation between age and MoCA score. Education was not associated with scores (B = .08, p = .33).

GABA Concentrations as a Function of Brain Region

A significant difference was found for GABA concentrations between the frontal (1.546 ± 0.305) and posterior (.7339 ± 0.264) voxels (t_{84} = −5.3373, $p < .001$), with a greater concentration of GABA in the posterior voxel.

GABA Concentrations as a Function of Age

Frontal Voxel. With the use of a linear regression model, lower GABA concentrations significantly predicted increased age (R^2 = .25, $F_{1,87}$ = 29.56, $p < .001$, B = −16.42, $p < .001$). Given that this decrease may have been a function of age-associated atrophy, rather than GABA-specific changes per se, we conducted a multiple regression, including CSF fraction and GABA concentration as predictors of age (R^2 = .38, $F_{2,86}$ = 26.19, $p < .001$). CSF concentrations were positively associated with age (B = 57.41, $p < .001$), and GABA concentrations were negatively associated with age (B = −9.378, $p < .01$). Notably, even when accounting for CSF fraction, GABA concentration remained a significant predictor of age. This association is depicted in Figure 2B.

Posterior Voxel. Linear regression revealed that lower GABA concentrations in the posterior voxel significantly predicted increased age (R^2 = .15, $F_{1,88}$ = 15.26, $p < .005$, B = −14.28, $p < .001$). To account for age-related atrophy, a multiple regression was conducted with CSF fraction and GABA concentration as predictors of age (R^2 = .38, $F_{2,86}$ = 26.19, $p < .001$). Greater age was related to lower GABA concentrations (B = −13.95, $p < .01$); no relation was found between CSF concentrations and age (B = 1.65, p = .93). This association is depicted in Figure 2C.

Cognitive Performance as a Function of GABA Concentrations

Frontal Voxel. The relation between frontal GABA concentration and the MoCA score was investigated using linear regression. The results of this regression indicated that GABA in this region accounted for a significant amount of variance in MoCA performance, such that higher concentrations of GABA

predicted better cognitive functioning (R^2 = .18, $F_{1,87}$ = 18.95, $p < .001$, B = 3.5, $p < .001$). On visual inspection, two data points appeared to be outliers. Although they did not fall beyond our outlier cutoff of 3 SDs above or below the mean, we reran the analyses without these participants. When their data were removed, the relation remained significant (R^2 = .12, $F_{1,85}$ = 11.63, $p < .001$), and GABA concentration continued to predict cognitive functioning (B = 3.3, $p < .001$).

Next, the relation between GABA concentration and MoCA score was queried, controlling for age, education, and CSF fraction. The results of this multiple regression demonstrated that the four predictors accounted for a significant amount of the variance in cognitive performance (R^2 = .22, $F_{4,84}$ = 5.775, $p < .001$). Within this model, higher GABA concentration significantly predicted better score, even when accounting for demographic influences and CSF fraction (B = 3.32, $p < .01$). Cognitive performance was not independently related to age, years of education, and/or CSF fraction (B = −.5, p = .12; B = .10, p = .24; B = 3.95, p = .37, respectively). We additionally reran the analyses without the two high-GABA participants. The overall model remained significant (R^2 = .16, $F_{4,82}$ = 3.87, $p < .01$). Higher GABA concentration continued to predict better MoCA scores (B = 3.14, $p < .01$), whereas the other covariates did not (B = −.5, p = .12; B = .10, p = .27; B = 3.85, p = .39, respectively). Figure 2D depicts the association between frontal GABA concentration and MoCA, controlling for age, education, and CSF fraction.

Posterior Voxel. The relation between posterior GABA concentration and MoCA score was investigated using a linear regression. The results of this regression indicated that posterior GABA concentration does not account for a significant amount of variance in performance (R^2 = .04, $F_{1,88}$ = 5.267, p = .07). Next, the relation between posterior GABA concentration and MoCA score was queried, controlling for age, education, and CSF fraction. The results of this multiple regression demonstrated that the four predictors accounted for a significant amount of variance in cognitive performance (R^2 = .12, $F_{4,85}$ = 2.84, $p < .05$). Among these variables, age was a significant predictor of cognitive performance (B = −.08, $p < .01$), such that greater age was associated with reduced performance. GABA concentration, years of education, and CSF fraction did not significantly predict cognitive performance (B = 1.4, p = .34; B = .07, $p > .44$; B = 3.44, p = .48, respectively). The addition of age, education, and CSF fraction reduced the contribution to the model of the posterior GABA concentration.

DISCUSSION

The primary findings of our study are that GABA concentrations in frontal and posterior regions decline with age and that decline in frontal, but not posterior, GABA concentration was associated with lower MoCA scores. The finding of reduced GABA in frontal and posterior cortices is consistent with previous work that has used ^{1}H-MRS to assess GABA in healthy adult populations (7), and it extends these findings by showing that this effect continues to occur with advanced age. Notably, the more aggressive rate of decline in frontal GABA concentrations is consistent with age-associated declines observed in other neuroimaging methods, including cortical volume (40) and white matter integrity (41,42), as well as with cognitive measures (43–45). Because a decline in GABA in the frontal region was evident even after controlling for atrophy by including CSF voxel fraction, we conclude that this effect is not simply a function of cortical atrophy, but rather a reduction of GABA concentration in brain tissue.

The age-related decline in GABA concentrations we report here is consistent with those previously reported by Gao *et al.* (7) in both frontal and posterior regions; however, other factors could account for the relation between GABA concentrations and MoCA scores. As such, we controlled for what were likely the strongest contributors: age and CSF fraction. Years of education was also included in the model because higher educational attainment is associated with superior cognitive function in old age in general (46) and on the MoCA specifically (30). Lower GABA concentrations, controlling for age, CSF fraction, and education, corresponded with lower MoCA scores in the frontal but not posterior voxel. Importantly, a one-unit increase in GABA corresponded to more than three-point increase in the MoCA score (B = 3.32), which is greater than estimates of test-retest reliability in the measure (30). Although the data presented here do not represent within-subject change, they suggest that a one-unit decrease in GABA would correspond to clinically significant cognitive decline. Given the small effect size, however, it should be contextualized as merely one factor contributing to age-related cognitive change. Other considerations influencing this relation are targets for future study and are further elucidated below.

Previous work has identified several specific cognitive domains that are associated with GABA concentration, including memory and attention (9,10,47). This investigation extends work on those specific domains to identify a connection between GABA and higher-order cognitive performance. Notably, although the MoCA is not designed for subdomain analysis, it is composed of a number of subtests tapping frontoexecutive functions. Given the significant GABA-cognition relation in the frontal but not posterior voxel, our results demonstrate some regional specificity of the impact of GABA concentration on cognition. Mechanistically, this relation may be subserved by the effect of GABA on signal-to-noise ratios in the implicated cortical regions. By increasing signal to noise, GABA likely facilitates information extraction and retention, abilities that are reflected in the total MoCA.

A number of questions remain unresolved with respect to GABA and cognition in the context of aging. Although we controlled for age, education, and atrophy as measured by the percentage of CSF brain tissue, it is possible that other factors contribute to the observed associations. That is, although the present study demonstrates an overall association between age, GABA, and cognition, it lacks sufficient power to explore all possible covariates that contribute to this association. Potential mechanisms that may underlie our findings and that cannot be ruled out include changes in macromolecule concentrations and gray or white matter alterations beyond the sensitivity of the relatively coarse measure used here. For example, white matter integrity, as reflected by frontal scalar measures of anisotropy on diffusion MRI, may be a contributing factor. Indeed, age-related white matter changes may, to

some extent, account for both the relation between age and cognition and the relation between GABA and cognition. Although we may have obliquely been able to address these changes by controlling for medical and/or behavioral comorbidities, this question would be more accurately addressed with a specific and intentional quantification of white matter changes. Therefore, future studies examining the relation between other neuroimaging methods such as diffusion MRI and GABA MRS would be valuable.

In addition, the present study queried potential comorbidities, including drug and alcohol abuse, through an extensive medical interview. However, we did not conduct toxicology screens on the participants to verify their statements, which may affect the generalizability of the results. Further studies specifically investigating the relation between GABA, age, cognition, and drug and alcohol use should use such an objective measurement. The relation between other comorbid factors that affect cortical GABA concentrations, such as insomnia and depression (48,49) and their interaction with aging, should also be investigated because these may modulate the relation between GABA and cognition.

Finally, the mechanisms underlying the influence of GABA on cognitive performance need to be investigated in greater detail. Decreases in GABA concentrations may indicate alterations in interneuron population or function, and these facilitator systems for neuronal communication may be sensitive to subclinical variations in brain health and function (e.g., neuroinflammatory factors or baseline and reactive shifts in autonomic nervous system mobilization). Although beyond the scope of the present study, additional research exploring the mechanisms of decline in GABA concentrations during normal aging and associated cognitive consequences would be beneficial. Results of the present investigation may have important clinical implications. Given the relation between GABA concentrations and cognitive function, it may be fruitful to explore the longitudinal trajectory of GABA and cognitive decline in the context of mild cognitive impairment and Alzheimer's disease. Furthermore, decline in frontal GABA concentrations may serve as both a predictor of neurodegenerative disease and an opportunity for pharmacological intervention. Future work, then, should establish the reliability of the relation between GABA and cognitive function in healthy older adults and examine it in clinical populations as well.

In summary, we demonstrate that the previously reported age-related decrease in GABA (7) continues into later life. Furthermore, we introduce evidence that frontal concentrations of GABA are predictive of general cognitive function in an aging population, even when controlling for well-known predicators of cognitive function, such as age, education, and brain atrophy. Future research will be well served to investigate tissue-specific concentrations of GABA and their relation to cognitive function to facilitate pharmacological or other intervention approaches.

ACKNOWLEDGMENTS AND DISCLOSURES

This work was supported in part by the Center for Cognitive Aging and Memory at the University of Florida, the McKnight Brain Research Foundation, the University of Florida Clinical and Translational Science Institute, which is supported in part by the National Institutes of Health (NIH) National Center for Advancing Translational Sciences (NCATS) under Award No. UL1TR001427; NIH/NCATS Clinical and Translational Science Awards Grant Nos. UL1TR000064 and KL2 TR000065; and the Claude D. Pepper Center at the University of Florida Grant No. P30 AG028740. This study applies tools developed under NIH Grant Nos. R01 EB016089 and P41 EB015909; RAEE also receives salary support from these grants.

The content is solely the responsibility of the authors and does not necessarily represent the official views of the National Institutes of Health.

All authors report no biomedical financial interests or potential conflicts of interest.

ARTICLE INFORMATION

From the Center for Cognitive Aging and Memory (ECP, AJW, HC, AMG, TRS, DGL, JBW, RAC), Institute on Aging, McKnight Brain Institute, Department of Aging and Geriatric Research; Department of Neuroscience (AJW), University of Florida, Gainesville, Florida; FM Kirby Center for Functional Brain Imaging (RAEE, NAJP, ADH), Kennedy Krieger Institute; Russell H. Morgan Department of Radiology and Radiological Science (RAEE, NAJP, ADH), The Johns Hopkins University School of Medicine, Baltimore, Maryland; Department of Radiology (ADH), CAIR Program (ADH), Alberta Children's Hospital Research Institute, University of Calgary; Hotchkiss Brain Institute (ADH), University of Calgary, Calgary, Alberta, Canada; Department of Biostatistics (HC); Department of Clinical and Health Psychology (AMG, TRS), University of Florida; Brain Rehabilitation and Research Center (DGL, JBW), Malcom Randall Veterans Affairs Medical Center; and Center for Neuropsychological Studies (JBW), Department of Neurology, University of Florida College of Medicine, Gainesville, Florida

Address correspondence to Eric C. Porges, Ph.D., University of Florida, 2004 Mowry Rd., Gainesville, FL 32610; E-mail: eporges@ufl.edu.

Received Mar 31, 2016; revised Jun 10, 2016; accepted Jun 11, 2016.

REFERENCES

1. Buzsáki G, Kaila K, Raichle M (2007): Inhibition and brain work. Neuron 56:771–183.
2. Lüscher C, Malenka RC (2012): NMDA receptor-dependent long-term potentiation and long-term depression (LTP/LTD). Cold Spring Harb Perspect Biol 4:a005710.
3. Nugent FS, Penick EC, Kauer JA (2007): Opioids block long-term potentiation of inhibitory synapses. Nature 446:1086–1090.
4. Castillo PE, Chiu CQ, Carroll RC (2011): Long-term plasticity at inhibitory synapses. Curr Opin Neurobiol 21:328–338.
5. Schultz LM (1997): REVIEW : GABAergic inhibitory processes and hippocampal long-term potentiation. Neuroscientist 3:226–236.
6. Inoue W, Baimoukhametova DV, Füzesi T, Wamsteeker Cusulin JI, Koblinger K, Whelan PJ, *et al*. (2013): Noradrenaline is a stress-associated metaplastic signal at GABA synapses. Nat Neurosci 16: 605–612.
7. Gao F, Edden RA, Li M, Puts NA, Wang G, Liu C, *et al*. (2013): Edited magnetic resonance spectroscopy detects an age-related decline in brain GABA levels. Neuroimage 78:75–82.
8. Ling LL, Hughes LF, Caspary DM (2005): Age-related loss of the GABA synthetic enzyme glutamic acid decarboxylase in rat primary auditory cortex. Neuroscience 132:1103–1113.
9. McQuail JA, Frazier CJ, Bizon JL (2015): Molecular aspects of age-related cognitive decline: the role of GABA signaling. Trends Mol Med 21:450–460.
10. Lasarge CL, Bañuelos C, Mayse JD, Bizon JL (2009): Blockade of GABA(B) receptors completely reverses age-related learning impairment. Neuroscience 164:941–947.
11. Bañuelos C, Beas BS, McQuail JA, Gilbert RJ, Frazier CJ, Setlow B, *et al*. (2014): Prefrontal cortical GABAergic dysfunction contributes to age-related working memory impairment. J Neurosci 34:3457–3466.
12. Mescher M, Merkle H, Kirsch J, Garwood M, Gruetter R (1998): Simultaneous in vivo spectral editing and water suppression. NMR Biomed 11:266–272.
13. Mescher M, Tannus A, Johnson MO, Garwood M (1996): Solvent suppression using selective echo dephasing. J Magn Reson Ser A 123:226–229.

14. Mullins PG, McGonigle DJ, O'Gorman RL, Puts NA, Vidyasagar R, Evans CJ, *et al*. (2014): Current practice in the use of MEGA-PRESS spectroscopy for the detection of GABA. Neuroimage 86: 43–52.
15. Edden RA, Barker PB (2007): Spatial effects in the detection of gamma-aminobutyric acid: Improved sensitivity at high fields using inner volume saturation. Magn Reson Med 58:1276–1282.
16. Gomez R, Behar KL, Watzl J, Weinzimer SA, Gulanski B, Sanacora G, *et al*. (2012): Intravenous ethanol infusion decreases human cortical γ-aminobutyric acid and N-acetylaspartate as measured with proton magnetic resonance spectroscopy at 4 tesla. Biol Psychiatry 71: 239–246.
17. Cai K, Nanga RP, Lamprou L, Schinstine C, Elliott M, Hariharan H, *et al*. (2012): The impact of gabapentin administration on brain GABA and glutamate concentrations: A 7T ^{1}H-MRS study. Neuropsychopharmacology 37:2764–2771.
18. Muthukumaraswamy SD, Edden RA, Jones DK, Swettenham JB, Singh KD (2009): Resting GABA concentration predicts peak gamma frequency and fMRI amplitude in response to visual stimulation in humans. Proc Natl Acad Sci U S A 106:8356–8361.
19. Donahue MJ, Near J, Blicher JU, Jezzard P (2010): Baseline GABA concentration and fMRI response. Neuroimage 53:392–398.
20. Gaetz W, Edgar JC, Wang DJ, Roberts TP (2011): Relating MEG measured motor cortical oscillations to resting γ-aminobutyric acid (GABA) concentration. Neuroimage 55:616–621.
21. Puts NA, Edden RA, Evans CJ, McGlone F, McGonigle DJ (2011): Regionally specific human GABA concentration correlates with tactile discrimination thresholds. J Neurosci 31:16556–16560.
22. Puts NA, Harris AD, Crocetti D, Nettles C, Singer HS, Tommerdahl M, *et al*. (2015): Reduced GABAergic inhibition and abnormal sensory symptoms in children with Tourette syndrome. J Neurophysiol 114: 808–817.
23. Edden RA, Muthukumaraswamy SD, Freeman TC, Singh KD (2009): Orientation discrimination performance is predicted by GABA concentration and gamma oscillation frequency in human primary visual cortex. J Neurosci 29:15721–15726.
24. Michels L, Martin E, Klaver P, Edden R, Zelaya F, Lythgoe DJ, *et al*. (2012): Frontal GABA levels change during working memory. PLoS One 7:e31933.
25. Evans CJ, McGonigle DJ, Edden RA (2010): Diurnal stability of gamma-aminobutyric acid concentration in visual and sensorimotor cortex. J Magn Reson Imaging 31:204–209.
26. Stuss DT, Alexander MP (2000): Executive functions and the frontal lobes: A conceptual view. Psychol Res 63:289–298.
27. Jurado MB, Rosselli M (2007): The elusive nature of executive functions: A review of our current understanding. Neuropsychol Rev 17:213–233.
28. Chan RC, Shum D, Toulopoulou T, Chen EY (2008): Assessment of executive functions: Review of instruments and identification of critical issues. Arch Clin Neuropsychol 23:201–216.
29. Alvarez JA, Emory E (2006): Executive function and the frontal lobes: A meta-analytic review. Neuropsychol Rev 16:17–42.
30. Nasreddine ZS, Phillips NA, Bédirian V, Charbonneau S, Whitehead V, Collin I, *et al*. (2005): The Montreal Cognitive Assessment, MoCA: A brief screening tool for mild cognitive impairment. J Am Geriatr Soc 53:695–699.
31. Julayanont P, Phillips N, Chertkow H, Nasreddine ZS (2012): Montreal Cognitive Assessment (MoCA): Concept and clinical review. In: Larner AJ, editor. Cognitive Screening Instruments: A Pract Approach. New York: Springer-Verlag, 111–152.
32. Oudman E, Postma A, Van der Stigchel S, Appelhof B, Wijnia JW, Nijboer TC (2014): The Montreal Cognitive Assessment (MoCA) is superior to the Mini Mental State Examination (MMSE) in detection of Korsakoff's syndrome. Clin Neuropsychol 28:1123–1132.
33. Harris AD, Puts NA, Barker PB, Edden RAE (2015): Spectral-editing measurements of GABA in the human brain with and without macromolecule suppression. Magn Reson Med 74:1523–1529.
34. Edden RAE, Puts NAJ, Harris AD, Barker PB, Evans CJ (2014): Gannet: A batch-processing tool for the quantitative analysis of gamma-aminobutyric acid–edited MR spectroscopy spectra. J Magn Reson Imaging 40:1445–1452.
35. Near J, Edden R, Evans CJ, Paquin R, Harris A, Jezzard P (2015): Frequency and phase drift correction of magnetic resonance spectroscopy data by spectral registration in the time domain. Magn Reson Med 73:44–50.
36. Harris AD, Puts NA, Edden RA (2015): Tissue correction for GABA-edited MRS: Considerations of voxel composition, tissue segmentation, and tissue relaxations. J Magn Reson Imaging 42:1431–1440.
37. Petrou M, Pop-Busui R, Foerster BR, Edden RA, Callaghan BC, Harte SE, *et al*. (2012): Altered excitation-inhibition balance in the brain of patients with diabetic neuropathy. Acad Radiol 19:607–612.
38. Foerster BR, Pomper MG, Callaghan BC, Petrou M, Edden RAE, Mohamed MA, *et al*. (2013): An imbalance between excitatory and inhibitory neurotransmitters in amyotrophic lateral sclerosis revealed by use of 3-T proton magnetic resonance spectroscopy. JAMA Neurol 70:1009–1016.
39. Ashburner J, Friston KJ (2005): Unified segmentation. Neuroimage 26: 839–851.
40. Good C, Johnsrude I (2001): A voxel-based morphometric study of ageing in 465 normal adult human brains. Neuroimage 14:21–36.
41. Pfefferbaum A, Adalsteinsson E, Sullivan EV (2005): Frontal circuitry degradation marks healthy adult aging: Evidence from diffusion tensor imaging. Neuroimage 26:891–899.
42. Zhu Z, Johnson NF, Kim C, Gold BT (2015): Reduced frontal cortex efficiency is associated with lower white matter integrity in aging. Cereb Cortex 25:138–146.
43. Salthouse TA (2009): When does age-related cognitive decline begin? Neurobiol Aging 30:507–514.
44. Salthouse T (2010): Selective review of cognitive aging. J Int Neuropsychol Soc 16:754–760.
45. Salthouse TA (2016): Continuity of cognitive change across adulthood. Psychon Bull Rev 23:932–939.
46. Wilson RS, Hebert LE, Scherr PA, Barnes LL, Mendes de Leon CF, Evans DA (2009): Educational attainment and cognitive decline in old age. Neurology 72:460–465.
47. Sumner P, Edden RA, Bompas A, Evans CJ, Singh KD (2010): More GABA, less distraction: A neurochemical predictor of motor decision speed. Nat Neurosci 13:825–827.
48. Plante DT, Jensen JE, Schoerning L, Winkelman JW (2012): Reduced γ-aminobutyric acid in occipital and anterior cingulate cortices in primary insomnia: A link to major depressive disorder? Neuropsychopharmacology 37:1548–1557.
49. Sanacora G, Mason GF, Rothman DL, Behar KL, Hyder F, Petroff OA, *et al*. (1999): Reduced cortical gamma-aminobutyric acid levels in depressed patients determined by proton magnetic resonance spectroscopy. Arch Gen Psychiatry 56:1043–1047.

frontiers in Aging Neuroscience

ORIGINAL RESEARCH
published: 02 May 2016
doi: 10.3389/fnagi.2016.00094

Cognitively Engaging Activity Is Associated with Greater Cortical and Subcortical Volumes

Talia R. Seider[1,2], Robert A. Fieo[1], Andrew O'Shea[1], Eric C. Porges[1], Adam J. Woods[1] and Ronald A. Cohen[1]*

[1] Center for Cognitive Aging and Memory, Department of Aging and Geriatric Research, Institute on Aging, University of Florida, Gainesville, FL, USA, [2] Department of Clinical and Health Psychology, University of Florida, Gainesville, FL, USA

As the population ages and dementia becomes a growing healthcare concern, it is increasingly important to identify targets for intervention to delay or attenuate cognitive decline. Research has shown that the most successful interventions aim at altering lifestyle factors. Thus, this study examined how involvement in physical, cognitive, and social activity is related to brain structure in older adults. Sixty-five adults (mean age = 71.4 years, standard deviation = 8.9) received the Community Healthy Activities Model Program for Seniors (CHAMPS), a questionnaire that polls everyday activities in which older adults may be involved, and also underwent structural magnetic resonance imaging. Stepwise regression with backward selection was used to predict weekly time spent in either social, cognitive, light physical, or heavy physical activity from the volume of one of the cortical or subcortical regions of interest (corrected by intracranial volume) as well as age, education, and gender as control variables. Regressions revealed that more time spent in cognitive activity was associated with greater volumes of all brain regions studied: total cortex ($\beta = 0.289$, $p = 0.014$), frontal ($\beta = 0.276$, $p = 0.019$), parietal ($\beta = 0.305$, $p = 0.009$), temporal ($\beta = 0.275$, $p = 0.020$), and occipital ($\beta = 0.256$, $p = 0.030$) lobes, and thalamus ($\beta = 0.310$, $p = 0.010$), caudate ($\beta = 0.233$, $p = 0.049$), hippocampus ($\beta = 0.286$, $p = 0.017$), and amygdala ($\beta = 0.336$, $p = 0.004$). These effects remained even after accounting for the positive association between cognitive activity and education. No other activity variable was associated with brain volumes. Results indicate that time spent in cognitively engaging activity is associated with greater cortical and subcortical brain volume. Findings suggest that interventions aimed at increasing levels of cognitive activity may delay cognitive consequences of aging and decrease the risk of developing dementia.

Keywords: cognitive aging, cognitive activity, healthy aging, brain volume, MRI, gray matter, social activity, physical activity

OPEN ACCESS

Edited by:
Michael Hornberger, University of East Anglia, UK

Reviewed by:
Agnes Lacreuse, University of Massachusetts, USA
Judith Machts, Otto-von-Guericke University Magdeburg, Germany

****Correspondence:***
Talia R. Seider
tseider@phhp.ufl.edu

Received: *21 January 2016*
Accepted: *14 April 2016*
Published: *02 May 2016*

Citation:
Seider TR, Fieo RA, O'Shea A, Porges EC, Woods AJ and Cohen RA (2016) Cognitively Engaging Activity Is Associated with Greater Cortical and Subcortical Volumes. Front. Aging Neurosci. 8:94. doi: 10.3389/fnagi.2016.00094

INTRODUCTION

Older age is the primary risk factor for neurodegenerative diseases such as Alzheimer's disease (AD). As the size and proportion of the population over age 65 increases, the number of people with dementia is expected to increase substantially, raising healthcare costs and caregiver burden (Alzheimer's Association, 2015). Thus, it is becoming increasingly important to identify targets for intervention with the aims of delaying or attenuating cognitive decline.

While several pharmaceuticals exist to delay cognitive decline, research has shown that the best results come from interventions aimed at altering lifestyle factors (Williams et al., 2010; Imtiaz et al., 2014). Greater self-reported levels of engagement in cognitive, social, and physical activity have frequently been associated with higher cognitive functioning scores (Barnes et al., 2004; Newson and Kemps, 2005; McGue and Christensen, 2007; Vemuri et al., 2012; Opdebeeck et al., 2016). Furthermore, physical activity and cognitive engagement are among the only factors consistently associated with decreased risk for AD and cognitive decline (Fratiglioni et al., 2004; Kramer et al., 2004; Hertzog et al., 2009; Williams et al., 2010). Still, the mechanisms of such effects remain poorly understood.

Brain structure and function presumably mediate the link between an active lifestyle and reduced risk for cognitive decline. Observational studies have shown that increased levels of physical activity are associated with larger brain volumes, especially in frontal and hippocampal areas (Rovio et al., 2010; Bugg and Head, 2011; Doi et al., 2015), and interventional studies have shown that physical activity can increase hippocampal (Erickson et al., 2011) and frontal volumes (Colcombe et al., 2006).

Research on the association between cognitive or social engagement and brain volume is less extensive. Proxy measures of cognitive reserve, such as intellectual attainment, have been linked with greater brain volume (Stern, 2009). New learning has been shown to cause increased parietal and hippocampal size in young adults (Draganski et al., 2006), and cognitive training has been associated with increased hippocampal volume and preserved white matter integrity in older adults (Engvig et al., 2014). Greater frequency of cognitive leisure activities has been associated with larger gray matter volume in frontal and limbic regions (Schultz et al., 2015), while higher scores on measures combining cognitive and social activities have been related to more normal-appearing white matter (Gow et al., 2012a) and reduced hippocampal decline over time (Valenzuela et al., 2008). More self-reported social engagement has also been associated with greater temporal and occipital gray matter volume (James et al., 2012), and an intervention study reported that increase in social activity was associated with increased total brain volume (Mortimer et al., 2012). Still, other research has shown no relationship between cognitive or social activity and volumetric data (Foubert-Samier et al., 2012; Vaughan et al., 2014; Van der Vegt, 2015), and the link between these lifestyle factors and regional cerebral volumes remains understudied.

The purpose of this study was to examine how physical, cognitive, and social activity is related to brain structure. Levels of engagement in everyday activities was measured via self-report. Based on previous research, we generally expected higher self-reported levels of physical, social, and cognitive activity to be associated with greater volumes, especially in frontal and limbic regions for physical activity, temporal and occipital regions for social activity, and parietal, frontal, and limbic regions for cognitive activity.

MATERIALS AND METHODS

Participants

Sixty-five community dwelling individuals in the Gainesville and North Florida region were recruited to complete a magnetic resonance imaging (MRI) scan and a cognitive assessment, including the Montreal Cognitive Assessment (MoCA), a brief screen of cognitive functioning. Exclusion criteria included history of head injury with loss of consciousness greater than 20 min, neurologic condition such as dementia, epilepsy, or stroke, major psychiatric illness such as schizophrenia or bipolar disorder, inability to undergo MRI, and MoCA score less than 20. Sample demographics and characteristics are listed in **Table 1**. Participants had a mean age of 71, they were generally well educated with a mean education of 17 years, slightly more than half were females, they were mostly Caucasian, and they were generally cognitively intact with a mean MoCA score of 26. The study was approved by University of Florida Institutional Review Board and written informed consent was obtained from all study participants.

Activity Assessment

The Community Healthy Activities Model Program for Seniors (CHAMPS) questionnaire was developed as part of an intervention study aimed at increasing participation in physical activities in community dwelling elderly. It was designed to measure current levels of energy expenditure by taking a poll of everyday activities in which older adults may be involved (Stewart et al., 1997). Participants were asked whether or not they engaged in a particular activity during a typical week in the past month. If they had, they were asked to fill in the number of times they engaged in the activity per week and mark the total number of hours spent in the activity per week. Total hours were grouped into 6 integer values such that 1 indicated less than 1 h was spent engaged in that activity per week, 2 indicated 1 – 2½ h spent, 3 indicated 3 – 4½ h, 4 indicated 5 – 6½ h, 5 indicated 7 – 8½ h, and 6 indicated 9 or more hours (**Figure 1**). Participants are also allowed to fill in "other" and record an activity that was not listed in the questionnaire.

Physical activities were divided into light and moderate-heavy groups based on the ratio of work metabolic rate to resting metabolic rate (MET) adjusted for older adults (Ainsworth et al., 1993) as was done in the original CHAMPS research (Stewart et al., 2001). Light physical activities were those with a MET

TABLE 1 | Sample characteristics ($N = 65$).

	Mean (SD)	Range
Age (years)	71.4 (8.9)	48–85
Education (years)	16.8 (2.5)	12–20
% male	43.1	
% Caucasian	95.4	
MoCA	26.0 (2.7)	20–30

MoCA, Montreal Cognitive Assessment.

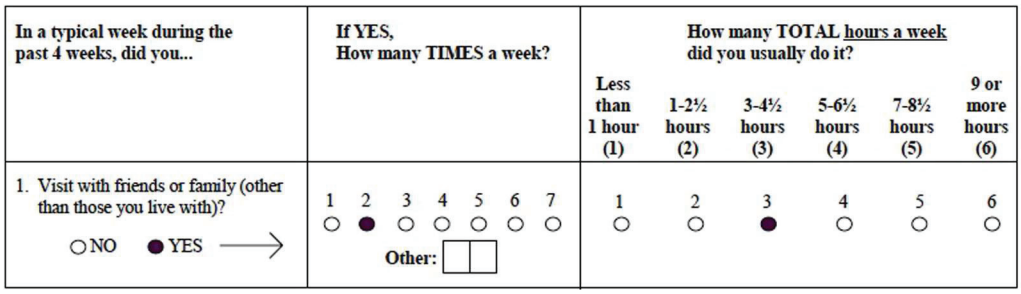

FIGURE 1 | Sample Community Healthy Activities Model Program for Seniors (CHAMPS) test item.

score below 30 and included conditioning training, yoga or tai chi, leisurely walking, walking to do errands, light gardening, light house work, golfing using a cart, and aerobic dancing. Moderate-heavy physical activities were those with a MET score equal to or above 30 and included sports, light or heavy strength training, swimming gently or fast, water exercises, working on aerobic machines, bicycling, fast walking, uphill walking or hiking, jogging or running, working on machinery (car, lawn mower, etc.), heavy gardening, heavy housework, singles or doubles tennis, golfing without use of a cart, dancing (such as square, folk, line, or ballroom), and skating (ice, roller, or in-line). Social activities were any for which the majority of time spent likely involved interpersonal interaction. These included visiting with family or friends, going to a senior center, volunteering, church-related activities, participating in clubs or groups, playing cards or board games with others, and shooting pool or billiards. Cognitive activities were those for which the majority of time spent was likely cognitively engaging rather than interpersonal. These included using a computer, doing arts or crafts, attending a concert, movie, lecture, or sport event, playing a musical instrument, and reading. If the "other" option was filled in, the activity described was placed in the most appropriate group. The integer measures (1 through 6) representing amount of time spent weekly in each activity were summed to create totals for light and moderate-heavy physical activities, social activities, and cognitive activities.

Magnetic Resonance Imaging

Acquisition

Magnetic resonance imaging data were acquired using a Philips Achieva 3.0 Tesla scanner (Achieva; Philips Electronics, Amsterdam, The Netherlands) at the McKnight Brain Institute (University of Florida, Gainesville, FL, USA) with a standard 32-channel receive-only head coil. High-resolution 3D T1-weighted MPRAGE scans were performed. Scans were acquired in a sagittal orientation with parameters as follows: voxel size = 1 mm isotropic; 1 mm slice thickness; TE = 3.2 ms; TR = 7.0 ms; FOV = 240 × 240; Number of slices = 170.

Analysis

T1-weighted MRIs were automatically segmented and volumes were calculated using FreeSurfer software, version 5.3.0, available at http://surfer.nmr.mgh.harvard.edu/ (Fischl et al., 2002). Following preprocessing, all results underwent quality control to confirm correct detection of gray and white matter. Any errors in segmentation were corrected manually and the T1 images were re-processed through FreeSurfer. Seventy one percentages of cases had some form of manual edit. These consisted of adding control points to extend the white matter boundary (55%), removing voxels from the brain mask (29%), and editing the white matter mask (6%). Some subjects had edits from more than one category, such as both control points and brain mask edits. Previous research has shown that this semi-automated procedure yields accurate and reliable results when compared to manual segmentation (Fischl et al., 2002; Jovicich et al., 2009; Morey et al., 2009) and histological measures (Morey et al., 2009). Automatically parcellated FreeSurfer gray matter regions of interest (ROIs) were based on the Desikan-Killiany atlas. Intracranial volume (ICV) was calculated based on the talairach transform (Buckner et al., 2004). ROIs for the left and right hemisphere were summed and corrected for ICV (by dividing ROI volume by ICV and multiplying by 100) to create bilateral, normalized ROIs. Some of these were then summed to create volumes for the four major lobes of the brain. Specifically, the frontal ROI consisted of the caudal and rostral anterior cingulate cortices, the caudal and rostral middle frontal cortices, the lateral and medial orbitofrontal cortices, the pars orbitalis, the superior frontal cortex, and the frontal pole; the parietal ROI consisted of the precuneus, the inferior and superior parietal lobules, and the supramarginal gyrus; the temporal ROI consisted of the entorhinal cortex, the inferior, middle, and superior temporal regions, the transverse temporal region, and the temporal pole; and the occipital ROI consisted of the lateral occipital region, the lingual and fusiform gyri, the pericalcarine region, and the cuneus. All four lobes were added together to create a measure of total cortical gray matter volume. Subcortical ROIs were chosen based on their relevance to cognitive and behavioral functioning and included the thalamus, caudate, hippocampus, and amygdala.

Statistical Analysis

All statistical analyses were performed using SPSS. Stepwise regression with backward selection was used to predict weekly time spent in either light physical, heavy physical, social, or cognitive activity using a cortical or subcortical ROI (corrected

by total ICV) as well as age, education, and gender as covariates. Individual regression analyses were conducted for each ROI. In stepwise regression with backward selection, all independent variables (predictors and covariates) are entered into the equation and sequentially removed based on the probability of F. The criterion used was $p \geq 0.10$. The first model for which all independent variables included explained significant variance in the dependent variable was chosen as the best model. The benefits of using this analytic method is that it allows for all variables to included, as it may be that a set of variables has better predictive validity than the subset, but it also removes those that may be falsely lowering the contribution of significant predictors by overlapping in variance explained. Thus, the final model efficiently explains the variance in the dependent variable and better identifies the unique contribution of the predictors.

RESULTS

Table 2 displays the percentage of ICV for cortical and subcortical regions in this sample. In regards to activity measures, scores do not refer directly to number of hours, but rather to ordinal measures reflecting roughly 1.5-h increments (**Figure 1**). Though it cannot be determined exactly how much time was spent in each of the activity categories, it appears that participants divided their time roughly evenly amongst light physical (mean = 8.7, SD = 5.1), heavy physical (mean = 8.4, SD = 5.7), social (mean = 10.5, SD = 6.0), and cognitive (mean = 11.3, SD = 4.5) activities.

Cognitive activity was the only outcome significantly associated with gray matter volume. **Table 3** lists these final, best-fitting models. Final models revealed a positive association with education ($p < 0.001$) and all cortical and subcortical ROIs examined (ps < 0.05). **Figure 2** depicts the relationships between cognitive activity and brain volumes, controlling for education. In each regression, variables excluded were age and sex.

In contrast, there were no significant associations observed between the volumes of these brain regions and engagement in light physical, heavy physical, or social activities as reported on the CHAMPS. More heavy physical activity was associated with younger age and male gender, whereas other activities were not associated with age or sex. Supplemental material includes these results.

TABLE 2 | Gray matter regions of interest presented as percentages of total intracranial volume.

Region of Interest	Mean (SD)	Range
Frontal lobe	7.83 (1.19)	6.18–11.52
Parietal lobe	5.77 (0.82)	4.34–8.35
Temporal lobe	4.75 (0.72)	3.48–6.94
Occipital lobe	4.43 (0.73)	3.43–6.33
Total cortex	22.78 (3.35)	18.14–32.43
Thalamus	0.91 (0.15)	0.71–1.35
Caudate	0.47 (0.08)	0.37–0.71
Hippocampus	0.54 (0.13)	0.30–1.01
Amygdala	0.22 (0.05)	0.13–0.37

DISCUSSION

In this study, we found that greater time dedicated to cognitively engaging activities was associated with greater cortical and subcortical brain volume. We did not find significant associations with physical or social activity level and volumetric data. Cognitive engagement activities represent one of three potential proxies for the construct of cognitive reserve. Epidemiologic-based support for the association between leisure and cognitive status has been accumulating for nearly a quarter of a century (Christensen and Mackinnon, 1993). In an effort to clarify causal attributions or directionality, other epidemiologic work has used sophisticated dynamic change models to show that *change* in cognitive leisure participation can result in higher scores on cognitive ability measures (Mitchell et al., 2012). Such evidence has sparked experimental investigations, with clinical trials demonstrating improved cognition over short periods (3–6 months) for those participating in cognitive leisure activities compared to controls (Stine-Morrow et al., 2008).

More recently, investigators have begun to examine imaging and volumetric evidence, showing that one's level of cognitive reserve is associated with brain volume. For instance, it has been shown that a more active cognitive lifestyle is associated with greater frontal and parietal brain volume in healthy older adults (Stine-Morrow et al., 2008). Our finding that higher cognitive engagement is associated with greater hippocampal volume was also reported in a longitudinal study (Valenzuela et al., 2008). Valenzuela et al. (2008) used the Lifetime of Experiences Questionnaire (LEQ), in which sample activities included creative arts, reading, writing, and socializing. The investigators reported a significant association between total LEQ and average hippocampal volume, controlling for age, gender, hypertension, and ICV. High LEQ individuals experienced an average loss of 3.6% of hippocampal volume over a 3-year period, while low LEQ individuals exhibited more than twice this volumetric loss (8.3%). It is important to note that these studies used a composite measure to establish these associations, which, in addition to cognitive engagement activities, also included education and job complexity. Yet cognitive engagement or cognitive leisure activities show unique contributions to cognitive health, independent of the variance attributed to education and occupational status (Stern, 2009; Foubert-Samier et al., 2012). Indeed, in the current investigation, the relationship between more involvement in cognitively engaging leisure activities and greater brain volumes was not explained by education.

Findings from the current study are similar to those of another observational study in which greater frequency of cognitive leisure activities (playing games like cards, checkers, crosswords, or other puzzles) was related to better cognitive performance and reduced brain atrophy (Schultz et al., 2015). Schultz et al. (2015) reported that higher activity scores were associated with greater gray matter volumes in several ROIs including the hippocampus, posterior cingulate, anterior

TABLE 3 | Best-fitting models predicting cognitive activity from gray matter region of interest, age, sex, and education.

Model/ROI	Variable	β	p	R^2	Model p	Excluded Variables
Frontal lobe	Frontal lobe	0.276	0.019*	0.247	<0.001*	Age
	Education	0.493	<0.001*			Sex
Parietal lobe	Parietal lobe	0.305	0.009*	0.262	<0.001*	Age
	Education	0.505	<0.001*			Sex
Temporal lobe	Temporal lobe	0.275	0.020*	0.246	<0.001*	Age
	Education	0.501	<0.001*			Sex
Occipital lobe	Occipital lobe	0.256	0.030*	0.237	<0.001*	Age
	Education	0.490	<0.001*			Sex
Total cortex	Total cortex	0.289	0.014*	0.253	<0.001*	Age
	Education	0.502	<0.001*			Sex
Thalamus	Thalamus	0.310	0.010*	0.261	<0.001*	Age
	Education	0.526	<0.001*			Sex
Caudate	Caudate	0.233	0.049*	0.227	<0.001*	Age
	Education	0.482	<0.001*			Sex
Hippocampus	Hippocampus	0.286	0.017*	0.250	<0.001*	Age
	Education	0.513	<0.001*			Sex
Amygdala	Amygdala	0.336	0.004*	0.280	<0.001*	Age
	Education	0.519	<0.001*			Sex

*ROI, region of interest. *$p < 0.05$.*

cingulate, and middle frontal gyrus. However, our findings differ from a longitudinal study that found no relationship between cognitive activity and MRI measures of whole brain volumes of gray and white matter (Vaughan et al., 2014). One potential reason for a lack of association in the Vaughan et al. (2014) study may be related to the items included in their 6-item measurement of cognitive activities. Like in the present study, they included reading and craft activities, but they also included group activities, social activities, and watching television. It is possible that group and social activities present with the local dependence, or relatedness; local independence, or unrelatedness, of items is a modern test theory assumption that, when violated, negatively impacts construct validity. Furthermore, television use has been shown to be negatively correlated with other cognitive activity items (Gow et al., 2012b; Fieo et al., 2014). Television time has also been associated with less frequent engagement in social and physical recreation (Hu et al., 2003) and increased risk for dementia (Rundek and Bennett, 2006). These factors may have reduced the power for detecting associations in the Vaughan et al. (2014) study. The current findings, combined with prior research in cognitive leisure activity, reinforce the relationship between hippocampal and cortical volumes and cognitive activity, consistent with our hypothesis.

It is somewhat surprising that heavy physical activity was not associated with volumetric data, as studies examining exercise effects on regional brain volume typically implicate frontal and hippocampal brain areas (Colcombe et al., 2006; Pereira et al., 2007; Erickson et al., 2011). Part of this discrepancy undoubtedly comes from the differences between intervention and observational studies. Intervention studies inherently involve introducing something novel in the lives of research participants. It may be that the amount of novelty an activity offers is more important than the type of activity itself in impacting cognitive and neurological functioning (Bielak, 2010). Thus, when intervention studies implement a physical activity regimen in sedentary adults (Colcombe et al., 2006), the novelty of the activity and significant change in lifestyle may very well impact brain structure.

Part of the discrepancy between the current findings and results from previous physical activity studies may be due to differences in methodology for measuring physical activity. The CHAMPS questionnaire asked participants to retrospectively indicate their levels of physical activity in a variety of class categories for a typical week over the previous month. Given the number of parameters that had to be remembered, it is possible that participants gave unreliable reports of their own activity (LaPorte et al., 1985). Indeed, Buchman et al. (2008) showed that objectively measured physical activity was associated with cognitive function, whereas self-reported daily physical activity in the same group was not. However, an evaluation of the CHAMPS questionnaire revealed a moderately strong correlation between self-reported engagement in moderate physical activity and activity objectively measured by a waist monitor ($r = 0.48$) (Harada et al., 2001). Furthermore, other self-report studies have shown associations between physical activity levels and cortical volumes (Erickson et al., 2010; Bugg and Head, 2011; Gow et al., 2012a; Benedict et al., 2013). As such, it is unlikely that the lack of association is entirely explained by the self-report nature of the physical activity measurement.

Our findings are consistent with Gow et al. (2012a), who measured baseline physical activity via self-report at age 70 years and administered MRIs at age 73. They found physical activity to be associated with white matter volume, but not gray matter volume. Thus, lack of findings in the

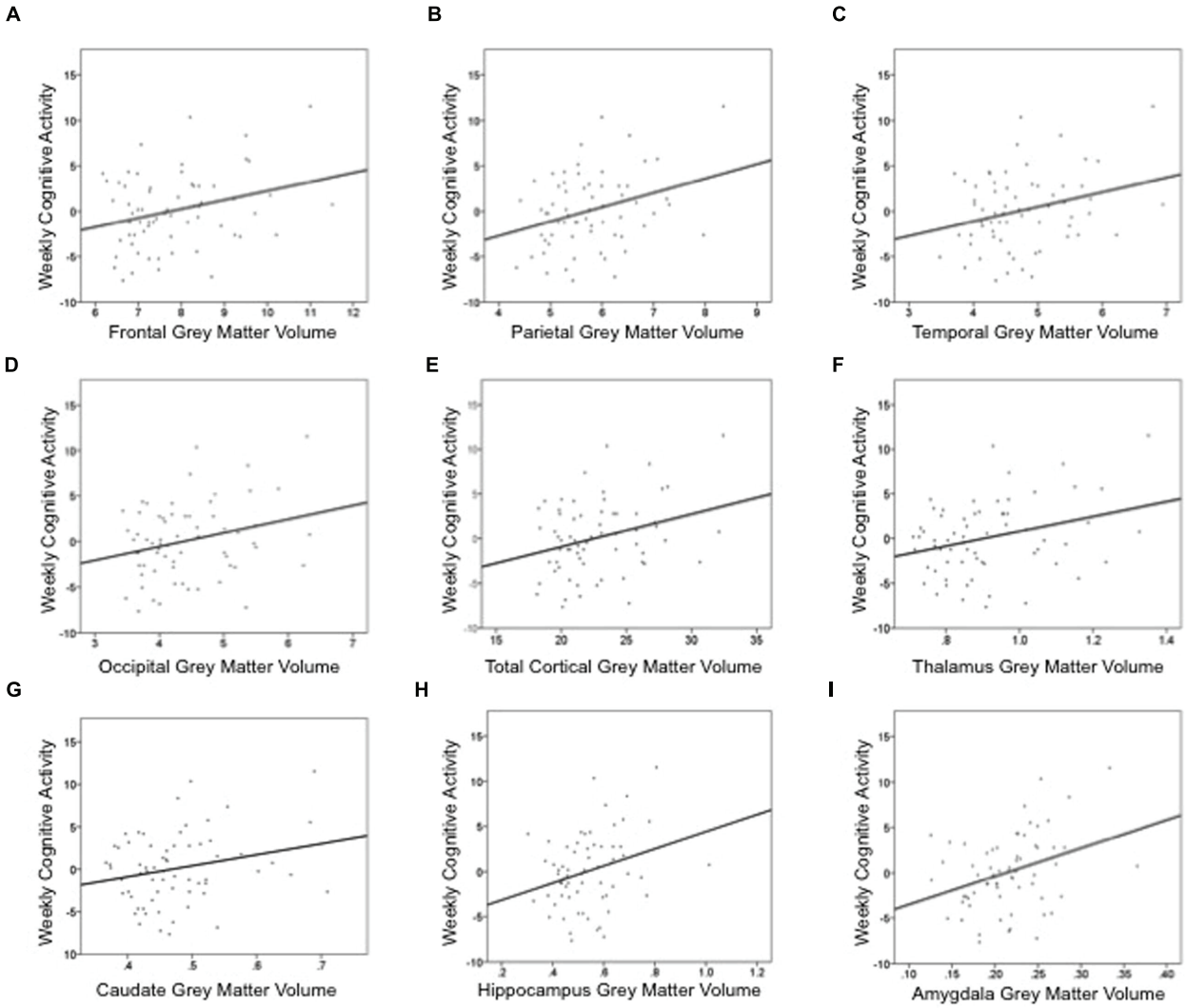

FIGURE 2 | Summed measures of weekly time spent in cognitively engaging activity are positively associated cortical and subcortical gray matter volumes: (A) frontal lobe, (B) parietal lobe, (C) temporal lobe, (D) occipital lobe, (E) total cortex, (F) thalamus, (G) caudate, (H) hippocampus, and (I) amygdala. These graphs depict the relationship between gray matter volume and cognitive activity, controlling for education. Thus, the *y*-axis is the unstandardized residual after regressing the effects of education out of cognitive activity. Gray matter volume is a percentage of intracranial volume.

present study may reflect the fact that only gray matter volume was measured. Given that the current findings are inconsistent with a large body of research on the impact of physical activity on brain volumes, we do not feel comfortable rejecting our hypothesis that greater physical activity is associated with greater volumes, particularly in frontal and limbic regions.

Social activity is more tenuously linked to brain volume than are physical and cognitive activity, and the relationship was not supported in the current investigation. Greater social involvement has been associated with greater normal-appearing white matter (Gow et al., 2012a), total brain (Mortimer et al., 2012), and gray matter (James et al., 2012) volumes. Yet methodological differences may explain discrepancies between prior results and our own.

Gow et al. (2012a) combined cognitive and social leisure activities when measuring the link between activity and brain structure. While greater cognitive and social activity was related to more normal-appearing white matter, these activities were not found to be associated with gray matter volume, consistent with the present data. Whether social activity has a stronger relationship to white matter than to gray matter volume deserves further investigation.

Mortimer et al. (2012) performed an intervention study and found that their social interaction groups showed significant increases in total brain volume over the study period. The fact that this study was an intervention may explain why their results differ from the current study, since, as previously discussed, the amount of novelty provided by an intervention may be a significant driver of results (Bielak, 2010). The intervention

group met three times per week at a neighborhood community center, the participants decided on their own to organize and select topics of conversation, and the discussions were described as extremely lively. Thus, lifestyle was significantly impacted in these participants.

James et al. (2012) demonstrated that higher social engagement was associated with greater total brain volume and total gray matter volume, as well as greater temporal and occipital gray matter lobar volumes. Yet methodological differences might also explain the discrepancies between their results and our own. The James et al. study included a question more related to physical than social activity in their eight-item measure of social engagement, as they asked participants how many times in the past week/month they had done any indoor or outdoor recreational activity like bowling, working out, fishing, hiking, boating, swimming, or golfing. Given that physical activity has a more robust association to gray matter volume than does social activity, responses to this question may have been a strong driver of results. Another important difference is in the study samples; the James sample was, for the most part, comprised of former lead workers who were recruited for a study of lead exposure and cognitive function. They were less socially engaged than population-based controls, who comprised 12% of the sample. Not only were the participants in the current study recruited from the same community population, but the sample size was significantly smaller compared to the James et al. sample of 348. Thus, differences in population and sample size may have given James et al. more statistical power to detect any relationship between the measured activities and gray matter volume.

Our null findings for social activity are similar to those of Foubert-Samier et al. (2012), who assessed activity in midlife and in retirement. They asked participants whether or not they engaged in a number of activities during midlife (when they worked) and currently (in retirement) and assigned one point for each activity. Social activity in both midlife and retirement was related to better semantic verbal fluency, but unrelated to total brain, gray matter, or white matter volumes.

Current findings are also consistent with Van der Vegt (2015), who found no association between social activity with family and friends and brain volume (Van der Vegt, 2015). In that study, participants were asked two questions: "In general, how often do you have contact with your family members (including telephone calls or letters)?" and, "In general, how often do you have contact with your friends or well-known acquaintances (including telephone calls or letters)?" Interestingly, factor analytic methods have shown that social activity can be presented as a bi-factor model: social-private and social-public (Jopp and Hertzog, 2010). Additionally, social-private was more highly correlated with cognitive functioning measures. As such, social-private may have a stronger relationship with brain volume than social private, and combining separable constructs may negatively impact predictive validity. The association between different types of social activity and volumetric data of cortical and subcortical regions warrants further study. Nevertheless, considering prior research and the results of the current study, we cannot support our hypothesis that social activity is associated with greater gray matter volumes in temporal and occipital regions.

As mentioned previously, novelty may be an important driving factor in the relationship between leisure activities that are engaging, cognitively or otherwise, and larger brain volumes. Animal models have shown that, in aged animals, environmental enrichment attenuates the age-related changes in cortical thickness (Mora et al., 2007). A defining feature of enrichment in animals is often novelty. For instance, repeatedly substituting and replacing the objects in the home cages creates a wide range of opportunities for enhanced cognitive stimulation, formation of tuned spatial maps, and proficient detection of novelty (Petrosini et al., 2009). In humans, one theoretical explanation for how novelty exerts a protective effect in older adults relates to non-adaptive "routinization" (Tournier et al., 2012). That is, as older adults continue to accumulate age-related insults (e.g., medical comorbidities or muscle related fatigue), some individuals may seek out more controlled, stable, predictive environments, thus limiting exposure to novel environments or experiences. Evidence in support of this can be found in a Bergua et al. (2006) study, demonstrating that preferences for routine were positively correlated with cognitive decline over 3 years. Additional support can be observed in the finding that greater variety of participation in cognitively stimulating activities was associated a ∼10% lower risk of cognitive impairment, regardless of how challenging these tasks were (Carlson et al., 2012). As such, though novel environments and situations may be more difficult to navigate as people age, they may be the most protective against neurological decline.

Limitations

The most common grouping scheme for investigating the efficacy of leisure activities has been the broad domains of physical, social activities, and other cognitive leisure activities, which is what we followed for this investigation. However, with such broad domains, many activities cannot be assigned unambiguously. Volunteering work, for instance, is likely to have a strong social component, but may in some instances entail more non-verbal cognitive or physical effort. Ideally, large item/activity pools would allow for the formation of more distinct, unidimensional activity constructs, for example, further delineating social activities into social-private and social-public (Jopp and Hertzog, 2010). Furthermore, historically, the evidence in observational studies, including the present study, has been limited to an examination of frequency of participation. However, contemporary conversations have moved beyond questioning the frequency of participation, placing greater emphasis on novelty/variety and cognitive challenge (Bielak, 2010; Chan et al., 2014). Finally, as previously mentioned, the accuracy of measurement in self-report questionnaires is questionable, as participants may have subjective biases and may, intentionally or unintentionally, misrepresent their objective activity levels (Erickson et al., 2012). Nevertheless, CHAMPS has several strengths, including robust psychometric properties (Harada et al., 2001; Wilcox et al., 2009), sensitivity to change

(Stewart et al., 1997), and correlations with objective measures of physical activity and functioning (King et al., 2000; Harada et al., 2001; Stewart et al., 2001).

CONCLUSION

Results of this study emphasize the relationship between volumetric data and the independent contribution of cognitively engaging activities. This process is of considerable value if we consider that cognitive leisure activities show unique contributions to cognitive health, independent of the variance attributed to other cognitive reserve proxies (e.g., education and occupational status) (Stern, 2009; Foubert-Samier et al., 2012). Results of the present study show that more time spent engaged in cognitive activity is associated with greater brain volume. Importantly, these lifestyle variables are modifiable, suggesting that interventions aimed at increasing levels of cognitive activity may delay onset or decrease risk of developing dementia. In fact, intervention studies have shown positive neurological effects of cognitive interventions. Still, the field of cognitive aging will benefit from more research investigating interventions aimed at increasing everyday cognitively engaging activities as well as the role of other biomarkers such as inflammatory agents and genetic factors in influencing brain structure and function.

AUTHOR CONTRIBUTIONS

TS was involved in the conception and writing of the manuscript and conducted statistical analyses. RF was involved in the writing of the manuscript. AO conducted volumetric analyses that were used in the manuscript. EP, AW, and RC were involved in the conception of the study, and RC was involved in the conception of the manuscript and data analysis. All authors contributed intellectual content and approved the version to be published.

ACKNOWLEDGMENT

This work was supported by an endowment from the McKnight Brain Research Foundation to the University of Florida Center for Cognitive Aging and Memory. This work was also supported by T32 AG020499 (TS).

SUPPLEMENTARY MATERIAL

The Supplementary Material for this article can be found online at: http://journal.frontiersin.org/article/10.3389/fnagi.2016.00094

REFERENCES

Ainsworth, B. E., Haskell, W. L., Leon, A. S., Jacobs, D. R. Jr., Montoye, H. J., Sallis, J. F., et al. (1993). Compendium of physical activities: classification of energy costs of human physical activities. *Med. Sci. Sports Exerc.* 25, 71–80. doi: 10.1249/00005768-199301000-00011

Alzheimer's Association (2015). Alzheimer's disease facts and figures. *Alzheimer's Dement.* 11, 332–384.

Barnes, L. L., Mendes de Leon, C. F., Wilson, R. S., Bienias, J. L., and Evans, D. A. (2004). Social resources and cognitive decline in a population of older African Americans and whites. *Neurology* 63, 2322–2326. doi: 10.1212/01.WNL.0000147473.04043.B3

Benedict, C., Brooks, S. J., Kullberg, J., Nordenskjold, R., Burgos, J., Le Greves, M., et al. (2013). Association between physical activity and brain health in older adults. *Neurobiol. Aging* 34, 83–90. doi: 10.1016/j.neurobiolaging.2012.04.013

Bergua, V., Fabrigoule, C., Barberger-Gateau, P., Dartigues, J. F., Swendsen, J., and Bouisson, J. (2006). Preferences for routines in older people: associations with cognitive and psychological vulnerability. *Int. J. Geriatr. Psychiatry* 21, 990–998. doi: 10.1002/gps.1597

Bielak, A. A. (2010). How can we not 'lose it' if we still don't understand how to 'use it'? Unanswered questions about the influence of activity participation on cognitive performance in older age–a mini-review. *Gerontology* 56, 507–519. doi: 10.1159/000264918

Buchman, A. S., Wilson, R. S., and Bennett, D. A. (2008). Total daily activity is associated with cognition in older persons. *Am. J. Geriatr. Psychiatry* 16, 697–701. doi: 10.1097/JGP.0b013e31817945f6

Buckner, R. L., Head, D., Parker, J., Fotenos, A. F., Marcus, D., Morris, J. C., et al. (2004). A unified approach for morphometric and functional data analysis in young, old, and demented adults using automated atlas-based head size normalization: reliability and validation against manual measurement of total intracranial volume. *Neuroimage* 23, 724–738. doi: 10.1016/j.neuroimage.2004.06.018

Bugg, J. M., and Head, D. (2011). Exercise moderates age-related atrophy of the medial temporal lobe. *Neurobiol. Aging* 32, 506–514. doi: 10.1016/j.neurobiolaging.2009.03.008

Carlson, M. C., Parisi, J. M., Xia, J., Xue, Q. L., Rebok, G. W., Bandeen-Roche, K., et al. (2012). Lifestyle activities and memory: variety may be the spice of life. The women's health and aging study II. *J. Int. Neuropsychol. Soc.* 18, 286–294. doi: 10.1017/S135561771100169X

Chan, M. Y., Haber, S., Drew, L. M., and Park, D. C. (2014). Training older adults to use tablet computers: does it enhance cognitive function? *Gerontologist* doi: 10.1093/geront/gnu057 [Epub ahead of print].

Christensen, H., and Mackinnon, A. (1993). The association between mental, social and physical activity and cognitive performance in young and old subjects. *Age Ageing* 22, 175–182. doi: 10.1093/ageing/22.3.175

Colcombe, S. J., Erickson, K. I., Scalf, P. E., Kim, J. S., Prakash, R., McAuley, E., et al. (2006). Aerobic exercise training increases brain volume in aging humans. *J. Gerontol. A Biol. Sci. Med. Sci.* 61, 1166–1170. doi: 10.1093/gerona/61.11.1166

Doi, T., Makizako, H., Shimada, H., Tsutsumimoto, K., Hotta, R., Nakakubo, S., et al. (2015). Objectively measured physical activity, brain atrophy, and white matter lesions in older adults with mild cognitive impairment. *Exp. Gerontol.* 62, 1–6. doi: 10.1016/j.exger.2014.12.011

Draganski, B., Gaser, C., Kempermann, G., Kuhn, H. G., Winkler, J., Buchel, C., et al. (2006). Temporal and spatial dynamics of brain structure changes during extensive learning. *J. Neurosci.* 26, 6314–6317. doi: 10.1523/JNEUROSCI.4628-05.2006

Engvig, A., Fjell, A. M., Westlye, L. T., Skaane, N. V., Dale, A. M., Holland, D., et al. (2014). Effects of cognitive training on gray matter volumes in memory clinic patients with subjective memory impairment. *J. Alzheimers Dis.* 41, 779–791. doi: 10.3233/JAD-131889

Erickson, K. I., Raji, C. A., Lopez, O. L., Becker, J. T., Rosano, C., Newman, A. B., et al. (2010). Physical activity predicts gray matter volume in late adulthood: the Cardiovascular Health Study. *Neurology* 75, 1415–1422. doi: 10.1212/WNL.0b013e3181f88359

Erickson, K. I., Voss, M. W., Prakash, R. S., Basak, C., Szabo, A., Chaddock, L., et al. (2011). Exercise training increases size of hippocampus and improves memory. *Proc. Natl. Acad. Sci. U.S.A.* 108, 3017–3022. doi: 10.1073/pnas.1015950108

Erickson, K. I., Weinstein, A. M., and Lopez, O. L. (2012). Physical activity, brain plasticity, and Alzheimer's disease. *Arch. Med. Res.* 43, 615–621. doi: 10.1016/j.arcmed.2012.09.008

Fieo, R., Manly, J. J., Schupf, N., and Stern, Y. (2014). Functional status in the young-old: establishing a working prototype of an extended-instrumental activities of daily living scale. *J. Gerontol. A Biol. Sci. Med. Sci.* 69, 766–772. doi: 10.1093/gerona/glt167

Fischl, B., Salat, D. H., Busa, E., Albert, M., Dieterich, M., Haselgrove, C., et al. (2002). Whole brain segmentation: automated labeling of neuroanatomical structures in the human brain. *Neuron* 33, 341–355. doi: 10.1016/S0896-6273(02)00569-X

Foubert-Samier, A., Catheline, G., Amieva, H., Dilharreguy, B., Helmer, C., Allard, M., et al. (2012). Education, occupation, leisure activities, and brain reserve: a population-based study. *Neurobiol. Aging* 33, 423.e15–423.e25. doi: 10.1016/j.neurobiolaging.2010.09.023

Fratiglioni, L., Paillard-Borg, S., and Winblad, B. (2004). An active and socially integrated lifestyle in late life might protect against dementia. *Lancet Neurol.* 3, 343–353. doi: 10.1016/S1474-4422(04)00767-7

Gow, A. J., Bastin, M. E., Munoz Maniega, S., Valdes Hernandez, M. C., Morris, Z., Murray, C., et al. (2012a). Neuroprotective lifestyles and the aging brain: activity, atrophy, and white matter integrity. *Neurology* 79, 1802–1808. doi: 10.1212/WNL.0b013e3182703fd2

Gow, A. J., Corley, J., Starr, J. M., and Deary, I. J. (2012b). Reverse causation in activity-cognitive ability associations: the Lothian Birth Cohort 1936. *Psychol. Aging* 27, 250–255. doi: 10.1037/a0024144

Harada, N. D., Chiu, V., King, A. C., and Stewart, A. L. (2001). An evaluation of three self-report physical activity instruments for older adults. *Med. Sci. Sports Exerc.* 33, 962–970. doi: 10.1097/00005768-200106000-00016

Hertzog, C., Kramer, A. F., Wilson, R. S., and Lindenberger, U. (2009). Enrichment effects on adult cognitive development: can the functional capacity of older adults be preserved and enhanced? *Psychol. Sci. Public Interest* 9, 1–65. doi: 10.1111/j.1539-6053.2009.01034.x

Hu, F. B., Li, T. Y., Colditz, G. A., Willett, W. C., and Manson, J. E. (2003). Television watching and other sedentary behaviors in relation to risk of obesity and type 2 diabetes mellitus in women. *JAMA* 289, 1785–1791. doi: 10.1001/jama.289.14.1785

Imtiaz, B., Tolppanen, A. M., Kivipelto, M., and Soininen, H. (2014). Future directions in Alzheimer's disease from risk factors to prevention. *Biochem. Pharmacol.* 88, 661–670. doi: 10.1016/j.bcp.2014.01.003

James, B. D., Glass, T. A., Caffo, B., Bobb, J. F., Davatzikos, C., Yousem, D., et al. (2012). Association of social engagement with brain volumes assessed by structural MRI. *J. Aging Res.* 2012, 512714. doi: 10.1155/2012/512714

Jopp, D. S., and Hertzog, C. (2010). Assessing adult leisure activities: an extension of a self-report activity questionnaire. *Psychol. Assess.* 22, 108–120. doi: 10.1037/a0017662

Jovicich, J., Czanner, S., Han, X., Salat, D., van der Kouwe, A., Quinn, B., et al. (2009). MRI-derived measurements of human subcortical, ventricular and intracranial brain volumes: reliability effects of scan sessions, acquisition sequences, data analyses, scanner upgrade, scanner vendors and field strengths. *Neuroimage* 46, 177–192. doi: 10.1016/j.neuroimage.2009.02.010

King, A. C., Pruitt, L. A., Phillips, W., Oka, R., Rodenburg, A., and Haskell, W. L. (2000). Comparative effects of two physical activity programs on measured and perceived physical functioning and other health-related quality of life outcomes in older adults. *J. Gerontol. A Biol. Sci. Med. Sci.* 55, M74–M83. doi: 10.1093/gerona/55.2.M74

Kramer, A. F., Bherer, L., Colcombe, S. J., Dong, W., and Greenough, W. T. (2004). Environmental influences on cognitive and brain plasticity during aging. *J. Gerontol. A Biol. Sci. Med. Sci.* 59, M940–M957. doi: 10.1093/gerona/59.9.M940

LaPorte, R. E., Montoye, H. J., and Caspersen, C. J. (1985). Assessment of physical activity in epidemiologic research: problems and prospects. *Public Health Rep.* 100, 131–146.

McGue, M., and Christensen, K. (2007). Social activity and healthy aging: a study of aging Danish twins. *Twin Res. Hum. Genet.* 10, 255–265. doi: 10.1375/twin.10.2.255

Mitchell, M. B., Cimino, C. R., Benitez, A., Brown, C. L., Gibbons, L. E., Kennison, R. F., et al. (2012). Cognitively stimulating activities: effects on cognition across four studies with up to 21 years of longitudinal data. *J. Aging Res.* 2012, 461592. doi: 10.1155/2012/461592

Mora, F., Segovia, G., and del Arco, A. (2007). Aging, plasticity and environmental enrichment: structural changes and neurotransmitter dynamics in several areas of the brain. *Brain Res. Rev.* 55, 78–88. doi: 10.1016/j.brainresrev.2007.03.011

Morey, R. A., Petty, C. M., Xu, Y., Hayes, J. P., Wagner, H. R. II, Lewis, D. V., et al. (2009). A comparison of automated segmentation and manual tracing for quantifying hippocampal and amygdala volumes. *Neuroimage* 45, 855–866. doi: 10.1016/j.neuroimage.2008.12.033

Mortimer, J. A., Ding, D., Borenstein, A. R., DeCarli, C., Guo, Q., Wu, Y., et al. (2012). Changes in brain volume and cognition in a randomized trial of exercise and social interaction in a community-based sample of non-demented Chinese elders. *J. Alzheimers Dis.* 30, 757–766. doi: 10.3233/JAD-2012-120079

Newson, R. S., and Kemps, E. B. (2005). General lifestyle activities as a predictor of current cognition and cognitive change in older adults: a cross-sectional and longitudinal examination. *J. Gerontol. B Psychol. Sci. Soc. Sci.* 60, 113–120. doi: 10.1093/geronb/60.3.P113

Opdebeeck, C., Martyr, A., and Clare, L. (2016). Cognitive reserve and cognitive function in healthy older people: a meta-analysis. *Neuropsychol. Dev. Cogn. B Aging Neuropsychol. Cogn.* 23, 40–60. doi: 10.1080/13825585.2015.1041450

Pereira, A. C., Huddleston, D. E., Brickman, A. M., Sosunov, A. A., Hen, R., McKhann, G. M., et al. (2007). An in vivo correlate of exercise-induced neurogenesis in the adult dentate gyrus. *Proc. Natl. Acad. Sci. U.S.A.* 104, 5638–5643. doi: 10.1073/pnas.0611721104

Petrosini, L., De Bartolo, P., Foti, F., Gelfo, F., Cutuli, D., Leggio, M. G., et al. (2009). On whether the environmental enrichment may provide cognitive and brain reserves. *Brain Res. Rev.* 61, 221–239. doi: 10.1016/j.brainresrev.2009.07.002

Rovio, S., Spulber, G., Nieminen, L. J., Niskanen, E., Winblad, B., Tuomilehto, J., et al. (2010). The effect of midlife physical activity on structural brain changes in the elderly. *Neurobiol. Aging* 31, 1927–1936. doi: 10.1016/j.neurobiolaging.2008.10.007

Rundek, T., and Bennett, D. A. (2006). Cognitive leisure activities, but not watching TV, for future brain benefits. *Neurology* 66, 794–795. doi: 10.1212/01.wnl.0000209497.38834.d7

Schultz, S. A., Larson, J., Oh, J., Koscik, R., Dowling, M. N., Gallagher, C. L., et al. (2015). Participation in cognitively-stimulating activities is associated with brain structure and cognitive function in preclinical Alzheimer's disease. *Brain Imaging Behav.* 9, 729–736. doi: 10.1007/s11682-014-9329-5

Stern, Y. (2009). Cognitive reserve. *Neuropsychologia* 47, 2015–2028. doi: 10.1016/j.neuropsychologia.2009.03.004

Stewart, A. L., Mills, K. M., King, A. C., Haskell, W. L., Gillis, D., and Ritter, P. L. (2001). CHAMPS physical activity questionnaire for older adults: outcomes for interventions. *Med. Sci. Sports Exerc.* 33, 1126–1141. doi: 10.1097/00005768-200107000-00010

Stewart, A. L., Mills, K. M., Sepsis, P. G., King, A. C., McLellan, B. Y., Roitz, K., et al. (1997). Evaluation of CHAMPS, a physical activity promotion program for older adults. *Ann. Behav. Med.* 19, 353–361. doi: 10.1007/BF02895154

Stine-Morrow, E. A., Parisi, J. M., Morrow, D. G., and Park, D. C. (2008). The effects of an engaged lifestyle on cognitive vitality: a field experiment. *Psychol. Aging* 23, 778–786. doi: 10.1037/a0014341

Tournier, I., Mathey, S., and Postal, V. (2012). The association between routinization and cognitive resources in later life. *Int. J. Aging Hum. Dev.* 74, 143–161. doi: 10.2190/AG.74.2.c

Valenzuela, M. J., Sachdev, P., Wen, W., Chen, X., and Brodaty, H. (2008). Lifespan mental activity predicts diminished rate of hippocampal atrophy. *PLoS ONE* 3:e2598. doi: 10.1371/journal.pone.0002598

Van der Vegt, E. (2015). *Social Activity and Brain Volume, White Matter Lesions and Cognitive Function. Are Low Levels of Social Activity Associated with Brain Abnormalities Observed on MRI and with Poor Cognitive Function?* Masters thesis, Utrecht University, Utrecht.

Vaughan, L., Erickson, K. I., Espeland, M. A., Smith, J. C., Tindle, H. A., and Rapp, S. R. (2014). Concurrent and longitudinal relationships between cognitive activity, cognitive performance, and brain volume in older adult

women. *J. Gerontol. B Psychol. Sci. Soc. Sci.* 69, 826–836. doi: 10.1093/geronb/gbu109

Vemuri, P., Lesnick, T. G., Przybelski, S. A., Knopman, D. S., Roberts, R. O., Lowe, V. J., et al. (2012). Effect of lifestyle activities on Alzheimer disease biomarkers and cognition. *Ann. Neurol.* 72, 730–738. doi: 10.1002/ana.23665

Wilcox, S., Dowda, M., Dunn, A., Ory, M. G., Rheaume, C., and King, A. C. (2009). Predictors of increased physical activity in the Active for Life program. *Prev. Chronic Dis.* 6, A25.

Williams, J. W., Plassman, B. L., Burke, J., and Benjamin, S. (2010). Preventing Alzheimer's disease and cognitive decline. *Evid. Rep. Technol. Assess. (Full Rep.)* 193, 1–727.

Conflict of Interest Statement: The authors declare that the research was conducted in the absence of any commercial or financial relationships that could be construed as a potential conflict of interest.

Copyright © 2016 Seider, Fieo, O'Shea, Porges, Woods and Cohen. This is an open-access article distributed under the terms of the Creative Commons Attribution License (CC BY). The use, distribution or reproduction in other forums is permitted, provided the original author(s) or licensor are credited and that the original publication in this journal is cited, in accordance with accepted academic practice. No use, distribution or reproduction is permitted which does not comply with these terms.

ORIGINAL ARTICLE: EPIDEMIOLOGY, CLINICAL PRACTICE AND HEALTH

Depressive symptoms modify age effects on hippocampal subfields in older adults

Sarah M Szymkowicz,[1] Molly E McLaren,[1] Andrew O'Shea,[2,3] Adam J Woods,[2,3,4] Stephen D Anton[2] and Vonetta M Dotson[1,4]

Departments of [1]Clinical & Health Psychology, [2]Aging & Geriatric Research, [3]Center for Cognitive Aging & Memory, and [4]Neuroscience, University of Florida, Gainesville, Florida, USA

Aim: Major depression is associated with hippocampal volume changes, especially in late-life depression. These changes usually consist of volume reductions, but depression-related increases in hippocampal volume have also been reported. Subfield analysis has identified structural changes primarily in the cornu ammonis (CA) 1, CA2–3 and subiculum of the hippocampus in individuals with major depression; however, it is unclear whether lower levels of depressive symptoms are also associated volume reduction, or if depressive symptoms interact with age to impact hippocampal subfields. The current study addressed these questions.

Methods: A total of 43 community-dwelling older adults completed the Center for Epidemiologic Studies Depression Scale and underwent magnetic resonance imaging. Hippocampal subfield segmentation was carried out using an automated procedure, and left and right volumes from CA1, CA2-3, and the subiculum served as outcome measures. Multiple hierarchical regressions were carried out with age, Center for Epidemiologic Studies Depression Scale scores and their interaction as the independent variables, and sex and total intracranial volume as covariates.

Results: Higher Center for Epidemiologic Studies Depression Scale scores were associated with less age-related volumetric decreases in the right subiculum and right CA1.

Conclusions: Age-related atrophy in the hippocampus might be counteracted by depressive symptom-related enlargement of CA1 and the subiculum. More research is required to better understand the functional significance of this relationship. **Geriatr Gerontol Int 2016; ••: ••–••.**

Keywords: aging, brain volume, depressive symptoms, hippocampus, magnetic resonance imaging.

Introduction

Major depression (MDD) is the most common psychiatric disorder seen in community-dwelling older adults.[1] Depression can be thought of as a continuum of symptoms that range from milder conditions, such as elevated depressive symptoms, to more severe forms of major depression. Elevated depressive symptoms are even more common than major depression in older adults, with an estimated prevalence of 7–15%.[2] These subthreshold depressive symptoms are of critical concern, as they are associated with similar cognitive and fronto-subcortical neural dysfunction, and adverse health outcomes as major depression, but are often undiagnosed and therefore untreated.[3,4]

For outcomes such as brain changes, the impact of subthreshold depressive symptoms might be greater in older adults compared with young adults as a result of the cumulative effect of depressive symptoms and normal age-related changes. In particular, depression-related hippocampal alterations can be more pronounced in older adults compared with their younger counterparts because of the cumulative effect of depression[5] and age-related hippocampal atrophy.[6] Older age is associated with hippocampal volume reduction, but findings in major and subthreshold depression vary, with many studies reporting smaller hippocampal volume,[7,8] but other studies reporting no differences[9,10] or larger hippocampal volume for at least some subgroups of depressed individuals.[11]

Inconsistencies in the depression literature might be due to heterogeneity within subregions of the hippocampus that is obscured when the hippocampus is examined globally. The hippocampus comprises histologically

Accepted for publication 24 July 2016.

Correspondence: Ms Sarah M Szymkowicz MS, Department of Clinical & Health Psychology, University of Florida, P.O. Box 100165, Gainesville, FL, 32610-0165. Email: smszymkowicz@phhp.ufl.edu

© 2016 Japan Geriatrics Society

doi: 10.1111/ggi.12901

distinct functional and structural subfields, including cornu ammonis (CA) 1–4, subiculum and dentate gyrus, that have different associations with memory and other functions, and might also be differentially related to both depressive disorders and non-pathological aging.[12] Findings for the relationships between hippocampal subfields, depression and aging are heterogeneous, with differing results for the subfield most affected. With respect to depression, some studies show smaller CA1, CA2–3 and subiculum volume in individuals with late-life depression,[13,14] and less dentate gyrus volume as a function of multiple depressive episodes in young to middle-aged adults.[15] In contrast, there is also evidence of larger volume of CA1 and portions of the subiculum bilaterally in unmedicated young to middle-aged depressed adults.[16] Similarly, findings on the effect of age on hippocampal subfields vary with some studies showing age effects on volume in the subiculum and relative sparing of CA1 and other subfields,[17] whereas others show age effects on volumes in CA2–3 and CA4–dentate gyrus.[18] Less is known about the potentially interactive effect of age and elevated depressive symptoms on hippocampal subfield volume.

The purpose of the current study was to determine whether or not age effects on volume of hippocampal subfields are modified by elevated depressive symptoms in older adults. Based on CA1, CA2–3 and the subiculum being most consistently related to late-life depression, we focused on these regions.[13] We predicted that older age would be associated with smaller volume in these hippocampal subfields, and that this association would be more pronounced at higher levels of depressive symptoms.

Methods

Participants

A total of 48 community-dwelling older adults (mean age 68.88 ± 7.21 years) were recruited for the present study. All participants were right-handed, native English speakers with at least 8 years of education. Participants were required to have a score of >30 on the Telephone Interview for Cognitive Status,[19] and a score of >24 on the Mini-Mental State Examination,[20] which are the suggested cut-offs for cognitive impairment, respectively. Exclusionary criteria included self-reported history of major neurological or other medical illness, head trauma, learning disorders, current epileptic or antipsychotic medication use, language comprehension difficulties and magnetic resonance imaging (MRI) contraindications. Participants with MDD were not excluded in order to increase the range of depressive symptom severity in the sample. Two participants met the criteria for MDD per clinical interview. Both were taking antidepressant medication, as were five additional individuals who did not meet the criteria for depression. Five individuals were excluded from analyses because of missing data, MRI evidence of past stroke, current substance abuse or a learning disorder diagnosis. Thus, our final sample comprised 43 individuals (9 young-old [aged 55–64 years], 24 middle-old [aged 65–74 years] and 10 old-old [aged ≥75 years]). Demographic data for this sample are presented in Table 1. All procedures were reviewed and approved by the University of Florida's institutional review board, and all participants provided verbal and written informed consent.

Measures

Participants completed the Center for Epidemiologic Studies Depression Scale (CES-D), which consists of 20 self-report questions assessing the frequency and severity of depressive symptoms over the previous week.[21]

MRI data acquisition

MRI data were collected within 1 week of completing the CES-D at the University of Florida's McKnight Brain Institute on the Advanced Magnetic Resonance Imaging and Spectroscopy (AMRIS) facility's Philips 3-Tesla scanner (Amsterdam, the Netherlands) using a Philips eight-channel radio-frequency coil. A high resolution, T_1-weighted turbo field echo anatomical scan was collected using the following parameters: TR = 81 ms, TE = 3.7 ms, 170 slices acquired in a sagittal orientation, flip angle = 8 degrees, 1 mm cubic resolution. To minimize noise while in the scanner, participants were given headphones and earplugs. Head movement was minimized by cushions positioned inside the head coil.

Table 1 Sample demographic characteristics

	Mean	SD	Range
Total sample (*n* = 43)			
Age (years)	68.79	7.00	55–81
Sex (% female)	69.76	–	–
Education (years)	15.07	2.53	10–20
MMSE total	28.91	1.25	25–30
CES-D total	7.84	8.90	0–45
Those using antidepressants (*n* = 7)			
Age (years)	62.57	6.78	56–72
Sex (% female)	71.46	–	–
Education (years)	15.57	2.64	12–19
MMSE total	29.42	0.79	28–30
CES-D total	17.29	16.09	1–45

CES-D, Center for Epidemiologic Studies Depression Scale; MMSE, Mini-Mental State Examination; SD, standard deviation.

© 2016 Japan Geriatrics Society

Hippocampal subfield measurement

The Freesurfer image analysis suite (version 5.3, http://surfer.nmr.mgh.harvard.edu) was used to quantify brain volumes.[22] Briefly, processing included motion correction, removal of non-brain tissue, automated Talairach transformation, segmentation of the gray and white matter tissue, and cortical surface inflation. Each image was also manually inspected for errors in the automatic processing by one of two raters. A two-way mixed effects model calculated the interclass correlation coefficient for manual volume adjustments. The interclass correlation coefficient between raters was extremely high (0.99), likely reflecting the minimal manual adjustments required after the automatic processing. Volumes of the bilateral hippocampi were obtained using an automated procedure for volumetric measurement of brain structure, which uses Bayesian inference and a probabilistic atlas of hippocampal formation based on manual delineations of subfields in ultra-high-T_1-weighted MRI scans from a number of participants.[23] The left and right hippocampi were segmented into seven subfields: CA1, CA2–3, CA4–dentate gyrus, subiculum, presubiculum, fimbria and hippocampal fissure. Average dice coefficients of approximately 0.7 for CA2-3 and subiculum were reported for overlap between manual and automated segmentation methods.[23] Regions of interest for the current study included left and right volumes from CA1, CA2–3 and the subiculum.

Statistical analysis

All analyses were carried out using SPSS 22.0 software (IBM, Armonk, NY, USA). Separate hierarchical regression analyses were carried out for the left and right CA1, CA2–3, and subiculum with age, CES-D scores and their interaction as the independent variables, and sex and total intracranial volume as covariates. Education and antidepressant use were initially entered as covariates, but were removed from final analyses due to a lack of statistical significance. CES-D scores were highly skewed; therefore, we applied a square root transformation to these data to ensure a more normal distribution. All variables besides sex were continuous measures in the models. Age and CES-D scores were mean-centered and multiplied to create the interaction terms. We used a statistical significance threshold of $\alpha \leq 0.05$. Because of the relatively small sample size, correcting for multiple comparisons would result in a highly stringent threshold for significance, and might increase the chance of type II error. We therefore present uncorrected results, but indicate when results met significance after Bonferroni multiple comparison correction.

Results

Results are summarized in Table 2 and Figure 1. With respect to the subiculum, there was a significant main effect of age, such that older age was associated with smaller

Table 2 Effects of age and Center for Epidemiologic Studies Depression Scale scores on hippocampal subfield volumes, adjusted for total intracranial volume and sex

	Total ICV			Sex			Age			CES-D			Age × CES-D		
	β	*t*	*P*	*β*	*t*	*P*	*β*	*t*	*P*	*β*	*t*	*P*	*β*	*t*	*P*
Right															
CA1	0.361	2.514	0.016*	−0.204	−1.452	0.155	−0.214	−1.612	0.116	−0.024	−0.155	0.877	0.356	2.375	0.023*
CA2-3	0.320	2.063	0.046*	−0.248	−1.632	0.111	−0.271	−1.893	0.066	−0.099	−0.594	0.556	0.113	0.698	0.490
Subiculum	0.151	1.107	0.276	−0.246	−1.844	0.073	−0.408	−3.236	0.003***	0.209	1.418	0.165	0.497	3.489	0.001***
Left															
CA1	0.456	2.875	0.007***	−0.096	−0.619	0.540	−0.206	−1.407	0.168	−0.081	−0.474	0.638	0.024	0.148	0.883
CA2–3	0.269	1.739	0.090	−0.316	−2.089	0.044*	−0.209	−1.463	0.152	−0.156	−0.933	0.357	0.104	0.644	0.523
Subiculum	0.360	2.467	0.018*	−0.177	−1.238	0.223	−0.376	−2.783	0.008***	0.166	1.050	0.301	0.277	1.818	0.077

*$P < 0.05$. **Significant after Bonferroni correction ($P \leq 0.008$). Men were coded as 0; women were coded as 1. CA, cornu ammonis; CES-D, Center for Epidemiologic Studies Depression Scale; ICV, intracranial volume.

© 2016 Japan Geriatrics Society

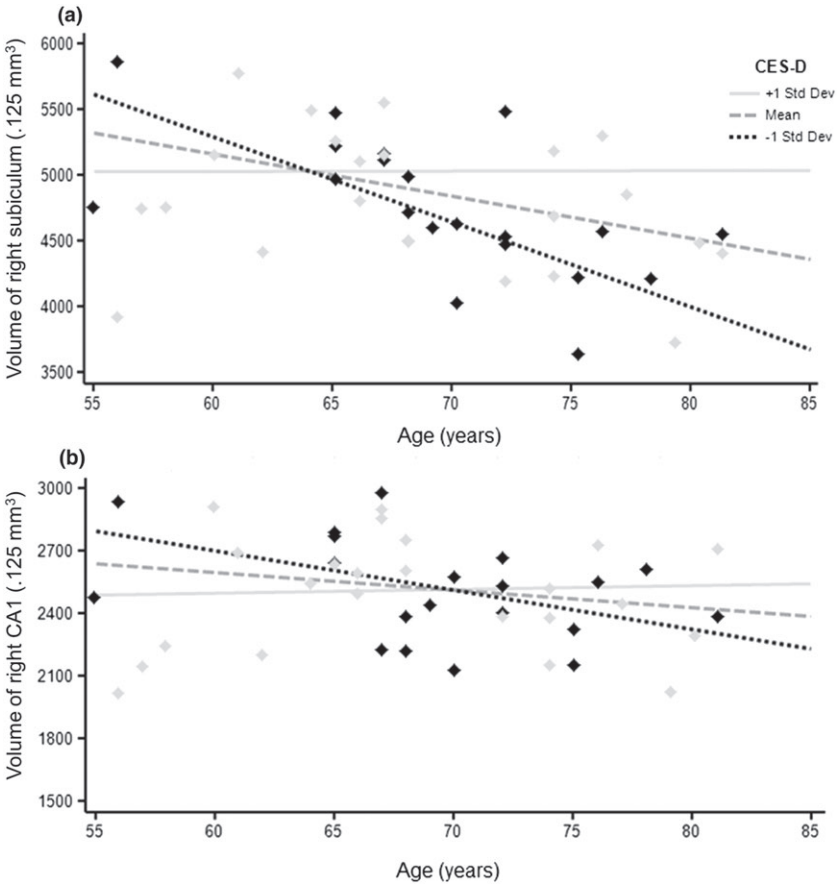

Figure 1 Significant results for the age × Center for Epidemiologic Studies Depression Scale (CES-D) interactions on volumes in the (a) right subiculum and (b) right cornu ammonis (CA) 1. Raw scores are presented for ease of display, but age and CES-D scores were entered as continuous variables in the statistical models and were centered around the mean in all analyses.

volume of the subiculum bilaterally (right: $P = 0.003$, left: $P = 0.008$; both significant after Bonferroni correction). This was further qualified by a significant age × CES-D interaction for the right subiculum ($P = 0.001$; significant after Bonferroni correction), suggesting that age effects on volume were greater in individuals with lower CES-D scores, but minimized in individuals with higher CES-D scores. A similar age × CES-D interaction was found for right CA1 subfield volume ($P = 0.023$). There were no other significant main effects or age × CES-D interactions for the other regions of interest. This pattern of results was unchanged when the two participants with MDD were excluded.

Discussion

The present study examined the interrelationships between depressive symptoms, age and hippocampal subfield volumes. Previous work has generally shown smaller volumes in the subiculum and CA1–3 subfields in both midlife and late-life depression, as well as smaller dentate gyrus volume in young depressed adults.[13,15] We add to this limited literature by investigating the interaction of age and depressive symptom severity in older adults with mostly subthreshold symptoms. This focus is important considering the high prevalence of subthreshold depressive symptoms in older adults[2] and the impact of non-pathological aging on hippocampal subfield volumes,[18] which raises the possibility of a cumulative effect of aging and depressive symptoms on hippocampal structure.

Our finding of greater age effects on volume in individuals with lower depressive symptoms and less of an age effect at higher depressive symptom severity is contrary to our hypothesis. Nevertheless, the results are not completely unexpected in the context of previous reports of larger volumes in the hippocampus. At least one study found larger hippocampal regions analogous to CA1 and the subiculum bilaterally in patients with MDD,[16] and depression-related enlargement of total hippocampal volume has also been reported.[11] In the present study, age effects on volume within the hippocampus might have been counteracted by depressive symptom-related enlargement of CA1 and the subiculum.

Although the functional significance of larger hippocampal volumes, particularly in CA1 and the subiculum, in individuals with elevated depressive symptoms remains unclear, it could be that CA1 and the subiculum are particularly vulnerable to the effects of depression, as the present study and others have found alterations in these subfields.[13,16] Post-mortem studies of individuals with mood disorders have also provided

© 2016 Japan Geriatrics Society

evidence of disproportionate structural changes in CA1 and the subiculum.[24] CA1 projects to the subiculum, which in turn provides the main output of the hippocampal formation to structures involved in mood regulation, including the entorhinal cortex, amygdala, ventromedial prefrontal cortex and striatum.[25] The subiculum is suggested to be integral to hippocampal interactions with the hypothalamic–pituitary–adrenal axis.[25] Hypothalamic–pituitary–adrenal axis dysfunction is thought to play a role in the pathophysiology of MDD, with persistent elevation of glucocorticoids leading to hippocampal atrophy.[26]

The mechanisms underlying larger, rather than smaller, hippocampal volume in relation to elevated depressive symptoms are unclear. Some researchers have argued that the early stages of depression are marked by a compensatory inflammatory response, which might modulate neurogenesis in the hippocampus through activation of pro-inflammatory cytokines [27] In addition to increased hippocampal volumes, increased blood flow to the hippocampus has been seen in acutely depressed patients, suggesting that these changes could reflect early or acute stages of depression.[28] It might only be through prolonged duration of depressive symptoms that hippocampal atrophy becomes evident.[29] Most of our participants had subthreshold depressive symptoms, and results were unchanged when excluding two participants with MDD. Combined with evidence that subthreshold depressive symptoms are often a precursor to MDD, this suggests the present findings might reflect neurobiological changes that increase the risk for future clinical depression, which might subsequently lead to smaller hippocampal volumes if untreated.[2]

The impact of depression treatment on hippocampal volumes has been highlighted by other investigations. There is evidence that longer duration of untreated depression is related to hippocampal volume reduction,[30] whereas antidepressant treatment is associated with increased volume over time.[31] Additional clinical variables might impact the relationship between depression and volume in the hippocampus. For example, morphological abnormalities were found in the left anterior subiculum and lateral CA1 in late-onset compared with early-onset depression in one study.[13] Other studies have found differences in first-episode compared with recurrent depression, including evidence of a positive relationship between total and subfield hippocampal volumes, and severity of depression in first-episode MDD.[15,32] Furthermore, comorbid symptoms of anxiety might also play a role in increased hippocampal volume, as research has suggested a positive relationship between increased anxiety and larger hippocampal volumes.[33] There is some suggestion from the pediatric depression literature that anxiety influences the ratio of hippocampal volumes to volumes in the amygdala.[34] The amygdala is a closely connected structure that is important for emotional expression and, together with the hippocampus, has a role in the formation of emotion-related memories.[35–37] Larger studies are required to investigate individual variability in anxiety and other clinical moderators, and their relationship to depression-related brain changes as possible methods for better understanding the underlying mechanisms of depression and improving intervention strategies.

The current findings should be interpreted in the context of limitations of the study, including the inherent limitations of the automated hippocampal segmentation program, as well as our relatively small sample size.[38] In addition, our sample included individuals taking antidepressants. Although we did not find any differences in subfield volumes between the two groups, it has been shown that antidepressant use can affect hippocampal volume, and that might have played a role in the present findings.[31] Furthermore, although all participants in the present study had Telephone Interview for Cognitive Status scores >30 and Mini-Mental State Examination scores >24, we cannot rule out the possibility that individuals with mild cognitive impairment were included, which could have affected the hippocampal subfield results. Moreover, information regarding anxiety symptoms was not available for all participants in the present study; therefore, we were unable to determine the influence of anxiety on the present results. Nevertheless, the study adds to the literature by investigating depressive symptoms as a continuous measure and not as a dichotomous variable (MDD *vs* healthy controls), as many other studies have previously done. Gaining a better understanding of the longitudinal relationship between depressive symptoms and age-related hippocampal volume change might increase our understanding of the pathophysiology of depression in older adults, and provide potential targets for behavioral and pharmacological treatments.

Acknowledgments

This work was supported by the McKnight Brain Research Foundation; the National Institute on Aging (under grants T32AG020499-11 and P30AG028740-01); the National Center for Advancing Translational Science (under grants UL1TR000064 and KL2TR000065); and the Thomas H Maren Foundation. Neuroimaging was carried out at the Advanced Magnetic Resonance Imaging and Spectroscopy (AMRIS) facility in the McKnight Brain Institute of the University of Florida, which is supported by National Science Foundation Cooperative Agreement No. DMR-1157490 and the State of Florida. SMS assisted with data collection and image processing, carried out statistical analyses, and took primary responsibility for manuscript writing. MEM assisted with image processing and manuscript writing. AO assisted with image processing and manuscript writing. AJW supervised all image processing and assisted with manuscript writing. SDA assisted with data collection and manuscript writing. VMD designed

© 2016 Japan Geriatrics Society

the study, supervised data collection, and supervised statistical analyses and manuscript writing.

Disclosure statement

The authors declare no conflict of interest.

References

1 Luijendijk HJ, van den Berg JF, Dekker MJ *et al.* Incidence and recurrence of late-life depression. *Arch Gen Psychiatry* 2008; **65**: 1394–1401. DOI:10.1001/archpsyc.65.12.1394.

2 Laborde-Lahoz P, El-Gabalawy R, Kinley J, Kirwin PD, Sareen J, Pietrzak RH. Subsyndromal depression among older adults in the USA: prevalence, comorbidity, and risk for new-onset psychiatric disorders in late life. *Int J Geriatr Psychiatry* 2015; **30**: 677–685. DOI:10.1002/gps.4204.

3 Kumar A, Jin Z, Bilker W, Udupa J, Gottlieb G. Late-onset minor and major depression: early evidence for common neuroanatomical substrates detected by using MRI. *Proc Natl Acad Sci U S A* 1998; **95**: 7654–7658.

4 Cuijpers P, Vogelzangs N, Twisk J, Kleiboer A, Li J, Penninx BW. Differential mortality rates in major and subthreshold depression: meta-analysis of studies that measured both. *Br J Psychiatry* 2013; **202**: 22–27. DOI:10.1192/bjp.bp.112.112169.

5 Fotuhi M, Do D, Jack C. Modifiable factors that alter the size of the hippocampus with ageing. *Nat Rev Neurol* 2012; **8**: 189–202. DOI:10.1038/nrneurol.2012.27.

6 Allen JS, Bruss J, Brown CK, Damasio H. Normal neuroanatomical variation due to age: the major lobes and a parcellation of the temporal region. *Neurobiol Aging* 2005; **26**: 1245–1260 discussion 79-82. DOI:10.1016/j.neurobiolaging.2005.05.023.

7 Cole J, Costafreda SG, McGuffin P, Fu CH. Hippocampal atrophy in first episode depression: a meta-analysis of magnetic resonance imaging studies. *J Affect Disord* 2011; **134**: 483–487. DOI:10.1016/j.jad.2011.05.057.

8 Spalletta G, Piras F, Caltagirone C, Fagioli S. Hippocampal multimodal structural changes and subclinical depression in healthy individuals. *J Affect Disord* 2014; **152-154**: 105–112. DOI:10.1016/j.jad.2013.05.068.

9 Greenberg DL, Payne ME, MacFall JR, Steffens DC, Krishnan RR. Hippocampal volumes and depression subtypes. *Psychiatry Res* 2008; **163**: 126–132. DOI:10.1016/j.pscychresns.2007.12.009.

10 Dotson VM, Davatzikos C, Kraut MA, Resnick SM. Depressive symptoms and brain volumes in older adults: a longitudinal magnetic resonance imaging study. *J Psychiatry Neurosci* 2009; **34**: 367–375.

11 Phillips JL, Batten LA, Tremblay P, Aldosary F, Blier P. A prospective, longitudinal study of the effect of remission on cortical thickness and hippocampal volume in patients with treatment-resistant depression. *Int J Neuropsychopharmacol* 2015; **18**: 1–9. DOI:10.1093/ijnp/pyv037.

12 Szabo K, Hennerici MG. *The Hippocampus in Clinical Neuroscience*. Switzerland: Karger, 2014.

13 Ballmaier M, Narr KL, Toga AW *et al.* Hippocampal morphology and distinguishing late-onset from early-onset elderly depression. *AJ Psychiatry* 2008; **165**: 229–237. DOI:10.1176/appi.ajp.2007.07030506.

14 Lim HK, Hong SC, Jung WS *et al.* Automated hippocampal subfields segmentation in late life depression. *J Affect Disord* 2012; **143**: 253–256. DOI:10.1016/j.jad.2012.04.018.

15 Treadway MT, Waskom ML, Dillon DG *et al.* Illness progression, recent stress, and morphometry of hippocampal subfields and medial prefrontal cortex in major depression. *Biol Psychiatry* 2015; **77**: 285–294. DOI:10.1016/j.biopsych.2014.06.018.

16 Bearden CE, Thompson PM, Avedissian C *et al.* Altered hippocampal morphology in unmedicated patients with major depressive illness. *ASN Neuro* 2009; **1**: e00020. DOI:10.1042/AN20090026.

17 La Joie R, Fouquet M, Mezenge F *et al.* Differential effect of age on hippocampal subfields assessed using a new high-resolution 3 T MR sequence. *Neuroimage* 2010; **53**: 506–514. DOI:10.1016/j.neuroimage.2010.06.024.

18 Pereira JB, Valls-Pedret C, Ros E *et al.* Regional vulnerability of hippocampal subfields to aging measured by structural and diffusion MRI. *Hippocampus* 2014; **24**: 403–414. DOI:10.1002/hipo.22234.

19 Brandt J, Spencer M, Folstein M. The telephone interview for cognitive status. *Neuropsychiatry Neuropsychol Behav Neurol* 1988; **1**: 111–117.

20 Folstein MF, Folstein SE, McHugh PR. "Mini-mental state". A practical method for grading the cognitive state of patients for the clinician. *J Psychiatr Res* 1975; **12**: 189–198.

21 Radloff LS. The CES-D Scale: A self-report depression scale for research in the general population. *Appl Psych Meas* 1977; **1**: 385–401.

22 Fischl B. *FreeSurfer Neuroimage* 2012; **62**: 774–781. DOI:10.1016/j.neuroimage.2012.01.021.

23 Van Leemput K, Bakkour A, Benner T *et al.* Automated segmentation of hippocampal subfields from ultra-high resolution in vivo MRI. *Hippocampus* 2009; **19**: 549–557. DOI:10.1002/hipo.20615.

24 Rosoklija G, Toomayan G, Ellis SP *et al.* Structural abnormalities of subicular dendrites in subjects with schizophrenia and mood disorders: preliminary findings. *Arch Gen Psychiatry* 2000; **57**: 349–356.

25 O'Mara S. The subiculum: what it does, what it might do, and what neuroanatomy has yet to tell us. *J Anat* 2005; **207**: 271–282. DOI:10.1111/j.1469-7580.2005.00446.x.

26 Conrad CD. Chronic stress-induced hippocampal vulnerability: the glucocorticoid vulnerability hypothesis. *Rev Neurosci* 2008; **19**: 395–411.

27 Dowlati Y, Herrmann N, Swardfager W *et al.* A meta-analysis of cytokines in major depression. *Biol Psychiatry* 2010; **67**: 446–457. DOI:10.1016/j.biopsych.2009.09.033.

28 Videbech P, Ravnkilde B, Pedersen AR *et al.* The Danish PET/depression project: PET findings in patients with major depression. *Psychol Med* 2001; **31**: 1147–1158.

29 Bell-McGinty S, Butters MA, Meltzer CC, Greer PJ, Reynolds CF 3rd, Becker JT. Brain morphometric abnormalities in geriatric depression: long-term neurobiological effects of illness duration. *AJ Psychiatry* 2002; **159**: 1424–1427.

30 Sheline YI, Gado MH, Kraemer HC. Untreated depression and hippocampal volume loss. *AJ Psychiatry* 2003; **160**: 1516–1518.

31 Frodl T, Jager M, Smajstrlova I *et al.* Effect of hippocampal and amygdala volumes on clinical outcomes in major depression: a 3-year prospective magnetic resonance imaging study. *J Psychiatry Neurosci* 2008; **33**: 423–430.

32 Cole J, Toga AW, Hojatkashani C *et al.* Subregional hippocampal deformations in major depressive disorder. *J Affect Disord* 2010; **126**: 272–277. DOI:10.1016/j.jad.2010.03.004.

33 Rusch BD, Abercrombie HC, Oakes TR, Schaefer SM, Davidson RJ. Hippocampal morphometry in depressed patients and control subjects: relations to anxiety symptoms. *Biol Psychiatry* 2001; **50**: 960–964.

© 2016 Japan Geriatrics Society

34 MacMillan S, Szeszko PR, Moore GJ *et al.* Increased amygdala: hippocampal volume ratios associated with severity of anxiety in pediatric major depression. *J Child Adolesc Psychopharmacol* 2003; **13**: 65–73. DOI:10.1089/104454603321666207.
35 Davis M. The role of the amygdala in fear-potentiated startle: implications for animal models of anxiety. *Trends Pharmacol Sci* 1992; **13**: 35–41.
36 LeDoux JE. Emotional memory systems in the brain. *Behav Brain Res* 1993; **58**: 69–79.
37 McGaugh JL, Introini-Collison IB, Nagahara AH, Cahill L, Brioni JD, Castellano C. Involvement of the amygdaloid complex in neuromodulatory influences on memory storage. *Neurosci Biobehav Rev* 1990; **14**: 425–431.
38 Wisse LE, Biessels GJ, Geerlings MI. A critical appraisal of the hippocampal subfield segmentation package in FreeSurfer. *Front Aging Neurosci* 2014; **6**: 261. DOI:10.3389/fnagi.2014.00261.

© 2016 Japan Geriatrics Society

ALCOHOLISM CLINICAL & EXPERIMENTAL RESEARCH

Current Heavy Alcohol Consumption is Associated with Greater Cognitive Impairment in Older Adults

Adam J. Woods, Eric C. Porges, Vaughn E. Bryant, Talia Seider, Assawin Gongvatana, Christopher W. Kahler, Suzanne de la Monte, Peter M. Monti, and Ronald A. Cohen

Background: The acute consumption of excessive quantities of alcohol causes well-recognized neurophysiological and cognitive alterations. As people reach advanced age, they are more prone to cognitive decline. To date, the interaction of current heavy alcohol (ethanol [EtOH]) consumption and aging remains unclear. This study tested the hypothesis that negative consequences of current heavy alcohol consumption on neurocognitive function are worse with advanced age. Further, we evaluated the relations between lifetime history of alcohol dependence and neurocognitive function

Methods: Sixty-six participants underwent a comprehensive neurocognitive battery. Current heavy EtOH drinkers were classified using National Institute on Alcohol Abuse and Alcoholism criteria (EtOH heavy, $n = 21$) based on the Timeline follow-back and a structured clinical interview and compared to nondrinkers, and moderate drinkers (EtOH low, $n = 45$). Of the total population, 53.3% had a lifetime history of alcohol dependence. Neurocognitive data were grouped and analyzed relative to global and domain scores assessing: global cognitive function, attention/executive function, learning, memory, motor function, verbal function, and speed of processing.

Results: Heavy current EtOH consumption in older adults was associated with poorer global cognitive function, learning, memory, and motor function ($ps < 0.05$). Furthermore, lifetime history of alcohol dependence was associated with poorer function in the same neurocognitive domains, in addition to the attention/executive domain, irrespective of age ($ps < 0.05$).

Conclusions: These data suggest that while heavy current alcohol consumption is associated with significant impairment in a number of neurocognitive domains, history of alcohol dependence, even in the absence of heavy current alcohol use, is associated with lasting negative consequences for neurocognitive function.

Key Words: Alcohol Consumption, Alcohol Dependence, Cognitive Aging, EtOH, Cognitive Impairment.

THE ACUTE CONSUMPTION of excessive quantities of alcohol causes well-recognized neurophysiological and cognitive alterations, including loss of consciousness, coma, or even death. Heavy alcohol consumption adversely affects the brain both directly and indirectly. Direct brain effects of alcohol include depression of central nervous system activity, alterations in cerebrovascular function, and neurotoxicity (Alexander et al., 2004; Haorah et al., 2005; Shih et al., 2001; Vinod and Hungund, 2005; Webb et al., 1997; Wilhelm et al., 2015). Indirect effects include neurotoxicity tied to hepatic, renal, and gastrointestinal dysfunction, as well as sleep disturbance, anoxia, head injury, and other disturbances that may occur with chronic alcohol intoxication (Marksteiner et al., 2002; O'Dell et al., 2012; Schuckit, 2009; Solomon and Malloy, 1992; Spirduso et al., 1989; Wilde et al., 2004).

Despite a growing literature concerning the effects of acute and chronic heavy alcohol consumption, the neurocognitive manifestations of heavy alcohol consumption remain unresolved. Findings from past studies conducted to address this question have not been ubiquitous. While the neurocognitive effects of alcohol consumption appear to depend on the amount of alcohol consumed, the duration of use, and various other clinical factors, including age and comorbid neurological conditions, not all studies agree (Carey et al., 2004a, b; Draper et al., 2011; Friend et al., 2005; Green et al., 2010; Houston et al., 2014; Marksteiner et al., 2002; Molina et al., 1994; O'Dell et al., 2012; Solomon and Malloy, 1992; Squeglia et al., 2009, 2014; Sullivan et al., 2002, 2010).

For example, in the MATCH study of drinkers undergoing alcohol treatment for alcohol abuse–dependence, Friend

From the Department of Aging and Geriatric Research (AJW, ECP, VEB, TS, RAC), Center for Cognitive Aging and Memory (CAM), Institute on Aging, University of Florida, Gainesville, Florida; Department of Psychiatry (AG), University of California San Diego, San Diego, California; Department of Behavioral and Social Sciences (CWK, PMM), Center for Alcohol and Addiction Studies and the Alcohol Research Center on HIV (ARCH), Brown University School of Public Health, Providence, Rhode Island; and Department of Pathology and Laboratory Medicine (SM), Department of Neurosurgery, Brown University, Providence, Rhode Island.

Received for publication March 29, 2016; accepted August 4, 2016.

Reprint requests: Adam J. Woods, PhD, Cognitive Aging and Memory Clinical Translational Research Program, Institute on Aging, Department of Aging and Geriatric Research, University of Florida, 2004 Mowry Road, Gainesville, FL 32610; Tel.: 352-294-5842; Fax: 352-294-5836; E-mail: ajwoods@ufl.edu

Copyright © 2016 by the Research Society on Alcoholism.

DOI: 10.1111/acer.13211

and colleagues (2005) found that while years of alcohol consumption was inversely associated with neuropsychological test scores, it did not account for much of the variance in these test scores. Yet, a recent study found in older adults that age of onset of alcohol dependence was not associated with greater cognitive deficits (Kist et al., 2014). However, this study also found that older adults had significantly poorer cognitive abilities when compared to nonalcohol-dependent controls. A recent study found age effects in 51 adults with alcohol dependence diagnoses who were abstinent from alcohol for 1 month (Durazzo et al., 2013). Mild deficits of learning, memory, cognitive efficiency, executive functions, processing speed, and fine motor skills were associated with alcohol dependence, although these deficits were greatest among people who also smoked cigarettes. In addition, another study found deficits in executive function in 560 heavy drinking men and women (Houston et al., 2014). In an earlier study, Drake and colleagues (1995) found that alcohol-dependent adults who abstained from alcohol after a 28-day treatment program showed recovery of cognitive functions. Another study found that moderate alcohol consumption was not associated with either the occurrence or exacerbation of dementia (Panza et al., 2009), and there have been reports that drinking 1 glass of wine a day may actually be associated with reduced rates of Alzheimer's disease (Solfrizzi et al., 2007). Yet, a recent study of brain morphometry and cognition reported that late life consumption of alcohol is associated with episodic memory difficulties and also reduced hippocampal volume in the Framingham cohort (Downer et al., 2015). These contrasting results demonstrate the need for further study of the influence of advanced age on possible heavy alcohol consumption effects on neurocognitive function. Further still, even less is known about the impact of advanced age on possible alcohol-related neurocognitive deficits.

In this study, we sought to understand the relationship between age, heavy alcohol consumption, and neurocognitive function. As people reach advanced age and are more prone to cognitive decline (Woods et al., 2012, 2013), the adverse effects of heavy alcohol use may be exacerbated (Riege et al., 1981). In fact, dementia secondary to alcoholism is commonly diagnosed in elderly adults whose cognitive and functional decline is inconsistent with progressive neurodegenerative disorders such as Alzheimer's disease and whose clinical history indicates chronic heavy alcohol consumption (Meyer et al., 1998; Tyas, 2001). As people reach more advanced age, they experience systemic physiological and neural alterations that may increase vulnerability to the effects of alcohol (Goldberg et al., 1994; Meyer et al., 1998; Snow et al., 2009; Tyas, 2001). Yet, relatively few studies have directly compared the neurocognitive performance of heavy drinkers with that of people who consume moderate quantities of alcohol or who are nondrinkers as a function of age. To address this question, this study was conducted to examine the association of heavy alcohol consumption with neurocognitive function at different ages. We hypothesized that heavy alcohol consumption would be associated with significant cognitive impairments and that the adverse effects of heavy alcohol consumption would be greatest among older adults.

MATERIALS AND METHODS

Participants

Sixty-six participants in a National Institute on Alcohol Abuse and Alcoholism (NIAAA) sponsored study of the effects of heavy alcohol use and aging on neurocognitive and brain functioning were assessed. The mean age of the sample was 38.5 ± 11.7 years (range = 21 to 69 years). Mean educational attainment was 13.7 ± 2.75 years. The racial composition of the overall sample was 30.3% African-American and 69.7% Caucasian. Thirty-five (53%) participants were women. The sample consisted of adults recruited from the Brown University Center for Aids Research, who were at risk for HIV or hepatitis C virus (HCV) infection based on their association with HIV-infected friends or family, prior injection drug use, or sexual risk, but who were not infected with either HIV or HCV. Participants were recruited over 30 months using clinician referral, word of mouth, and flyers. All participants underwent a neurological examination and thorough medical history assessment. HIV infection was ruled out based on enzyme-linked immunosorbent assay (ELISA) and confirmed by Western blot, while active HCV infection was ruled out by negative anti-HCV ELISA and negative qualitative HCV RNA by polymerase chain reaction. Participants were also excluded for history of (1) head injury with loss of consciousness > 10 minutes; (2) history of severe anxiety, depression, or neurological disorders, including dementia, seizure disorder, stroke, and opportunistic brain infection; (3) severe psychiatric illness that might impact brain function (e.g., schizophrenia, bipolar illness); and (4) current (6-month) substance dependence or positive urine toxicology screen for cocaine, opiates, or illicit stimulants or sedatives. Inclusion/exclusion criteria were assessed using structured clinical interview by the study physician and self-reported medical history. The study was approved by the institutional review boards, and informed consent was obtained from each participant before enrollment.

Alcohol Consumption. Participants were recruited with the goal of obtaining relatively equal samples of nondrinkers, people who drink moderate quantities of alcohol, and heavy alcohol users (ethanol [EtOH] none; EtOH moderate, EtOH high) based on current use. Participants were categorized into alcohol groupings based on NIAAA criteria (see Alcoholism NIoAAa: http://rethinkingdrinking.niaaa.nih.gov/IsYourDrinkingPatternRisky/WhatsAtRiskOrHeavyDrinking.asp) derived from Timeline followback (TLFB; Fals-Stewart et al., 2000) and a structured clinical interview by the study physician. The TLFB involves a self-report of drinking behavior over the past 90 days and was used to calculate the average number of drinks per week over the past 3 months. The EtOH heavy group consisted of people who reported drinking 5 or more drinks in a single day for men (or average more than 14 per week), and 4 or more in a single day (or average more than 7 in a week) for women. The EtOH moderate group consisted of people who reported consuming less than EtOH heavy quantities, while EtOH none reported no consumption of alcohol.

Given the study hypotheses of adverse neurocognitive effects among heavy drinkers, the EtOH none and EtOH moderate groups were pooled into a single group consisting individuals who were currently drinking below the NIAAA threshold for "at-risk" alcohol consumption (EtOH low). About 31.8% (n = 21, 8 women) were heavy alcohol consumers compared to 68.2% (n = 45, 27 women) who were not. There were no significant differences by EtOH level

or age between EtOH none ($n = 11$) versus moderate ($n = 34$) participants on any cognitive domain examined, $F(1, 45) < 1.4$, $ps > 0.05$. Age and years of education were not significantly different between the EtOH heavy and EtOH low-risk groups ($ps > 0.05$). There was not a significant difference in racial composition between EtOH groups ($p > 0.05$). There were a greater percentage of women in the EtOH low group ($p > 0.05$, addressed below in the statistical section). Demographic characteristics by EtOH grouping are presented in Table 1.

Drug and Alcohol Dependence. No participants were currently using cocaine or opiates based on self-report and urinalysis, and no participants met criteria for current cocaine or opiate dependence based on the Kreek–McHugh–Schluger–Kellogg scale (KMSK scale; Kellogg et al., 2003). KMSK scale was also used to assess lifetime history of alcohol dependence. The KMSK quantifies self-reported exposure to opiates, cocaine, alcohol, and/or tobacco. Each section of the KMSK scale assesses the frequency, amount, and duration of use of a substance during the person's period of highest consumption. The scale also assesses the mode of use, whether the substance use is current or past, and whether each substance is the substance of choice. Six participants were excluded from alcohol dependence analyses because of incomplete KMSK scores. Thirteen women ($n = 32$, 53.3%) of the sample ($n = 60$) had a history of alcohol dependence, while 46.7% ($n = 28$, 18 women) did not have a lifetime history of alcohol dependence. About 21.6% ($n = 13$) of participants with past history of alcohol dependence were currently alcohol dependent. Thus, 13 of 32 persons with current alcohol dependence overlapped with the total number of people with a lifetime history. Age was not significantly different between lifetime alcohol dependence groups ($p > 0.05$), but education and sex were significantly different ($ps < 0.05$; addressed below in Statistical Analyses). There was not a significant difference in racial composition between dependence groups ($p > 0.05$). Demographic characteristics by lifetime alcohol dependence grouping are presented in Table 1. It is important to note that lifetime alcohol dependence was assessed based on positive or negative history of alcohol dependence, not a quantification of amount of alcohol consumed over the lifetime.

Neurocognitive Assessment. All participants completed a battery of standardized neuropsychological tests widely used in past studies by our group and others to assess the following cognitive domains: speed of information processing, attention/executive functioning, learning, recall memory, verbal fluency, and psychomotor speed. The battery was comprised of the following tests chosen for their sensitivity to HIV-associated neurocognitive deficit: Hopkins Verbal Learning Test—Revised (HVLT-R; verbal learning and memory; Benedict et al., 1998; Brandt and Benedict, 1991); Brief Visuospatial Memory Test—Revised (BVMT-R; visuospatial learning and memory; Benedict, 1997); Controlled Oral Word Association Test (COWAT–FAS; verbal fluency [Benton et al., 1994]; category fluency [animals; categorical verbal fluency]); Stroop Color and Word Test (attention/executive function; Golden, 1978); Trails Making Test, Parts A and B (executive function; Reitan, 1992); Letter–Number Sequencing (working memory) from the Wechsler Adult Intelligence Scale—Third Edition (WAIS-III; Wechsler, 1997); Grooved Pegboard Test (fine motor speed; Kløve, 1963); and the Digit Symbol–Coding and Symbol Search (speed of processing measures) tests from the WAIS-III (Wechsler, 1997). *T*-scores from delayed recall on the HVLT-R and BVMT-R were averaged to calculate the delayed recall domain. Learning trial performance (*T*-scores) on these 2 tasks was averaged to create the learning domain. COWAT and animal naming *T*-scores were averaged for the verbal fluency domain. Stroop, Letter–Number Sequencing, and Trails A and B *T*-scores were averaged to compute the attention/working memory/executive functioning domain. Digit Symbol–Coding and Symbol Search were averaged to calculate the speed of processing domain. The Grooved Pegboard Test *T*-score was used for the psychomotor speed domain.

Demographically (age, education, gender, race) corrected *T*-scores were calculated using established norms. A global index of neurocognitive function was calculated by averaging all domain composite *T*-scores.

Table 1. Sample Demographics by Ethanol (EtOH) and Lifetime Alcohol Dependence History Groupings

	EtOH group	Mean	Std. dev.	Range
Age	EtOH– ($n = 45$)	39.82	12.21	21 to 69
	EtOH+ ($n = 21$)	35.38	10.20	22 to 54
	Dependence– ($n = 28$)	38.57	13.82	21 to 69
	Dependence+ ($n = 32$)	38.84	9.87	22 to 56
Education	EtOH– (w = 27)	13.84	2.80	8 to 20
	EtOH+ (w = 8)	13.05	2.94	7 to 18
	Dependence–* (w = 18)	14.61	2.47	11 to 20
	Dependence+* (w = 13)	12.53	2.92	7 to 18

EtOH+ = heavy EtOH consumption; EtOH– = nonheavy EtOH consumption; Dependence– = no history of alcohol dependence; Dependence+ = history of alcohol dependence; *n* = sample size, w = women.
*$p < 0.05$.

Statistical Analyses

Statistical analyses were performed using SPSS-22 software (IBM, Armonk, NY). Demographic and clinical characteristics of the overall sample were determined, and differences in these characteristics among the EtOH low and EtOH high groups examined using independent *t*-tests and χ^2. Differences in neurocognitive performance as a function of alcohol grouping or lifetime alcohol dependence groups and age were examined using general linear modeling. The primary analyses consisted of 2-way analyses of variance (ANOVAs) (e.g., EtOH × age or dependence × age), in which the dependent measure was each of the domain scores and the global index. Age was dichotomized based on the median of the sample (median = 39 years) such that adults 40 years or older were compared to adults younger than 40 years. As age was corrected for using *T*-scores in the dependent measures, age was included in the models to specifically assess for abnormal change in the normal trajectory of age-related neurocognitive decline. Thus, the presence of an age effect denotes exacerbation of normal age-related decline in neurocognitive function. Interactions and simple effects were examined based on the results of the overall ANOVAs. Both EtOH groupings and lifetime dependence groupings had significant differences in the distribution of sex. Analyses including sex as a factor in each of the 2-way ANOVAs failed to show any significant interactions or main effects of sex on cognitive measures ($ps > 0.05$). Thus, sex was not included in the models presented below. Tables 2 and 3 provide mean values in *T*-scores used for analyses. Except for Fig. 1, *T*-scores were transformed into *z*-score format for ease of interpretation. Figure 1 depicts performance per domain by *T*-scores.

RESULTS

Current Alcohol Consumption

Descriptive statistics for EtOH high and low groups by age group are provided in Table 2 (*T*-scores) and 3 (raw scores). The interactions of age by EtOH for global cognitive performance, learning, memory, and motor function are shown in Fig. 2.

Table 2. Cognitive Performance by Ethanol (EtOH) and Age Groups (*T*-scores)

Domain score	EtOH group	Age group	Mean	Std. error	95% Confidence interval Lower bound	95% Confidence interval Upper bound
Global cognition*	EtOH–	Younger	48.274	1.644	44.987	51.560
		Older	51.616	1.681	48.255	54.976
	EtOH+	Younger	51.666	2.107	47.453	55.878
		Older	45.489	2.980	39.532	51.446
Speed of processing	EtOH–	Younger	52.551	1.887	48.779	56.322
		Older	54.227	1.929	50.371	58.083
	EtOH+	Younger	54.381	2.418	49.547	59.215
		Older	48.643	3.420	41.807	55.479
Attention/ executive	EtOH–	Younger	53.841	1.755	50.333	57.348
		Older	54.227	1.794	50.641	57.814
	EtOH+	Younger	54.381	2.249	49.885	58.877
		Older	49.714	3.181	43.356	56.073
Learning*	EtOH–	Younger	39.030	2.456	34.120	43.940
		Older	44.545	2.511	39.524	49.565
	EtOH+	Younger	45.417	3.148	39.123	51.710
		Older	34.662	4.452	25.762	43.562
Memory*	EtOH–	Younger	38.762	2.632	33.501	44.024
		Older	47.720	2.691	42.341	53.100
	EtOH+	Younger	45.072	3.374	38.328	51.816
		Older	38.097	4.771	28.560	47.634
Verbal	EtOH–	Younger	52.391	2.087	48.220	56.563
		Older	55.932	2.134	51.667	60.197
	EtOH+	Younger	54.571	2.675	49.225	59.918
		Older	55.500	3.783	47.938	63.062
Motor*	EtOH–	Younger	48.217	2.292	43.635	52.800
		Older	50.432	2.344	45.747	55.117
	EtOH+	Younger	53.857	2.938	47.984	59.730
		Older	43.643	4.155	35.337	51.949

EtOH+ = heavy EtOH consumption; EtOH– = nonheavy EtOH consumption; Std. = standard; Younger = years of age < 40 years; Older = years of age ≥ 40 years; Age range of sample = 21 to 69 years.
*Significant age × EtOH interaction at $p < 0.05$.

Global Cognitive Function. A significant age by EtOH interaction was found for global cognitive function, $F(1, 62) = 4.80$, $p < 0.05$, partial eta squared = 0.07. Overall cognitive performance varied as a function of level of alcohol consumption and age. Tests of simple effects revealed a significant effect of age on cognitive performance for the EtOH high group ($p < 0.05$). Heavy drinkers 40 years and older had lower global cognitive scores than younger heavy drinkers (Fig. 2). There was not an age effect on cognitive performance for the EtOH low group. Tests of simple effects conducted to examine EtOH high and EtOH low groups further demonstrate this relationship between age and alcohol use. Cognitive performance did not vary as a function of level of alcohol consumption for participants under the age of 40 years. In contrast, cognitive performance differed between the EtOH high and EtOH low groups for participants 40 years and older, with heavy drinkers showing lower cognitive scores ($p < 0.05$; Fig. 2*A*).

Learning and Memory. A significant age by EtOH interaction was found for composite learning performance, $F(1, 62) = 6.30$, $p < 0.05$, partial eta squared = 0.09 (Fig. 2*B*). Tests of simple effects revealed that among people in the EtOH high group, a significant age effect existed ($p < 0.05$). Heavy drinkers 40 years and older had lower learning scores than younger heavy drinkers. Age group effects were not evident for the EtOH low group. Tests of simple effects conducted to compare EtOH high and EtOH low separately for the young and older age groups indicated similar effects. Among young drinkers, EtOH high and EtOH low did not differ significantly, whereas a significant EtOH effect existed among the older drinkers, with lower learning scores for the EtOH high group ($p < 0.05$).

A significant age by EtOH interaction was also found for composite memory performance, $F(1, 62) = 5.25$, $p < 0.05$, partial eta squared = 0.08. Heavy drinkers 40 years and older had lower memory recall score than younger heavy drinkers. An age effect was not evident for the EtOH low group. Tests of simple effects conducted to compare EtOH high and EtOH low separately for the young and older age groups indicated similar effects. Among young drinkers, EtOH high and EtOH low did not differ significantly, whereas a significant EtOH effect existed among the older drinkers with lower memory scores for EtOH high group ($p < 0.05$). The interaction of age by EtOH for learning and memory is shown in Figs 2*B,C*.

Motor Function

A significant age by EtOH interaction was also found for motor function, $F(1, 62) = 4.2$, $p < 0.05$, partial eta squared = 0.06 (Fig. 2*D*). Tests of simple effects comparing EtOH high and EtOH low separately indicated that differences between the age groups existed for the EtOH high group ($p < 0.05$), but not the EtOH low group. For the EtOH high group, older heavy drinkers had poorer fine motor function than younger heavy drinkers, whereas young and older adults in the EtOH low group did not differ in their motor function.

Other Cognitive Functions

There were not interactions of age by EtOH for the verbal, speed of processing, or attention/executive domains, $F(1, 62) < 2.2$, $ps > 0.05$. Accordingly for these cognitive domains, performance did not differ among young and older participates based on their level of current alcohol consumption. There were also not significant main effects for age or EtOH with respect to these cognitive domains, $F(1, 62) < 0.8$, $ps > 0.05$.

Alcohol Dependence

In subsequent analyses, the influence of lifetime alcohol dependence history was analyzed to determine whether dependence was also associated with reduced cognitive performance. Unlike current heavy alcohol use, lifetime history of alcohol dependence did not interact with age to adversely affect cognitive performance, $F(1, 60) < 1.5$, $ps > 0.22$).

Table 3. Cognitive Performance by Ethanol (EtOH) and Age Groups (Raw Scores)

Test name	EtOH group	Age group	Mean	Std. error	Test name	EtOH group	Age group	Mean	Std. error
HVLT-R Learning	EtOH–	Younger	23.65	1.23	Trails A (seconds)	EtOH–	Younger	28.04	1.84
		Older	23.91	0.93			Older	29.41	1.75
	EtOH+	Younger	25.50	1.48		EtOH+	Younger	28.00	2.39
		Older	18.86	1.72			Older	36.86	1.96
HVLT-R Delayed	EtOH–	Younger	7.91	0.59	Trails B (seconds)	EtOH–	Younger	64.83	5.33
		Older	9.00	0.44			Older	81.45	10.31
	EtOH+	Younger	8.93	0.69		EtOH+	Younger	82.79	15.42
		Older	7.00	0.78			Older	81.14	6.39
BVMT-R Learning	EtOH–	Younger	22.30	1.57	Letter Number Sequencing	EtOH–	Younger	10.74	0.74
		Older	23.41	1.24			Older	10.23	0.71
	EtOH+	Younger	26.14	1.81		EtOH+	Younger	11.64	0.85
		Older	20.43	2.74			Older	9.43	1.08
BVMT-R Delayed	EtOH–	Younger	8.61	0.57	Grooved Pegboard (D, seconds)	EtOH–	Younger	71.17	4.39
		Older	9.27	0.51			Older	74.14	2.65
	EtOH+	Younger	9.86	0.74		EtOH+	Younger	63.57	4.38
		Older	7.71	1.12			Older	84.71	4.68
COWAT	EtOH–	Younger	37.43	2.55	Grooved Pegboard (ND, seconds)	EtOH–	Younger	76.68	3.51
		Older	40.86	2.98			Older	79.36	3.79
	EtOH+	Younger	40.86	3.14		EtOH+	Younger	75.00	6.05
		Older	37.29	4.05			Older	100.29	5.65
Animal Naming	EtOH–	Younger	21.96	1.51	Digit Symbol–Coding	EtOH–	Younger	71.26	4.25
		Older	21.00	0.95			Older	66.55	3.82
	EtOH+	Younger	22.69	1.72		EtOH+	Younger	77.21	4.41
		Older	19.71	1.97			Older	63.00	4.28
Stroop Color and Word Test	EtOH–	Younger	83.48	1.61	Symbol Search	EtOH–	Younger	38.87	2.02
		Older	38.00	2.28			Older	32.55	1.57
	EtOH+	Younger	43.50	2.82		EtOH+	Younger	39.36	3.20
		Older	32.14	0.80			Older	28.71	1.88

HVLT-R = Hopkins Verbal Learning Test—Revised; BVMT-R = Brief Visual Memory Test—Revised; COWAT = Controlled Oral Word Association Test; D = dominant; ND = nondominant; EtOH+ = heavy EtOH consumption; EtOH– = nonheavy EtOH consumption; Std. = standard; Younger = years of age < 40 years; Older = years of age ≥ 40 years; Age range of sample = 21 to 69 years.

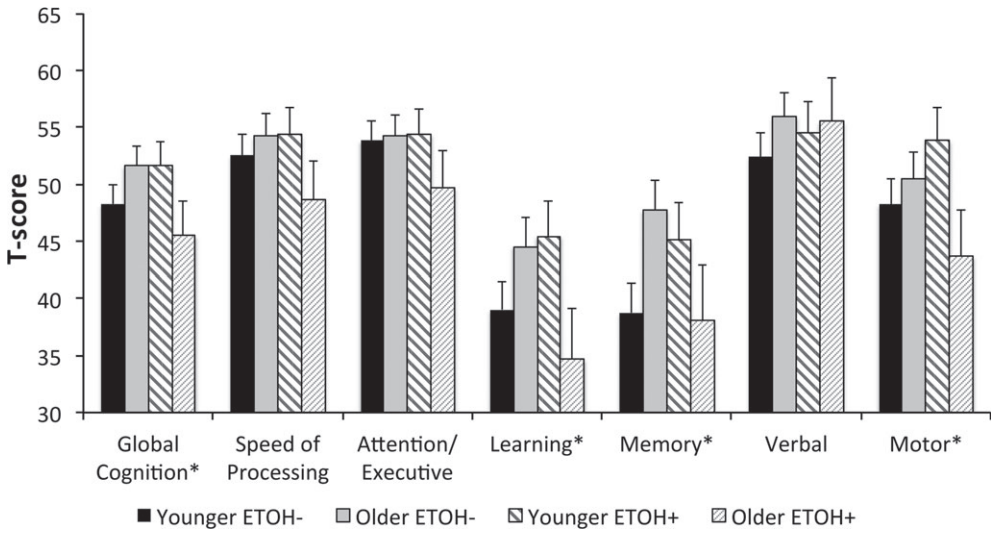

Fig. 1. Cognitive performance by ethanol (EtOH) and age groups. *T*-score data are presented with standard error bars for each age and EtOH group. Although visually different, younger EtOH– and younger EtOH+ were not significantly different on learning and memory domains, *F*s < 2.1, *p*s > 0.15.

There was also not a main effect of age, $F(1, 60) < 1.5$, ps > 0.22. In contrast, the main effect of alcohol dependence was significant for global cognitive function, $F(1, 60) = 7.35$, $p = 0.001$, partial eta squared = 0.017 (Fig. 3*A*), learning, $F(1, 60) = 7.35$, $p = 0.001$, partial eta squared = 0.22 (Fig. 3*B*), memory, $F(1, 60) = 7.35$, $p = 0.001$, partial eta squared = 0.32 (Fig. 3*C*), motor function, $F(1, 60) = 7.35$, $p = 0.001$, partial eta squared = 0.12 (Fig. 3*D*), and attention/executive function, $F(1, 60) = 7.35$, $p = 0.001$, partial eta squared = 0.08 (Fig. 3*E*), with cognitive performance lower in people with a history of lifetime alcohol dependence (ps < 0.05; Table 4). Lifetime alcohol

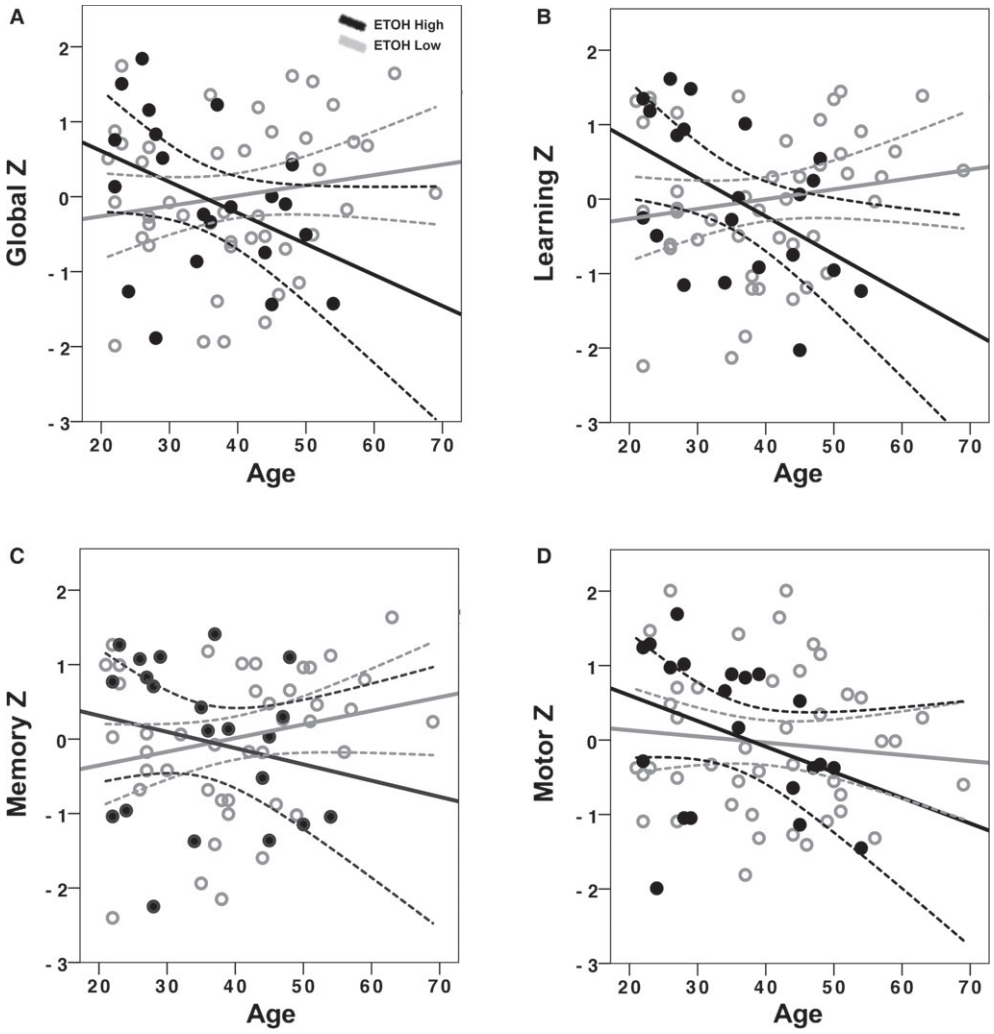

Fig. 2. Effects of age and current alcohol consumption on neurocognitive domains. *T*-scores were converted to *z*-scores for ease of interpretation. (**A**) Global cognitive function, (**B**) Learning, (**C**) Memory, (**D**) Motor. Ethanol (EtOH) high = heavy alcohol consumption, EtOH low: none/moderate alcohol consumption. Dashed lines represent 95% confidence limits.

dependence did not significantly affect verbal or speed of processing ($ps > 0.05$).

DISCUSSION

The results of this study indicate an interaction between quantity of current alcohol consumption and age with respect to global cognitive performance, as well as performance in the cognitive domains of learning, memory, and motor function. Current heavy drinkers who, by definition, consumed more alcohol on a weekly basis than the NIAAA threshold for "high-risk" drinking (EtOH high) exhibited greater cognitive deficits as a function of age compared to younger current heavy drinkers and compared to adults who were current nonheavy drinkers or abstainers (EtOH low). There was not an age association with cognitive performance for the EtOH low group. Adults who were not currently heavy drinkers tended to have average cognitive performance, relative to demographically corrected normative values. The fact that people who did not drink alcohol at all did not differ significantly from people who consumed minimal to moderate quantities on any cognitive domain supports our original hypothesis that adverse cognitive effects would primarily be observed among current heavy drinkers.

That neurocognitive performance did not vary as a function of age in the EtOH low group is perhaps not surprising given that the mean age of the study cohort was only 39 years, with no participants over the age of 65. Age-associated cognitive decrements are not expected among healthy adults during midlife and are usually minimal until the seventh decade of life. The absence of aging associations in the EtOH low group, after normative correction for age, education, and socioeconomic status, demonstrates that neither abstaining from alcohol nor nonheavy drinking altered the normal trajectory of cognitive aging. The observed age findings among heavy drinkers are more the anomaly, suggesting that people who consume large quantities of alcohol may be prone to premature cognitive aging.

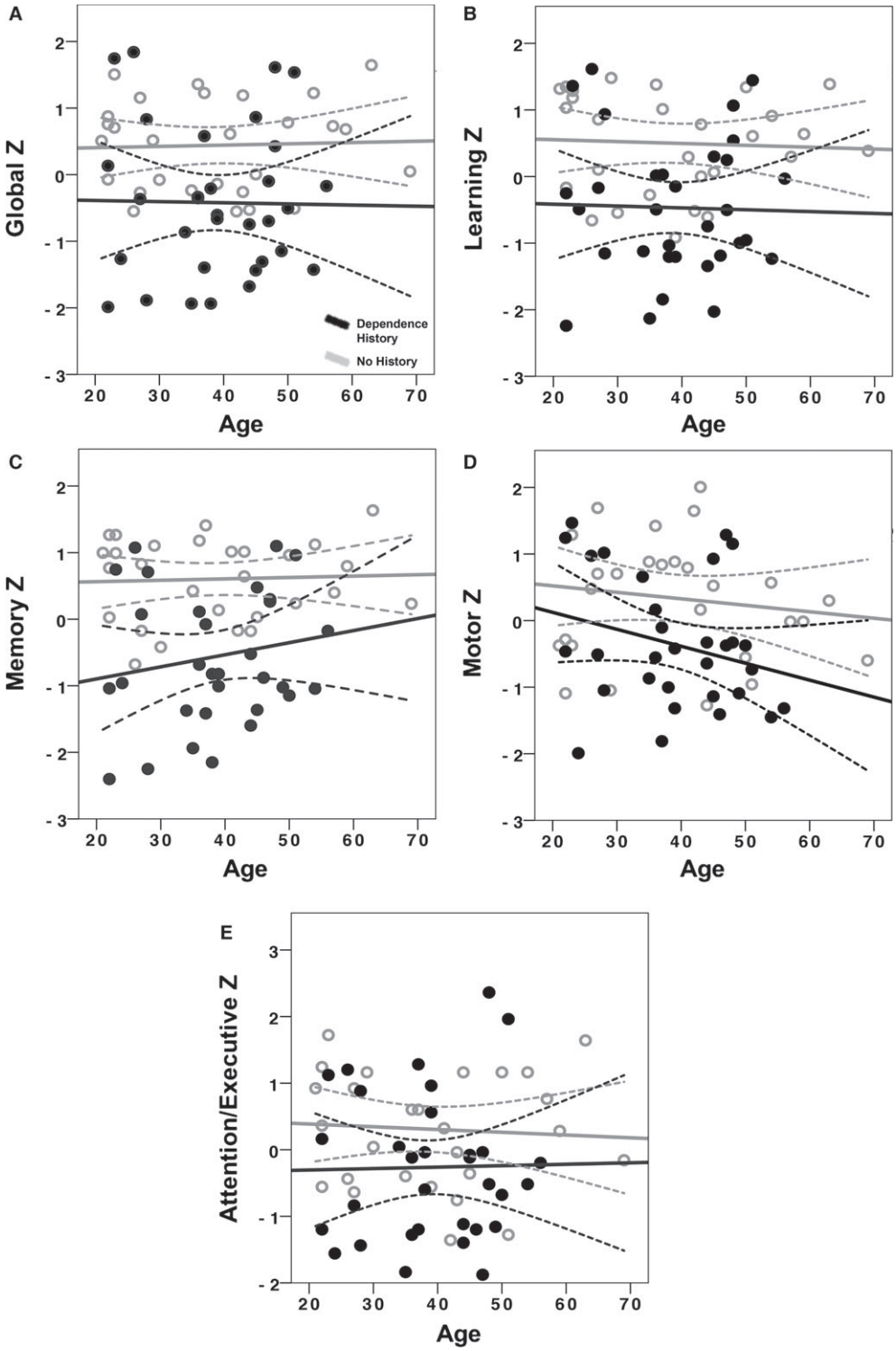

Fig. 3. Effects of lifetime history of alcohol dependence on neurocognitive domains. *T*-scores were converted to *z*-scores for ease of interpretation. (**A**) Global cognitive function, (**B**) Learning, (**C**) Memory, (**D**) Motor, (**E**) Attention/executive function. Dependence history = lifetime alcohol dependence history. Dashed lines represent 95% confidence limits.

Neurocognitive deficits in older current heavy drinking were not universal. Specifically, older current heavy drinkers had significantly lower performance on tasks related to learning, memory, and motor function. In contrast, attention/executive functions, verbal fluency, and speed of processing did not differ as a function of age and current alcohol consumption. In terms of motor function, the measure used in the current study was designed to assess psychomotor speed

Table 4. Cognitive Performance by Lifetime Alcohol Dependence History (*T*-scores)

Composite cognitive measure	EtOH DH	Mean	Std. error	95% Confidence interval Lower bound	Upper bound
Global cognition*	None	53.313	1.463	50.382	56.243
	DH	46.522	1.376	43.766	49.278
Speed of processing	None	54.244	1.799	50.640	57.847
	DH	51.990	1.692	48.601	55.379
Attention/executive*	None	56.163	1.597	52.964	59.362
	DH	51.390	1.502	48.382	54.399
Learning*	None	47.753	2.131	43.484	52.022
	DH	36.216	2.004	32.202	40.231
Memory*	None	50.849	2.103	46.636	55.063
	DH	36.226	1.978	32.263	40.188
Verbal	None	55.754	1.929	51.889	59.619
	DH	52.855	1.814	49.221	56.490
Motor*	None	53.359	2.016	49.319	57.398
	DH	45.629	1.896	41.830	49.428

EtOH DH = alcohol dependence history; DH = lifetime alcohol dependence history; None = no dependence history; Std. = standard.
*Main effect of lifetime alcohol dependence history at $p < 0.05$.

in a fine motor control task. Learning and memory composite scores were calculated using both visual and verbal learning and memory indices. These functionally specific results may provide insight into candidate neural structures for future investigations into the neural correlates of our findings, such as hippocampus, cerebellum, and primary and supplementary motor association cortices. As the functions of these brain regions are impacted acutely during heavy alcohol consumption (e.g., blackouts, loss of coordination, etc.), our data may suggest that these acute effects are more lasting in consequence.

In contrast to findings for current heavy alcohol consumption, lifetime history of alcohol dependence did not interact with age. Rather, neurocognitive deficits were evident in persons with a history of alcohol dependence irrespective of age. Global cognitive performance with specific deficits in learning, memory, motor function, and attention/executive function was associated with lifetime history of alcohol dependence. While neurocognitive effects of current heavy alcohol consumption appear to be exacerbated by age, long-term decline in cognitive function from lifetime history of alcohol dependence does not. Regardless, the same functions affected by current heavy consumption of alcohol were also affected in those with a lifetime history of alcohol consumption, in addition to attention/executive function. As with current heavy alcohol consumption, neurocognitive effects were not universal, with no evidence of change in speed of processing or verbal fluency. The consistency between current and lifetime history, as well as anecdotal reports of acute effects of heavy alcohol consumption, suggests that these patterns represent a consistent cascade of short- and long-term consequences from heavy alcohol consumption.

Our current findings provide evidence that the adverse effects of alcohol use on neurocognitive function may interact with both age and quantity of alcohol consumed. Heavy alcohol consumption appears to have adverse cognitive effects, whereas drinking minimal to moderate amounts of alcohol does not produce these associations, even in older adults. The fact that heavy alcohol effects on cognition were associated with age in a cohort that was less than 70 years of age suggests that very advanced age is not a prerequisite for these adverse effects and that susceptibility may increase dramatically during midlife. Evidence for greater compromise of neurocognitive function in older adults with current heavy alcohol consumption may have significant implications for personal and public health, as these individuals are likely more susceptible to decline in driving performance, increased rates of injury, hospitalization and dependence on assisted living, poorer medical outcomes, increased mortality rates, and other factors commonly associated with cognitive decline in older adults (Woods et al., 2011, 2013). Evidence for long-term consequences of alcohol dependence is also potentially important. These data suggest that those with a lifetime history of alcohol dependence may suffer deleterious effects that compromise neurocognitive function throughout life, not merely during acute periods of heavy alcohol consumption. However, the alternative is also possible and cannot be discounted in the current study. That is to say, premorbid deficits in neurocognitive function may predispose people toward alcohol abuse and dependence. It is also important to note that these findings are specifically relevant to the presence or absence of lifetime history of alcohol dependence, not a direct quantification of the amount of alcohol consumed over the lifetime. Such data may be important for further exploring these effects.

Furthermore, prior studies found mixed results when investigating the consequences of heavy alcohol consumption on neurocognitive function. Our results provide evidence supporting recent studies on the interaction of age and heavy alcohol consumption and extend our understanding of their neurocognitive consequences. This study provides strong evidence that heavy alcohol consumption has both short- and long-term consequences for neurocognitive function and that these consequences increase with advancing age. Furthermore, our data suggest that heavy alcohol consumption is associated with accelerated cognitive aging.

Limitations and Future Directions

The population of noninfected but at-risk persons recruited from a larger EtOH-focused study on HIV may represent a significant sampling bias that could exaggerate the impact of EtOH on cognitive function. However, these data also represent realistic insight into a population with high rates of EtOH abuse and thus are, at the very least, representative of similar populations. Use of normative data between groups to assess age effects over different test measures might be viewed as a limitation versus a matched sample control across groups. Future study of persons not at risk

for contracting HIV and HCV will help to support the applicability of these data to the population at large. In addition, longitudinal studies would allow for better understanding of the long-term consequences of these effects. Use of self-report measures of alcohol consumption and lifetime history of dependence may have introduced an extra degree of variability over objective measurement. However, such objective measures are often impossible, especially when assessing past alcohol consumption. These self-report measures may actually underestimate the level of current consumption and presence of past dependence. While this study demonstrates the neurocognitive consequences of heavy alcohol consumption, the structural, metabolic, and functional brain changes underlying long-term consequences of heavy alcohol consumption remain unclear. Furthermore, the causal direction of the relationship between neurocognitive function and alcohol abuse–dependence requires further study. As such, future studies are needed to characterize the relationship between alcohol-associated cognitive impairments versus cognitive deficit-associated increase in alcohol consumption, metabolic and functional brain abnormalities that can be assessed using neuroimaging and other methods, and the amount of recovery of function versus persistent brain dysfunction that is likely to occur with reduced alcohol consumption as people age.

FUNDING

The research was supported in part by the NIAAA P01AA019072, P30 AG028740, KL2TR001429, the McKnight Brain Research Foundation, and the UF Center for Cognitive Aging and Memory. The authors have no conflicts of interest to report.

REFERENCES

Alexander S, Kerr ME, Yonas H, Marion DW (2004) The effects of admission alcohol level on cerebral blood flow and outcomes after severe traumatic brain injury. J Neurotrauma 21:575–583.

Benedict RHB (1997) Brief Visuospatial Memory Test-Revised. Psychological Assessment Resources, Odessa, FL.

Benedict RHB, Schretlen D, Groninger L, Brandt J (1998) Hopkins verbal learning test – revised: normative data and analysis of inter-form and test-retest reliability. Clin Neuropsychol 12:43–55.

Benton AL, Hamsher K, Sivan AB (1994) Multilingual Aphasia Examination. AJA Associates, Iowa City.

Brandt J, Benedict RHB (1991) Hopkins Verbal Learning Test-Revised (HVLT-R). Psychological Assessment Resources Inc., Lutz, FL.

Carey CL, Woods SP, Gonzalez R, Conover E, Marcotte TD, Grant I, Heaton RK, Group H (2004a) Predictive validity of global deficit scores in detecting neuropsychological impairment in HIV infection. J Clin Exp Neuropsychol 26:307–319.

Carey CL, Woods SP, Rippeth JD, Gonzalez R, Moore DJ, Marcotte TD, Grant I, Heaton RK, Group H (2004b) Initial validation of a screening battery for the detection of HIV-associated cognitive impairment. Clin Neuropsychol 18:234–248.

Downer B, Jiang Y, Zanjani F, Fardo D (2015) Effects of alcohol consumption on cognition and regional brain volumes among older adults. Am J Alzheimers Dis Other Demen 30:364–374.

Drake AI, Butters N, Shear PK, Smith TL, Bondi M, Irwin M, Schuckit MA (1995) Cognitive recovery with abstinence and its relationship to family history for alcoholism. J Stud Alcohol 56:104–109.

Draper B, Karmel R, Gibson D, Peut A, Anderson P (2011) Alcohol-related cognitive impairment in New South Wales hospital patients aged 50 years and over. Aust New Zealand J Psychiat 45:985–992.

Durazzo TC, Pennington DL, Schmidt TP, Mon A, Abe C, Meyerhoff DJ (2013) Neurocognition in 1-month-abstinent treatment-seeking alcohol-dependent individuals: interactive effects of age and chronic cigarette smoking. Alcohol Clin Exp Res 37:1794–1803.

Fals-Stewart W, O'Farrell TJ, Freitas TT, McFarlin SK, Rutigliano P (2000) The timeline follow-back reports of psychoactive substance use by drug-abusing patients: psychometric properties. J Consult Clin Psych 68:134–144.

Friend KB, Malloy PF, Sindelar HA (2005) The effects of chronic nicotine and alcohol use on neurocognitive function. Addict Behav 30:193–202.

Goldberg RJ, Burchfiel CM, Reed DM, Wergowske G, Chiu D (1994) A prospective study of the health effects of alcohol consumption in middle-aged and elderly men. The Honolulu Heart Program. Circulation 89:651–659.

Golden CJ (1978) Stroop Color and Word Test. Stoelting, Chicago.

Green A, Garrick T, Sheedy D, Blake H, Shores EA, Harper C (2010) The effect of moderate to heavy alcohol consumption on neurpopscyhological performance as measured by the repeatable battery for the assessment of neuropsychological status. Alcohol Clin Exp Res 34:442–450.

Haorah J, Knipe B, Leibhart J, Ghorpade A, Persidsky Y (2005) Alcohol-induced oxidative stress in brain endothelial cells causes blood-brain barrier dysfunction. J Leukoc Biol 78:1223–1232.

Houston RJ, Derrick J, Leonard K, Testa M, Quigley B, Kubiak A (2014) Effects of heavy drinking on executive cognitive functioning in a community sample. Addict Behav 39:345–349.

Kellogg SH, McHugh PF, Bell K, Schluger JH, Schluger RP, LaForge KS, Ho A, Kreek MJ (2003) The Kreek-McHugh-Schluger-Kellogg scale: a new, rapid method for quantifying substance abuse and its possible applications. Drug Alcohol Depend 69:137–150.

Kist N, Sandjojo J, Kok RM, van den Berg JF (2014) Cognitive functioning in older adults with early, late, and very late onset alcohol dependence. Int Psychogeriatr 26:1863–1869.

Kløve H (1963) Grooved Pegboard. Lafeyette Instruments, Lafeyette, IN.

Marksteiner J, Bodner T, Gurka P (2002) Alcohol-induced cognitive disorder: alcohol dementia. Wien Med Wochenschr 152:98–101.

Meyer JS, Terayama Y, Konno S, Akiyama H, Margishvili GM, Mortel KF (1998) Risk factors for cerebral degenerative changes and dementia. Eur Neurol 39(Suppl 1):7–16.

Molina JA, Bermejo F, del Ser T, Jimenez-Jimenez FJ, Herranz A, Fernandez-Calle P, Ortuno B, Villanueva C, Sainz MJ (1994) Alcoholic cognitive deterioration and nutritional deficiencies. Acta Neurol Scand 89:384–390.

O'Dell KM, Hannay HJ, Biney FO, Robertson CS, Tian TS (2012) The effect of blood alcohol level and preinjury chronic alcohol use on outcome from severe traumatic brain injury in Hispanics, anglo-Caucasians, and African-Americans. J Head Trauma Rehabil 27:361–369.

Panza F, Capurso C, D'Introno A, Colacicco AM, Frisardi V, Lorusso M, Santamato A, Seripa D, Pilotto A, Scafato E, Vendemiale G, Capurso A, Solfrizzi V (2009) Alcohol drinking, cognitive functions in older age, predementia, and dementia syndromes. J Alzheimers Dis 17:7–31.

Reitan RM (1992) Trail Making Test. Reitan Neuropsychology Laboratory, Tucson, AZ.

Riege WH, Holloway JA, Kaplan DW (1981) Specific memory deficits associated with prolonged alcohol abuse. Alcohol Clin Exp Res 5:378–385.

Schuckit MA (2009) Alcohol-use disorders. Lancet 373:492–501.

Shih CL, Chi SI, Chiu TH, Sun GY, Lin TN (2001) Ethanol effects on nitric oxide production in cerebral pial cultures. Alcohol Clin Exp Res 25:612–618.

Snow WM, Murray R, Ekuma O, Tyas SL, Barnes GE (2009) Alcohol use and cardiovascular health outcomes: a comparison across age and gender in the Winnipeg Health and Drinking Survey Cohort. Age Ageing 38:206–212.

Solfrizzi V, D'Introno A, Colacicco AM, Capurso C, Del Parigi A, Baldassarre G, Scapicchio P, Scafato E, Amodio M, Capurso A, Panza F (2007) Alcohol consumption, mild cognitive impairment, and progression to dementia. Neurology 68:1790–1799.

Solomon DA, Malloy PF (1992) Alcohol, head injury, and neuropsychological function. Neuropsychol Rev 3:249–280.

Spirduso WW, Mayfield D, Grant M, Schallert T (1989) Effects of route of administration of ethanol on high-speed reaction time in young and old rats. Psychopharmacology 97:413–417.

Squeglia LM, Boissoneault J, Van Skike CE, Nixon SJ, Matthews DB (2014) Age-related effects of alcohol from adolescent, adult, and aged populations using human and animal models. Alcohol Clin Exp Res 38: 2509–2516.

Squeglia LM, Spadoni AD, Infante MA, Myers MG, Tapert SF (2009) Initiating moderate to heavy alcohol use predicts change in neuropsychological functioning for adolescent rils and boys. Psychol Addict Behav 23:715–722.

Sullivan EV, Fama R, Rosenbloom MJ, Pfefferbaum A (2002) A profile of neuropsychological deficits in alcoholic women. Neuropsychology 16:74–83.

Sullivan EV, Harris RA, Pfefferbaum A (2010) Alcohol's effects on brain and behavior. Alcohol Res Health 33:127–143.

Tyas SL (2001) Alcohol use and the risk of developing Alzheimer's disease. Alcohol Res Health 25:299–306.

Vinod KY, Hungund BL (2005) Endocannabinoid lipids and mediated system: implications for alcoholism and neuropsychiatric disorders. Life Sci 77:1569–1583.

Webb B, Heaton MB, Walker DW (1997) Ethanol effects on cultured embryonic hippocampal neuronal calcium homeostasis are altered by nerve growth factor. Alcohol Clin Exp Res 21:1643–1652.

Wechsler D (1997) Wechsler Adult Intelligence Scale-III (WAIS-III). The Psychological Corporation, San Antonio, TX.

Wilde EA, Bigler ED, Gandhi PV, Lowry CM, Blatter DD, Brooks J, Ryser DK (2004) Alcohol abuse and traumatic brain injury: quantitative magnetic resonance imaging and neuropsychological outcome. J Neurotrauma 21:137–147.

Wilhelm CJ, Hashimoto JG, Roberts ML, Bloom SH, Beard DK, Wiren KM (2015) Females uniquely vulnerable to alcohol-induced neurotoxicity show altered glucocorticoid signaling. Brain Res 1601:102–116.

Woods AJ, Cohen RA, Pahor M (2013) Cognitive frailty: frontiers and challenges. J Nut Health and Aging 17:741–743.

Woods AJ, Mark VW, Pitts AC, Mennemeier M (2011) Pervasive cognitive impairment in acute rehabilitation inpatients without brain injury. PM R 3:426–432; quiz 432.

Woods AJ, Mennemeier M, Garcia-Rill E, Huitt T, Chelette KC, McCullough G, Munn T, Brown G, Kiser TS (2012) Improvement in arousal, visual neglect, and perception of stimulus intensity following cold pressor stimulation. Neurocase 18:115–122.

frontiers in Aging Neuroscience

ORIGINAL RESEARCH
published: 08 December 2016
doi: 10.3389/fnagi.2016.00298

Cognitive Aging and the Hippocampus in Older Adults

Andrew O'Shea[1], *Ronald A. Cohen*[1], *Eric C. Porges*[1], *Nicole R. Nissim*[1,2] *and Adam J. Woods*[1,2]*

[1]*Center for Cognitive Aging and Memory, McKnight Brain Institute, Department of Clinical and Health Psychology, University of Florida, Gainesville, FL, USA,* [2]*Department of Neuroscience, University of Florida, Gainesville, FL, USA*

The hippocampus is one of the most well studied structures in the human brain. While age-related decline in hippocampal volume is well documented, most of our knowledge about hippocampal structure-function relationships was discovered in the context of neurological and neurodegenerative diseases. The relationship between cognitive aging and hippocampal structure in the absence of disease remains relatively understudied. Furthermore, the few studies that have investigated the role of the hippocampus in cognitive aging have produced contradictory results. To address these issues, we assessed 93 older adults from the general community (mean age = 71.9 ± 9.3 years) on the Montreal Cognitive Assessment (MoCA), a brief cognitive screening measure for dementia, and the NIH Toolbox-Cognitive Battery (NIHTB-CB), a computerized neurocognitive battery. High-resolution structural magnetic resonance imaging (MRI) was used to estimate hippocampal volume. Lower MoCA Total ($p = 0.01$) and NIHTB-CB Fluid Cognition ($p < 0.001$) scores were associated with decreased hippocampal volume, even while controlling for sex and years of education. Decreased hippocampal volume was significantly associated with decline in multiple NIHTB-CB subdomains, including episodic memory, working memory, processing speed and executive function. This study provides important insight into the multifaceted role of the hippocampus in cognitive aging.

Keywords: cognitive aging, hippocampus, MoCA, NIH toolbox, structural magnetic resonance imaging

OPEN ACCESS

Edited by:
Ashok Kumar,
University of Florida, USA

Reviewed by:
Michael R. Foy,
Loyola Marymount University, USA
Con Stough,
Swinburne University of Technology, Australia

***Correspondence:**
Adam J. Woods
ajwoods@ufl.phhp.edu

Received: *11 May 2016*
Accepted: *22 November 2016*
Published: *08 December 2016*

Citation:
O'Shea A, Cohen RA, Porges EC, Nissim NR and Woods AJ (2016) Cognitive Aging and the Hippocampus in Older Adults. Front. Aging Neurosci. 8:298. doi: 10.3389/fnagi.2016.00298

INTRODUCTION

From the discovery of its role in episodic memory following bilateral resection in patient "HM" to the discovery of its role in symptoms of Alzheimer's disease (AD), the hippocampus is considered a structure fundamental for human cognition (Scoville and Milner, 1957; Squire, 1992; Jack et al., 1999). In addition to its well-documented role in memory function, recent research demonstrates that the hippocampus also plays a role in executive function, processing speed, intelligence, path integration and spatial processing (Reuben et al., 2011; Papp et al., 2014; Yamamoto et al., 2014). Each of these cognitive processes is shown to decline in the context of cognitive aging, in the absence of neurodegenerative diseases or neurological injury (Salthouse, 2010). Thus, understanding how change in hippocampal structure impacts cognition in the context of aging may prove important for identifying: (a) critical neural underpinnings of the cognitive aging process; and (b) intervention targets for combating cognitive aging.

Most of our knowledge of hippocampal structure-function relationships in humans is based on the findings in various disease states or following resection of the medial temporal

lobes resulting in gross memory disturbance. Models of structure-function relationships in non-human animals have highlighted the hippocampus as a spatial map, crucial for navigation and spatial memory (O'Keefe and Dostrovsky, 1971; O'Keefe, 1979). In addition, recent functional magnetic resonance imaging (MRI) findings have provided insight into the functional role of the hippocampus in various cognitive abilities beyond episodic and spatial memory (Eldridge et al., 2000; Iaria et al., 2007; Woods et al., 2013). However, the impact of subtle changes in hippocampal structure in the context of normal aging, in the absence of neurodegenerative or other disease states, remains poorly understood.

Individuals with diagnoses of mild cognitive impairment (MCI) and dementia have smaller hippocampi than age-matched controls in numerous MRI studies (Shi et al., 2009). Hippocampal atrophy is considered a hallmark of Alzheimer's disease (AD) (Jack et al., 1999). Premorbid hippocampal volume in patients with MCI predicts future conversion to AD (Jack et al., 1999). Thus, change in the structure of the hippocampus appears to play an important role in dementia. However, hippocampal volume is also well-documented to decline in normal aging (Raz et al., 2005). Yet, the functional consequences of this age-related volumetric loss is not well characterized in the context of aging in the absence of neurodegenerative disease. While changes in cognitive scores on dementia screening and cognitive assessment measures in patients with MCI and AD are associated with smaller hippocampal volume, it is unclear whether these findings are unique to dementia/disease states or extend to more subtle variations in hippocampal structure from normal aging.

The few studies that have investigated cognitive aging and the hippocampus have produced results that contrast significantly with prior research in neurological and neurodegenerative disease (Van Petten, 2004; Paul et al., 2011; Colom et al., 2013). For example, Van Petten (2004), in a meta-analysis, reported that the relationship between hippocampal size and episodic memory were weak. These inconsistencies between aging and disease-related findings highlight the need for further investigation of the role of the hippocampus in cognitive aging. Understanding the relationship between hippocampal structure and function in cognitive aging may have predictive value for identifying persons at higher risk for future cognitive decline, cognitive frailty and conversion to MCI (Woods et al., 2013). The prevalence of older adults is expected to accelerate over the coming decades. With this shift in the age of the world population comes an increase in the number of people that will suffer from MCI and other neurodegenerative disorders. Thus, there is a pressing need to identify predictive markers of decline. However, pursuit of such markers is difficult, if not impossible, without first understanding the normal variation present in the aging brain, as well as the overall structure-function relationship between the hippocampus and different components of cognitive function.

In the current study, we sought to examine the relationship between hippocampal volume and a commonly administered dementia-screening tool and a comprehensive cognitive battery in a cohort of 93 older adults without neurological injury, neurodegenerative disease or major psychiatric illness to: (1) better understand the structure-function relationship between the hippocampus and cognitive aging; and (2) to providing a foundation for development of predictive biomarkers by characterizing the sensitivity of commonly administered MCI screening and cognitive assessment tools to age-related structural changes in the hippocampus. We specifically examined the relationship between the Montreal Cognitive Assessment (MoCA) and the NIH Toolbox Cognitive Battery (NIHTB-CB). The MoCA is a brief (10 min) screening tool for MCI (Nasreddine et al., 2005), whereas the NIH toolbox cognitive assessment is a brief comprehensive computerized cognitive battery (∼60 min) consisting of tests to assess executive function, attention, episodic memory, language, processing speed and working memory. These measures are sub-divided into two composite cognitive scores comprising cognitive abilities that change with age (fluid cognitive function) or remain stable over time (crystalized cognitive functions). The delineation of a two-factor model (a fluid factor and a crystalized factor) instead of a single general intelligence factor is valuable when studying cognitive aging due to differences in the age curves of fluid and crystalized abilities (Cattell, 1987). Mungas et al. (2014) found a two-factor solution fit the NIHTB-CB validation data better than a single general intelligence factor; however, the best fitting model was a five-factor solution comprised of the following: reading, vocabulary, episodic memory, working memory and executive function/processing speed. An extension of the two-factor, fluid and crystalized model, the Cattell-Horn-Carroll (CHC) theory of cognition extends the factors of general intelligence to nine broad abilities (fluid reasoning, comprehension-knowledge, short-term memory, visual processing, auditory processing, long-term storage and retrieval, cognitive processing speed, quantitative knowledge and reading and writing; McGrew, 2009). The CHC taxonomy may provide a more thorough description of individual domains of the NIHTB-CB. However, a single NIHTB-CB task would likely incorporate multiple factors of the CHC model, rather than representing distinct entities.

We hypothesized that older adults with smaller hippocampal volumes would evidence lower performance on both the MoCA and NIHTB fluid cognition scores. In contrast, language-based cognitive abilities (i.e., crystalized cognition) would not change as a function of hippocampal volume. Furthermore, we hypothesized that hippocampal volume would be most strongly associated with performance on the memory domain of the MoCA and NIHTB. In addition, we also predicted that smaller hippocampal volume would be associated with slower processing speed and poorer executive functions. These data would not only support the role of the hippocampus in cognition as shown in prior research on neurodegenerative disease and neurological disease states, but also extend these findings to cognitive aging. Furthermore, these data would provide a strong foundation for development of predictive hippocampal biomarkers for future decline in longitudinal cohorts by characterizing cognitive aging in the hippocampus

in the absence of neurological and neurodegenerative disease.

MATERIALS AND METHODS

Participants

Ninety-three older adults (60% female) were recruited from the north-central Florida community through newspaper advertising, fliers and community outreach. Participants had a mean age of 71.7 years (SD = 9.8 years) and an average of 16.26 years education (SD = 2.61, see **Table 1** for detailed demographics). All participants provided written informed consent prior to enrollment. All study procedures were approved by the University of Florida Institutional Review Board prior to the start of the study. Participants had the opportunity to ask the researchers any questions about study procedures prior to the start of the study. No vulnerable populations were studied. Exclusionary criteria included pre-existing neurological or psychiatric brain disorders, MRI contraindications (such as metal or medical devices inside the body not approved to be scanned at 3T), reported diagnosis of a neurodegenerative brain disease (i.e., dementia or Alzheimer's) or self-reported difficulty with thinking and memory.

Study Procedures

Participants completed a neuropsychological battery (see "Measures" Section for more details) that included the NIHTB-CB and MoCA. Neuropsychological tasks were administered at an onsite clinical research facility by trained study staff. The neuropsychological battery was completed as a single visit. Neuroimaging scanning was completed at a subsequent MRI visit.

Measures

NIH Toolbox

In this study, NIH Toolbox was used as a brief, comprehensive assessment to examine neurological and behavioral function, allowing for the study of functional changes across the lifespan. The cognitive domain measure was used which covered subdomains of: executive function and attention, episodic memory, language, processing speed and working memory. Executive function and attention was measured by NIH-Toolbox Flanker Inhibitory Control and Attention test and the Dimensional Change Card Sort test. Flanker measures the ability to inhibit visual attention to irrelevant task dimensions. The Dimensional Card Sort test was used to assess the set-shifting component of executive function. Working memory was tested by the List Sorting test. Episodic Memory was assessed by Picture Sequence memory test and the Auditory Verbal Learning (Rey) test. To test language, the Oral Reading Recognition test and the Picture Vocabulary test were used. Processing speed was assessed by the Pattern Comparison test and the Oral Symbol Digit test. The fluid cognition composite is composed of the following tasks: Dimensional Change Card Sort, Flanker, Picture Sequence Memory, List Sorting and Pattern Comparison. The crystalized cognition composite is composed of the Picture Vocabulary Test and the Oral Reading Recognition Test. The NIH toolbox cognitive battery has been shown to have high test-retest reliability, as well as high convergent validity with "gold standard" measures of crystalized and fluid cognition (Heaton et al., 2014).

TABLE 1 | Sample demographics.

	Mean	*SD*	*Range*
Age	71.69	9.45	43–85
Education	16.26	2.61	12–20
Sex distribution			
	Number	*% of sample*	
Male	37	40	
Female	56	60	

MoCA

The MoCA is a 10-min, 30-point clinical assessment of multiple cognitive functions, including orientation (6 points), attention (6 points), short-term memory recall (5 points), abstract thinking (2 points), visuospatial executive function assessed by a clock-drawing task, trails task and reproducing a geometrical figure (5 points), naming task (3 points) and language function assessed by verbal fluency test (3 points). An additional one point was added for subjects with less than/equal to 12 years in education (per guidelines of MoCA administration (Nasreddine et al., 2005)). The suggested cut-off point on the MoCA is below 26 for MCI.

Neuroimaging Acquisition

All participants were imaged in a Philips 3.0 Tesla (3T) scanner (Achieva; Philips Electronics, Amsterdam, Netherlands) at the McKnight Brain Institute (University of Florida, Gainesville, FL, USA) with a 32-channel receive-only head coil. A pillow was placed under the head to limit motion during the scan. A high-resolution 3D T1 weighted MPRAGE scan was performed. Scanning parameters consisted of: voxel size = 1 mm isotropic; 1 mm slice thickness; TE = 3.2 ms; TR = 7.0 ms; FOV = 240 × 240; Number of slices = 170; acquired in a sagittal orientation.

Neuroimaging Processing

T_1-weighted MRI scans were processed with the software FreeSurfer version 5.3. To measure hippocampal volume, the automated subcortical segmentation stream in FreeSurfer was used. The software uses Bayesian inference methods relying on prior anatomical probabilities in a labeled data set, along with *a priori* known T_1 intensity characteristics of subcortical regions, as well as T_1 intensity information from the scan being processed, in order to label discrete regions (Fischl et al., 2002). Previous research has shown this automated procedure produces accurate and reliable results, while taking a fraction of the time of the gold standard of manual segmentation (Fischl et al., 2002;

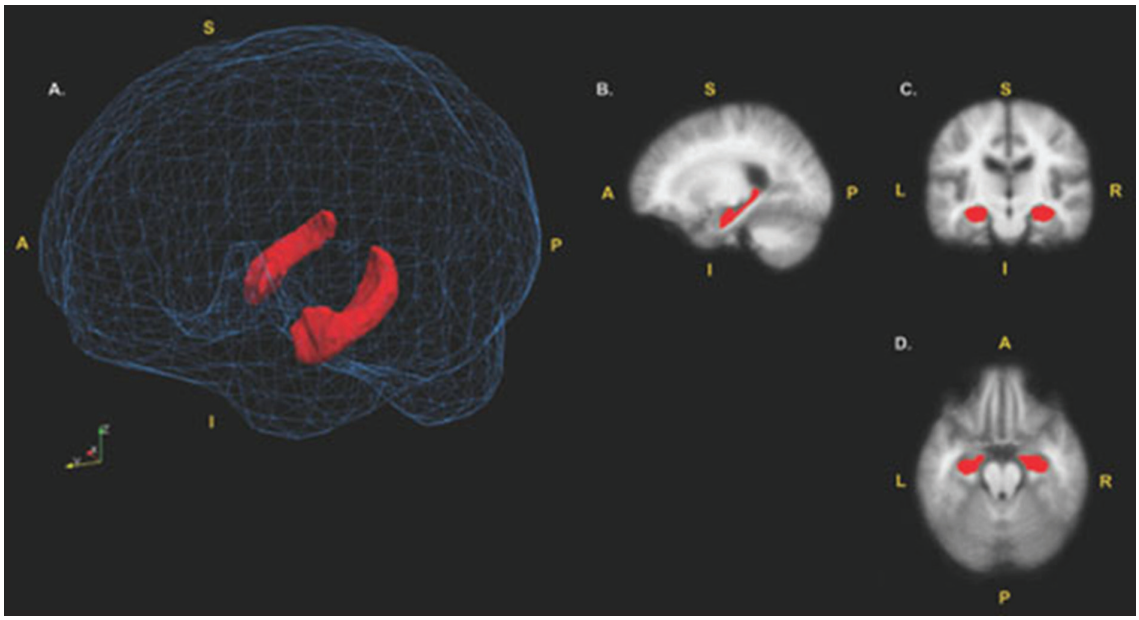

FIGURE 1 | Hippocampal region of interest (ROI). (A) surface models of the left and right hippocampi ROIs displayed in red. The hippocampi are visualized inside a wireframe mesh provided by Madan (2015). **(B)** Sagittal view (x = 105), **(C)** coronal view (z = 110) and **(D)** axial view (y = 151) of the hippocampi displayed in red. Coordinates are in MNI305 space. A, Anterior; P, Posterior; I, Inferior; S, Superior.

Jovicich et al., 2009). This makes automated segmentation well suited for large samples. Any errors in segmentation were fixed manually, and were re-processed through FreeSurfer, producing results that have been validated against manual segmentation (Morey et al., 2009) and histological measures (Cardinale et al., 2014). Whole hippocampal volume was computed as a sum of left and right hemisphere measures; this measure was then normalized in respect to total intracranial volume. All subsequent uses of the term "hippocampal volume" refer to the normalized value. See **Figure 1** for a visual depiction of the hippocampal region of interest (ROI; mesh provided by Madan, 2015).

Statistical Analyses

Neuroimaging data was analyzed using a ROI approach predicting hippocampal volume. MoCA and NIHTB-CB composite scores were used as predictor variables. Descriptive statistics and inter-measure correlations can be found in **Tables 2**, **3**. Hippocampal volume was normalized using estimated total intracranial volume, to control for differences in head size. Covariates of sex and education years were included in all models. A secondary set of analyses was aimed at examining the sub-scales of MoCA and NIH toolbox fluid cognition composite to determine whether a sub-scale was driving the relationship in the total score. Due to the characteristics of MoCA, certain sub-scales did not lend themselves to further analyses. Naming, Language, Abstraction and Orientation sections were excluded due to a restriction of range in observation (i.e., a 1 point scale) and/or a lack of variability. Two subjects were excluded as outliers because they had values greater than 2.5 the standard deviation from the mean (1 hippocampal volume outlier; 1 crystallized cognition outlier).

TABLE 2 | Descriptive statistics.

Measure	*Mean*	*SD*	*Range*
NIH Toolbox crystalized cognition	127.54	11.05	100–154
NIH Toolbox fluid cognition	96.21	9.72	80–133
MoCA	25.74	2.53	20–30

SD, Standard Deviation.

TABLE 3 | Correlation matrix.

	MoCA	Crystal	Fluid
MoCA	1	0.37**	0.42**
Crystal	0.37**	1	0.28**
Fluid	0.42**	0.28**	1

Crystal, NIH Toolbox crystallized cognition; Fluid, NIH Toolbox fluid cognition. $^{**}p < 0.01$.

RESULTS

NIH Toolbox

Relationship Between NIH Toolbox Fluid Cognition and Neuroimaging Measures

There was a significant positive linear relationship between hippocampal volume and fluid cognition composite score (t = 3.3, p = 0.001, partial η^2 = 0.11; see **Figure 2**) while controlling for sex and years of education (full model ($F_{(3,89)} = 3.81$, $p = 0.013$, $r^2 = 0.11$).

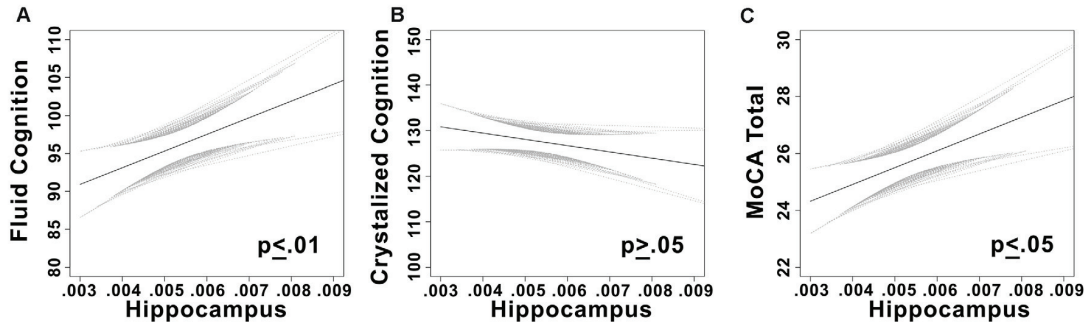

FIGURE 2 | (A) Plots the linear relationship between fluid cognition and hippocampal volume. **(B)** Plots the linear relationship between crystalized cognition and hippocampal volume. **(C)** Plots the linear relationship between Montreal Cognitive Assessment (MoCA) total score and hippocampal volume. Confidence bands are 95% confidence intervals of the regression line.

Relationship Between NIH Toolbox Crystallized Cognition and Neuroimaging Measures

As expected, no relationship was observed between hippocampal volume and crystallized cognition while controlling for covariates ($t = -0.21$, $p = 0.84$). Univariate models were nonsignificant as well; neither composite nor individual sub-scales of crystallized cognition were significantly related to hippocampal volume (p's > 0.05).

Relationship Between NIH Toolbox Sub-Scales and Neuroimaging Measures

Five linear models were analyzed using each sub-scale of the NIH toolbox fluid cognition composite while controlling for sex and years of education. Dimensional Change Card Sorting ($p = 0.027$, partial $\eta^2 = 0.05$, observed power = 0.60), Picture sequence memory ($p = 0.001$, partial $\eta^2 = 0.11$, observed power = 0.90), List Sorting ($p = 0.04$, partial $\eta^2 = 0.05$, observed power = 0.54) and Pattern comparison ($p = 0.002$, partial $\eta^2 = 0.11$, observed power = 0.89) were predicted by hippocampal volume. The attention domain flanker task was not significantly ($p > 0.25$) related to hippocampal volume. The strongest predictor of hippocampal volume was the pattern comparison task, which is in the processing speed domain. The episodic memory (picture sequence memory task) domain and the working memory domain (list sorting task) were both significantly related to hippocampal volume. Two supplemental tasks, the symbol digit search and Rey verbal learning were also analyzed (these tasks do not factor into the fluid cognition composite score, but were including in our NIH-Toolbox cognitive module). Rey verbal learning ($p = 0.008$, partial $\eta^2 = 0.08$, observed power = 0.77) and symbol digit search ($p = 0.073$, partial $\eta^2 = 0.04$, observed power = 0.44) scores showed a positive relationship with hippocampal volume. See **Figure 3** for a summary.

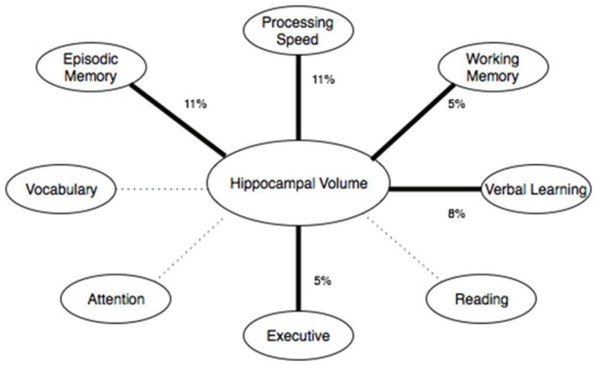

FIGURE 3 | Shows the cognitive domains of the NIH toolbox and their relationship with hippocampal volume. Thick, solid lines represent significant ($p < 0.05$) effects. Dashed lines represent non-significant effects. The percentage represents the effect size (percent variance explained by the predictor variable).

MoCA

Relationship Between MoCA and Neuroimaging Measures

There was a significant positive linear relationship between hippocampal volume and total MoCA score while controlling for sex and years of education ($t = 2.36$, $p = 0.02$, partial $\eta^2 = 0.06$).

Relationship Between MoCA Subscales and Neuroimaging Measures

Three subscales of the MoCA were analyzed individually: delayed recall, attention and visual-spatial/executive. As hypothesized, delayed recall was associated with hippocampal volume ($t = 1.96$, $p = 0.052$). No associations were found between attention ($t = 0.75$, $p = 0.454$) or visual-spatial/executive ($t = 0$ 0.88, $p = 0.382$).

DISCUSSION

Hippocampal volume predicted cognitive performance on both the MoCA and NIH toolbox fluid cognition composite score in a community sample of 93 older adults without clinical history of MCI, neurodegenerative disease, neurological injury or self-reported memory problems. This finding supports the study hypothesis that smaller hippocampal volume is associated with poorer cognitive performance in older adults, particularly with respect to memory-related functions. A relationship in hippocampal volume was found only for fluid abilities, and not crystallized abilities such as vocabulary or reading. This

disassociation has been described in patient studies such as HM, where bilateral hippocampal resection caused profound memory disturbances while general knowledge remained intact (Scoville and Milner, 1957).

Prior literature demonstrates a strong relationship between the hippocampus and learning, memory and other fluid cognitive functions in both animals and humans (Raz et al., 1998; Petersen et al., 2000), with smaller volumes associated with poorer performance (Persson et al., 2006). However, these results have not been universal in older adults (Van Petten, 2004). Our data not only demonstrate a strong relationship between hippocampal volume and episodic memory, but also relationships with executive function, working memory and speed of processing.

Cognitive Subdomains and Hippocampal Volume

Within the MoCA and NIHTB, subtests that targeted the memory domain were significantly related to hippocampal volume. This replicates previous research showing a positive relationship between hippocampal atrophy and memory measures in non-demented subjects (Golomb et al., 1996; Persson et al., 2006). However, as mentioned, not all studies have replicated this finding. A meta-analysis by Van Petten (Van Petten, 2004) suggested that overall evidence in the literature for a positive relationship between hippocampal size and episodic memory in older adults was "surprisingly weak." In addition, a prior study investigating the relationship between hippocampal volume and MoCA failed to find such a relationship (Paul et al., 2011). While the current study and Paul et al. (2011) were similar in statistical power, imaging methods, and study inclusion/exclusion criteria, our sample was approximately 10 years older. As the relationship between hippocampal volume and memory is non-linear with age, this difference in our cohort's average age may account for the difference in our findings (Chen et al., 2016).

Regardless, this study is the first to report a significant positive relationship between hippocampal volume, MoCA and NIHTB-CB memory measures. However, caution in the interpretation of these findings is warranted. "Bigger is better" is certainly an oversimplification; smaller hippocampi have been associated with better memory in children and adolescents (Sowell et al., 2001). Furthermore, in pathological conditions, such as Fragile X syndrome, enlarged hippocampi are associated with poorer memory performance (Molnár and Kéri, 2014). The biological change associated with increased or decreased brain volume could be the result of multiple processes, which we are unable to elucidate with T1 structural MRI techniques. For example, increased volume could be the result of increased neuronal cell bodies, increases in glia or astrocytes, neuroinflammation or insufficient neuronal pruning. Nonetheless, our results demonstrate that smaller hippocampal volume is associated with decreased performance on two well validated and commonly administered measures of cognitive function in older adults, with particular sensitivity to memory function across both tasks.

Hippocampal volume was associated with performance in other cognitive domains besides memory on the NIHTB Cognitive Battery, specifically speed of processing, working memory and executive function (see **Figure 3**). In fact, the association between hippocampal volume and processing speed on the NIHTB was slightly stronger than for episodic memory. As delayed recall is not assessed by the NIH-Toolbox, it is possible that the relationship with delayed recall observed on the MoCA was not detectable from the NIH-Toolbox Cognitive Battery. Regardless, our results highlight the multifaceted role of the hippocampus in cognitive aging. The hippocampus contributes to other cognitive functions besides memory, and optimal learning and memory depends on other cognitive functions, such as working memory, processing speed and executive functioning, in addition to encoding and storage. A relationship between speed of processing and hippocampal volume has been shown in some (Tisserand et al., 2000), but not all past studies (Colom et al., 2013). An association between hippocampal volume and executive functioning was only evident on the NIH toolbox (dimension change card sorting), not for the MoCA executive-visual spatial sub-scale. Dimensional Change Card Sorting has greater cognitive demand and requires higher-order executive processes compared to the MoCA executive tasks. For example, the Dimensional Change Card Sorting task would require effort from multiple CHC factors, such as fluid reasoning, short-term memory, visual processing and reaction speed. Even though the executive tasks in NIH Toolbox and MoCA are classified as part of the same domain, performance on these tasks was not correlated ($r = 0.07$, $p > 0.05$). This supports the conclusion that these tests measure different elements of executive functioning. While the relationship between fluid cognition and hippocampal volume may seem surprising due to the traditional association of fluid abilities (particularly executive function and processing speed) and the pre-frontal cortex, previous studies have implicated hippocampal volume as a predictor of fluid ability in older adults (while no such association was found in younger adults; Reuben et al., 2011). A potential mechanism of the hippocampal association with fluid ability in older adults may relate to compensatory processes in the hippocampus as a result of the pre-frontal atrophy observed with age. Further research, particularly longitudinal studies, are needed to clarify whether the relationship between hippocampal volume and fluid ability changes throughout the lifespan, and which potential mechanisms may account for such change.

CONCLUSION

Prior research has produced controversy over the role of the hippocampus in cognitive aging, casting doubt on its role in episodic memory, as well as other domains (e.g., speed of processing, Van Petten, 2004; Colom et al., 2013). Our findings demonstrate that the hippocampus is a critical structure in cognitive aging, playing a role not only in episodic memory, but also processing speed, working memory and executive function. Whether effects of the hippocampus on domains outside of episodic memory are direct or meditational in nature remains to be seen. Our findings also demonstrate that performance on

a commonly used bedside dementia screening (MoCA) and a comprehensive cognitive battery (NIH Toolbox) are significantly related to hippocampal volume. Whereas, a prior study failed to find a relationship between MoCA and hippocampal volume in an older adult population (Paul et al., 2011), we found that our cohort, approximately 10 years senior in average age, evidenced a significant relationship. These data suggest a foundation for longitudinal research investigating hippocampal volume in older adults as a possible predictor of future decline or MCI conversion. Such data would help to elucidate issues of acute vs. progressive atrophy in the study, and further clarify potential implications for pathologies like MCI and AD. More importantly, our data provide strong evidence in support of the multifaceted role of the hippocampus in cognitive aging.

AUTHOR CONTRIBUTIONS

AO, RAC, ECP, NRN and AJW contributed text to the manuscript. AO and AJW performed data analysis. All authors provided edits and approved the final version of the manuscript.

FUNDING

AJW and AO are partially supported by the McKnight Brain Research Foundation and the University of Florida Cognitive Aging and Memory Clinical Translational Research Program. AJW is partially supported by the NIH/NCATS CTSA grant UL1 TR000064 and KL2 TR000065, NIA K01AG050707-A1 and R01AG054077. The funding sources had no involvement in the study design, collection, analysis and interpretation of the data, in the writing of the manuscript and in the decision to submit the manuscript for publication. Neuroimaging was performed at the Advanced Magnetic Resonance Imaging and Spectroscopy (AMRIS) facility in the McKnight Brain Institute of the University of Florida, which is supported by National Science Foundation Cooperative Agreement no. DMR-1157490 and the State of Florida.

REFERENCES

Cardinale, F., Chinnici, G., Bramerio, M., Mai, R., Sartori, I., Cossu, M., et al. (2014). Validation of FreeSurfer-estimated brain cortical thickness: comparison with histologic measurements. *Neuroinformatics* 12, 535–542. doi: 10.1007/s12021-014-9229-2

Cattell, R. B. (1987). *Intelligence: Its Structure, Growth and Action.* Amsterdam, New York, NY: North-Holland.

Chen, H., Zhao, B., Cao, G., Porges, E. C., O'Shea, A., Woods, A. J., et al. (2016). Statistical approaches for the study of cognitive and brain aging. *Front. Aging Neurosci.* 8:176. doi: 10.3389/fnagi.2016.00176

Colom, R., Stein, J. L., Rajagopalan, P., Martínez, K., Hermel, D., Wang, Y., et al. (2013). Hippocampal structure and human cognition: key role of spatial processing and evidence supporting the efficiency hypothesis in females. *Intelligence* 41, 129–140. doi: 10.1016/j.intell.2013.01.002

Eldridge, L. L., Knowlton, B. J., Furmanski, C. S., Bookheimer, S. Y., and Engel, S. A. (2000). Remembering episodes: a selective role for the hippocampus during retrieval. *Nat. Neurosci.* 3, 1149–1152. doi: 10.1038/80671

Fischl, B., Salat, D. H., Busa, E., Albert, M., Dieterich, M., Haselgrove, C., et al. (2002). Whole brain segmentation: automated labeling of neuroanatomical structures in the human brain. *Neuron* 33, 341–355. doi: 10.1016/S0896-6273(02)00569-X

Golomb, J., Kluger, A., de Leon, M. J., Ferris, S. H., Mittelman, M. P., Cohen, J., et al. (1996). Hippocampal formation size predicts declining memory performance in normal aging. *Neurology* 47, 810–813. doi: 10.1212/WNL.47.3.810

Heaton, R. K., Akshoomoff, N., Tulsky, D., Mungas, D., Weintraub, S., Dikmen, S., et al. (2014). Reliability and validity of composite scores from the NIH toolbox cognition battery in adults. *J. Int. Neuropsychol. Soc.* 20, 588–598. doi: 10.1017/S1355617714000241

Iaria, G., Chen, J.-K., Guariglia, C., Ptito, A., and Petrides, M. (2007). Retrosplenial and hippocampal brain regions in human navigation: complementary functional contributions to the formation and use of cognitive maps. *Eur. J. Neurosci.* 25, 890–899. doi: 10.1111/j.1460-9568.2007.05371.x

Jack, C. R. Jr., Petersen, R. C., Xu, Y. C., O'Brien, P. C., Smith, G. E., Ivnik, R. J., et al. (1999). Prediction of AD with MRI-based hippocampal volume in mild cognitive impairment. *Neurology* 52, 1397–1403. doi: 10.1212/WNL.52.7.1397

Jovicich, J., Czanner, S., Han, X., Salat, D., van der Kouwe, A., Quinn, B., et al. (2009). MRI-derived measurements of human subcortical, ventricular and intracranial brain volumes: reliability effects of scan sessions, acquisition sequences, data analyses, scanner upgrade, scanner vendors and field strengths. *Neuroimage* 46, 177–192. doi: 10.1016/j.neuroimage. 2009.02.010

Madan, C. R. (2015). Creating 3D visualizations of MRI data: a brief guide. *F1000Res.* 4:466. doi: 10.12688/f1000research.6838.1

McGrew, K. S. (2009). CHC theory and the human cognitive abilities project: standing on the shoulders of the giants of psychometric intelligence research. *Intelligence* 37, 1–10. doi: 10.1016/j.intell.2008.08.004

Molnár, K., and Kéri, S. (2014). Bigger is better and worse: on the intricate relationship between hippocampal size and memory. *Neuropsychologia* 56, 73–78. doi: 10.1016/j.neuropsychologia.2014.01.001

Morey, R. A., Petty, C. M., Xu, Y., Hayes, J. P., Wagner, H. R. II., Lewis, D. V., et al. (2009). A comparison of automated segmentation and manual tracing for quantifying hippocampal and amygdala volumes. *Neuroimage* 45, 855–866. doi: 10.1016/j.neuroimage.2008.12.033

Mungas, D., Heaton, R., Tulsky, D., Zelazo, P. D., Slotkin, J., Blitz, D., et al. (2014). Factor structure, convergent validity and discriminant validity of the NIH toolbox cognitive health battery (NIHTB-CHB) in adults. *J. Int. Neuropsychol. Soc.* 20, 579–587. doi: 10.1017/S1355617714000307

Nasreddine, Z. S., Phillips, N. A., Bédirian, V., Charbonneau, S., Whitehead, V., Collin, I., et al. (2005). The montreal cognitive assessment, MoCA: a brief screening tool for mild cognitive impairment. *J. Am. Geriatr. Soc.* 53, 695–699. doi: 10.1111/j.1532-5415.2005.53221.x

O'Keefe, J. (1979). A review of the hippocampal place cells. *Prog. Neurobiol.* 13, 419–439. doi: 10.1016/0301-0082(79)90005-4

O'Keefe, J., and Dostrovsky, J. (1971). The hippocampus as a spatial map. Preliminary evidence from unit activity in the freely-moving rat. *Brain Res.* 34, 171–175. doi: 10.1016/0006-8993(71)90358-1

Papp, K. V., Kaplan, R. F., Springate, B., Moscufo, N., Wakefield, D. B., Guttmann, C. R. G., et al. (2014). Processing speed in normal aging: effects of white matter hyperintensities and hippocampal volume loss. *Neuropsychol. Dev. Cogn. B Aging Neuropsychol. Cogn.* 21, 197–213. doi: 10.1080/13825585.2013.795513

Paul, R., Lane, E. M., Tate, D. F., Heaps, J., Romo, D. M., Akbudak, E., et al. (2011). Neuroimaging signatures and cognitive correlates of the montreal cognitive assessment screen in a nonclinical elderly sample. *Arch. Clin. Neuropsychol.* 26, 454–460. doi: 10.1093/arclin/acr017

Persson, J., Nyberg, L., Lind, J., Larsson, A., Nilsson, L.-G., Ingvar, M., et al. (2006). Structure-function correlates of cognitive decline in aging. *Cereb. Cortex* 16, 907–915. doi: 10.1093/cercor/bhj036

Petersen, R. C., Jack, C. R. Jr., Xu, Y.-C., Waring, S. C., O'Brien, P. C., Smith, G. E., et al. (2000). Memory and MRI-based hippocampal volumes in aging and AD. *Neurology* 54, 581–581. doi: 10.1212/WNL.54.3.581

Raz, N., Gunning-Dixon, F. M., Head, D., Dupuis, J. H., and Acker, J. D. (1998). Neuroanatomical correlates of cognitive aging: evidence from structural

magnetic resonance imaging. *Neuropsychology* 12, 95–114. doi: 10.1037/0894-4105.12.1.95

Raz, N., Lindenberger, U., Rodrigue, K. M., Kennedy, K. M., Head, D., Williamson, A., et al. (2005). Regional brain changes in aging healthy adults: general trends, individual differences and modifiers. *Cereb. Cortex* 15, 1676–1689. doi: 10.1093/cercor/bhi044

Reuben, A., Brickman, A. M., Muraskin, J., Steffener, J., and Stern, Y. (2011). Hippocampal atrophy relates to fluid intelligence decline in the elderly. *J. Int. Neuropsychol. Soc.* 17, 56–61. doi: 10.1017/S135561771000127X

Salthouse, T. A. (2010). Selective review of cognitive aging. *J. Int. Neuropsychol. Soc.* 16, 754–760. doi: 10.1017/S1355617710000706

Scoville, W. B., and Milner, B. (1957). Loss of recent memory after bilateral hippocampal lesions. *J. Neurol. Neurosurg. Psychiatry* 20, 11–21. doi: 10.1136/jnnp.20.1.11

Shi, F., Liu, B., Zhou, Y., Yu, C., and Jiang, T. (2009). Hippocampal volume and asymmetry in mild cognitive impairment and Alzheimer's disease: meta-analyses of MRI studies. *Hippocampus* 19, 1055–1064. doi: 10.1002/hipo.20573

Sowell, E. R., Delis, D., Stiles, J., and Jernigan, T. L. (2001). Improved memory functioning and frontal lobe maturation between childhood and adolescence: a structural MRI study. *J. Int. Neuropsychol. Soc.* 7, 312–322. doi: 10.1017/s135561770173305x

Squire, L. R. (1992). Memory and the hippocampus: a synthesis from findings with rats, monkeys, and humans. *Psychol. Rev.* 99, 195–231. doi: 10.1037//0033-295x.99.2.195

Tisserand, D. J., Visser, P. J., van Boxtel, M. P. J., and Jolles, J. (2000). The relation between global and limbic brain volumes on MRI and cognitive performance in healthy individuals across the age range. *Neurobiol. Aging* 21, 569–576. doi: 10.1016/s0197-4580(00)00133-0

Van Petten, C. (2004). Relationship between hippocampal volume and memory ability in healthy individuals across the lifespan: review and meta-analysis. *Neuropsychologia* 42, 1394–1413. doi: 10.1016/j.neuropsychologia.2004.04.006

Woods, A. J., Cohen, R. A., and Pahor, M. (2013). Cognitive frailty: frontiers and challenges. *J. Nutr. Health Aging* 17, 741–743. doi: 10.1007/s12603-013-0398-8

Yamamoto, N., Philbeck, J. W., Woods, A. J., Gajewski, D. A., Arthur, J. C., Potolicchio, S. J., et al. (2014). Medial temporal lobe roles in human path integration. *PLoS One* 9:e96583. doi: 10.1371/journal.pone.0096583

Conflict of Interest Statement: The authors declare that the research was conducted in the absence of any commercial or financial relationships that could be construed as a potential conflict of interest.

The handling Editor declared a shared affiliation, though no other collaboration, with the authors and states that the process nevertheless met the standards of a fair and objective review.

Copyright © 2016 O'Shea, Cohen, Porges, Nissim and Woods. This is an open-access article distributed under the terms of the Creative Commons Attribution License (CC BY). The use, distribution and reproduction in other forums is permitted, provided the original author(s) or licensor are credited and that the original publication in this journal is cited, in accordance with accepted academic practice. No use, distribution or reproduction is permitted which does not comply with these terms.

UF | Evelyn F. & William L. McKnight Brain Institute
UNIVERSITY *of* FLORIDA

Evelyn F. and William L. McKnight Brain Institute of the University of Florida
P.O. Box 100015 • Gainesville, FL 32610-0015
352.273.8500

Revised 1/17/17 PS118660